Interplay of EGFR and Notch signaling pathways via mitochondrial shape and activity during *Drosophila* development

A thesis

Submitted in partial fulfilment of the requirements

of the degree of

DOCTOR OF PHILOSOPHY

By

DARSHIKA TOMER

20113119

INDIAN INSTITUTE OF SCIENCE EDUCATION AND RESEARCH PUNE

Dedicated to my parents…

CERTIFICATE

It is certified that the work incorporated in the thesis entitled ("Interplay of EGFR and Notch signaling pathways via mitochondrial shape and activity during *Drosophila* development") submitted by Darshika Tomer was carried out by the candidate, under my supervision. The work presented here or any part of it has not been included in any other thesis submitted previously for the award of any degree or diploma from any other University or institution.

Date:

Dr. Richa Rikhy
(Supervisor)

DECLARATION

I declare that this written submission represents my research work in my own words and where others' ideas or works have been included, I have adequately cited and referenced the original sources. I also declare that I have adhered to all principles of academic honesty and integrity and have not misrepresented or fabricated or falsified any idea/data/fact/source in my submission. I understand that violation of the above will because for disciplinary action by the Institute and can also evoke penal action from the sources which have thus not been properly cited or from whom proper permission has not been taken when needed.

Date:

Darshika Tomer

Reg. No: 20113119

ACKNOWLEDGEMENT

Thesis writing is an individual effort but Ph.D is a collective task. So I will not take the whole blame; here are some of the people who I want to thank for this adventure.

Ph.D has been a learning experience and as a bonus, I met great people enroute. I can't recall a time when my guide, Dr. Richa Rikhy has not been there to discuss a question. I always look up to her for advice in work as well as figuring other things out. Being the second student in the lab I was showered with attention which juniors are envious of. She allowed us to try out a lot of new things, and even if they did not work out, she never lost patience over it. I would also like to thank her for constantly encouraging me to attend conferences and interact to with fantastic people in the field. Faculty at IISER are approachable and always ready to discuss work or life at IISER in general. It's an honor to know them and listen to their work. Especially Dr. Girish Ratnaparkhi, with whose lab we shared lab meetings, has always put forth the most basic questions and helped me guide the project. His smart come backs are an inspiration to any apprentice of sarcasm. Dr. Anuradha Ratnaparkhi, my external RAC member shared her vast fly knowledge, as well as reagents thus making the Ph.D ride smoother. I am grateful to my RAC members, Dr. L.S. Shashidhara who has been patient and offered critical comments time to time during the Ph.D. Dr. Aurnab Ghose took time to explain the nuances of research during RAC meetings which were very helpful. In addition I would like to thank Dr. Thomas Pucadyil for help with Drp1 point mutants and Dr. Kundan Sengupta, Dr. Saikrishnan Kayarat, Dr. Sanjeev Galande for reagents.

IISER provides excellent infrastructure for a fly lab. The campus is unlike any college I had been to, it's a much smaller and intimate place where everybody knows everybody. BS-MS organized activities from Karvaan to Friday night movies and quilling classes which have given me memories that will be cherished forever. I would like to thank UGC, DBT and Infosys foundation for providing me opportunity to attend conferences and make new friends. I would like to thank Vijay, Snehal, Yashwant, Piyush, Kalpesh, Mrinalini, Shabnam for making work smoother and Mahesh and Tushar for help with conference paperwork.

Friends did a wonderful job of constantly distracting me from my work and in general get me into trouble of all sorts. Our lab is bound together by the philosophy of having a good time no matter what. Experiments which have not worked out were turned into inspiration to try out more things. They were always there to lend a hand in return for little food or money. Sayali was instrumental in scaring number of juniors. I would like to thank Dnyanesh-Rohan for scientific inputs, biased views and their acting skills. Swati has pan-IISER presence and kept us entertained with her ideas about life. Thank you Sameer and Bipasha for the food, trips and selfless help. Gossip sessions with Manasi Gangan and Aparna offered much needed respite from work. I am grateful to Devashree and Radhika for help me with my project work. I know I have found friends for life in these guys.

Being mainly a fly lab, we hardly had any molecular biology reagents in the beginning and most of the time I borrowed heavily from Girish lab. I thank Girish lab members for inputs in work and for reagents.

Neha has been a friend on whom I can completely rely, talk freely and get away from work with, which is most needed. I will cherish a lifetime of memories with her; of all the great things Ph.D was about.

I want to thank countless scientists who have awed everybody with their cool experiments and ideas. I am particularly thankful to Dr. Barbara McClintock for showing that genes can jump too. Dr. Thomas Hunt Morgan and his lab members for introducing fruit flies. I am also grateful for generally well behaved *Drosophila* for giving up its ovaries for the noble task of my Ph.D.

Thank you Pune, for being imperfect, so that we could constantly complain about there being no transport, heavily charging autowallahs, no places to see while all the time enjoying excellent weather. I am going to miss the breeze, the rain, but not the sun.

Thank you yearly book sales for helping me expand my library; Prison break, Friends, Rick and Morty, Game of thrones for guilt filled entertainment.

Thank you, Ravi for the discussions and being open to ideas, I know I have found a friend for life in you and I think you are really lucky.

Family is the support system which we all take for granted a lot. I love my brother for always being there no matter what and being the cool person that he is. I am extremely lucky to have parents who cheerfully donated me to science, braving the jibes from ‘society’ alone and tried their best to understand my work. No words can sum up my love for you both.

Sometimes the questions are complicated and the answers are too.
Modified from Dr. Seuss

TABLE OF CONTENT

LIST OF FIGURES

LIST OF TABLES

ABBREVIATIONS

PFC- Posterior follicle cells

FC- Follicle cells

FSC- Follicle stem cell

AFC- Anterior follicle cells

MBC- Main body follicle cells

ROS- Reactive oxygen species

ETC- Electron transport chain

FCCP- Carbonyl cyanide-p-trifluoromethoxyphenylhydrazone

NOX- NADPH oxidase

UPR- Unfolded protein response

ER- Endoplasmic reticulum

Drp1- Dynamin related protein 1

Marf- Mitochondrial assembly regulatory factor

Mfn- Mitofusin

Opa1- Optic atrophy 1

Fzo- Fuzzy onions

Mdv1- Mitochondrial division protein 1

Caf4- CCR4- associated factor 4

Mid51- Mitochondrial dynamics protein

MARCM- Mosaic analysis with a repressible cell marker

hsflp- Heat shock flippase

FRT- Flippase recognition target

aPKC- Atypical protein kinase C

Dlg- Discs large 1

NC- Nuclear cycle

EGFR- Epidermal growth factor receptor

JNK- c-Jun N-terminal kinase

NICD- Notch intracellular domain

Hnt- Hindsight

AMPK- 5' adenosine monophosphate-activated protein kinase

SOD- Superoxide dismutase

ERK- Extracellular signal-regulated kinase

Arp2/3- Actin related protein

NAD- Nicotinamide adenine dinucleotide

QH2- Ubiquinone

CDK1- Cyclin dependent kinase 1

DILPs- Insulin- like peptide 1

MCU- Mitochondrial calcium uniporter

MAMs- Mitochondria associated membrane

VDAC- Voltage dependent anion channel

p38K- p38 kinase

CHOP- c(EBP) homologues protein

ATF2- Activating transcription factor 2

AP1- Activator protein 1

Par1- Partitioning defective 1

Patj- PALS1 associated TJ1 protein

Lgl- Lethal giant larvae

TMRE- tetramethylrhodamine, ethyl ester

CoVa- Cytochrome C oxidase subunit Va

DHE- dihydroethidium

2-DG- 2-Deoxy-2-Glucose

PAGFP- Photo activable GFP

LKB1- Liver kinase B1

CAMKK2- Calcium/calmodulin-dependent protein kinase kinase 2

PI3K- Phosphatidylinositol-4,5-bisphosphate 3-kinase

Scrib- Scribbled

ADAM- A disintegrin and metaalloproteinase

HIF- Hypoxia inducible factor

mitoPLD- mitochondrial phospholipase D

ABSTRACT

Mitochondrial shape is modulated to regulate their function. The regulation of this modulation by cell signalling is not understood well in the field. The EGFR and Notch signaling pathways interact with mitochondrial metabolism and morphology during development however the mechanism of interplay is unknown. *Drosophila melanogaster* posterior follicle cells (PFCs) deficient in mitochondrial fission protein Drp1 showed loss of EGFR signaling driven oocyte axial patterning and Notch signaling mediated PFC differentiation. This study elucidates the interaction of these pathways with mitochondrial bioenergetics in the form of electron transport chain (ETC) activity. We show that PFCs deficient for Drp1 have increased mitochondrial membrane potential in addition to aggregated mitochondrial morphology. Even though *drp1* mutant PFCs show defective oocyte migration, phosphorylated ERK (dpERK), a downstream component of EGFR signaling is elevated in these cells. We find that ERK regulates mitochondrial membrane potential at wild type levels in PFCs and increased dpERK in *drp1* mutant PFCs is responsible for higher mitochondrial membrane potential. Pharmacological inhibition of ETC does not result in change in aggregated mitochondrial morphology in *drp1* mutant PFCs or loss of oocyte patterning. Notably, ETC inhibition activates Notch signaling in wild type ovarioles at an earlier stage and reverses the loss of Notch signaling in *drp1* mutant PFCs. The positive correlation between EGFR and fragmented mitochondria seems to hold true for *Drosophila* wing as well. Hence, EGFR-mitochondria might interact in multiple tissues during development. Our study thus shows that the EGFR-Ras-ERK pathway maintains mitochondrial morphology and membrane potential in follicle cells (FCs) for appropriate activity for oocyte axial patterning and mitochondrial bioenergetics specifically affects Notch mediated differentiation.

SYNOPSIS

Name of the Student: Darshika Tomer
Registration number: 20113119
Name of Thesis advisor: Dr. Richa Rikhy
Date of Registration: 1st August 2011
Place: Indian Institute of Science Education and Research, Pune
Title: **Interplay of EGFR and Notch signaling pathways via mitochondrial shape and activity during *Drosophila* development**

Introduction

Mitochondria are dynamic organelles which in addition to their chief function of energy generation, perform a number of other tasks in a cell such as regulation of calcium levels, the release of ROS and lipid metabolism etc. (Javadov and Kuznetsov 2013). Dynamicity of mitochondria arises on account of its variable architecture; it can be present in the form of a dense network or small fragments (Bereiter-Hahn and Vöth 1994). Inner mitochondrial cristae structure also varies. It can be sparse or abundant, depending on the ATP output required by the cell (Frey and Mannella 2000). Mitochondrial architecture governs its functions and is dependent on cell type. For example, *Drosophila* embryo has small fragmented mitochondria while *Drosophila* muscle cells have elongated tubular mitochondria (Wang *et al.* 2016; Chowdhary *et al.* 2017). Mitochondrial surface acts as a platform to facilitate interactions with other organelles such as ER and signaling molecules such as the apoptotic family protein Bax (Karbowski *et al.* 2002; Korobova *et.al.* 2013). By virtue of these diverse functions and interactions, the organelle is understood to be a master regulator in several signaling pathways and more aspects are being added through ongoing studies (Soubannier and McBride 2009). Thus mitochondria are now known to have an instructive rather than standby role in the determination of cellular identity and functions.

There are several studies in diverse model systems signifying the role of mitochondria in cell fate decision making, cell number control and patterning in a tissue

(Tsang and Lemire 2003; Mitra *et al.* 2012; Lee *et al.* 2016). Mitochondria can exert control over cellular processes due to its ability to coordinate with the nucleus and ER. This coordination can be in the form of direct transcriptional regulation of ETC genes, retrograde signal through UPR etc. (Biswas *et al.* 1999; Zhao *et al.* 2002). Another mode of interaction can be by cytoplasmic compartmentalization of signaling molecules, thus preventing their nuclear access. For example, processed Notch is present in T-cell mitochondrial fraction (Perumalsamy *et al.* 2010). Mitochondrial shape can indirectly influence its ATP yield, its ability to signal ER and nucleus and its ability to sequester signaling molecules (Westermann 2010). Abrogation of mitochondrial architecture is lethal in early development (Chen *et al.* 2003; Ishihara *et al.* 2009). Hence, this warrants a thorough analysis of the signaling elements downstream of mitochondria; lack of which can be the root of some of the diseases. Moreover, the knowledge of 'why and how' a developing animal maintains particular mitochondrial morphology and activity is fascinating. This fascination is what drove us; this study aimed to analyze the role of mitochondria in EGFR and Notch pathway on account of its architecture and energetics during *Drosophila* development.

This piece of work characterized mitochondria-signaling pathway interaction primarily in *Drosophila* ovary FCs. FCs are epithelial cells, enclosing the germline cells in *Drosophila* ovarioles. Their development can be followed from stem cell to differentiated cell stage. Further it attempted to show that similar relations hold true for other *Drosophila* tissues such as wing and embryo as well. The thesis also summarizes protocols necessary to understand mitochondrial functions quantitatively in addition to qualitative assessment in tissues. Here are the key findings:

Results and Discussion

1. Fission deficient mitochondria in *drp1*^{KG} mutant disrupt tissue organization in *Drosophila* ovary

MARCM is a specific strategy which used to generate GFP marked clones mutant for the protein of choice (Golic and Lindquist 1989). This technique results in generation of marked cells homozygous for the mutation of interest in an otherwise heterozygous background enabling an analysis of fate of these cells in vivo in the tissue of interest. MARCM clones for the mitochondrial fission protein, Drp1 in FCs displayed multilayering and their mitochondria were aggregated. We found lowering of cell number in the *drp1* mutant clone in comparison to FRT 40A control which did not have any mutation. *drp1*^{KG} cells were also deficient in the apical polarity marker, aPKC. Further, the decrease in cell number was found to be on account of slower division cycles as read by aberrant Cyclin B and E immunostaining in the mutant.

2. *drp1* mutant cells have higher mitochondrial membrane potential and ROS

We formulated protocols to quantify mitochondrial membrane potential, amount of ROS in the cell, ATP output and connectivity of mitochondrial network in *Drosophila* clonal FCs and *Drosophila* embryo. We observed that *drp1*^{KG} mutant mitochondria in the FCs had higher mitochondrial membrane potential difference and the cells also had elevated ROS. Fused mitochondria typically have greater potential difference across their inner mitochondrial membrane (Chen *et al.* 2005). However, increase in ROS generally correlates with fragmented architecture (Röth *et al.* 2014). We need to figure out if augmented ROS is outcome of cytoplasmic enzymes such as NOX in these cells (Nauseef 2008). We also found that lowering of mitochondrial membrane potential using drugs such as FCCP and by RNAi against ETC proteins resulted in quantifiable decrease in the potential difference.

In addition, it was established that *Drosophila* embryos rely on ETC for their energy demands and perturbations in ETC lead to disrupted actin dynamics probably via increase in pAMPK levels in the embryo (Chowdhary *et al.* 2017). pAMPK, the ATP sensor, is a prominent signaling pathway which orchestras stress related transcription regulation. It is a known cell cycle regulator (Motoshima *et al.* 2006). Our findings hinted at AMPK interaction with cytoskeleton during cell divisions.

Hence we were able to show how mitochondrial membrane potential can be used as a readout for status of the mitochondria and effect of its loss on the cell. We further wanted to test this abrogation with respect to the signaling pathways EGFR and Notch during development.

3. Increased ERK in *drp1*^{KG} mutant is responsible for multilayering and cell number defect

EGFR pathway is a known modulator of mitochondrial morphology (Mitra *et al.* 2012); hence next we assessed signaling molecules downstream of EGFR in *drp1*^{KG} mutant. Immunostaining for activated ERK (dpERK) and Ras showed them to be higher in *drp1*^{KG} mutant clones. Depletion of Ras and ERK using RNAi lines in the *drp1*^{KG} mutant background, rescued the defect in cell arrangement and number. Surprisingly, *drp1*^{KG} mutant despite elevated dpERK, exhibited defect in oocyte position which is downstream of EGFR in the ovaries. We further probed the localization of dpERK in the *drp1* mutant and found loss in its nuclear staining. This suggested that due to inability of ERK to enter nucleus it cannot activate transcription factors required for the oocyte movement to occur.

4. Lowering ERK rescued the mitochondrial aggregation and morphology defect

EGFR is known to regulate mitochondrial energy output (Boerner *et al.* 2004). In our assessment as well, it was noted that it controls mitochondrial membrane potential in the *Drosophila* FCs. Lowering of ERK drops mitochondrial membrane potential in *erk*^{i} alone and in *drp1*^{KG} mutant background as well. ERK depletion also reverted the aggregated mitochondrial network in *drp1*^{KG} mutant to dispersed as in the control cells.

This suggested that EGFR is upstream of mitochondrial shape and membrane potential in *Drosophila* FCs (Figure 1).

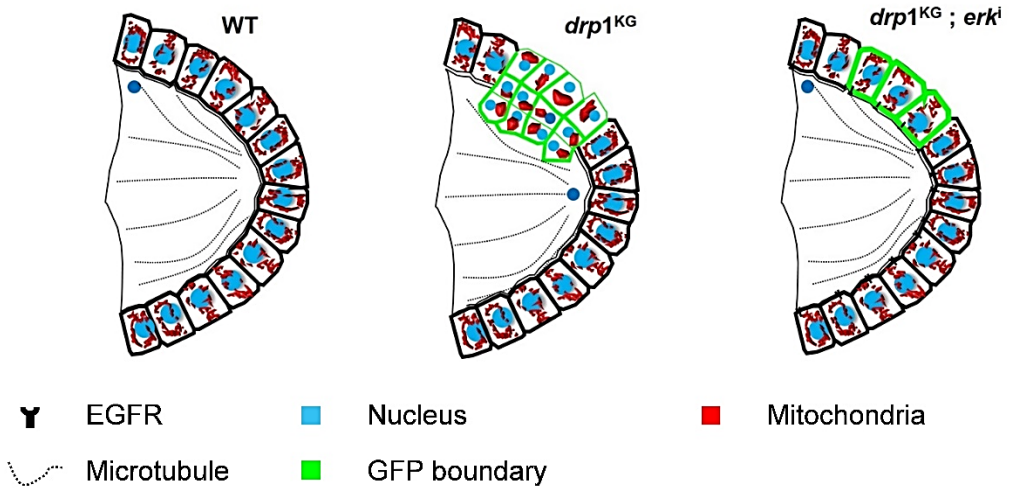

Figure 1. Increased cytoplasmic ERK is responsible for multilayering and cell number defect in *drp1* mutant. In the wild type ovariole FCs surrounding the oocyte communicate via EGFR signaling with the oocyte. The oocyte in stage 8 chamber is adjacent to anterior FCs. Mitochondria are distributed in the cytoplasm. *drp1* mutant has aggregated mitochondria and cells arrange in multiple layers. There is a loss of oocyte's positional information. ERK lowering the *drp1* mutant background rescues the multilayered phenotype and resolves the aggregated mitochondrial network. The oocyte position is however not reverted to the dorso-anterior position.

5. *drp1*^{KG} mutant exhibits loss of Notch pathway, which is rescued on Ras/ERK lowering

drp1^{KG} mutant are defective for Notch pathway as well (Mitra *et al.* 2012), and the mutant cells do not enter endocycle. EGFR is known to regulate Notch via the transcription factor Groucho in *Drosophila* FCs (Johnston *et al.* 2016). We checked for Notch pathway components in *drp1*^{KG}; *erk*^{i} and saw that there is a rescue and Notch pathway is activated. The cells enter endocycle and the Cyclin defect in *drp1* mutant is

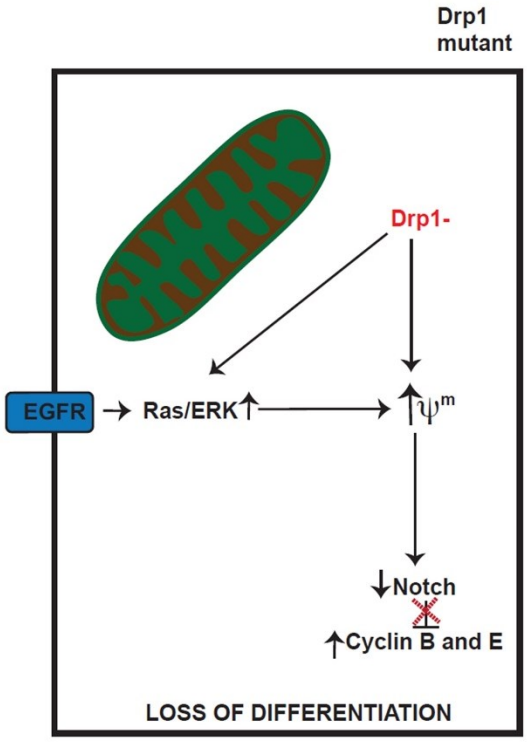

Figure 2. EGFR pathway regulates Notch via mitochondrial morphology and membrane potential in PFCs. Notch defective *drp1* mutant is rescued by removal of ERK via RNAi and lowering of mitochondrial membrane potential using ETC mutants. ERK lowering also rescues the slow cell cycle defect and Cyclins are lowered, thus initiating endocycle in the FCs.

reverted. This suggested that increased Ras/ERK was responsible for loss of Notch (Figure 2).

6. Increased mitochondrial membrane potential leads to Notch defect

We wanted to know if ERK reduction of mitochondrial membrane potential is what rescued Notch pathway. Hence mitochondrial membrane potential was reduced in *drp1* mutant background using RNAi against *pdsw*. We discerned that reduction of mitochondrial membrane potential is sufficient to rescue Notch pathway. In order to test if this would hold true for the wild type as well, we treated wild type to FCCP; thus lowering mitochondrial membrane potential in the entire ovariole and found that Notch pathway is now activated not stage 6 onwards but stage 5. This established that in wild type, Notch pathway is dependent on the mitochondrial energetics for its activation at appropriate stage.

In summary, we propose that EGFR pathway regulates mitochondrial morphology and activity and thereby interacts with Notch signaling. *Drosophila* FC development hence is

synchronized by a state of balance between levels of EGFR, ERK localization, mitochondrial morphology and membrane potential. We found a similar relationship to hold true for the *Drosophila* wing as well, where we found that defects in dominant negative EGFR can be rescued, by just increasing mitochondrial fragmentation in the cells. This again shows us that mitochondrial morphology is part of the EGFR pathway and together they are required for tissue organization and development.

7. References

1. Bereiter-Hahn J., Vöth M., **1994** Dynamics of mitochondria in living cells: shape changes, dislocations, fusion, and fission of mitochondria. Microsc. Res. Tech. **27**: 198–219.
2. Biswas G., Adebanjo O. A., Freedman B. D., Anandatheerthavarada H. K., Vijayasarathy C., Zaidi M., Kotlikoff M., Avadhani N. G., **1999** Retrograde Ca2+ signaling in C2C12 skeletal myocytes in response to mitochondrial genetic and metabolic stress: a novel mode of inter-organelle crosstalk. EMBO J. **18**: 522–533.
3. Boerner J. L., Demory M. L., Silva C., Parsons S. J., **2004** Phosphorylation of Y845 on the Epidermal Growth Factor Receptor Mediates Binding to the Mitochondrial Protein Cytochrome c Oxidase Subunit II. Mol. Cell. Biol. **24**: 7059–7071.
4. Chen H., Detmer S. a., Ewald A. J., Griffin E. E., Fraser S. E., Chan D. C., **2003** Mitofusins Mfn1 and Mfn2 coordinately regulate mitochondrial fusion and are essential for embryonic development. J. Cell Biol. **160**: 189–200.
5. Chen H., Chomyn A., Chan D. C., **2005** Disruption of fusion results in mitochondrial heterogeneity and dysfunction. J. Biol. Chem. **280**: 26185–92.
6. Chowdhary S., Tomer D., Dubal D., Sambre D., Rikhy R., **2017** Analysis of mitochondrial organization and function in the *Drosophila* blastoderm embryo. Sci. Rep.: 1–17.
7. Farida Korobova, Vinay Ramabhadran and H. N. H., **2013** An Actin-Dependent Step in Mitochondrial Fission Mediated by the ER-Associated Formin INF2.

Science (80-.). **76**: 211–220.

8. Frey T. G., Mannella C. A., **2000** The internal structure of mitochondria. Trends Biochem. Sci. **25**: 319–324.
9. Golic K. G., Lindquist S., **1989** The FLP recombinase of yeast catalyzes site-specific recombination in the *Drosophila* genome. Cell **59**: 499–509.
10. Ishihara N., Nomura M., Jofuku A., Kato H., Suzuki S. O., Masuda K., Otera H., Nakanishi Y., Nonaka I., Goto Y.-I., Taguchi N., Morinaga H., Maeda M., Takayanagi R., Yokota S., Mihara K., **2009** Mitochondrial fission factor Drp1 is essential for embryonic development and synapse formation in mice. Nat. Cell Biol. **11**: 958–966.
11. Javadov S., Kuznetsov A., **2013** Mitochondria: the cell powerhouse and nexus of stress . Front. Physiol. **4**: 207.
12. Johnston M. J., Bar-Cohen S., Paroush Z., Nystul T. G., **2016** Phosphorylated Groucho delays differentiation in the follicle stem cell lineage by providing a molecular memory of EGFR signaling in the niche. Development: dev.143263.
13. Karbowski M., Lee Y. J., Gaume B., Jeong S. Y., Frank S., Nechushtan A., Santel A., Fuller M., Smith C. L., Youle R. J., **2002** Spatial and temporal association of Bax with mitochondrial fission sites, Drp1, and Mfn2 during apoptosis. J. Cell Biol. **159**: 931–938.
14. Lee S., Lee K., Huh S., Hong S. H., Lee S., Lee K., Huh S., Liu S., Lee D., Hong S. H., Yu K., **2016** Polo Kinase Phosphorylates Miro to Control ER- Mitochondria Contact Sites and Mitochondrial Ca 2 + Homeostasis in Neural Stem Cell Development Article Polo Kinase Phosphorylates Miro to Control ER-Mitochondria Contact Sites and Mitochondrial Ca 2 + Homeos. Dev. Cell **37**: 174–189.
15. Mitra K., Rikhy R., Lilly M., Lippincott-Schwartz J., **2012** DRP1-dependent mitochondrial fission initiates follicle cell differentiation during *Drosophila* oogenesis. J. Cell Biol. **197**: 487–97.
16. Motoshima H., Goldstein B. J., Igata M., Araki E., **2006** AMPK and cell proliferation – AMPK as a therapeutic target for atherosclerosis and cancer. J. Physiol. **574**: 63–71.

17. Nauseef W. M., **2008** Biological roles for the NOX family NADPH oxidases. J. Biol. Chem. **283**: 16961–16965.
18. Perumalsamy L. R., Nagala M., Sarin A., **2010** Notch-activated signaling cascade interacts with mitochondrial remodeling proteins to regulate cell survival. Proc. Natl. Acad. Sci. U. S. A. **107**: 6882–6887.
19. Röth D., Krammer P. H., Gülow K., **2014** Dynamin related protein 1-dependent mitochondrial fission regulates oxidative signalling in T cells. FEBS Lett. **588**: 1749–1754.
20. Soubannier V., McBride H. M., **2009** Positioning mitochondrial plasticity within cellular signaling cascades. Biochim. Biophys. Acta **1793**: 154–70.
21. Tsang W. Y., Lemire B. D., **2003** The role of mitochondria in the life of the nematode, Caenorhabditis elegans. Biochim. Biophys. Acta - Mol. Basis Dis. **1638**: 91–105.
22. Wang Z.-H., Clark C., Geisbrecht E. R., **2016** Analysis of mitochondrial structure and function in the *Drosophila* larval musculature. Mitochondrion **26**: 33–42.
23. Westermann B., **2010** Mitochondrial fusion and fission in cell life and death. Nat. Rev. Mol. Cell Biol. **11**: 872–84.
24. Zhao Q., Wang J., Levichkin I. V, Stasinopoulos S., Ryan M. T., Hoogenraad N. J., **2002** A mitochondrial specific stress response in mammalian cells. EMBO J. **21**: 4411–9.

CHAPTER 1

Introduction

Mitochondria are double membrane bound organelles whose chief function is energy production in the cell. Mitochondria originated as endosymbionts, they are semi-autonomous in nature and there are two major theories to explain their origin. The conflicting theories state that the evolution of Eukaryote occurred simultaneously or before the endocytic event. Mitochondria evolved from proto-mitochondrion, a member of proteobacteria (Boussau *et al.* 2004). It is hypothesized that they were endocytosed around 2 billion years ago and gave a selective advantage to their hosts on account of oxidative phosphorylation (Embley 2006; de Duve 2007). Genome sequence comparisons show that mitochondria is close to the α-proteobacteria, *Rickettsia prowazekii* and they both diverged from a common ancestor (Gray 2012). Mitochondria utilize actin polymerization via Arp2/3 complex and another member of *Rickettsia* family, also uses this mode to transverse host cell cytoplasm (Gouin *et al.* 2005), hence actin interactors could have been passed on from the common ancestor. Rho-zero cells lack electron transport chain (ETC) components in the mitochondria. They depend on glycolysis for cell survival. Mitochondrial ROS and calcium related functions are hindered in these cells (Chandel and Schumacker 1999). Hence such studies have shown that mitochondria not only contribute ATP, but in addition have various diverse functions (Figure 1.1A-F). It is fascinating to note this transition of mitochondria from the humble beginnings to its current status in the cell.

Mitochondria is a double membrane bound organelle, the inner mitochondrial membrane is folded to form cristae. The folds increase the surface area available for respiration. Mitochondrion generates ATP by means of ETC and Krebs cycle in a eukaryotic cell. Krebs cycle takes place in the mitochondrial matrix and contributes ATP, NADH, QH_2 and CO_2. The inner mitochondrial membrane is embedded with electron carrier protein complexes which utilize the products of Krebs cycle and facilitate formation of active gradient of electrons. Oxidative phosphorylation complex proteins are contributed by nuclear as well as mitochondrial genome (Figure 1.1E). ETC establishes a transmembrane pH difference and the enzyme ATP synthase utilizes this

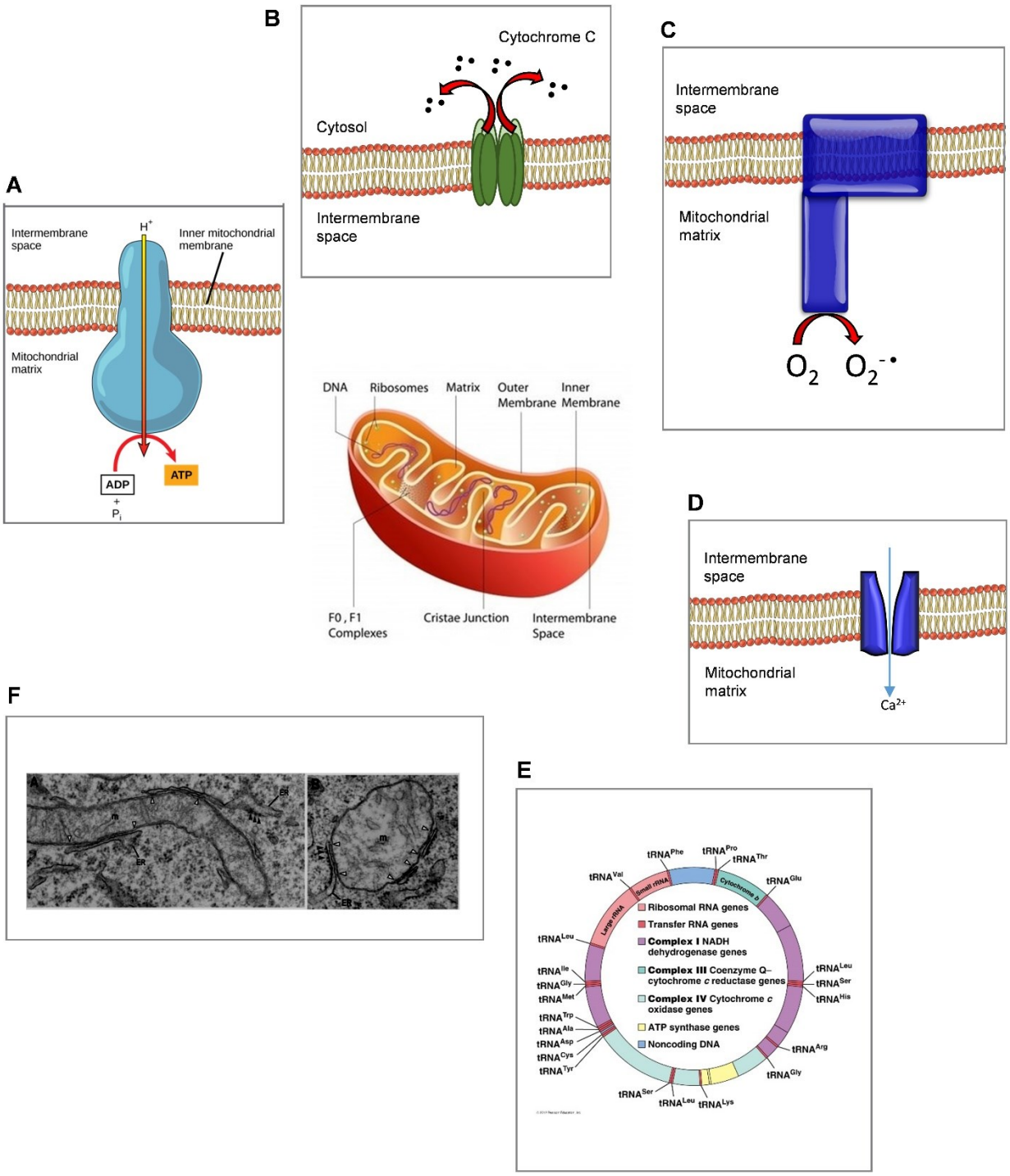

Figure 1.1. Multiple facets of the organelle mitochondria. (A) Mitochondria is the primary source of energy in the cell. It generates ATP with the help of ETC complexes housed on the inner mitochondrial membrane. Complex V shown here is the ATP synthase which translocates protons from the intermembrane space into the mitochondrial matrix to power ADP phosphorylation and produce ATP.

(B) Mitochondria participate in apoptosis mediated cell death. On receiving apoptotic signal, Bax family proteins get activated. These bind and permeate mitochondrial membrane thus facilitating release of Cytochrome C, which is critical for the activation of downstream Caspases.
(C) As a byproduct of the process of oxidative phosphorylation, ROS species such as superoxide ions are released. Mitochondria is one of the source of ROS in the cell in addition to cytoplasmic ROS generators such as NOX.
(D) Mitochondrial membrane houses calcium channels, hence regulating cytoplasmic calcium levels in coordination with the ER. These channels take up calcium from the cytoplasm or the exchange with ER.
(E) Mitochondrion has its own genome as well using which ETC components are transcribed and translated. I
(F) Mitochondria exhibit variable morphologies in the cell. SEM images depict variable mitochondrial shapes present; they can be present in the form of long tubules or short globules in a cell (EMs from Cosson *et al.* 2012).

pH difference to convert ADP to ATP, the energy currency of a cell. ATP synthase is part of the larger family of proteins whose counterparts in plants are involved in converting chemiosmotic potential into ATP. Similar proteins in plant thylakoid drive potential difference across grana. The transfer of electrons from one membrane bound enzyme to another ends in reduction of an oxygen molecule to release water (Figure 1.2A). A cell is able to synthesize 2 moles of ATP per mole of glucose by glycolysis. Kreb cycle and oxidative phosphorylation together bring the total up to 36 moles of ATP (Ernster L 1981). However this is not a rule, in fact there are organisms which generate far less moles of ATP for each mole of glucose consumed. For example mitosomes, which exist as compartments in the microorganism *Entamoeba histolytica* are a form of mitochondrion but are not involved in energy generation (Tovar *et al.* 1999). By compartmentalization mitochondrion makes the process efficient and allows the organism to survive in an aerobic environment.

Mitochondria are divided among daughter cells by a process of fission (Nunnari *et al.* 1997). Fission involves scission of both outer and inner membranes to form smaller units. Similarly mitochondria can fuse to form a large continuous network and the process is mediated by fusion proteins (Figure 1.3A-B). Mitochondrial network are

A

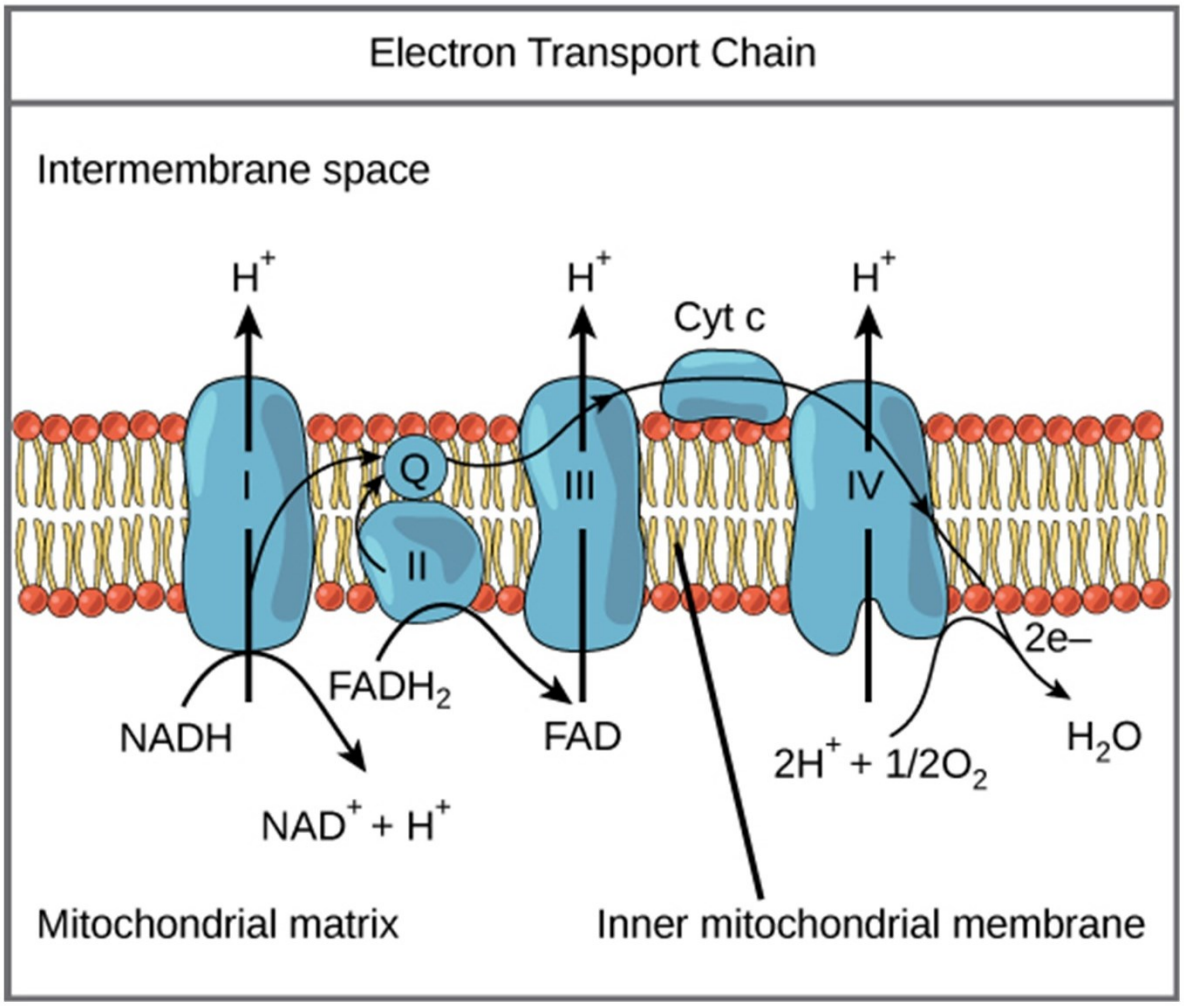

Figure 1.2. Mitochondria generate ATP with the help of ETC mediated redox reactions. (A) Inner membrane of the mitochondria harbours the ETC. ETC consists of multi subunit complexes; complex I is NADH dehydrogenase which reduces ubiquinone to oxidize NADH, in the process transporting 4 electrons out into the intermembrane space. Complex II- Succinate dehydrogenase again generates ubiquinol and passages electrons to add to the potential difference across the inner membrane. Reduced ubiquinone reacts with the third complex, cytochrome bc1 to push electrons out. Cytochrome oxidase or complex IV oxidizes Cytochrome c, in turn reducing oxygen to water. The process serves to create a difference in electron concentration, which is translated into potential energy to feed into complex V, which uses the potential energy to generate ATP.

malleable as and when cellular processes demand, hence making the matrix dynamic.

Constant fusion and fission allow efficient exchange of mitochondrial proteins and the nucleoids. This allows diseased and mutant mitochondria to survive, hence benefiting the population as a whole. Mitochondrial distribution to daughter cells as well as its transport within a cell is attained by mitochondrial fission (Shaw and Nunnari 2002) (Figure 1.4A).

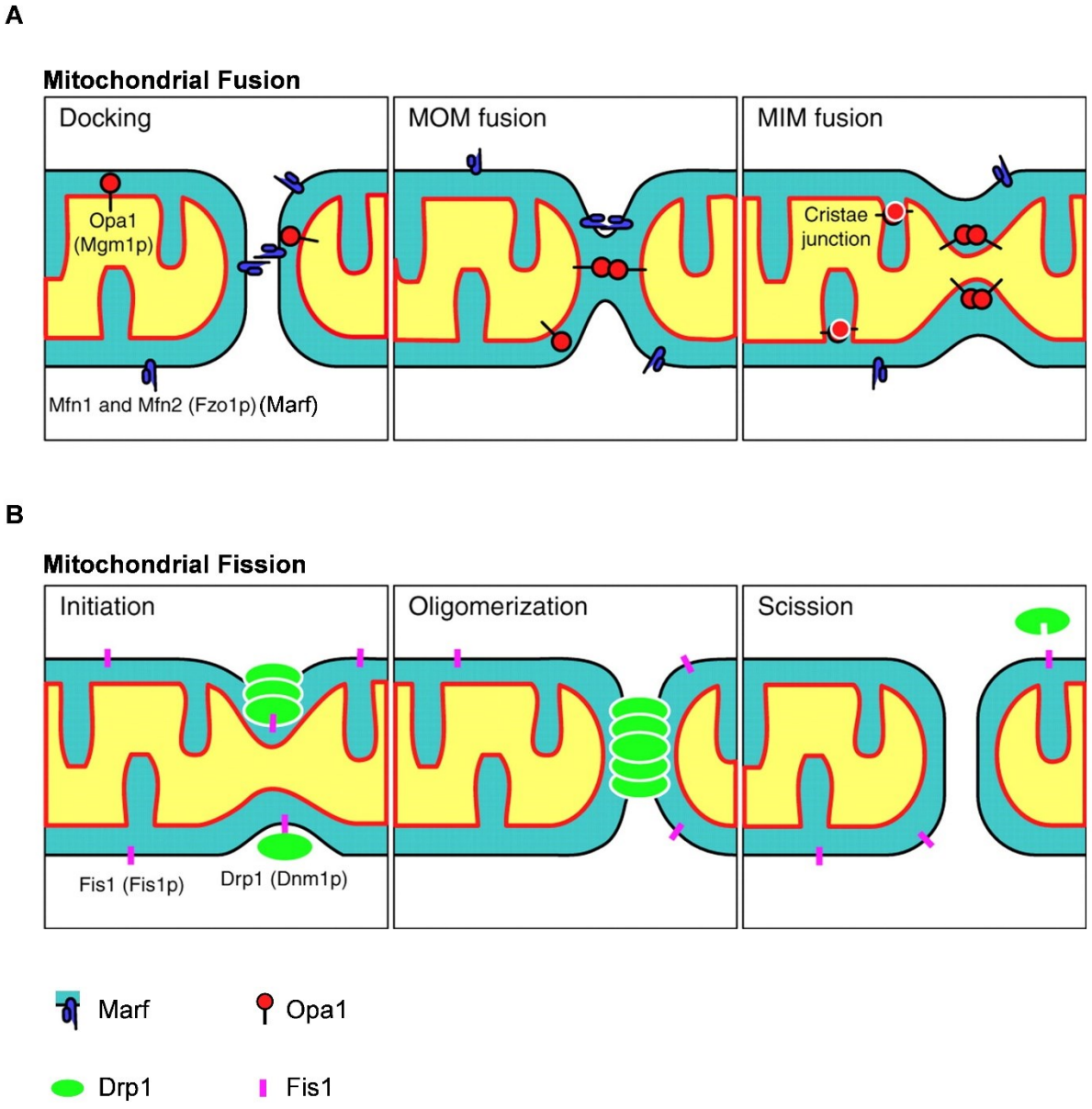

Figure 1.3. Regulators of mitochondrial shape in a cell. Mitochondria can acquire diverse morphologies depending on their function. (A) Fusion of mitochondria to form

tubular network is brought about by outer membrane fusion protein Marf and inner membrane fusion protein Opa1. Both are transmembrane proteins and they act in a Snare like manner to bring the membranes closer to each other followed by merging of lipids in the membrane.
(B) Mitochondrial network can be fragmented into smaller structures with the help of the cytoplasmic fission protein, Drp1. In the cytoplasm, Drp1 is present as dimers and tetramers. It assembles around the mitochondrial membrane with the help of proteins such as Fis1 and forms a helical ring around the organelle. This ring uses GTP to constrict mitochondria to a certain diameter, subsequently scission follows the constriction.
(Image modified from Seo *et al.* 2010)

Role of mitochondria in cellular physiology was first shown in apoptosis (Martinou 1999). Mitochondrial fragmentation enables release of cytochrome C into the cytoplasm, which activated downstream effectors. Reactive oxygen species (ROS) are a byproduct of ETC in mitochondria. Presence of ROS in a cell elicits expression of a number of genes to tackle its increased levels in a cell. They are known to act as secondary messengers as well, as they can oxidize signalling pathway proteins. ROS synthesized by leaky mitochondria is also one of the indicators of mitochondrial function and induces oxidative stress in a cell (Dröge 2002). Other indicators include membrane potential and ATP: ADP ratio. Hence these indicators can establish retrograde signalling from mitochondria to the cell. Unfolded protein response similar to that in ER is activated in a cell on accumulation of proteins in the mitochondria (Figure 1.5A). A signal is relayed to nucleus to increase transcription of genes encoding proteases as well as molecular chaperones such as Hsp60, Hsp70 (Haynes *et al.* 2007). Thus a number of studies have characterized physiological roles of mitochondria.

Signaling pathways act as the steering controls in a cell. They decide the lifetime, the lifestyle of a cell and its interaction with the neighbors and tissue as a whole. Activation of signalling pathways vary spatiotemporally. Pathways can be apposing in function so as to fine tune a response or work in concert to together bring about a change. The cascade of signalling involves activation of secondary messengers. Docking of these signalling molecules onto the mitochondria can enable a direct and

quick control over the organelle. Both the dynamicity in shape and the control over

A

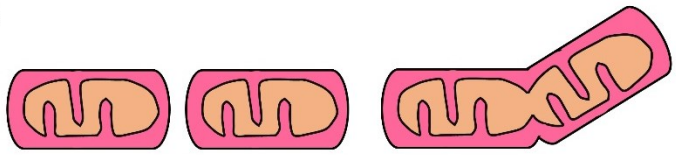

Mitochondrial fission seen during	Mitochondrial fusion seen during
Mitotic phase cell division	G1-S phase cell cycle
Calcium release	Calcium store
Quality control	Autophagy
Transport	Innate Immunity
Apoptosis	

Figure 1.4. Mitochondrial architecture is closely regulated during key cellular processes. (A) Mitochondria undergo fragmentation during mitosis and divided to daughter cells. Increased in mitochondrial fission correlates with release of calcium into the cytosol. Fission is necessary for removal of diseased mitochondria from the cellular pool and thus maintain the high efficiency of the energy production. Mitochondrion are transportated to specific regions in the cytoplasm via microtubular network. Apoptotic proteins cause mitochondria to fragment and Cytochrome C is released. Factors which promote mitochondrial fusion are autophagy as it makes mitochondria less suspectible to degradation. During G1-S phase of the cell cycle mitochondria are maintain in a fused state by Cyclins. Innate immunity requires mitochondria fusion as immunity related proteins dock onto mitochondrial membrane.

energy make mitochondria a good candidate to act as a signalling platform. There are speculations that the shape change of mitochondria itself is capable of giving rise to downstream responses (Mcbride and Neuspiel 2006; Youle 2009). Energy changes originating in the mitochondria dictate a cell's activity (Aon and Camara 2015). Studies

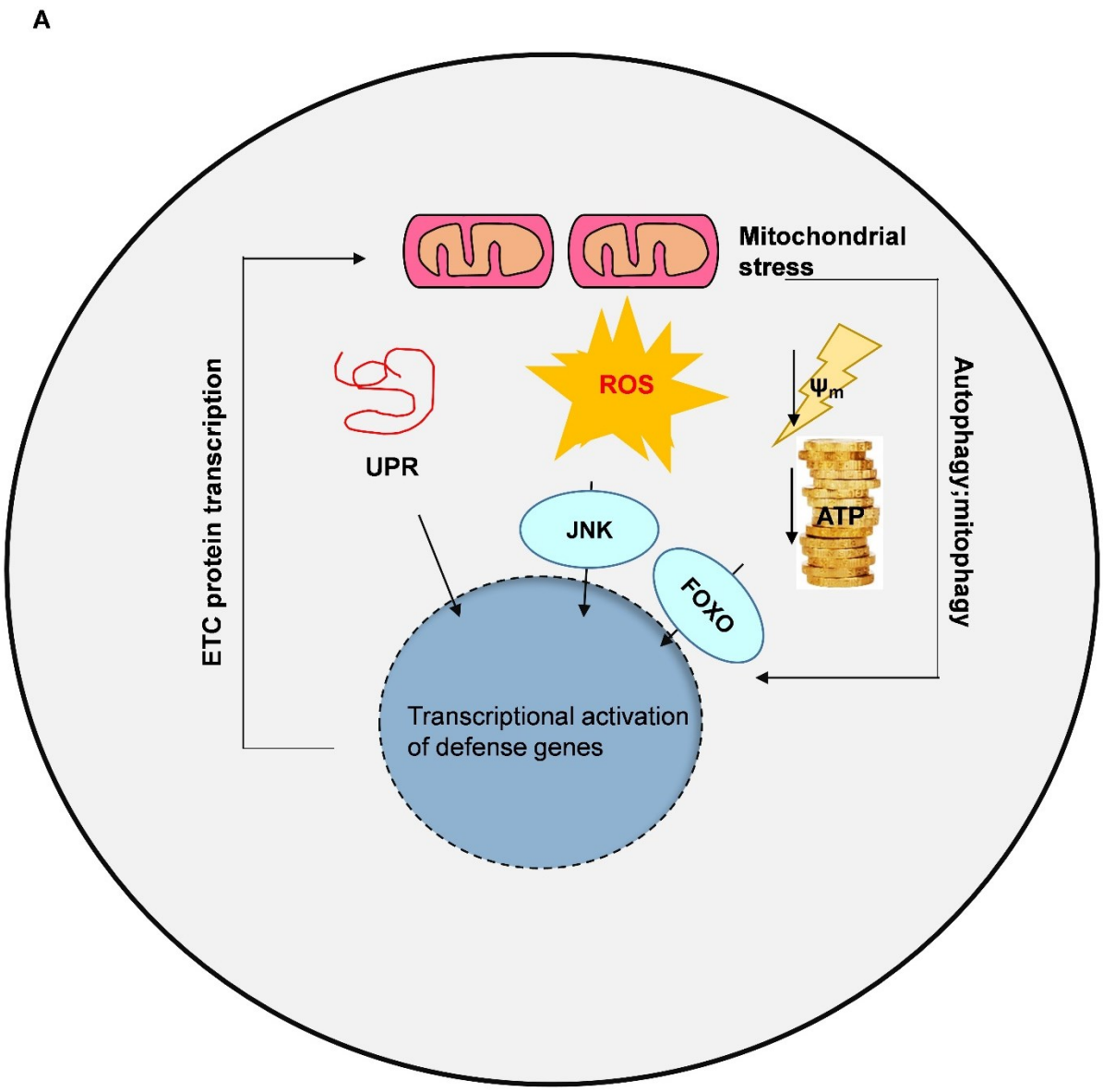

Figure 1.5. Physiological roles of mitochondria. (A) A healthy cell signals mitochondria to transcribe ETC components and maintain steady state of energy production as required for its functions. In conditions of stress such as due to increased ROS under low oxygen conditions, decrease in ATP and mitochondrial membrane potential; mitochondria signals the nucleus via activating transcription factors like JNK or FOXO to activate anabolic pathways. This reduces the burden on the mitochondria. Accumulation of unfolded proteins in the mitochondria also sends a signal to the cell via UPR. Mitochondrial pool in the cell in turn relieves itself of stress, removes damaged mitochondria and replenishes its proteins by fusing with healthier mitochondria in the cell.

suggest that mitochondrial shape and energy generation affect each other

interchangeably (Mishra and Chan 2016). Hence if any, a complex network of relationships exists between signaling, mitochondrial shape and metabolism. The introduction will attempt to bring to focus the role of mitochondria in various tissues and developmental phenomenon and its interaction with signaling pathways.

1.1 Regulation of mitochondrial shape

Mitochondria were first observed to have variable shapes in rat liver cells in 1931 (Smith 1931). Efforts were subsequently directed towards finding out the reason behind the variability. These were followed by mutational studies in *Saccharomyces cerevisiae* which were aimed at identifying the proteins involved in mitochondrial shape regulation (McConnell 1990; Burgess *et al.* 1994; Hermann *et al.* 1998). However Hales and Fuller figured the first protein Fuzzy onions (Fzo) by their work in the fruit fly *Drosophila melanogaster* (Hales and Fuller 1997). Fzo is a transmembrane dynamin like GTPase located on the outer mitochondrial membrane. It is involved in tethering two membranes resulting in distortion and fusion of membranes. The process of fusion and fragmentation in mitochondria shares a striking resemblance to fission and fusion of vesicles during endocytosis of receptors from the plasma membrane (Heymann and Hinshaw 2009). Another dynamin family, Dynamin related protein (Drp1) is the chief protein involved in mitochondrial fission in *Drosophila*. It is a cytoplasmic protein assembled onto the mitochondrial membrane by scaffolding proteins located on the membrane. A major scaffolding protein is Fis1, known to interact with Drp1, whereby it holds two membranes in close apposition (Mozdy *et al.* 2000). Subsequent scission of the membrane occurs after a constricting effect of Drp1 assembly on the mitochondrial membrane (Figure 1.6A). Endophilin B1 is a BAR domain protein involved in membrane pinching downstream of Drp1 (Karbowski *et al.* 2004). The recruitment of Drp1 differs in both yeast and higher organisms. Proteins Mdv1 and Caf4 act as scaffolding factors for binding of Dnm1 (yeast homologue of Drp1) to the membrane (Shaw and Nunnari 2002; Okamoto and Shaw 2005). In higher organisms no protein equivalent for Mdv1 and Caf4 has been found. Studies with MEFs have revealed MiD49 and MiD51 as proteins present on outer mitochondrial membrane which interact and assemble Drp1 onto the

mitochondria (Palmer *et al.* 2011). Another possible candidate is mitochondrial fission factor (MFF), it is a tail anchored protein suggested to be involved in both mitochondrial and peroxisomal division (Gandre-Babbe and van der Bliek 2008). Mitochondrial fission occurs most frequently at sites of ER-mitochondria interaction. These sites attract actin which provides the initial force for membrane scission, Drp1 is also shown to be

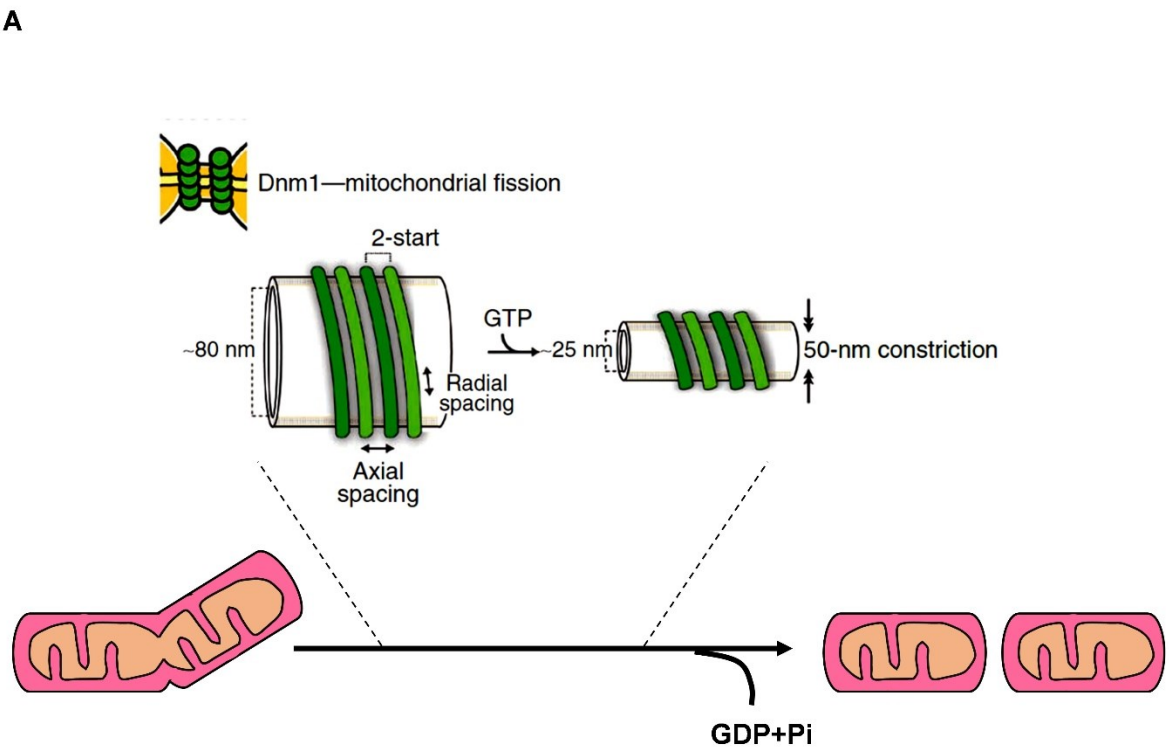

Figure 1.6. Drp1, a dynamin family GTPase causes mitochondrial fission. (A) Drp1 is known to assemble in the form of two-start helix around the mitochondrial membrane. With the hydrolysis of GTP, the ring constricts to around 80nm-25nm inner diameter. It is now postulated that on this constricted structure, Dynamin2 assembles and further constricts the membrane to around 15nm to cause scission with the release of GDP and a phosphate.
(Image modified from Mears *et al.* 2011).

enriched at these focal points (Korobova. al., 2013). Hence mitochondrial fragmentation is governed by Drp1 and its recruiting proteins can differ across organisms.

Mitochondrial fusion is separate for the outer and the inner membrane. Both processes are independent of each other but involve the same principle of membrane

apposition followed by distortion of lipids. This is followed by mixing of lipids and formation of continuous lipid bilayer (Koshiba *et al.* 2004; Martens and McMahon 2008). Outer membrane fusion is mediated by Mitofusins (Mfn), Dynamin family GTPases and they are assisted by mitophosholipase D and cardiolipins (DeVay *et al.* 2009). Mfn1/2 is coiled coil domain containing protein which can form homo or heterodimers with their counterparts present on a closely apposed membrane, thereby assisting in the fusion of the two membranes. Inner membrane fusion is brought about by yet another Dynamin family protein, Optic atrophy 1 (Opa1) which exists in number of isoforms differing in the presence of transmembrane domains (Griparic *et al.* 2007). It is cleaved by a host of proteases situated on inner mitochondrial membrane and in intermembrane matrix space such as Presenillin associated proteases, Rhomboid like proteases, mAAA and i-AAA proteases. These are all membrane anchored proteases, Yme1 is intermembrane space protease. Recent experiments in mice have revealed that ablation of metalloprotease OMA leads to faulty processing of OPA1 resulting in metabolism related disorders (Korwitz *et al.* 2016). It has been observed that increased cleavage to S isoforms results in reduced function of the protein. Decrease in mitochondrial membrane potential leads to increase in S isoforms and increased mitochondrial fission (Eura *et al.* 2006). Hence mitochondrial fusion is driven by Mfn and Opa isoforms in the cell.

Most of the morphology regulating proteins are GTPases. GTPases are switched from an active/ inactive conformation by hydrolysis of GTP, hence mitochondrial morphology regulating proteins behave differently under different GTP concentrations. Mfn 1/2 is activated by low GTP conditions and Opa1 is activated under high GTP conditions. GTP hydrolysis is followed by membrane constriction by Drp1 during fission (Hoppins *et al.* 2007). Drp1 constricts the mitochondrial membrane to a diameter of 50nm (Mears *et al.* 2011). In order to cause membrane scission, the membrane has to be half that diameter, which is proposed to be brought about by another GTPase, classical dynamin family protein, Dynamin 2 (Lee *et al.* 2016a). Fzo mediated membrane tethering is also dependent on its GTPase activity (Cohen *et al.* 2011). Thus mitochondrial morphology is dependent on GTPase activity.

Other than GTP concentration, mitochondrial morphology proteins are also

regulated via posttranslational modifications (Table 1.1). GTPase effector domain

		Interactor	Effect	Reference
Drp1	**Enhancers**	Nitric oxide	S-nitrosylation	Cho et. al., 2009
		CDK/CyclinB, ERK	Phosphorylation at S585, S616 respectively	Taguchi et. al., 2007, Kashatus et.al., 2015
		Calcineurin	Dephosphorlytion at S637	Cereghetti et. al., 2008
		SENP3	Desumoylation	Guo et. al., 2013
	Suppressors	APC/C, MARCH V	Ubiquitinylation	Karbowski et. al., 2007
		cAMP	Phosphorylation at S637	Cribbs et. al., 2007
		Sumo1	Sumoylation at multiple sites	Harder et. al., 2004, Figueroa-Romero et. al., 2009
Opa1	**Enhancers**	Presenillin associated, i-AAA, m-AAA	Proteases at S1 and S2	Anand et. al., 2014, Song et. al., 2007
		SIRT3	Acetylation at K926 and K931	Samant et. al., 2013
Marf	**Enhancers**	MitoPLD	Hydrolyzes Cardiolipin	Choi et. al., 2006
	Suppressors	Pink1 , Parkin	Ubiquitinylation	Gegg et. al., 2010
		JNK, ERK	Phosphorylation at S27, T562 respectively	Leboucher et. al., 2012, Pyakurel et. al., 2015

Table 1.1. Post translational modification of mitochondrial morphology regulators. Mitochondrial fission protein Drp1 undergoes posttranslational modifications such as S-nitrosylation, phosphorylation, sumoylation etc. CDK/cyclin B for example phosphorylate Drp1 to activate mitochondrial fragmentation during cell cycle. These modifications are crucial for enhancement or repression of the protein. Mitochondrial fusion proteins, Marf and Opa1 are also known to be modified postranslation, however not a lot of targets are

known for them. Opa1 is processed by proteases to generate various isoforms thus modifying the activity of the protein. Marf undergoes suppression post phosphorylation at specific sites.

(GED) of Drp1 is phosphorylated as well as sumoylated at number of residues (Anderson and Blackstone 2013). Phosphorylation by CDK1 activates mitochondrial fission while cAMP inhibits Drp1 via phosphorylation (Taguchi *et al.* 2007; Cribbs and Strack 2007). Marf homologues undergo ubiquitination by Parkin and Pink1, in order to mark uncapacitated mitochondria in a cell (Gegg *et al.* 2010). Phosphorylation of Mfn2 by JNK inactivates the fusion protein (Perumalsamy *et al.* 2010). Opa acetylation reduces its activity in cardiomyocytes under stress (Samant *et al.* 2014). Hence, posttranslational additions are a mode of morphology regulation in a cell and it is believed, that a lot more post translational modifications will come to light in future. In addition to these master players, a number of accessory proteins work towards mitochondrial shape regulation. Rab32 is a mitochondrial membrane anchored G protein of Ras superfamily known to tether cAMP dependent kinase protein onto the mitochondrial membrane (Alto *et al.* 2002). The anchoring helps in orchestrating signal transduction events efficiently by concentrating signaling molecules in vicinity of targets. It is possible that kinases associated with Rab32 relay signals to the organelle. Pink is a mitochondrially localized serine threonine kinase which is involved in pathogenesis of Parkinson's disease (Valente *et al.* 2004; Silvestri *et al.* 2005). Pink1 is known to be involved in functions such as mitophagy (Matsuda *et al.* 2010) and its overexpression induces mitochondrial fission. Fis 1 acts as the mediator between Pink1 and Drp1 (Yang *et al.* 2008). These studies bring out the fact that mitochondrial shape is tightly regulated but why is this regulation important for the cell?

Mitochondrial shape regulation is crucial for a cell; loss of fission mediating protein in mice leads to early embryonic lethality (Ishihara *et al.* 2009). Mitochondria undergo fragmentation during apoptosis, by association of Bax with Drp1 (Karbowski *et al.* 2002; Martinou and Youle 2006). Decrease in fission machinery proteins leads to delay in apoptosis (Frank *et al.* 2001). Mitochondria undergo regulated cyclic changes during cell cycle. During interphase they exist in a fused state. As cell cycle proceeds

through mitosis, fragmentation occurs by activation of Drp1 (Mitra *et al.* 2009). This activation is mediated by phosphorylation of Drp1 molecules by CDK1/Cyclin B (Taguchi *et al.* 2007) (Figure 1.7A). Hence mitochondrial shape has physiological relevance and more studies are required to delve deeper into its coordination.

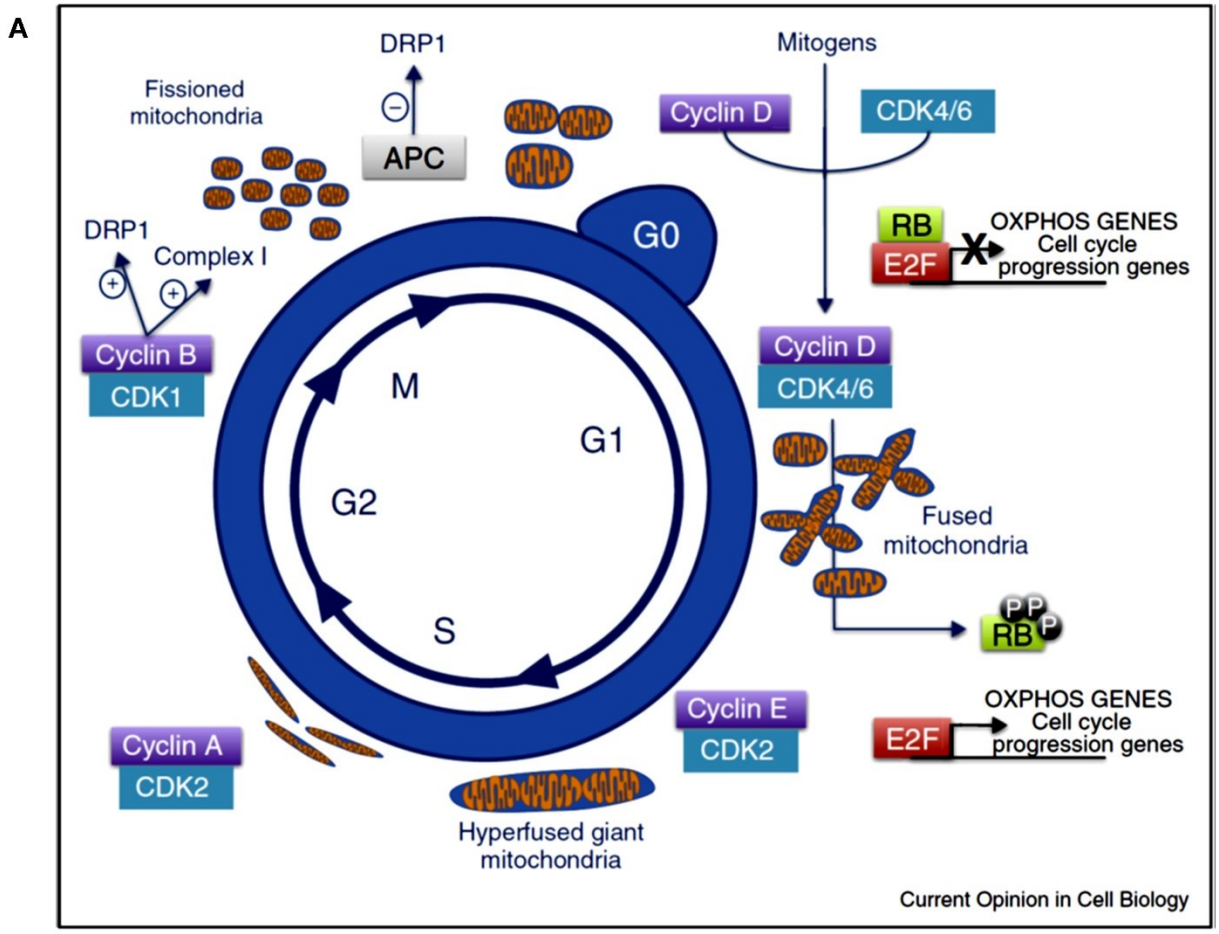

Figure 1.7. Mitochondrial morphology varies during cell cycle phases. (A) Mitochondrial architecture is regulated very tightly during cell cycle. Mitochondria are fragmented by the CDK1/CyclinB complex during mitosis to ensure distribution to both the daughter cells. G1-S phase cell has fused mitochondria with the activation of oxidative phosphorylation, the mitochondrial membrane potential is also higher in this stage as compared to M phase.
(Image modified from Lopez-Mejia and Fajas 2015).

1.2 Mitochondrial shape and energy are interdependent

Mitochondrial architecture and its energy status guide each other (Mishra and Chan 2016). Fusion of inner membrane, increases the surface area available for ETC and also allows more supercomplex assemblies. Supercomplexes usually consist of Complex I, III and IV in mammals. Complex V, ATP synthase is usually found in the form of dimers. Supercomplexes strengthen ATP production because of localization of substrates and faster transfer to next complex (Schägger and Pfeiffer 2000). Increasing the phospholipids in inner mitochondrial membrane decreases the efficiency of oxidative phosphorylation by 60-85% in vitro (Schneider *et al.* 1980). In cell lines it has been seen that larger mitochondrial networks are present to allow increased dissipation of energy (Skulachev 2001). A number of experiments have been done to look at the effect of perturbation of mitochondrial shape on its energy status and vice versa. Any slight change in cell energy status has an impact on mitochondria (Figure 1.8A). Increase in AMPK, which is activated downstream of ATP loss, causes mitochondrial fragmentation leading to subsequent cell death (Toyama *et al.* 2016). Sensors such as AMPK are used to relay the nutrient stress to the whole cell so that the cell can readjust its expenditure. Mitochondrial ETC also regulate ROS, and via ROS as well mitochondrial shape can be perturbed. For example, exposure to low concentrations of H_2O_2 resulted in change in morphology from long tubules to fragmented mitochondria. Mitochondrial morphology was restored by upregulation of both fusion and fission mediating proteins, Drp1 and Mfn1, hence the dynamicity of the organelle was reestablished (Jendrach *et al.* 2008). Increase in glucose concentration leads to increased fragmentation of mitochondria by Drp1 mediated fission. This increase in respiration was accompanied by increased ROS production as well (Yu *et al.* 2006). ATP levels have been shown to regulate Mgm1 (yeast analogue of Opa1) proteolysis by Pcp1, a rhomboid protease found on mitochondrial membrane in Yeast. The activity of the protease is influenced by change in hydrophobicity of the amino terminal of Mgm1. The exact mechanism of how ATP production or membrane potential change leads to the above is not understood yet (Reichert et. al. 2004). Studies have demonstrated that downregulation of Mfn2 expression leads to reduction in mitochondrial membrane potential in rat muscle cells

(Bach *et al.* 2003). A follow up study to this illustrated that this decrease in mitochondrial potential occurs possibly because of repression of components of protein complexes involved in oxidative phosphorylation (Pich *et al.* 2005). In conclusion, mitochondrial architecture is interwoven with ATP, ROS and mitochondrial membrane potential difference in a cell.

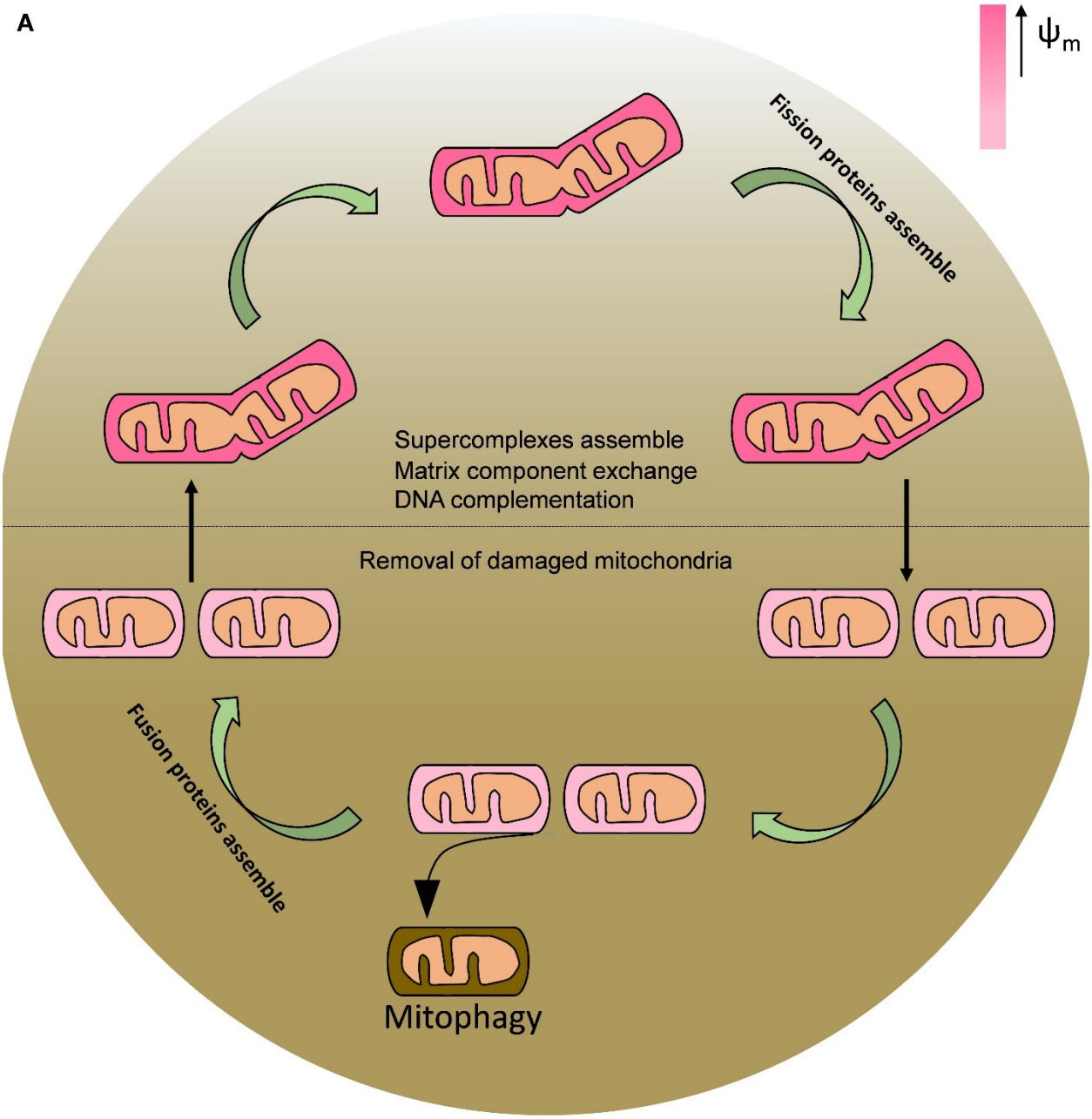

Figure 1.8. Mitochondrial shape and energy impact each other. (A) Fused mitochondria usually contain more supercomplexes, which are assembly of ETC

complexes to enable faster relay of electrons and higher membrane potential difference across the inner membrane. Mitochondrial membrane potential in small fragmented mitochondria is usually low and they are useful to segregate the mutant and diseased mitochondria which are under-performing from the sturdier mitochondrial pool. (Redrawn from Vásquez-Trincado *et al.* 2016).

The study of both shape and energy becomes a little tricky because of its multifactorial nature. Both shape and energy are connected hence any change in one influences the other. Attempts have been made to do experiments where only one single factor is modified and rest remains the same. Rho zero cells lack mitochondrial respiratory chain components (Chandel and Schumacker 1999). They serve as ideal cells to look at role of mitochondrial shape in a cell. Another study looks at the effect of substrate change on mitochondrial shape and energy production, as well as ROS production and membrane potential. They found that nature of substrate changes the mitochondrial positioning in a cell line as well as its shape. This change is probably necessary such that energy production is adjusted to a favorable level (Rossignol *et al.* 2004; Liesa and Shirihai 2013). Hence both shape and energy are highly supervised factors and there is a lot of crosstalk between them.

1.3 Mitochondria in stem cells and cancer cells

Mitochondrial cristae are essentially immature in stem cells. Electron micrographs show tube like mitochondria in wild type stem cells but the cristae is not very dense. These structures are primarily found around the nuclei and the ATP production is also relatively low (Teixeira *et. al*. 2015). These attributes indicate that most of the stem cells rely on bare minimum mitochondrial functions and concentrate on maintaining a state of low metabolism. Low metabolic state also means low ROS production and less susceptibility to ROS induced DNA damage to the stem cell genome. Activation by appropriate signals induces transformation into sophisticated mitochondrial network and subsequent cell differentiation. Studies place mitochondrial differentiation upstream of cell differentiation as it has been shown that abrogation of mitochondrial cristae

transformation affects cell number, replicative potential and cell fate. Inhibition of mitochondrial ETC proteins via mutants or drugs and mitochondrial morphology proteins or mitochondrial localization leads to defect in embryonic stem cell proliferation and differentiation potential in *Drosophila* and mice (Schieke *et al.* 2008; Mandal *et al.* 2011a; Pereira *et al.* 2013; Kowno *et al.* 2014; Kim *et al.* 2015). Mitochondrial calcium regulation is also important for mouse neural cell development (Lee *et al.* 2016).

Majority of data on bioenergetics of germ cells in organisms is from assessment of their nutritional status, and their response to starvation. Germ cell number in niche is governed by a combination of systemic signals, intrinsic factors and local signals. Germ cell number decreases invariably with age. Systemic signals which regulate their number can be for example insulin in *Drosophila ge*rm cells in stage 1 ovariole chamber. These signals can originate from fat body via *Drosophila* insulin like peptides (DILPs) as well. Nutrient sensor TOR is the master regulator for both insulin dependent and independent pathways (Clancy 2001; Tatar *et al.* 2001; Shingleton *et al.* 2005). Germ line stem cells also depend on non-cell autonomous factors such as amino acid concentration in adipocytes (Armstrong *et al.* 2014). Thus global energy decides the investment of the organism in germ cell number. There are other interesting pathways such as Notch pathway as well involved in local signals. These will be discussed in detail in later chapters.

In most of the cancerous cells due to Warburg effect, pyruvate does not enter the ETC instead glycolysis is used even at high oxygen concentration (Warburg 1956). They can be used to look at mitochondrial morphology in cells in which energy synthesis by ETC is divorced from cell growth. A number of studies have looked for the difference in cancerous and non-cancerous cell mitochondrial morphology however there is no one consistent story (Scatena 2012; Vyas *et al.* 2016) (Figure 1.9A). Under induced hypoxic conditions cancerous cells have enlarged mitochondrial network which helps in evading apoptosis (Chiche *et al.* 2010). Other studies have shown prevalence of fragmented mitochondria in cancer cell lines (Kashatus *et al.* 2015; Serasinghe *et al.* 2015; Senft and Ronai 2016). Therefore, in cancer cells mitochondrial network is usually

fragmented and cells rely on glycolysis for ATP.

A

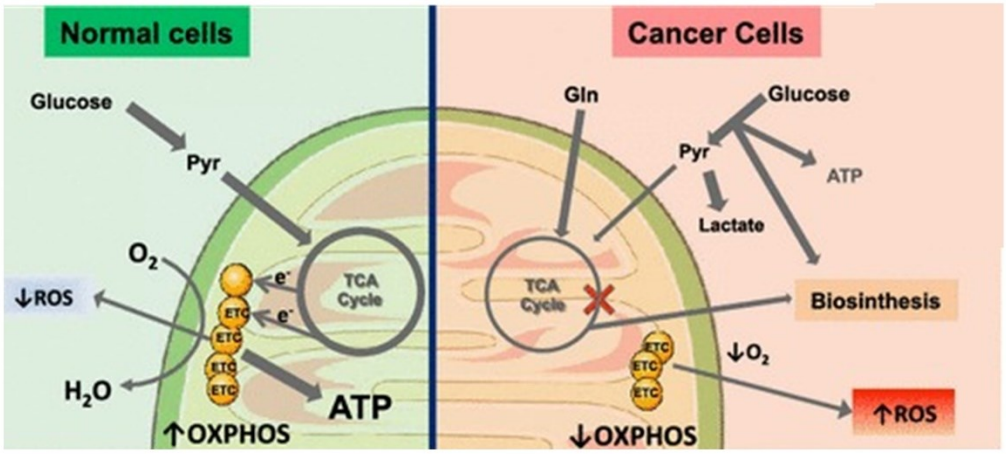

Figure 1.9. Cancer cell metabolism does not rely on ETC. (A) Cells in a growing organism utilize glucose to contribute substrates to oxidative phosphorylation in the mitochondria. In turn ROS, H_2O and ATP are released into the cell. Cancer cell primarily relies on glycolysis due to hypoxic condition and ETC activity is reduced in them. High amount of ROS and lactic acid are generated in the mitochondria (Ribas *et al.* 2016).

1.4 Emerging role of mitochondria in signaling pathways

Signaling pathways involved in universal mechanisms such as cell cycle regulation, glucose metabolism, apoptosis, and differentiation utilize some global molecules and some specific molecules. These pathways are conserved among species and have a defined spatio-temporal pattern. The functions controlled by these pathways almost always involves a change in mitochondrial energy generation. Since mitochondrial shape change is one of effectors of mitochondrial energy it is possible that above pathways exert influence on mitochondrial shape as well. A possible integration of all the mitochondrial functions will provide a cohesive view of mitochondrial control in a cell.

1.4.1 Mitochondrial morphology proteins are key determinants in growth and differentiation pathways in a cell

Mitochondrial morphology is downstream of EGFR and upstream of Notch in PFCs (Mitra *et al.* 2012). Mfn2 has been known to have a direct interaction with p21 Ras (a member of EGFR pathway) by its N terminal domain in mouse embryonic fibroblasts (de Brito and Scorrano 2009). The interaction in this particular study was found to be essential for Mitochondria-ER association. They found that Mfn2 null cells not only exhibit a change in mitochondrial morphology but also in the ER morphology. Mfn2 is found to localize on the mitochondrial membrane as well as on mitochondria associated membranes and ER network. Sequestration of Ras by Mfn2 binding leads to abrogation of MAPK pathway and G0-G1 cell cycle arrest in vascular smooth muscle cells (Chen *et al.* 2004). Drp1 is shown to be phosphorylated by ERK at S616 to cause mitochondrial fragmentation, which is necessary for Ras mediated tumorigenicity (Kashatus *et al.* 2015). Mfn1 and Mfn2 are phosphorylated by MAPKs under tumorous or stress conditions (Leboucher *et al.* 2012; Pyakurel *et al.* 2015). Yorkie activation enhances Marf and Opa1 transcription, reduces ROS levels and thereby promotes cell proliferation (Nagaraj *et al.* 2012). Hence, key mitochondrial morphology proteins crosstalk with signaling molecules (Table 1.2) and a lot of potential interactions still need to be uncovered.

Signaling molecules	Nature of interaction	Reference
Yorkie	Transcriptional upregulation of *marf* and *opa*	Nagaraj et. al., 2012
ERK	Activation of Drp1 by phosphorylation	Kashatus et. al., 2015
JNK	Gets activated by AMPK released as result of Complex I subunit downregulation	Owusu-Ansah et. al., 2008
JNK	Inactivates Marf by phosphorylation	Leboucher et al. 2012
Bax , Bac	Activate Drp1 to induce apoptosis	Frank et. al., 2001
Wnt	Regulates mitochondrial architecture via Alex-3	Serrat et. al., 2013

Table 1.2. Mitochondria interacts with signaling pathways to modulate cellular

function. Table lists the signaling molecules known to interact with and regulate mitochondria in a cell. Signaling molecules interact with varying aspects of mitochondria such as proteins controlling its architecture and its ATP production.

1.4.2 Mitochondria interacts with signaling molecules via regulating calcium levels in the cell

Mitochondria and ER are calcium storehouses, buffering its amount in the cell. Mitochondrial calcium channels (MCU) are low affinity channels present on the inner mitochondrial membrane and pump calcium into the mitochondria depending on the proton gradient across the membrane. Calcium is sent out via exchange with other positively charged ions such as sodium via Sodium or proton calcium exchangers. Calcium influx into the cell is followed by rapid bursts of calcium into the mitochondria. Entry of calcium into the mitochondria, on account of the positive charge dissipates the mitochondrial membrane potential transiently. A lot of calcium is taken up into mitochondria at the mitochondria associated membranes (MAMs) in close proximity to the ER. VDAC on the outer mitochondrial membrane is signaled by inositide 3, 4, 5-phosphate (IP3) on ER to uptake calcium (Szabadkai *et al.* 2006). In addition to IP3, factors such as distance and volume between ER and MAMs are also important factors governing calcium influx. Scorrano and de Brito have shown that Mfn2 is also enriched at the MAMs and downregulation of Mfn1/2, disrupts ER morphology as well as calcium uptake into mitochondria (de Brito and Scorrano 2009).

Study in mouse embryonic fibroblasts has shown that downregulation of fusion mediating proteins lead to increased calcium and calcineurin in the cells. Increased calcineurin leads to increased Notch in the cells and inhibition of differentiation. Depletion of calcineurin, a calcium dependent phosphatase was able to rescue the phenotype and correction of cell differentiation defect (Kasahara *et. al.* 2013). To summarize, mitochondrial calcium can regulate signaling pathways such as Notch in a cell.

1.4.3 ETC and its byproducts regulate growth via signaling

A cell tightly regulates its energy synthesis and expenditure hence it's not a surprise that signaling pathways end up controlling a host of mitochondrial genes. Cell manipulates the ATP synthesis, ROS release and substrate availability and there is feedback from these. There is a lot literature spanning 50 years correlating how mitochondrial energy production is tailored to fit cellular needs. I will be covering some salient points which are of relevance to the thesis and capture gist of the relationship.

1.4.3.1 ROS is known modulator of kinase mediated cellular signaling

It is now known a substantial number of signal transduction mechanisms employ the oxidation of downstream effectors to pass the message. Presence of ROS results in activation of a number of genes encoding for enzymes to tackle them such as superoxide dismutase (SOD). It is known that oxidative stress evokes the MST-FOXO pathway to signal transcriptional changes. MST kinases are known to phosphorylate FOXO for its activation on sensing oxidative stress (Lehtinen *et al.* 2006). p38 kinase (p38K) is a stress activated kinases downstream of MAPK pathway proteins. It activates transcription factor Mef2 which has conserved binding sites upstream of gene of manganese superoxide dismutase (MnSOD) protein located on mitochondrial membrane (Vrailas-Mortimer *et al.* 2011). Hence, it can directly influence ROS quenching.

ROS is a manifestation of mitochondrial stress, which itself acts as a retrograde signal. Accumulation of unfolded proteins in mitochondrial matrix activates proteases such as ClpXP, m- AAA family proteases (Haynes *et al.* 2007). In rat hepatoma cells, where this phenomenon was first observed, it was seen that there was a loss of mtDNA as well (Martinus *et al.* 1996). C/EBP homologous protein (CHOP) is one of the conserved sites for Upr signal (Zhao *et al.* 2002). This site has an activator protein-1 (AP1) binding element (Horibe and Hoogenraad 2007). It is known that JNK pathway binds AP1 site (Weiss *et al.* 2003). It is also known that mitochondria to nuclei signal propagates on activation of transcription factor ATF2, which is known to be associated with JNK (Biswas *et al.* 1999). Hence, it is possible that the retrograde stress signalling

utilizes JNK pathway for modulation of cell machinery. ROS levels have been found to increase apoptosis via inducing phosphorylation of p38K. AKT pathway increases ROS production by increasing oxidative metabolism and increasing the amount of oxygen consumed. Increased ROS levels induce phosphorylated p38K (Ushio-Fukai *et al.* 1998). Hence, the site and the amount of ROS dictates the outcome on the cellular signaling.

1.4.3.2 Mitochondrial membrane potential in relation to cellular signaling

Decrease in mitochondrial membrane potential is signaled by mitochondria to the cell. This signalling can be through AMP kinase which acts as a sensor of ADP: ATP ratio and decreases anabolic reactions in the cell (Hardie and Carling 1997). Utpal Banerjee lab proposes a pathway activated by inefficiency of ETC. Complex I subunit inhibition leads to increased ROS in the cell and activation of JNK. Depletion in complex IV lead to low ATP and AMP kinase activation. Inhibition of either complex converges onto inhibition of Cyclin E leading to cell cycle arrest in an energy deficient situation (Owusu-Ansah *et. al*. 2009). AMPK induces mitophagy by activating ULK1 in murine hepatocytes (Egan *et al.* 2011). Most of the signaling is ATP dependent on account of phosphorylation. Kinase dependent growth pathways such as EGFR are shut down in ATP deficit conditions. ATP via P2 GPCRs activate calcium and subsequent transcription factor signaling in osteoblasts (Grol *et al.* 2012). Hence most phenotypes of change in mitochondrial membrane potential are attributed to change in ATP levels in the cell. However it can have direct effects as well by modulating pH conditions in inner mitochondrial membrane. Till now most correlations between signaling and mitochondrial membrane potential are indirect.

Hence, with this discussion I hope I have sufficiently piqued the reader's interest towards the organelle mitochondria and its multiples roles in the development of an organism. Through this thesis I plan to ask the broad question:

How does mitochondria interact with signaling pathways during development?

Specifically the question can be divided into following subparts, which form the aims of the thesis:

1. Manipulation of mitochondrial morphology proteins leads to change in tissue morphology during oogenesis.
2. Formulate protocols to assess mitochondrial attributes in *Drosophila* tissues
3. Understand interaction of EGFR and fission deficient mitochondria during *Drosophila* follicle cell development
4. Analyze Notch pathway in mitochondrial fission mutant *Drosophila* follicle cells
5. Analyze effect on mitochondrial manipulation on *Drosophila* wing development

CHAPTER 2

Manipulation of mitochondrial morphology proteins leads to change in tissue morphology during oogenesis

2.1 Introduction

Mitochondria are involved in a plethora of cellular functions such as energy metabolism, calcium homeostasis, cell cycle, cell death and cellular signaling. Many of these functions are modulated by mitochondrial morphology changes. For example, periodic changes in mitochondrial morphology and mitochondrial membrane potential occur during the cell cycle (Schieke *et al.* 2008; Mitra *et al.* 2009). On account of their diverse roles in the key cellular phenomenon, they play a determinative role in development and differentiation (Maeda and Chida 2013; Wanet *et al.* 2015). They have been shown to regulate neuronal differentiation, germ cell, FC and hemocyte differentiation (Williams *et al.* 2010; Mitra *et al.* 2012; Gao *et al.* 2014; Teixeira *et. al.* 2015). Mitochondria in stem cells exist in a rudimentary form and cells rely on glycolysis for energy. Cellular differentiation is accompanied by the presence of a more elaborate mitochondrial network along with aerobic glycolysis. This transition is likely to be regulated by key signaling pathways that impact the synthesis of mitochondrial proteins, increase the mitochondrial DNA replication cycles and increase the activity of large GTPase proteins dedicated to mitochondrial fusion and fission.

Drosophila melanogaster ovaries were chosen as the model system to study the impact of mitochondrial protein manipulation because of large cell size, ease of imaging, availability of genetic and cell biological manipulation techniques, reagents and most importantly the presence of cells in progressive stages of growth and differentiation. *Drosophila* ovary consists of chains of successively mature FC chambers housing the oocyte. FCs undergo mitotic divisions from stage 2-6, then they start endocycling and form differentiated cells. Endocycling is mediated by activation of Notch pathway. EGFR pathway is activated in the PFCs covering the oocyte in stage 8 by the ligand Gurken. This activation is responsible for the movement of the oocyte to the dorso-anterior position; thus patterning the dorso-ventral axis of the embryo (Figure 2.1A-B). EGFR

pathway is known to modulate mitochondrial morphology in *Drosophila* ovarian FCs (Mitra et. al., 2012). Hence *Drosophila* FCs can be used to assay role of mitochondria in the cell cycle, signaling pathways and thus in development during oogenesis.

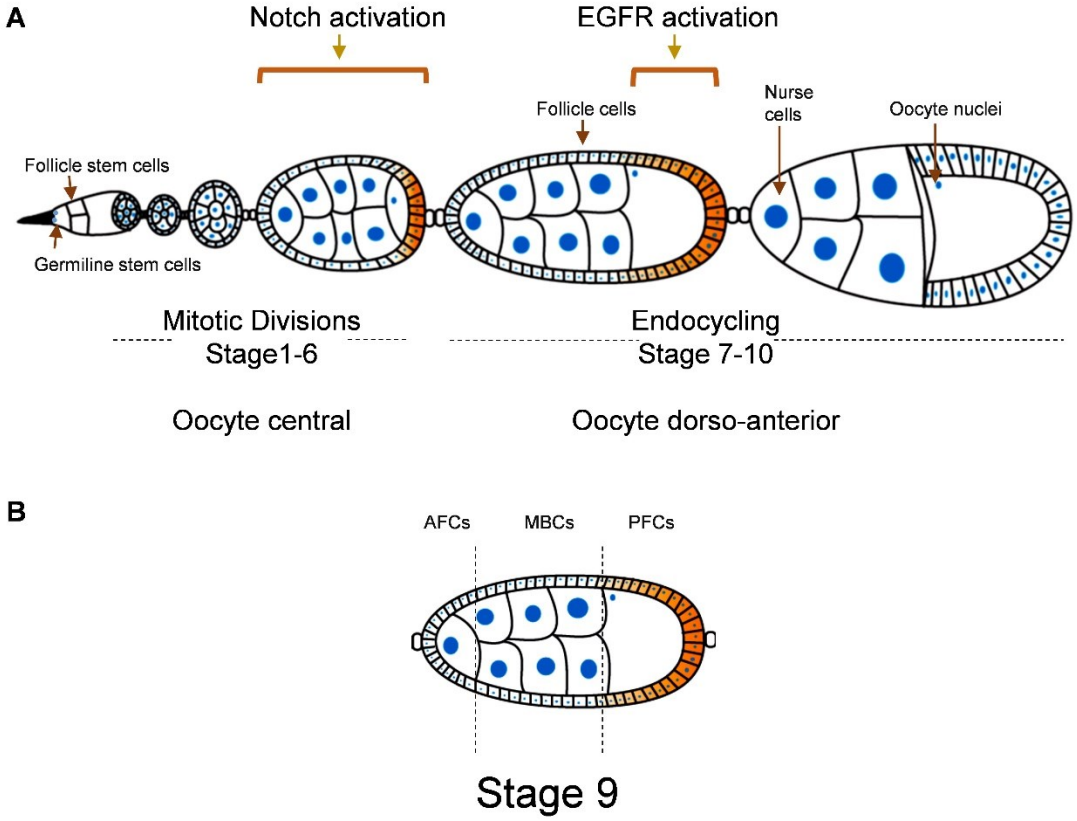

Figure 2.1. *Drosophila* ovary as a model system. (A) *Drosophila* ovariole is a chain of chambers of successively increasing age. Leftmost chamber is the stage 1 which contains the germline stem cells adhered to the niche with the help of DE-Cadherin. It also contain a pair of FSC which give rise to the prefollicle cells and subsequently the FCs. The FCs are epithelial cells which enclose the cyst containing the oocyte and the nurse cells. FCs divide upto stage 6 and the chambers steadily grow in size. FCs switch to endocycling from stage 7 on Notch pathway activation. EGFR pathway is activated in Stage 8 and the oocyte nuclei (in centre in stage 6) moves to dorso-anterior position in the mature chamber. (B) Stage 8-9 chamber can be divided into three regions depending on the follicle cell population; anterior follicle cells (AFCs), main body follicle cells and PFCs. Only the PFCs are subject to EGFR signaling. AFCs experience JAK-STAT signal.

2.2 Materials and Methods

2.2.1 *Drosophila* genetics

All *Drosophila* crosses were performed in standard cornmeal agar medium at 25^{o}C. The *drp1*^{KG03815}, *drp1*^{i}, *marf*^{i}, *opa*^{i}, *erk*^{i}, *ras*^{i}, *pdsw*^{i}, UAS-*drp1*, UAS-*marf*, *hs*-flp; ubi-nls-GFP, FRT40A/CyO, *c306*-Gal4, *e22c*-Gal4, *gr1*-Gal4 lines were obtained from Bloomington Stock Center. The stock *hsflp*; Gal80FRT40A/CyO;*tub*-Gal4, UAS CD8GFP/TM6 was obtained from Nicole Grieder. The *marf*$^{(MG)}$ line was a gift from Ming Guo lab. The *drp1*^{KG03815}FRT40A/CyO stock was generated using standard genetic crosses.

2.2.2 Generation of FC clones

Homozygous *drp1*^{KG} mutant clones were generated by the FLP-FRT mediated site-specific recombination and twin spot (Griffin *et al.* 2009) or MARCM system (Golic and Lindquist 1989) (Figure 2.2A-B). Flies containing *drp1*^{KG03815}FRT40A were crossed with *hs*-flp; Gal80 FRT40A/CyO; *tub*-Gal4, UAS CD8GFP/TM6 or *hs*-flp; ubi-nls-GFP, FRT40A/CyO. 1-3 day adult females carrying the genotype hsflp/+; *drp1*^{KG03815}FRT40A/Gal80 FRT40A; *tub*-Gal4, UAS CD8GFP/+ or hsflp/+; *drp1*^{KG03815}FRT40A/ubi-nls-GFP FRT40A were heat pulsed at 37.5 ^{o}C for 60 min in a water bath to generate FC clones. After the heat shock, flies were transferred to fresh vials supplemented with yeast granules. Twin spot flies were dissected after an interval of 6-8d. MARCM flies were dissected at 10days to maximise on clones arising from early cell divisions or from stem cells. Clones were marked with plasma membrane associated CD8GFP in the MARCM system or absence of GFP with the twin spot strategy (Figure 2.2A-B). The staging of the egg chambers was done following (Spradling 1993). For epistasis experiments, mosaic females were obtained by crossing control FRT40A/CyO to *hsflp*; Gal80 FRT 40A/CyO; *tub*-Gal4, UAS CD8GFP/TM6. The protocol and time of heat shock followed by dissection was maintained identical across genotypes allowing quantification of numbers of cells per clone across genotypes.

2.2.3 Immunostaining of FCs

Ovaries dissected in Schneider's medium were fixed with 4% PFA in PBS,

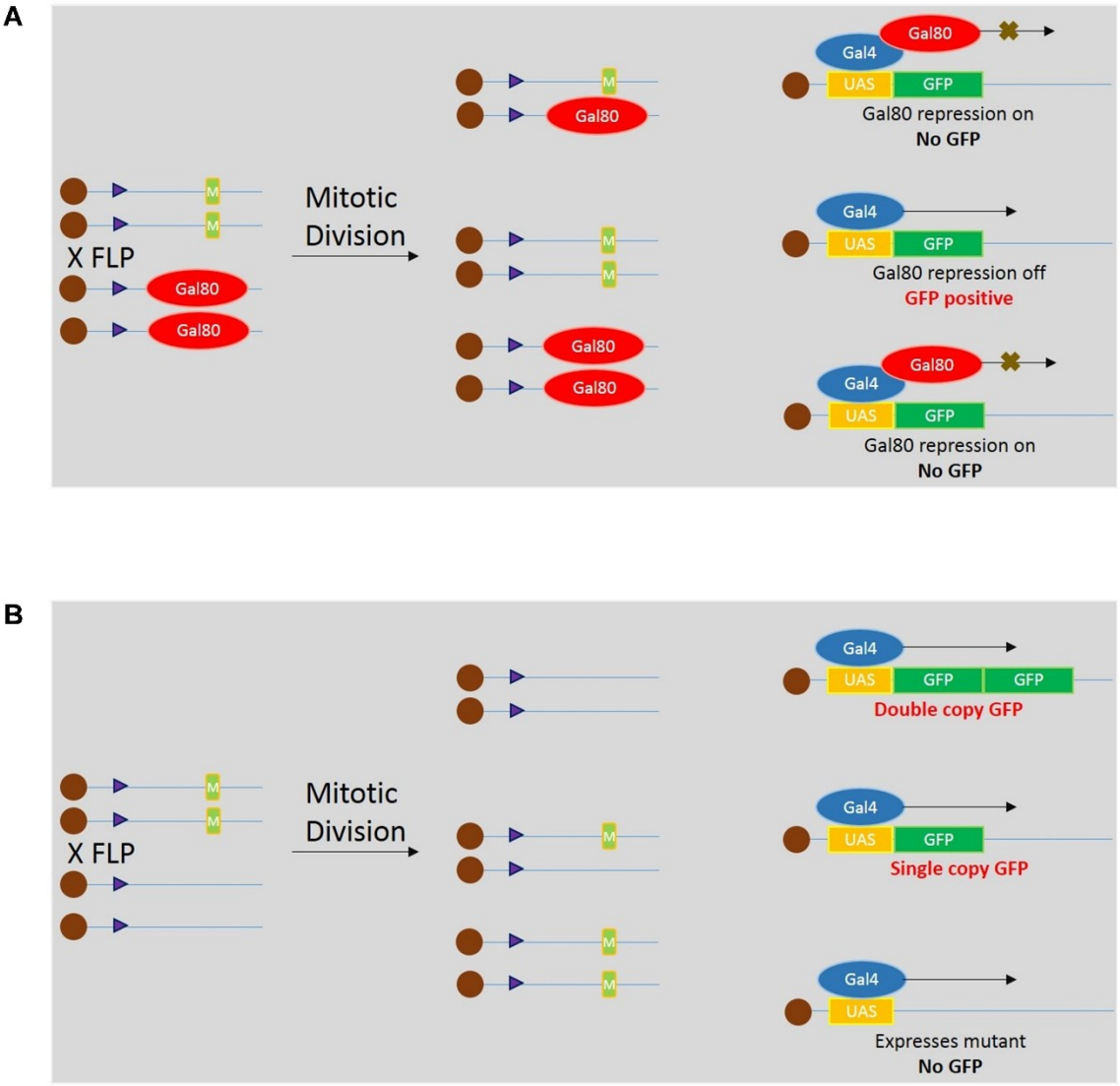

Figure 2.2. FLP-FRT mediated strategies to generate mutant clones in *Drosophila*. (A-B) Heatshock activates the enzyme flippase (hsFLP) which is under heatshock promoter, causing FRT element coordinated recombination. This results in removal of Gal80 inhibition on Gal4 in one of the combinations culminating in Gal4 driven GFP expression. GFP positive tissue is interspersed with non-GFP heterozygous background resulting in a mosaic pattern (A). Twin spot generates two marked populations, single copy GFP heterozygous and wild type double copy GFP background. In this strategy mutant is GFP negative (B). Both strategies provide excellent control environment to compare and contrast mutant and wild type growth and development.

permeabilized with 0.3% Triton-X-100 in PBS (0.3% PBST), blocked in 2% BSA in 0.3% PBST, stained with primary antibody overnight at 4 ^{0}C, washed in 0.3% PBST, stained

with secondary antibody for 1 hour in 0.3% PBST at RT, washed and mounted in Slow-fade Gold (Molecular Probes). 5-15 animals were dissected for each experiment at 10d after heat shock. All the ovarioles (30-35 per fly) containing clones at the stage 7-9 were imaged and experiments were repeated 2 or more times as indicated by “N” value in the figure legends. The primary antibodies used were: mouse anti-CycB 1:10 (DSHB), rabbit anti-CycE 1:500 (Santacruz), mouse anti-aPKC 1:1000 (DSHB), rabbit anti-Dlg 1:200 (DSHB), rabbit anti-cleaved Caspase-3 1:200 (Cell Signaling), rat anti-DE Cadherin 1:10 (DSHB). mouse anti-βPS(myospeheroid) (Integrin) 1:10 (DSHB). Fluorescently coupled Streptavidin 633 (Molecular Probes) (1:1000) was used to mark mitochondria in FCs and fluorescently coupled secondary antibodies (Molecular Probes) were used at dilution 1:1000.

2.2.4 Image acquisition and phenotypic estimation in FCs

The ovaries were imaged using a Plan apochromat 40X 1.3/1.4 NA objective on Zeiss LSM 710/780. The images were grabbed with an averaging of 4 at 512 x 512 pixels. The laser power was kept similar between samples and the gain varied between 800-850 for antibody staining. The range indicator mode was used for the acquisition of each image so that the intensity did not reach 255 on an 8-bit scale. An ROI of 5-30 cells across an optical plane was chosen in each clone for estimation of phenotypes and “n” refers to the numbers of clones in different ovarioles observed for 2 or more experiments as represented by “N” value in the figure legends. Percentage values in the figures with aggregated mitochondria and multilayering are representative of the percentage of independent clones showing the defective phenotype.

2.2.5 Estimation of cell numbers per FC clone

Cell counts using the twin spot or the MARCM strategy were done from independent clones across multiple experiments using ImageJ. Optical slice thickness of acquisition was 1.08 μm, the smallest cell being approximately 5μm and care was taken to not mark the same cell twice. GFP positive in case of MARCM and GFP negative in case of twin spot cell nuclei stained with Hoescht were marked manually and counted in the control FRT40A and mutant clones. Cell numbers were compared using non-parametric

two-tailed Kruskal Wallis, Mann Whitney and Dunn's test for statistical analysis to allow comparison of different sample sizes and non-gaussian distribution.

2.2.6 Image analysis for estimation of fluorescence in FCs

Quantification of aPKC, cleaved-Caspase, Dlg, Integrin, DE-cadherin, Cyclin B, Cyclin E signal was performed using ImageJ. The optical slice was manually chosen depending on clone visibility and the GFP boundary in the MARCM system. A region of interest in one independent clone containing cell numbers between 5-30 across an optical plane was marked and average fluorescence intensity for GFP positive (clonal) and GFP negative (background) region was computed. A ratio of these intensities was obtained for each clone thus normalizing for variations in accessibility to dyes, drugs, antibodies or imaging conditions. The non-parametric two-tailed Kruskal Wallis test, Dunn's test and Mann-Whitney test were used to compare non-gaussian distribution of fluorescence ratios between different genotypes.

2.2.7 High resolution imaging of mitochondria

For visualization of mitochondrial morphology, immunostained FCs were imaged using a Plan-Apochromat 63X Oil, 1.4 NA objective of Zeiss LSM 800 microscope with a AiryScan module (Engelmann and Weisshart 2014). Images were deconvolved and surface rendered using AutoQuant X3 and BitPlane Imaris version 8.0 respectively.

2.3 Results

2.3.1 Drp1 deficient FCs contain aggregated mitochondria

We depleted *drp1* in ovarian FCs using the transposon tagged mutation *drp1*^{KG03815} (*drp1*^{KG}). The *drp1*^{KG} mutant is a null allele via P-element insertion in the 1st intron (Figure 2.3A) and its mitochondrial phenotype is reversed by a genomic duplication or a transgene expressing *drp1* (Rikhy *et al.* 2007; Mitra *et al.* 2012). *drp1*^{KG} is known to be homozygous lethal, hence clones were generated for the allele allowing us to mutate the gene in only a subset of cells in the tissue. We made use of the twin-spot and the MARCM system to generate clones. GFP positive FCs homozygous for the *drp1*^{KG} mutant and control FRT40A were generated using heat shock. *drp1*^{KG} FCs showed an

aggregated mitochondrial mass as compared to background heterozygous control cells and FRT40A control cells (Figure 2.3B). This consists of fused mitochondria as assessed previously by micro irradiation of the mitochondrial membrane potential sensitive dye TMRE (Mitra *et al.* 2012).

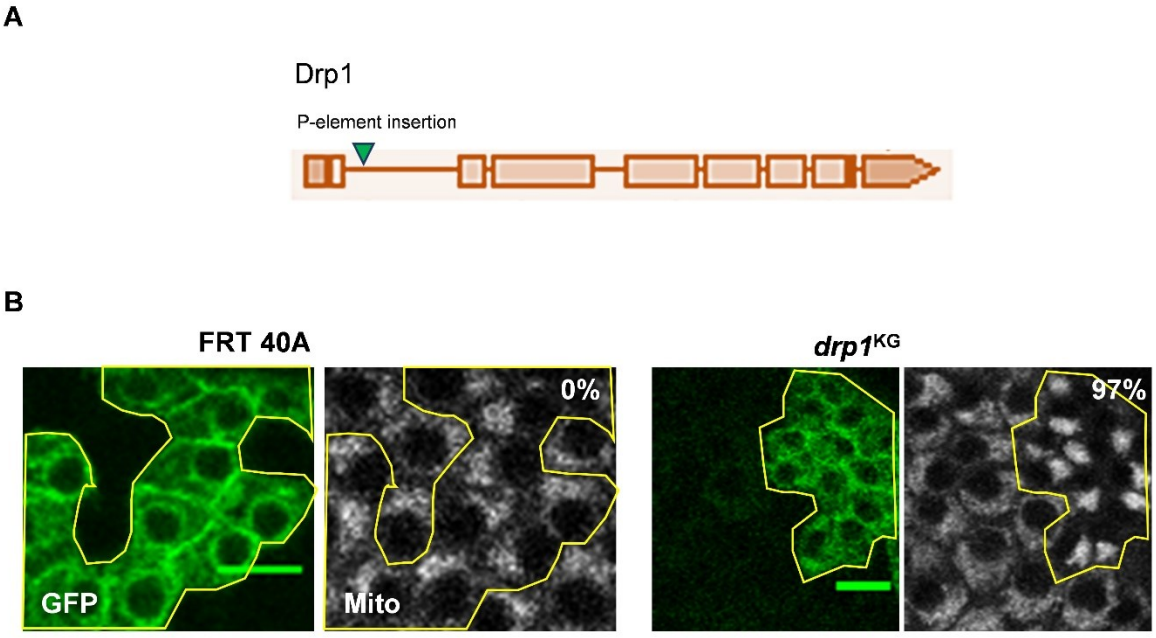

Figure 2.3. Mitochondria are aggregated in *drp1*^{KG} FCs. (A) *drp1*^{KG} mutant is a P-element mutant with insertion in the 1st intron.
(B) *drp1*^{KG} homozygous mutant cells (CD8GFP; yellow boundary) are generated by mitotic recombination in a heterozygous background. Mitochondria labelled by fluorescent Streptavidin (grey) are aggregated in *drp1*^{KG} PFCs (97%, percentage of chambers with fused mitochondria; n=47, N=4) while FRT 40A clones have dispersed mitochondria as in the background (0%, n= 40, N=3).
Scale bar: 10 µm. n=FC clones in independent ovarioles, N=Experimental replicates.

We used ovary specific Gal4s, *c306* (expression in anterior follicle cells (AFCs)), *gr1*-Gal4 (expression in FCs covering the oocyte, stage 8 onwards) and *e22c*-Gal4 (expressed in all FCs) (Figure 2.4A-C) to monitor overexpression of fusion protein Marf and found similar aggregation, however visually the mitochondria was most highly

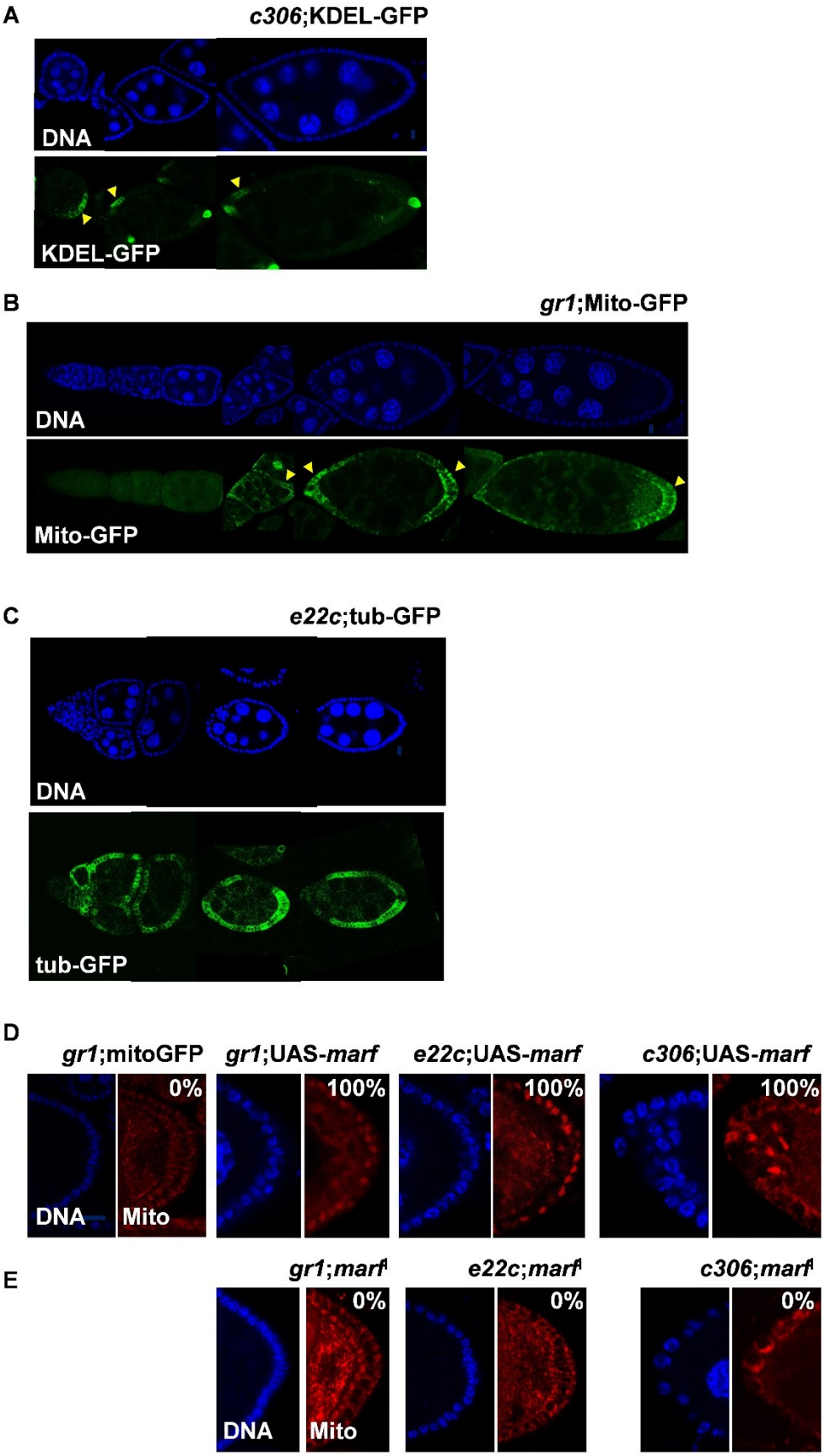
A
c306;KDEL-GFP
DNA
KDEL-GFP
B
gr1;Mito-GFP
DNA
Mito-GFP
C
e22c;tub-GFP
DNA
tub-GFP
D
gr1;mitoGFP
gr1;UAS-marf
e22c;UAS-marf
c306;UAS-marf
0%
100%
100%
100%
DNA
Mito
E
gr1;marf1
e22c;marf1
c306;marf1
0%
0%
0%
DNA
Mito

Figure 2.4. Marf overexpression leads to mitochondrial aggregation. (A-C) FC expression domains of ovary specific Gal4. *c306*-Gal4 is restricted to AFCs, KDEL-GFP driven by *c306*-Gal4 is seen only in AFCs (A). *gr1*-Gal4 is expressed in PFCs and AFCs stage 7 onwards, seen here with Mito-GFP (B). *e22c*-Gal4 expresses in a variegated fashion in entire ovariole in all the stages as seen with tubulin-GFP staining (C).
(D) Marf overexpression shows aggregation of mitochondrial network in the PFCs. Mitochondria are dispersed around the nucleus in PFCs and AFCs. Overexpression of Mito-GFP shows aggregated mitochondria with *gr1* (n=15, N=2)/*e22c* (n=12, N=3) (in PFCs) /*c306* (n=10, N=2) (in AFCs) (D;*gr1*-Gal4 control n=40, N=3, percentage in all the panels represents chambers with defect in mitochondrial distribution).
(E) Marf downregulation did not show any change in morphology with any of the three Gal4s. (*gr1*-Gal4; n= 20, N=2, *e22c*-Gal4; n= 15, N=2, *c306*-Gal4; n= 25, N=2, percentage in all the panels represents chambers with defect in mitochondrial distribution).
Scale bar: 10 µm. n=FC clones in independent ovarioles, N=Experimental replicates.

aggregated in *drp1*^{KG} mutant (Figure 2.4D). Downregulation of the fusion protein, Marf, with the above Gal4s, induced no change in mitochondrial morphology in PFCs (Figure 2.4E). This suggests that mitochondria are already in a state of fragmentation and decrease in fusion proteins further does not alter the equilibrium so that morphology change can be discerned using a confocal microscope.

2.3.2 *drp1*^{KG} mutant exhibits multilayering and decrease in cell numbers

The *drp1*^{KG} mutant tissue was arranged in multilayers of epithelial cells (Figure 2.5A). Multilayering can be because of change in cell number or loss of polarity and subsequent disarrangement of cells. We tested both the scenarios to find out the cause of multilayering. In order to estimate cell number two strategies were used to generate clones: Twin spot and MARCM. Twin spot generates control and mutant clones from mitotic sister cells in the same tissue at the same time in development thus allowing accurate comparison of proliferation rate of two cell types. The clones thus generated undergo exact same development. The control clone is brighter for GFP than the background, the mutant, on the other hand does not have GFP positive cells. *drp1*^{KG} clones were found to be much smaller in comparison to control twin spots.

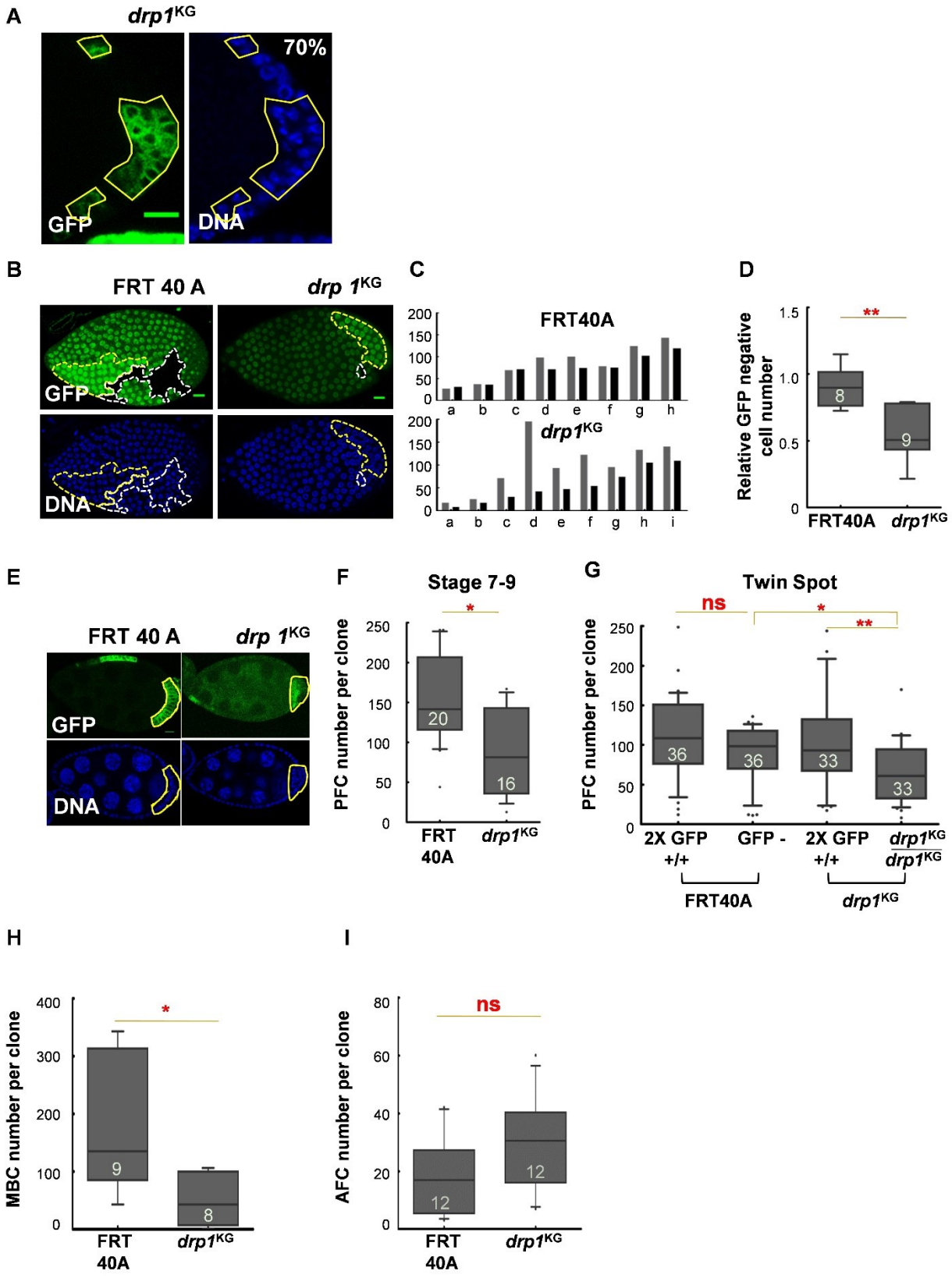
A
drp1KG
70%
GFP
DNA
B
FRT 40 A
drp 1KG
GFP
DNA
C
FRT40A
drp1KG
a b c d e f g h
a b c d e f g h i
D
Relative GFP negative cell number
**
FRT40A
drp1KG
E
FRT 40 A
drp 1KG
GFP
DNA
F
Stage 7-9
PFC number per clone
*
FRT 40A
drp1KG
G
Twin Spot
ns
*
**
PFC number per clone
2X GFP +/+
GFP -
2X GFP +/+
drp1KG drp1KG
FRT40A
drp1KG
H
MBC number per clone
*
FRT 40A
drp1KG
I
AFC number per clone
ns
FRT 40A
drp1KG

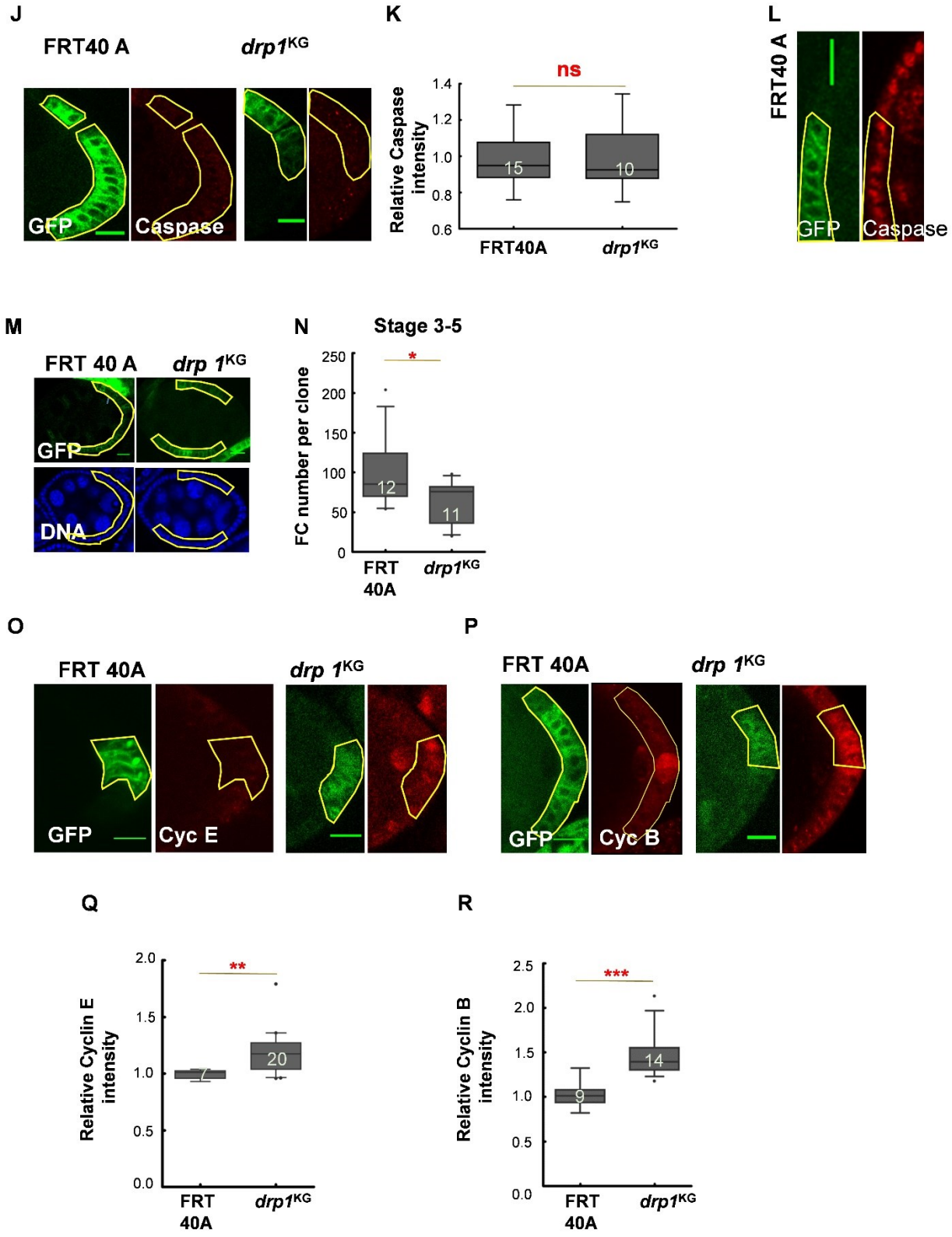
J
FRT40 A
drp1KG
GFP
Caspase
K
ns
Relative Caspase intensity
1.4
1.2
1.0
0.8
0.6
15
10
FRT40A
drp1KG
L
FRT40 A
GFP
Caspase
M
FRT 40 A
drp 1KG
GFP
DNA
N
Stage 3-5
*
FC number per clone
250
200
150
100
50
0
12
11
FRT 40A
drp1KG
O
FRT 40A
drp 1KG
GFP
Cyc E
P
FRT 40A
drp 1KG
GFP
Cyc B
Q
**
Relative Cyclin E intensity
2.0
1.5
1.0
0.5
0.0
20
FRT 40A
drp1KG
R
***
Relative Cyclin B intensity
2.5
2.0
1.5
1.0
0.5
0.0
14
9
FRT 40A
drp1KG

Figure 2.5. *drp1*^{KG} mutant tissue is multilayered and cell proliferation is decreased.
(A) *drp1*^{KG} PFCs show multilayering. *drp1*^{KG} (CD8GFP) PFCs are present in multiple layers (70%, percentage of chambers with multilayering, n=47, N=4) as compared to neighbouring control cells.
(B-D) *drp1*^{KG} PFC clone cell numbers are reduced compared to homozygous wild-type twin spot. The representative image shows an optical slice in the surface view of stage 9 chamber twin spot clones for FRT40A (control) and *drp1*^{KG}. *drp1*^{KG} (blank or GFP minus: white dashed border line) spot is smaller than the wild-type clone (2XGFP: yellow dashed border line, nls-ubiGFP; green, DNA; blue) (B). Histogram depicting variation in clone sizes for stage 9 chambers. Wild-type bars (grey) are arranged according to increasing size of GFP negative spots (black) for both FRT40A and *drp1*^{KG} (C). Ratio of number of cells for 2XGFP to GFP negative is less for *drp1*^{KG} as compared to FRT40A twin spots (D) (n= 8,9, N=3,**,P$\leq$0.01, two tailed Mann-Whitney test).
(E-F) *drp1*^{KG} PFC numbers per clone are decreased in the MARCM system. A representative image showing a CD8GFP (green) clone in a stage 8 chamber contains fewer cells in *drp1*^{KG} as compared to FRT40A (DNA; blue) (E) Quantitative analysis of PFCs per clone in *drp1*^{KG} ovarioles is significantly less than FRT40A (n=20,16, N=3, *,P $\leq$ 0.05, two-tailed Mann-Whitney) (F).
(G) Average number of control and *drp1*^{KG} mutant FCs are comparable between the twin spot and MARCM strategy. Graph depicting distribution of 2X GFP (nls-ubiGFP; green) and GFP negative clone sizes for FRT 40A and *drp1*^{KG} (DNA; blue) (G). (n=36, 36, 33, 33, N=3, **,*, P $\leq$ 0.01, P $\leq$ 0.05, Kruskal Wallis and Dunn's Test).
(H-I) *drp1*^{KG} MBCs but not AFCs show cell proliferation defect. Quantification of *drp1*^{KG} clones (CD8GFP) showed a decrease in MBCs as compared to FRT 40A control MBC and AFC clones respectively (H, n=9,8,N=3,*,P$\leq$0.05, two tailed Mann-Whitney test). AFCs number is not significantly different in *drp1*^{KG} clones compared to FRT 40A clones (I, n=12, 12, N=3, two tailed Mann-Whitney test).
(J-L) *drp1*^{KG} cells do not undergo apoptosis. *drp1*^{KG} cells (CD8GFP;green) are negative for cleaved Caspase staining (red) (J). Quantification shows no significant difference from control FRT 40A cells (K, n=15, 10, N=2, two tailed Mann-Whitney test). Cleaved Caspase staining in early FRT 40A control cells confirms the antibody (L).
(M-N) *drp1*^{KG} FCs show proliferation defect in mitotic stages. A representative image showing a clone (CD8GFP;green) in stage 5 chamber (mitotic stages) in *drp1*^{KG} ovarioles is smaller than control FRT40A (DNA; blue) (M).

Significant difference is seen in quantitative analysis of cell number in FRT40A and *drp1*^{KG} mutant clones in mitotic stages (n=12, 11 each, N=3, *, P ≤ 0.05, two-tailed Mann-Whitney test) (N).
(O-R) *drp1*^{KG} FCs have increased Cyclin E and B. *drp1*^{KG} PFCs show increased Cyclin E (red) (O), quantification in (P, n=7, 20, N=3 ,**, P≤0.01, two tailed Mann-Whitney test). Cyclin B accumulation is also seen in *drp1*^{KG} PFCs (Q). Quantification for Cyclin B comparison to FRT 40A control in (R, n=9, 14, N=3, ***, P≤0.001, two tailed Mann-Whitney test).
Data is presented as box plots where horizontal bar represents mean, box limits 25th and 75th percentiles, whiskers 10th and 90th percentiles and dots are observations outside 10th and 90th percentiles. Numbers within the box represent number of data points (n). Each data point in the box plot is an average from 5-30 cells. ns= not significant, Scale Bar: 10μm. n=FC clones in independent ovarioles, N=Experimental replicates.

FRT 40A clones had equal sized twin spots (Figure 2.5B-D). Hence the loss of Drp1 is debilitating to the cell and leads to decrease in proliferation. We found a similar decrease in the cell number using MARCM as well (Figure 2.5E-F). The ratio of decrease in cell numbers was also similar in both the techniques (Figure 2.5G). We quantified the impact on cell number in midbody follicle cells (MBCs) as well as AFCs using MARCM. We found a significant change in cell number in the MBC population, however, the cell number was not different for AFC populations (Figure 2.5H-I). This can be because the number of AFCs is much smaller than PFC and MBC, and the tissue is able to compensate for their loss. This count was done only for MARCM technique as it was difficult to find the exact twin clone in the chambers with multiple clone populations.

The lowering of cell number can be because of lowered cell divisions or increased cell death. We checked for both in MARCM clones. We did not expect cell death in *drp1*^{KG} mutant because *drp1* negative cells are known to be incapable of undergoing apoptosis as mitochondria cannot be fragmented and cytochrome C cannot be released (Frank *et al.* 2001). Immunostaining for cleaved-Caspase 3 (activated form of Caspase 3) was found to be similar to neighboring non-GFP control cells. Immunofluorescence intensity was measured in both GFP-positive as well as neighbouring GFP-negative cells (description of quantification in Material and Methods

section 2.2.6). The difference in intensity is represented in the form of a ratio between GFP positive and negative. Thus allowing normalization for factors such as age, nutrition and antibody penetrance. We compared these ratios between *drp1*^{KG} clones as well FRT40A clones, there was no significant difference between the two (Figure 2.5J-L). Another mode of programmed cell death is via autophagy. Autophagy during early and mid oogenesis is mediated by the caspase Dcp1 (Hou *et al.* 2008). Dcp1 is also elicited downstream of Cytochrome C release, hence again dependent on mitochondrial fragmentation. Hence cell number lowering is not on account of cell death.

Next, we tried to estimate cell division rate. The FCs undergo division up to stage 6 and enter endocycle as mentioned earlier. Cell numbers were counted in early stages using MARCM and found that the cell number is less for *drp1*^{KG} in these stages as well (Figure 2.5M-N). Hence the *drp1*^{KG} clones are small because of cell division defects in early stages. The *drp1* mutant FCs have been previously shown to have an increased incorporation of BrdU indicating that the cells were indeed proliferating, albeit slowly (Mitra *et al*. 2012). A similar decrease in proliferation is seen in *drp1* deficient mouse embryonic fibroblasts in low cell densities (Parker *et al.* 2015). Defective spindle orientation can also be a causative agent for disarrangement of cells, which can be checked using tubulin immunostaining. However, all attempts to do the same have unfortunately failed till now.

Cyclin B and E are downregulated in stage 7 endocycling FCs in the wild type. *drp1*^{KG} FCs at stage 7-9 clones did not enter the endocycle and had increased Cyclin B and Cyclin E antibody staining consistent with sustained proliferation in these cells. The immunostaining was comparable between GFP and non-GFP cells in control FRT40A ovarioles (Figure 2.5O-R). Hence cell division is slowed down in *drp1*^{KG} mutant and Cyclins accumulate in them, this leads to decrease in clonal cell number.

2.3.3 Apical polarity is lost in *drp1*^{KG} mutant cells

If multilayering is not on account of increased cell numbers, the loss of polarity can be the answer. Literature suggests that multilayering can result from loss of polarity proteins. FCs are epithelial cells with well-defined apical, lateral and basal domains. Follicle stem cells (FSCs) in Stage 1 chamber have basal and lateral domain markers

but lack apical domain. As the daughter cells are formed, EGF is downregulated, prefollicle cells come in contact with germ cells which they have to envelop and consequently apical domain is formed (Castanieto *et al.* 2014). In agametic ovaries apical domain is found to absent (Tanentzapf *et al.* 2000), hence contact with germ cells is essential. Hence FCs undergo mesenchymal to epithelial like transition. Bazooka (Baz) is the first polarity marker to appear. It is followed by Atypical protein kinase (aPKC) which restricts Baz to the lateral domain. aPKC recruits Crumbs, another apical marker to establish an apical domain. It has been shown that the apical complex is essential for correct positioning of the lateral domain proteins (Rolls *et al.* 2003). Integrin is a basal marker and its loss leads to multilayering in mouse lung epithelial cells (Chen and Krasnow 2012). Multilayering has been reported from loss of Crumbs, Armadillo (interactor of DE and DN Cadherin adhesion complex), Braniac and egghead (glycosyl transferases which regulate FC adhesion (Goode *et al.* 1996)), α-spectrin and 14-3-3 (cytoskeleton interactors), Par-1 (lateral domain protein) and PatJ (apical protein, part of Crumbs complex (Sen *et al.* 2015). Multilayering defect in most instances is seen in posterior large clones indicating the susceptibility of the cells and ability to compensate for small clones but not big ones (Tanentzapf and Tepass 2002). Localisation of the aPKC also affects future axis in fly as aPKC phosphorylates Lgl and leads to activation of microtubule polarity and oocyte movement (Tian and Deng 2008). Hence the loss of the most of polarity proteins results in multilayering in FCs.

Loss of one polarity component usually abrogates other markers as well. Loss of apical polarity marker Crumbs causes a reduction in other apical polarity markers Disc lost and α-spectrin. Crumbs overexpression also shows mild disruption of lateral membrane proteins. Loss of DE-Cad alone does not severely impair FC development. Arm mutants display multilayering and loss of Crumbs (Tanentzapf et. al., 2000).

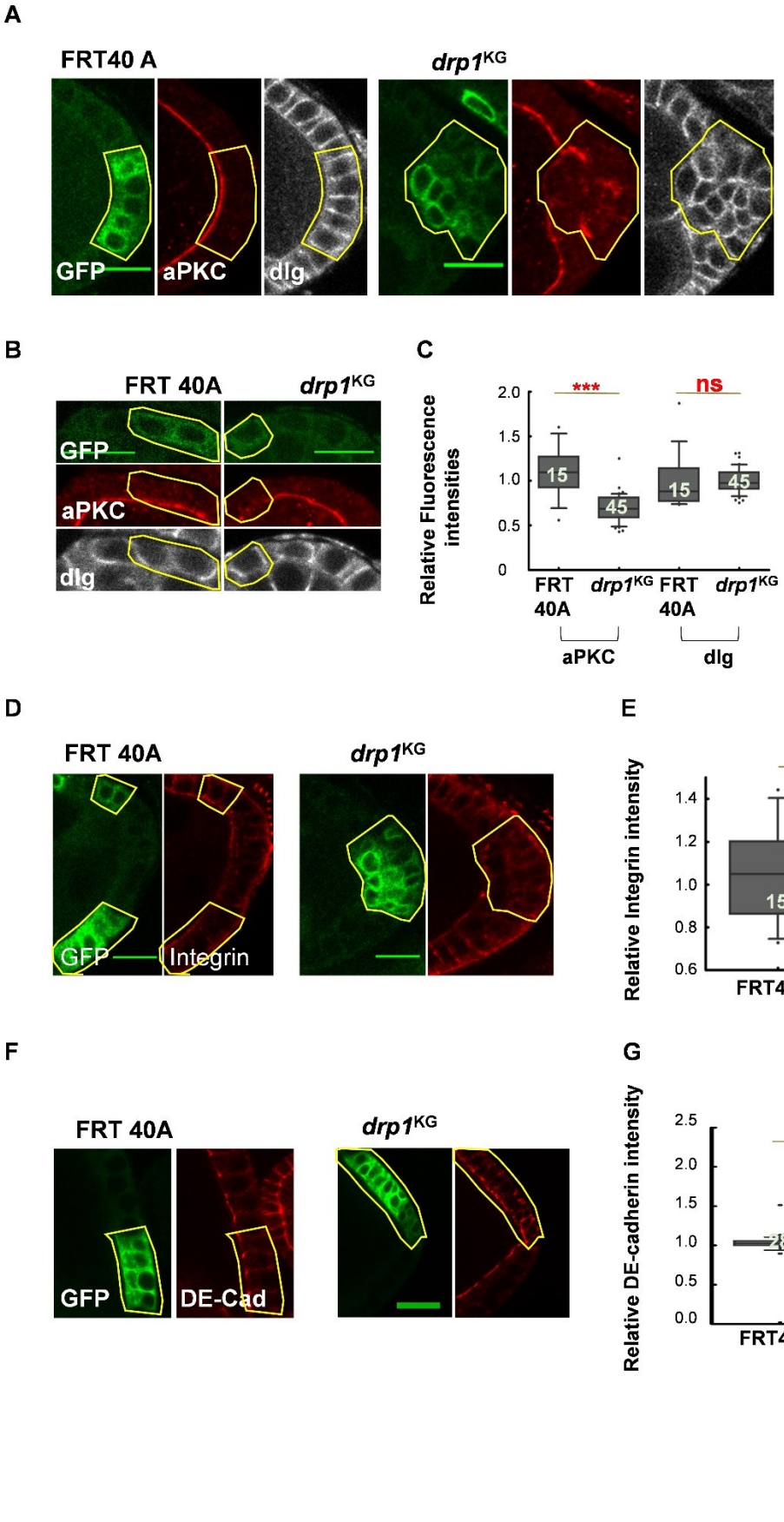
A
FRT40 A
drp1KG
GFP
aPKC
dlg
B
FRT 40A
drp1KG
GFP
aPKC
dlg
C
Relative Fluorescence intensities
***
ns
2.0
1.5
1.0
0.5
0
15
45
15
45
FRT 40A
drp1KG
FRT 40A
drp1KG
aPKC
dlg
D
FRT 40A
drp1KG
GFP
Integrin
E
Relative Integrin intensity
ns
1.4
1.2
1.0
0.8
0.6
15
15
FRT40A
drp1KG
F
FRT 40A
drp1KG
GFP
DE-Cad
G
Relative DE-cadherin intensity
ns
2.5
2.0
1.5
1.0
0.5
0.0
29
FRT40A
drp1KG

Figure 2.6. *drp1*^{KG} FCs lack apical polarity. (A-C) Apical polarity marker, aPKC lost in *drp1*^{KG} FCs. aPKC (red) is present on the apical membrane while Dlg marks the lateral membrane in control FRT 40A cells. *drp1*^{KG} PFCs lacks aPKC, Dlg however is intact (A). aPKC is absent in early FC clones of *drp1*^{KG} (B). Quantification shows the depletion in aPKC in *drp1*^{KG} FCs (C, n=15, 45, 15, 45, N=2, ***, P≤0.001, two tailed Mann-Whitney test).
(D-F) Adhesion proteins are intact *drp1*^{KG} PFCs. Integrin immunostaining is undamaged in *drp1*^{KG} PFCs compared to control FRT 40A cells (D). Quantification in (E,n=15,15, N=2, two tailed Mann-Whitney test). DE-Cadherin is present in the *drp1*^{KG} PFCs same as FRT 40A (F). Quantification in (G) depicts DE-Cadherin immunostaining in a mutant cell compared to neighboring control cells (n=28, 29, N=2, two tailed Mann-Whitney test). Data is presented as box plots where horizontal bar represents mean, box limits 25th and 75th percentiles, whiskers 10th and 90th percentiles and dots are observations outside 10th and 90th percentiles. Numbers within the box represent number of data points (n). Each data point in the box plot is an average from 5-30 cells. ns=not significant, Scale Bar: 10μm. n=FC clones in independent ovarioles in (C) and (E), in (G) n=number of cells in which DE-cadherin was quantified from 3 ovariole chambers, N=Experimental replicates.

Bazooka mutants lacking activating sites for 14-3-3 lack distinction of apical and lateral domains (Benton and St Johnston, 2003). In *Drosophila* embryo it has been shown that lateral and apical domain function to restrict each other and absence of Lgl leads to non-requirement of Crumbs (Tanentzapf and Tepass, 2002).

We performed immunostaining for apical, lateral and adhesion complex proteins. aPKC showed an apical enrichment in FRT 40A control clones. Dlg exhibited lateral membrane localization. DE- cadherin marked the adhesion belt in all the FC. aPKC was significantly reduced in the *drp1*^{KG} mutant cells, Dlg was similar in intensity in both control and mutant cells (Figure 2.6A-C). Integrin was intact in *drp1*^{KG} mutant FCs; DE-cadherin was also equal in intensity (Figure 2.6D-E). Hence apical membrane polarity is lost in *drp1*^{KG} mutant cells leading to multilayering in the tissue.

2.4 Discussion

The impact of *drp1*^{KG} on mitochondrial fusion and tissue multilayering was known earlier (Mitra et. al., 2012). Aberrant tissue morphology in *drp1*^{KG} clones results from loss of apical polarity and slower division cycles. Disorganized multilayered tissue resembles a tumorous phenotype visually, however, the opposite, mitochondrial fragmentation has been associated with a tendency to metastasize (Zhao *et al.* 2013). Therefore, the cell number comparison using MARCM and Twin spot provided a mode of quantification of cell population and identify the root of multilayering. FCs arise from the FSCs present in the Stage 1 ovariole chamber. They are held in the niche with the help of Integrin and DE-cadherin. Mitochondrial ETC complex I mutant leads to a decrease in FSC number. An increase in ROS also decreases the FSC stemness (Wang *et al.* 2012). Using MARCM, the *drp1*^{KG} mutant cell is generated at the FSC stage and the subsequent daughter cells are mutant and GFP positive. In a non-mutant clone, the GFP positive and negative FSC will be equal and grow together to give rise to equal population of daughter cells, which divide further and finally large GFP positive clones will be generated. Hence in FRT 40A control clones, we saw huge clones spanning 200 cells and entire chamber sometimes in case both FSCs flipped and became GFP positive. In *drp1*^{KG} mutant the clones were almost half in size than FRT 40A clones, also if rare complete chamber clones were seen, the chamber was found be dead. Persistent Cyclin E seen in the *drp1*^{KG} mutant cells, is also seen in mdivi-1 (fission inhibitor) treated cells (Mitra et. al., 2009). Thus, cell number is reduced in the multilayered *drp1*^{KG} clones. This is similar to effects of change in ETC or ROS hinting that the cell division process can be dependent on mitochondria via either of the above factors.

Role of mitochondria in the regulation of polarity is not understood well. Cytoskeletal components can crosstalk with mitochondria in turn regulating polarity (Muliyil *et al.* 2011; Morlino *et al.* 2014; Li *et al.* 2015). CRB1, the homologue of Crumbs is observed in vicinity of the mitochondria in retinal cells (Quinn *et al.* 2017). DE-Cadherin upregulation rescues increased ROS mediated defect in FSCs (Wang *et.al.*, 2012). EGFR downregulation is necessary for apical polarity to arise in FCs. Is the impact on EGFR signaling responsible for aPKC loss or direct effect on cellular polarity?

We will attempt to answer this question by looking at EGFR pathway in *drp1*^{KG} mutant cells in Chapter 4. To conclude mitochondria and cell polarity can be interlinked through ROS or AMPK and it will be an interesting field to explore.

Now let us look at methods to characterise mitochondria in a cell with respect to its activity, ATP production and ROS output in the next chapter.

CHAPTER 3

Characterization of mitochondrial organization and activity in cells during *Drosophila* oogenesis and embryogenesis

3.1 Introduction

Mitochondrial function can be assessed by not only characterising shape but also their activity. Mitochondria are susceptible to slight fluctuations in their environment (Abele *et al.* 2002; Rossignol 2004; Gui *et al.* 2016). Hence it is crucial to analyze its properties in homeostatic conditions close to that in a cell. This chapter will discuss how mitochondrial output in the form of its membrane potential, ATP and ROS can be quantified and analyzed.

As discussed in Chapter 1, mitochondrial ATP synthesis, calcium regulation, ROS production, mitochondrial network architecture crosstalk with each other. For example, mitochondrial ROS should not be measured in isolation as it is dependent on mitochondrial membrane potential and shape (Suski *et al.* 2012; Ahmad *et al.* 2013). Tissues have a characteristic mitochondrial architecture which is dictated by their primary function (Noguchi and Kasahara 2017). Hence factors such as tissue stress can influence the mitochondrial properties. These effects can manifest differentially by short term or long term perturbations. Therefore different phenotypes are observed after acute and chronic mitochondrial treatments (Fernández-Mosquera *et al.* 2017). In fact differences in both can offer nice insight into how a tissue adapts its mitochondria in diverse situations. Within a cell as well there can be differences in mitochondria, depending on their location. In neurons, mitochondria present in axonal lamellipodia have higher mitochondrial membrane potential than rest of the axon. This difference is on account of increased growth factor signaling in the lamellipodia via PI3K. Administration of U0126, an inhibitor of kinases downstream of EGFR abolishes the increased mitochondrial membrane potential difference (Verburg and Hollenbeck 2008). Hypoxia driven transcription regulation is dependent on increased ROS release by perinuclear mitochondria (Al-Mehdi *et al.* 2012). Hence there is a correlation between mitochondrial function and its position in the cell. Mitochondria are also known to differ

in membrane potential in different cell cycle stages. Mitochondria are electrically continuous as monitored by loss of TMRE (Tetramethyl rhodamine ethylamine, a mitochondrial membrane potential sensitive fluorescent dye) in G1-S phase. This continuity is lost during mitotic phase. ATP production also depletes during the mitotic phase (Mitra et. al., 2009). Hence mitochondrial functions depend on cell cycle stage, cell type, developmental stage and subcellular localisation.

A number of fluorescence based assays are used routinely, and can be easily adapted for tissue of interest to ask questions regarding the status of mitochondria. Let us discuss some of these assays and how they can be used to comment on mitochondrial status.

3.2 Materials and methods

3.2.1 *Drosophila* genetics

All *Drosophila* crosses were performed in standard cornmeal agar medium at 25ºC. The *pdsw*^{i}, *cova*^{i}, *ampk*^{i}, *lkb*^{i} lines were obtained from the Bloomington Stock Center. *drp1*^{KG} FRT 40A/CyO; *pdsw*^{i}/TM6 and *nanos*-Gal4,Mito-GFP line was generated by standard genetic crosses. The UASP-Mito-GFP flies were obtained from Rachel Cox (Cox and Spradling 2003).

3.2.2 Generation of FC clones

drp1^{KG} and *drp1*^{KG} ;*pdsw*^{i} clones were generated as described in Materials and Methods of Chapter 2 (section 2.2.2).

3.2.3 Immunostaining of FCs

Immunostaining protocol has been described in Chapter 2 Material and Method section 2.2.3. The primary antibodies used were: pAMPK (1:200, Cell signaling), total AMPK-α (1:200, Abcam). Fluorescently coupled Streptavidin 633 (Molecular Probes) (1:1000) was used to mark mitochondria in FCs and fluorescently coupled secondary antibodies (Molecular Probes) were used at dilution 1:1000.

3.2.4 Immunostaining of Embryo

nanos-Gal4,Mito-GFP/+ (Control) or F1 flies from RNAi lines crossed to *nanos*-Gal4 were transferred to embryo collection cages with Agar (3%) sugar plates with yeast paste. *nanos*-Gal4,Mito-GFP embryos were collected and divided after dechorionation into control and experiment vials to maintain uniformity in terms of embryo age, drug treatment, immunostaining protocol. Embryos for *pdsw* and *cova* RNAi were collected and immunostained at the same time as the *nanos*-Gal4,Mito-GFP control embryos. Embryos were washed, dechorionated using 100% bleach for 1-2 min, washed and fixed in heptane (Sigma): 4% paraformaldehyde (1:1) in PBS for 20 mins at room temperature. Vitellin membrane was removed by 1:1 methanol: heptane mix for pAMPK and AMPK-α immunostaining and for Phalloidin hand devitellinization was used. Further processing was done in a similar manner to *Drosophila* ovary. Primary antibodies used and their dilutions were as follows: pAMPK 1:200 (Cell Signaling), AMPK-α 1:200 (Abcam). Fluorescently coupled secondary antibodies (Alexa Fluor 488, 568, 633, Molecular Probes) were used at 1:1000 dilution in PBST. Fluorescently tagged Phalloidin (1:500, Molecular Probes) and Streptavidin (1:1000, Molecular Probes) were added with secondary antibodies. DNA was labelled using Hoechst 33342 (1:1000, Molecular probes). Embryos were imaged using Plan apochromat 40X/63X/1.4 objectives on the Zeiss LSM710/780.

3.2.5 Measurement of mitochondrial membrane potential using CMXRos assay

CMXRos (Molecular Probes) (100nM) in Schneider's medium was added to live ovaries for 30min. Subsequently, ovaries were washed thrice in Schneider's medium for 5min each. Fixation was done in 4%PFA in PBS for 15min. The experiments for control and mutant samples used the same CMXRos dye aliquot, were done at the same time and imaged on the same day. Uncoupler FCCP (10μM) (Sigma) was added after 3 washes for 30 min followed by one 5min wash and fixation followed by staining. CMXRos fluorescence was compared using non-parametric two-tailed Kruskal Wallis, Mann Whitney and Dunn's test for statistical analysis to allow comparison of different sample sizes and non-gaussian distribution.

3.2.6 Measurement of ROS using DHE and MitoSOX in FCs

In order to estimate ROS using DHE, ovaries were carefully dissected in Schneider's medium and incubated in 30nM DHE for 7 min. Tissue was then washed once in Schneider's and transferred to poly L-Lysine treated chamber. Ovaries were allowed to stick to the surface of the chamber and 1X PBS was added slowly along the sides and the sample was imaged live.

Freshly dissected ovaries were incubated in 5mM MitoSOX for 10 min and then given a single Schneider's medium wash. The tissue was allowed to bind Labtek chambers and imaged in 1X PBS to monitor mitochondrial ROS live.

3.2.7 ETC disruption, glycolysis inhibition using drug treatment

Dechorionated embryos were permeabilized using D-Limonene (Sigma Aldrich) : Heptane (1:1) (LH) containing drugs and incubated at RT for the time indicated. Subsequently, embryos were fixed and stained as mentioned above. Drug concentrations and their respective incubation times were as follows, FCCP: 10 µM (Sigma Aldrich); 15 mins, Rotenone: 5 µM; 30 mins (Sigma Aldrich), Oligomycin: 10 µM; 5 mins (Sigma Aldrich), 2-Deoxy-D-Glucose (2-DG): 100uM; 15mins (Sigma Aldrich). 5 mM Rotenone, 10 mM Oligomycin and 5 mM 2-DG were made in DMSO and 10mM FCCP stock was prepared in 100% ethanol. Control embryos were treated with an equivalent concentration of DMSO or ethanol. All the treatments were done for both the control and experiment at the same time. 2DG was added along with 5 µM FM464-FX (Molecular Probes) in order to establish permeabilization of the embryos.

3.2.8 Image acquisition and phenotypic estimation in FCs

The method for this has been summarized in Chapter 2, Materials and Methods section 2.2.4.

3.2.9 Image acquisition and quantification in *Drosophila* embryos

For imaging, all the samples were first checked and saturation for pAMPK and AMPK-α (total AMPK) was set according to the highest intensity sample to maintain uniform

imaging conditions. Images were taken at 512X512 with an averaging of 2 at 2X Zoom for 63X lens. Quantification of pAMPK and AMPK-α was done by measuring average image intensity for the channel using ImageJ. This mean intensity was normalized by subtracting the corresponding minimum. An average of these was taken for the respective control and each normalized mean was divided by this average so as to represent each value as a fold change. Normalized means as ratio were compared using GraphPad Prism 6.0 and plotted in the form of boxplots. Furrow length was measured from sagittal sections of the embryos using ImageJ line tool. Furrows for each cycle were compared to corresponding control cycles in GraphPad Prism 6.0 and plotted in the form of boxplots.

3.2.10 Image analysis for estimation of fluorescence in FCs

Fluorescence estimation was done as stated in Chapter 2, Materials and Methods section 2.2.6.

3.2.11 Estimation of embryo lethality

Embryonic lethality was determined by hatch assay. Flies were allowed to grow in cages with Agar (3%) Sugar as the food source. Yeast paste was supplemented to this media when embryo collection was done. 3 hour embryo collection was done using sieves. The collected embryos were carefully laid onto an Agar (3%) Sugar plate in the form of 10X10 matrix. Plates were incubated at 25 °C and checked for hatched embryos after 24 and 48 hrs. Lethality was depicted as percentage embryos which did not hatch.

3.2.12 ATP estimation

ATP estimation was carried out from embryo extracts by using luciferase based ATP determination Kit (Thermo Fisher Scientific). Briefly, 3 hour old embryos were collected and rinsed in heptane twice and subsequently dried completely. Embryos were manually crushed on ice using 1.5 ml microfuge tube pestle in homogenisation buffer (Tris (100 mM) and EDTA (100 µM)) till a uniform extract was obtained. The extract was lysed by boiling for 5 min and the supernatant was collected by spinning at 21000 g at 4^{O}C. Supernatant was diluted (1:10) in dilution buffer (25 mM Tris, 100 µM EDTA) and

again spun at 21000 g at 4^{O}C. After diluting appropriately, Luciferin and firefly luciferase in buffer provided in the kit were added to the samples in 96 well white plates and ATP concentration dependent luminescence was measured immediately on a Varioskan Spectrometer at 560 nm. In order to ascertain reproducibility, both experimental and control samples were assayed at three different dilutions. Each dilution was loaded in triplicates and readings for the entire plate were taken thrice. All measurements were normalized to total protein content of the embryos. Protein estimation was done using BCA kit (Thermo Fisher Scientific) against standard BSA concentrations. Each sample was loaded in three different wells and emission for each well was measured thrice. All the experiments were repeated 3 times. The graph represents the percentage reduction corresponding to controls estimated at the same time. Means were compared using one tailed Mann-Whitney test in GraphPad prism 6.0.

3.2.13 Live Imaging of ovarioles

Freshly emerged pUASP-Mito-PAGFP flies were kept in media supplemented with dry yeast for 2 days. Flies were subsequently dissected in Schneider's medium and ovaries were separated using insect pins. Labtek chambers were treated with poly L-lysine for 5 min. The chamber was washed continuously under tap water for 10 min. Ovaries were transferred in minimal medium onto the Labtek chambers and allowed to stick to the surface. PBS was added to the chamber carefully along the sides. Ovaries were imaged using Plan Apochromat 40x/1.4 objective on the Zeiss LSM780; 488 nm and 561 nm lasers were used at 2% power with an appropriate gain, within the dynamic range for imaging GFP.

3.2.14 Photoactivation of Mito-PAGFP in ovarioles

Photoactivation in nurse cells and oocyte expressing Mito-PAGFP was performed in selected ROIs using the 405 nm laser with 100% power and 50 iterations by Plan Apochromat 40x/1.4 NA objective on the Zeiss LSM780. Images were acquired using 488 nm laser at 2% power. The data obtained was analyzed using ImageJ. For nurse cells, equidistant region in adjacent nurse cells and region in same nurse cell was

monitored at the same time as the ROI. Intensities were normalised to the background and increase in fluorescence in comparison to post activated fluorescence intensity was calculated for each. For the oocyte, four equidistant reference regions in different directions were compared to the ROI.

3.3 Results

3.3.1 Mitochondrial membrane potential is elevated in FCs mutant for mitochondrial fission protein

Cells lacking mitochondrial fusion proteins Mfn1/2 show fragmentation and loss of membrane potential (Chen *et al.* 2003). Mitochondrial membrane potential can be measured by a number of fluorescence dyes such as JC1, Mitotracker green/red/far red. These dyes accumulate in the mitochondria and fluoresce depending on the proton gradient across the mitochondrial inner membrane. We used the dye Mitotracker Red CMXRos as it is retained after fixation, allowing us to combine it with primary antibodies of our choice. CMXRos forms thiol conjugates with peptides thereby making it resistant to depletion on fixation with paraformaldehyde (Susin *et al.* 1999; Cottet-Rousselle *et al.* 2011). We compared CMXRos fluorescence in living and fixed ovarioles containing *drp1*^{KG} PFCs and did not find a significant difference (Figure 3.1A-B). Fused mitochondria in PFCs depleted of Drp1 were checked for mitochondrial membrane potential using CMXRos. The fluorescence in clones was normalized relative to the surrounding control PFCs. The fluorescence ratio was close to 1 when control FRT40A clone cells were compared to the corresponding background cells (Figure 3.1C, F). The relative fluorescence ratio of more than 1 showed greater accumulation of the potentiometric dye CMXRos and an increase in mitochondrial membrane potential. This allowed us to control for variations in the data arising out of differential dye uptake, sample preparation and experimental fluctuations. *drp1*^{KG} PFCs showed increased CMXRos fluorescence as compared to background control cells and the GFP:non-GFP ratio was more than 1 (Figure 3.1D, F).

In order to validate the dye further, we used a number of drugs which target

either the whole ETC or individual complexes and deplete the mitochondrial membrane potential. We standardized the ETC uncoupler FCCP (Carbonyl cyanide-*4*-(trifluoromethoxy) phenylhydrazone) (Nicholls and Budd 2000). FCCP is an ionophore and mediates passage of hydrogen ions across the mitochondrial inner membrane thereby dissipating the mitochondrial membrane potential difference. We tried range of FCCP concentrations (1 µM-100 µM) for varying durations (15 min-2 hour) and found that 30 min treatment with 10 µM FCCP disrupted the mitochondrial membrane potential in control FCs (Figure 3.1C, F). Quantification of CMXRos fluorescence confirmed a drop in mitochondrial membrane potential in the whole tissue. We also tested the same in *drp1*^{KG} FCs and found a drop in fluorescence similar to the control (Figure 3.1D, F). FCCP treatment reduced mitochondrial membrane potential in the entire tissue and similarly in control FRT40A GFP and non-GFP cells, hence maintaining the ratio at 1.

FCCP treatment has been shown to cause mitochondrial fragmentation in cell lines (Cereghetti *et al.* 2008). No significant difference was found in mitochondrial architecture in FCCP treated FCs (Figure 3.1C, D). Even a two hour treatment did not alter mitochondrial architecture. This can be either because the treatment is insufficient to bring about a change or mitochondrial shape is not dependent on mitochondrial membrane potential in this tissue.

In addition, to compare pharmacological inhibition of the ETC, with genetic manipulation, RNAi was used to deplete ETC protein. RNAi against *pdsw*, a complex I subunit was used. Downregulation of *pdsw* showed a significant drop in membrane potential using CMXRos dye. We observed a very subtle difference in mitochondrial morphology in *pdsw* RNAi, however the phenotype was not consistent. A stronger mutant can perhaps help accentuate the alteration in morphology if any. The observation that mitochondrial distribution is unaffected on *pdsw* loss indicates that the status of mitochondrial morphology proteins in PFCs. Mitochondrial morphology is susceptible to change in mitochondrial membrane potential up to early stages (stage 6-7), subsequently stages mature, FCs differentiate and acquire characteristic mitochondrial shapes. The mitochondrial morphology regulating proteins also increase in amount and hence mitochondria resist change in their shape. This is beneficial for the cell as it is able to stringently maintain the mitochondrial shape it requires for

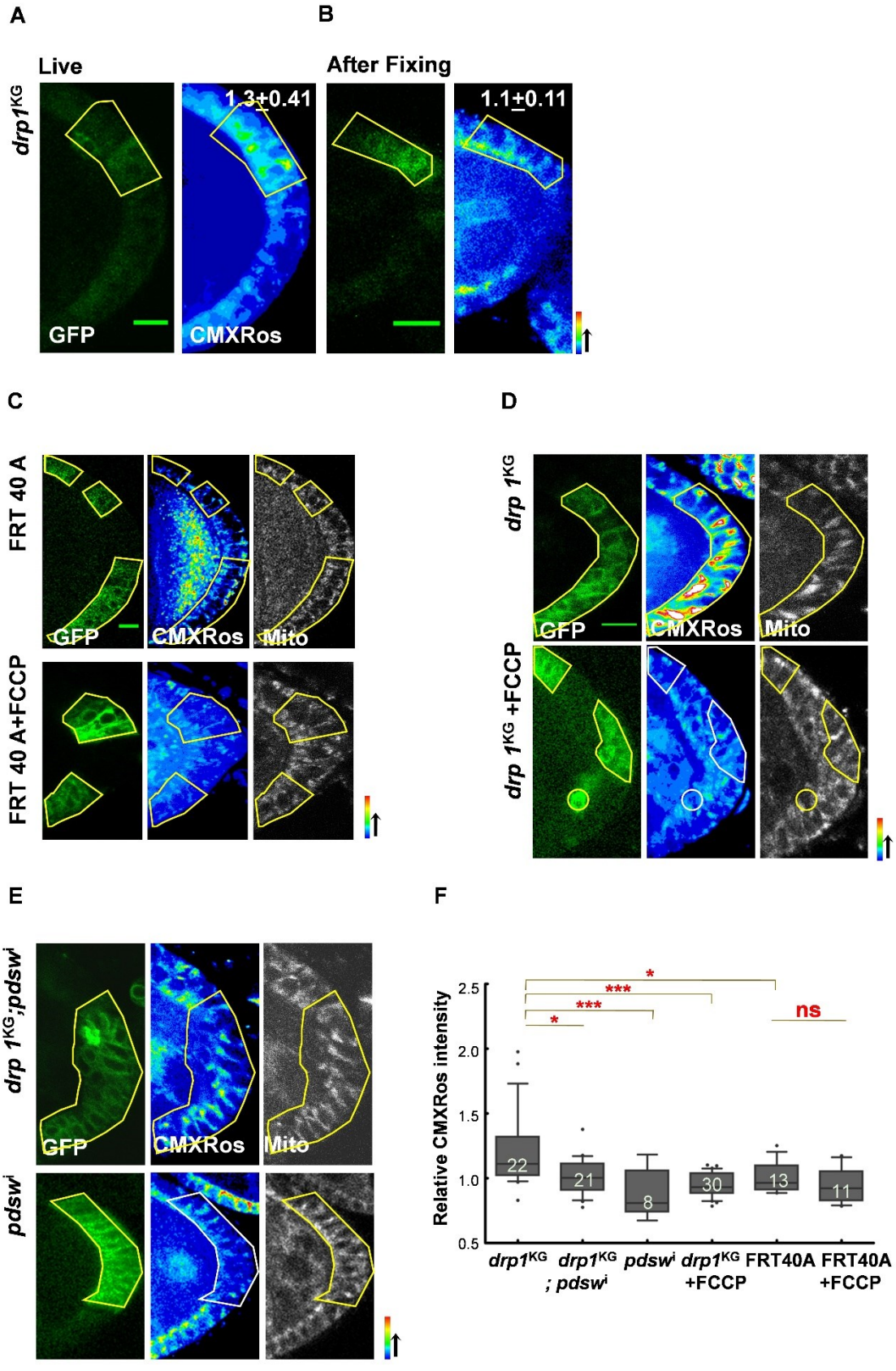
A
B
Live
After Fixing
drp1KG
1.3±0.41
1.1±0.11
GFP
CMXRos
C
D
FRT 40 A
FRT 40 A+FCCP
drp 1KG
drp 1KG +FCCP
GFP
CMXRos
Mito
E
F
drp 1KG;pdswi
pdswi
Relative CMXRos intensity
2.5
2.0
1.5
1.0
0.5
*
***
***
*
ns
22
21
8
30
13
11
drp1KG
drp1KG ; pdswi
pdswi
drp1KG +FCCP
FRT40A +FCCP

Figure 3.1. *drp1*^{KG} cells have higher mitochondrial membrane potential. (A-B) CMXRos (pseudocolored where red is the highest intensity pixel and blue is the lowest) uptake in living and fixed *drp1*^{KG} PFCs. Ratio of CMXRos intensity in GFP to control cells is similar before (A) and after fixation (B) of FCs. (n= 4).
(C-F) *drp1*^{KG} PFCs have increased and *pdsw*^{i} have decreased mitochondrial membrane potential. The CMXRos signal overlaps with the mitochondria signal in FRT 40A as well as mutants. CMXRos intensity ratio in control FRT40A GFP to non-GFP cells is close to 1 with and without FCCP treatment (n= 12, 11, N=3) (C). *drp1*^{KG} FCs (n=22, N=5) show higher CMXRos fluorescence as compared to background control cells (ratio higher than 1) and this is not seen in the presence of FCCP (n=30, N=4) (D). CMXRos fluorescence ratio decreases in *drp1*^{KG}; *pdsw*^{i} and in *pdsw*^{i} compared to background control cells (n=21, 8, N=4) (E). CMXRos intensity ratio quantification shows a significant decrease on FCCP addition and in *pdsw*^{i} (n=30, 8, N=4,4; FRT40A (n=13, N=3), ***,P $\leq$ 0.001, *,P $\leq$ 0.05,two tailed Kruskal Wallis and Dunn's test) (F).
Data is presented as box plots where horizontal bar represents mean, box limits 25th and 75th percentiles, whiskers 10th and 90th percentiles and dots are observations outside 10th and 90th percentiles. Numbers within the box represent number of data points (n). Each data point in the box plot is an average from 5-30 cells. ns=not significant, Scale Bar: 10µm. n=FC clones in independent ovarioles, N=Experimental replicates.

appropriate function.

In conclusion, CMXRos is an excellent fixable dye to assess mitochondrial membrane potential in the *Drosophila* FCs and *drp1*^{KG} FCs have heightened mitochondrial membrane potential difference.

3.3.2 Monitoring ATP levels in FCs and embryogenesis

Higher mitochondrial membrane potential difference results in higher ATP output from ETC. ATP levels can be monitored by measuring ATP using luciferase based kits or indirectly by estimating AMPK levels in the cell. Decrease in ATP leads to increased activation of AMPK, the energy sensor of the cell via LKB1. AMPK is upstream of number of transcription factors such as FOXO, responsible for promoting catabolism and inhibiting anabolism (Steinberg and Kemp 2009; Mihaylova and Shaw 2011). I will

summarize analysis, of ATP levels in FCs and then go on to describe the protocol used for *Drosophila* embryo.

3.3.2.1 *drp1*^{KG} FCs have higher pAMPK levels

AMPK levels were monitored in FCs by using antibody against activated AMPK (pAMPK) and pAMPK levels were found to be higher in early FCs (stage 1-6) as compared to stage 7-9 in wild type. Early FCs had bright bursts of pAMPK, which overlapped with the nuclear staining indicating nuclear localisation of pAMPK. These bright bursts were frequently seen in cells undergoing metaphase. Stage 7 onwards FCs had dispersed cytoplasmic pAMPK signal (Figure 3.2A-B).

Drosophila ovaries undergo an insulin pathway mediated switch from stage 12 in their glycogen content. This is on account of major rearrangement in metabolites in these stages (Sieber *et al.* 2016). However, the study does not discuss metabolism in early FCs, for example if early FCs depend on glycolysis for ATP. In order to estimate the ATP contribution via glycolysis, we treated *Drosophila* ovaries with 2-DG. 2-DG treated ovariole chambers had increased pAMPK immunostaining and it was completely nuclear in all the cells (Figure 3.2C). This suggests that glycolysis is responsible for ATP production in FCs and under starvation, pAMPK can activate transcriptional targets to help in the ovariole survival. It would be interesting to utilize the 2-DG assay to ask questions about downstream targets of pAMPK and how they affect ovary development. Another burning question is if there is difference in response to 2-DG depending on the ovariole stage.

drp1^{KG} PFCs exhibit increased pAMPK immunostaining in comparison to the neighbouring control cells (Figure 3.2D). This was a surprise as high mitochondrial membrane potential is usually translated into increased ATP. We were not able to use the luciferase based assay with the MARCM as it requires tissue extracts and will be very erroneous if performed from clonal tissue. Hence this was used for whole embryos and pAMPK levels were used for the clonal tissue. It is possible that Complex V is not able to function at an optimal level in these mutant cells. pAMPK also might be activated in response to other stresses rather than lack of ATP. Increased expenditure of energy

can also activate AMPK. SIRTs are activated by increased exercise and they, in turn, activate LKB1 to phosphorylate more AMPK (Lan *et al.* 2008). Further experiments are required to understand the pAMPK increase in *drp1*^{KG} PFCs. Response of fission deficient mitochondria in *drp1*^{KG} PFCs to 2-DG treatment would also be interesting to analyze. It is possible that pAMPK mediated effects are worsened as glycolysis is shut down in the FCs.

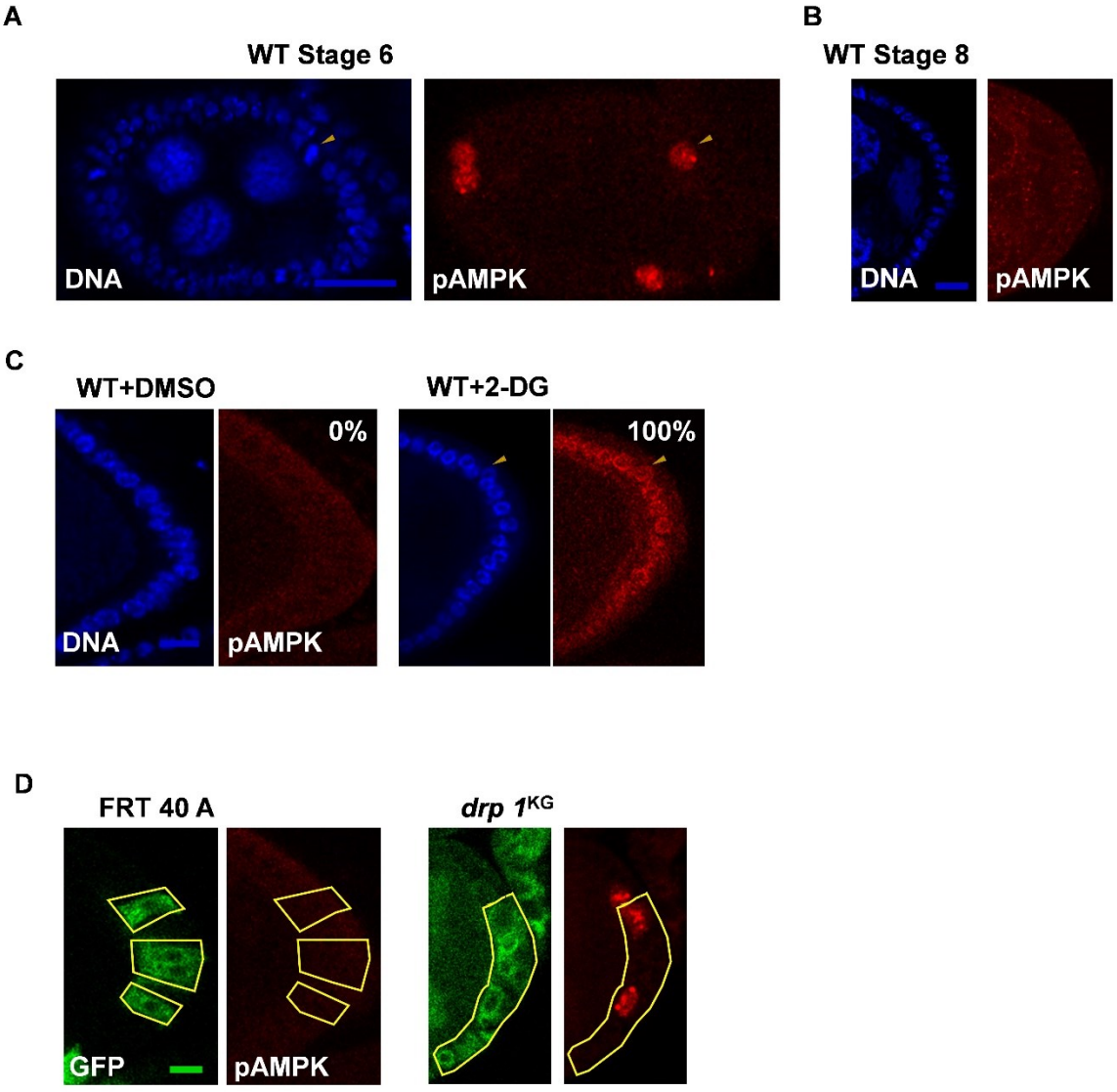

Figure 3.2. *drp1*^{KG} cells have elevated pAMPK. (A-B) Early stage FCs are rich in activated AMPK signal. Immunostaining for pAMPK (red) shows bright signals (marked by yellow arrow head) in stage 3-6 FCs (DNA;blue). Stage 7 onwards pAMPK signal is faint and dispersed in the PFC cytoplasm (100%, n=25, N=3) (A).
(C) 2-DG treatment increases nuclear pAMPK signal. Treatment of cells with glycolysis inhibitor 2-DG shows completely nuclear signal of pAMPK (marked by yellow arrowhead) in all the FCs as compared to DMSO treated control (100% 2-DG treated ovarioles show nuclear pAMPK, while 0% DMSO treated show pAMPK in nucleus, n=10,10, N=2) (C).
(D) *drp1*^{KG} PFCs (CD8GFP;green) show pAMPK (red) enrichment. pAMPK bursts can be seen in *drp1*^{KG} mutant cells stage 7 and later (62%, n=8, N=2), while FRT 40A lacks them (0%, n=10, N=2) (D).
Scale bar: 10 µm. n=FC clones in independent ovarioles, N=Experimental replicates.

3.3.2.2 Mitochondrial activity is required for furrow formation in the *Drosophila* early embryo

This work was done in collaboration with Sayali Chowdhary, Dnyanesh Dubal and Devashree Sambre and is part of the publication '**Analysis of mitochondrial organization and function in the *Drosophila* blastoderm embryo', Nature Scientific Reports (doi:10.1038/s41598-017-05679-1)**

We monitored both pAMPK and ATP levels in *Drosophila* embryos. *Drosophila* embryogenesis begins as a single cell surrounded by copious amount of yolk rich in lipid droplets, signalling molecules, nutrients and mRNA required for patterning. The single cell undergoes 8 rounds of division and the 256 nuclei thus formed start moving towards periphery of the embryo. The cells continue sharing the yolk at the periphery for next 4 rounds of division, hence *Drosophila* early embryo is syncytial. After completing NC13, the nuclei acquire basal boundaries and form complete cells, which then go on to acquire different identities and form an adult fly (Figure 3.3A). Each syncytial cell has a pool of basally localized mitochondria (Chowdhary *et al.* 2017). Cells are partially compartmentalized on account of short membrane extensions known as furrows screening them from their neighbors (Figure 3.3B).

We collected synchronized embryos and measured the amount of ATP in them depending on activation of the enzyme luciferase. In order to maintain homogeneity, the sensitivity range of the kit and fold change in ATP with dilution of embryo extract was measured. Care was taken such that there is no inactivation of ATP content in the extracts.

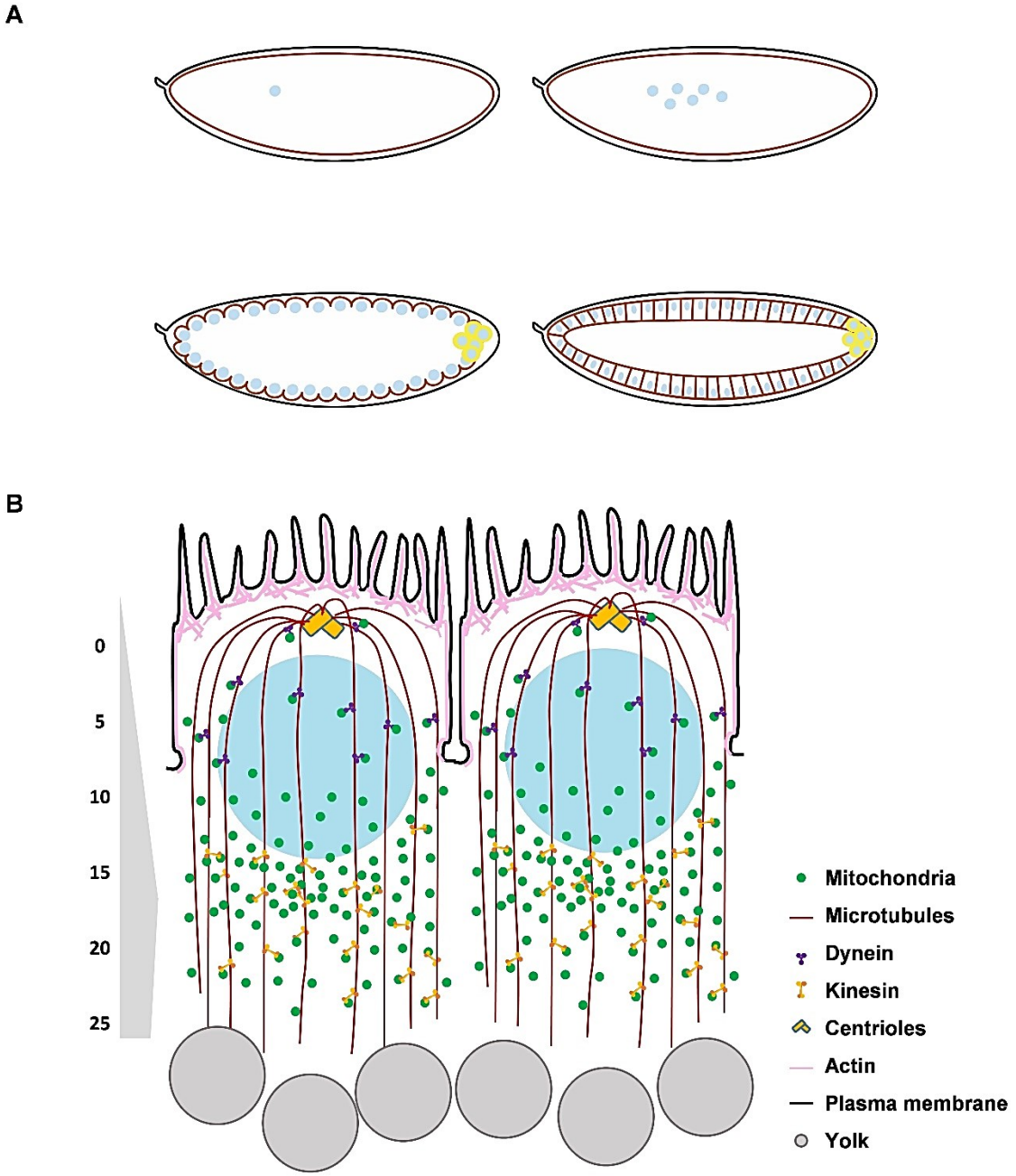

Figure 3.3. Syncytial *Drosophila* embryo as a model system to study role of mitochondria. (A-B) *Drosophila* embryo begins as a single nucleus (A, first panel), which undergoes 9 cycles of division inside the embryo (second panel), in stage 10 the nuclei move up to the boundary and are partially separated from each other by plasma membrane (third panel). After 4 more divisions, complete membrane forms at stage 14; cellularization (fourth panel) (A). Syncytial nucleus has its mitochondrial pool concentrated in the basal region. Mitochondria use the tubulin network to travel apically as the cell divisions progress. The basal region in the *Drosophila* embryo is rich in yolk particles. Each nuclei is partially confined with the help of membrane furrow (B).

Next robustness of the assay was checked by changing the mitochondrial ETC activity in *Drosophila* embryo. We used both drug based and genetic approaches to modify ETC activity in the syncytial embryo. *Drosophila* ovaries are easily permeable to drugs through basement membrane. During dissection, muscle fibre sheath has to be carefully removed to allow maximum passage of drug. However, *Drosophila* embryo has two layers of impermeable membranes to protect itself from outside assault. Number of different combinations of organic as well as inorganic solutions were used to allow the drug to penetrate the embryo. We found limonene and heptane in a combination of 1:1 to work best. In order to disrupt the output of entire ETC, the uncoupler FCCP was used. In germline cells, FCCP treatment has also been shown to impair mtDNA replication (Hill *et al.* 2014). Rotenone was used as a complex I inhibitor. It has been used to model Parkinson's disease in *Drosophila* and study its downstream effectors (Coulom and Birman 2004). It inhibits complex I subunit by preventing electron transfer to ubiquinone. Oligomycin acts on the ATP synthase (Complex V) by blocking the F0 subunit. As a result of this inhibition, there is a transient spike in mitochondrial membrane potential as there is no pumping of electron from intermembrane space to the matrix, however there is a subsequent dip in the membrane potential on account of disruption of the whole chain. A lot of studies have been undertaken to under the effect of these drugs on ETC and subsequent impact on the cell itself.

Drosophila embryo has a huge reserve of lipid droplets and amino acids. It has to undergo fast cycles of initial division to transform from syncytial to cellularized embryo. Mass spectrometry studies have shown that amino acids are the primary metabolites in

the *Drosophila* early embryo (Tennessen *et al.* 2014; Sieber *et al.* 2016). A Similar abundance of amino acids has been observed in mouse and human embryos as well (Houghton1 *et al.* 2002; Martin *et al.* 2003; Sturmey *et al.* 2008). A number of early studies have been conducted on mammalian preimplantation embryos to shed light on their key source of energy (Leese, 2012). The preimplantation embryo is relatively quiescent to reduce its ROS footprint. In vitro studies have shown that embryos which burn less fuel, have a better chance of surviving (Houghton *et al.* 1996). Similar pattern has been seen for *Drosophila* and mice embryo as mitochondria are maternally transmitted to the embryo. In order to maintain high fidelity and prevent accumulation of mutations, oocyte mitochondria are maintained in a relatively nascent state (Babayev and Seli 2015; Sieber *et al.* 2016). The adjoining nurse and FCs support the oocyte development. There is no study to characterise the contribution of mitochondria and specifically the mitochondrial ETC during embryo development. Hence we used these tools to understand the role of ETC in syncytial divisions.

3.3.2.2.1 ETC inhibition leads to decrease in ATP and increased pAMPK in *Drosophila* syncytial embryo

In order to inhibit ETC acutely, *nanos*-Gal4, Mito-GFP embryos were collected and treated with drugs and subsequently their ATP and AMPK levels were estimated. In control embryos, pAMPK is faintly distributed in nucleus in prophase and exhibits a kinetochore like structure in metaphase (Figure 3.4A). ATP levels analyzed via luciferase based assay were found to be lowered significantly in all the drug treatments as compared to the controls, establishing that the drugs are effective in their function (Figure 3.4B). There was also a significant increase in pAMPK levels. In the drug treated embryos pAMPK was mainly nuclear (Figure 3.4C-E), which again corresponds to active state of the protein (Ju *et al.* 2011; Kazgan *et al.* 2010). We then looked for ATP depletion in RNAi lines against complex I, *pdsw* and complex IV, *cova* depletion using *nanos*-Gal4 as driver. Genetic manipulation of ETC also yielded similar ATP lowering in the embryo (Figure 3.4B). In addition, we found that pAMPK was also higher in both the RNAi lines while AMPK-α was similar to controls (Figure 3.4F-G). AMPK-α

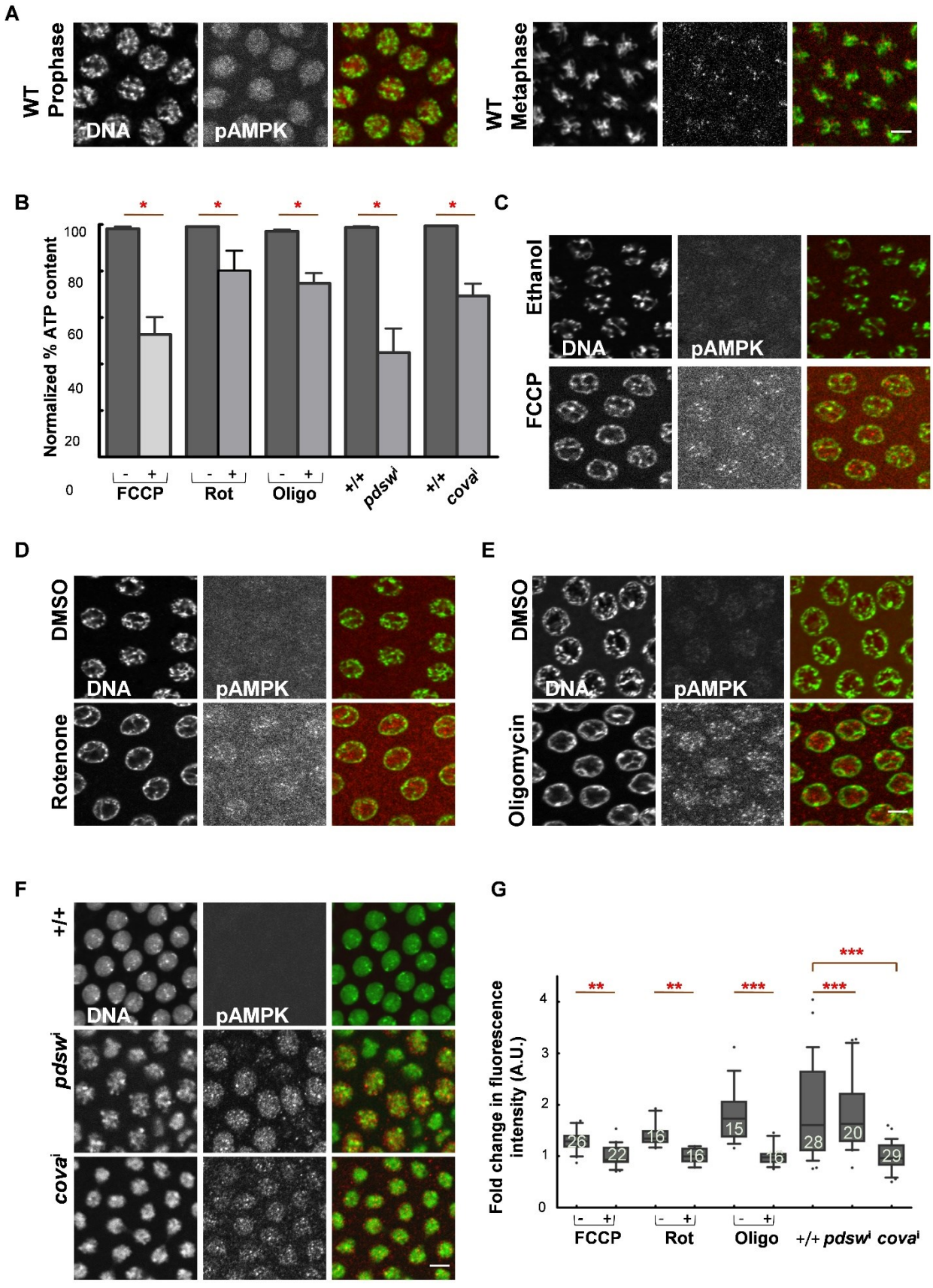
A
WT Prophase
DNA
pAMPK
WT Metaphase
B
Normalized % ATP content
100
80
60
40
20
0
FCCP
Rot
Oligo
+/+ pdsw^i
+/+ cova^i
C
Ethanol
FCCP
DNA
pAMPK
D
DMSO
Rotenone
DNA
pAMPK
E
DMSO
Oligomycin
DNA
pAMPK
F
+/+
pdsw^i
cova^i
DNA
pAMPK
G
Fold change in fluorescence intensity (A.U.)
FCCP
Rot
Oligo
+/+ pdsw^i cova^i

Figure 3.4. ETC impairment decreases ATP and activates AMPK in the syncytial *Drosophila* embryo. (A) pAMPK (green in merge) is nuclear (DNA; red in merge) in prophase and cytoplasmic in metaphase in wild type embryos. pAMPK shows a kinetochore like pattern in the metaphase.
(B) ATP luciferase assay shows a depletion in ATP levels in *Drosophila* embryos treated with ETC inhibiting drugs; oligomycin, FCCP and rotenone. Depletion of ETC proteins, *pdsw* and *cova* also leads to decrease in ATP (n=9, N=3,*, $P \leq 0.05$, one tailed Mann-Whitney test).
(C-G) Increased pAMPK (red in merge, DNA green in merge) is seen on treatment of embryo with ETC inhibitior drugs in comparison to the DMSO or ethanol treated control embryos (C-E, G). Similarly *pdsw* and *cova* downregulation shows increased pAMPK signal in comparison to the wild type control (+/+) (F-G). (n= 26,22,16,16,15,16,28,20,29 embryos ***,$P \leq 0.001$,**,$P \leq 0.01$,*,$P \leq 0.05$, two tailed Mann-Whitney test).
Scale bar: 5 μm. Histogram in (A) represents average of luminescence from 3 samples, intensity measured thrice for each and normalized to the average. + represents drug treated samples and – represents DMSO/ethanol treated samples, +/+ represents wild type control in (G). Data in (G) is presented as box plots where horizontal bar represents mean, box limits 25th and 75th percentiles, whiskers 10th and 90th percentiles and dots are observations outside 10th and 90th percentiles. Numbers within the box represent number of data points (n). Each data point in the box plot is an average from 25-40 cells in an embryo. ns=not significant. n=embryos, N=experimental replicates. (Adapted from Chowdhary et. al., 2017).

levels however were not affected in the *pdsw* and *cova* downregulation lines (Figure 3.5A), indicating that more of AMPK is getting activated on ETC manipulation.

One of the surprising observation was the rapid response that the embryo had towards the ETC inhibitor drugs. Oligomycin treatment for just 5 min was sufficient to increase the amount of pAMPK to 1.8 times the control. Cell lines have been reported to show pAMPK response in a similar manner in short span of time (Fujii *et al.* 2000; Tsou *et al.* 2011). This result allowed us to reflect on the reaction time of *Drosophila* embryo to metabolic offence.

In conclusion, acute as well as severe abrogation of ETC leads to ATP depletion in the early embryo leading to increase in active AMPK and glycolysis does not

significantly contribute to ATP synthesis. We next went on to analyze the effect of ATP depletion in the growing embryo.

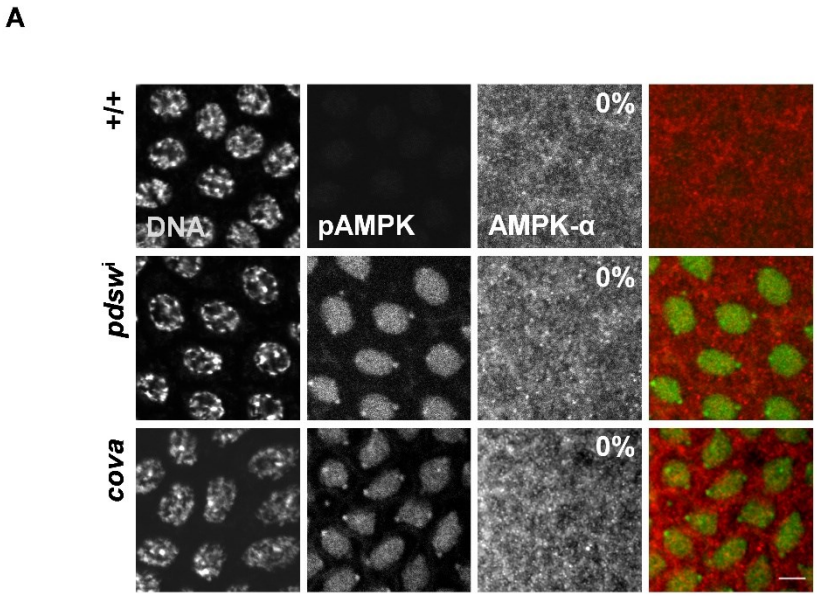

Figure 3.5. Total AMPK levels do not change on genetic depletion of ETC (A) AMPK-α (red in merge) is seen dispersed in the cytoplasm as well as nucleus in the control syncytial embryo. AMPK-α (red in merge, pAMPK;green in merge) intensity is not changed in *pdsw*^{i} and *cova*^{i} expressing embryos compared to the wild type control (0% embryos show defect in AMPK-α immunostaining, n=12,13,15,N=3 each).
Scale: 5 µm. n=embryos, N=experimental replicates. (Adapted from Chowdhary et. al., 2017).

3.3.2.2.2 ETC disruption causes shortening of metaphase furrows

pdsw and *cova* depleted embryos were fragile and exhibited defects in Phalloidin immunostaining which binds to F-actin. The architecture was disrupted and the membrane was loosened as opposed to compact actin network in control embryos (Figure 3.6A). *Drosophila* syncytial embryo has well defined apical and lateral membrane but no basal membrane. After cellularization each cell is sealed off into individual compartments. The lateral membrane is short during interphase and extends down during metaphase forming metaphase furrows. Metaphase furrow length is dependent on actin dynamics (Afshar *et al.* 2000). Furrows in drug treated embryos

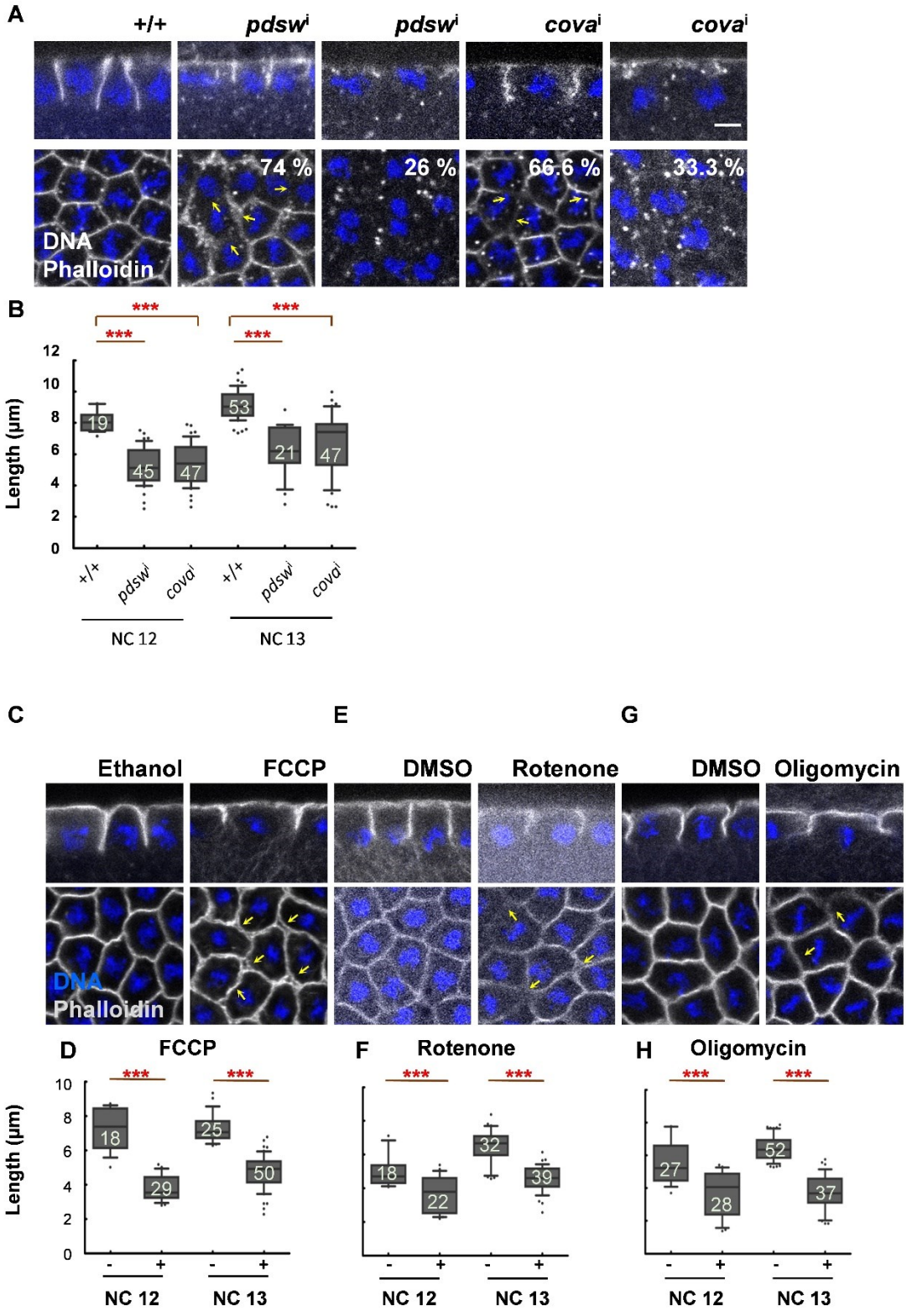
A
+/+
pdsw^i
pdsw^i
cova^i
cova^i
74 %
26 %
66.6 %
33.3 %
DNA
Phalloidin
B
***
***
***
***
Length (µm)
12
10
8
6
4
2
0
19
45
47
53
21
47
+/+
pdsw^i
cova^i
+/+
pdsw^i
cova^i
NC 12
NC 13
C
E
G
Ethanol
FCCP
DMSO
Rotenone
DMSO
Oligomycin
DNA
Phalloidin
D
FCCP
F
Rotenone
H
Oligomycin
***
***
Length (µm)
10
8
6
4
2
0
18
29
25
50
18
22
32
39
27
28
52
37
-
+
-
+
NC 12
NC 13

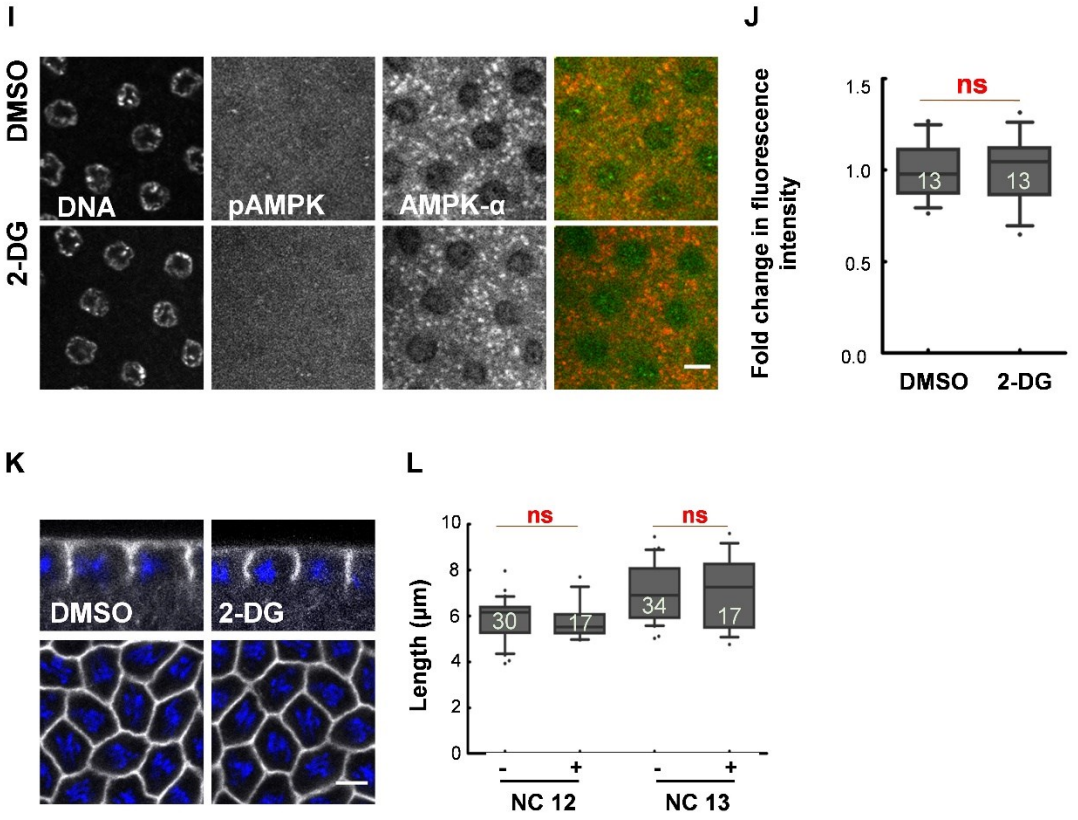

Figure 3.6. ETC inhibition causes furrow shortening in syncytial embryos. (A-B) Downregulation of ETC proteins disrupts actin network in early syncytial embryo. *pdsw*^{i} embryos have shorter furrows and membrane loosening (74%) or complete loss of Phalloidin immunostaining (26%). Downregulation of *cova* as well shows severe loss of actin network (33.3%) and membrane loosening (66.6%) (A). Quantification of furrow length shown in (B, NC12 control 19 (4 embryos) *pdsw*^{i} n = 45 metaphase furrows (8) and *cova*^{i} 47 (8), and; NC13 control 53 (8), *pdsw*^{i} 21 (4) and *cova*^{i} 47 (7), ***, P ≤ 0.001, two tailed Mann-Whitney test). (C-G) Uncoupling of ETC by FCCP causes shortening of metaphase furrows (Phalloidin;grey, DNA;blue) compared to ethanol treated controls (Top panel, saggital section). XY section shows that the actin network is loosened (marked by yellow arrows) (C). Quantification in (D, NC12 Control n = 18 (4 embryos), FCCP: 29 furrows (6); NC13 control n = 25 (6) and FCCP: 50 (11), ***, P ≤ 0.001, two tailed Mann-Whitney test). Rotenone causes similar shorter furrows and dispersed actin network between two cells. In the early embryo (E). Quantification compares furrow length in rotenone treated to DMSO and rotenone treated embryos in NC12 and 13 (F,NC 12 control n = 18 (5), rotenone n = 22 (4); NC13 control n = 32 (5), Rotenone n = 39 (6), ***,

P ≤ 0.001, two tailed Mann-Whitney test). Oligomycin treatment leads to furrow shortening in comparison to DMSO control (G), quantification in H, NC12 control n = 18 (4) and oligomycin n = 28 (7) and NC13 control 52 (10) and oligomycin 37 (7), ***, P ≤ 0.001, two tailed Mann-Whitney test). (I-L) Glycolysis inhibition by 2-DG treatment does not alter pAMPK levels and metaphase furrow length. Treatment of syncytial *Drosophila* embryos with 2-DG does not show increase in the levels of pAMPK (green-merged, α-AMPK in red in merge) (I). Quantification in (J), n = 13, 13 embryos and 310 and 300 cells, N=2; for treated and control embryos respectively. (two tailed Mann Whitney test). Metaphase furrow length is not reduced in 2-DG treated embryos compared to control embryos (K). NC 12 control metaphase furrows n = 30 furrows (8 embryos), 2DG n = 17 (5); NC13 control n = 32 (7), 2DG n = 17 (5), N=3. (two tailed Mann Whitney test) (L)
Scale bar: 5 μm. Data is presented as box plots where horizontal bar represents mean, box limits 25th and 75th percentiles, whiskers 10th and 90th percentiles and dots are observations outside 10th and 90th percentiles. Numbers within the box represent number of data points (n). Each data point in the box plot is an average from 25-40 cells in an embryo. ns=not significant. n=embryos, N=experimental replicates. (Adapted from Chowdhary et. al., 2017).

were significantly shortened in the *pdsw* and *cova* depletion. We compared Nuclear Cycle 12 as well as 13 furrow lengths and found significant shortening (Figure 3.6A-B). Similarly, furrow length in drug treatments were shorter as well (Figure 3.6C-H). Hence, furrow formation is an energy intensive process and ATP depletion leads to its abrogation. Other than the fact that the process itself requires a lot of energy, it is also possible that pAMPK dependent signaling is responsible for impairment of actin dynamics.

In order to check contribution of glycolysis in *Drosophila* embryo development, we inhibited glycolysis by 2-DG. If glycolysis contributed significantly to ATP production in the *Drosophila* embryo, we would again see a spike in pAMPK and furrow disruption. No significant difference in pAMPK was found (Figure 3.6I-J). 2DG treated embryos did not show any change in furrow length as compared to control (Figure 3.6K-L).

Hence ETC disruption by acute as well as chronic treatment leads to short metaphase furrow.

3.3.3 Monitoring ROS in FCs

ROS production is perhaps the most studied mitochondrial output after ATP. It is a master regulator of several signaling pathways and is controlled stringently in a cell. Change in ROS levels are crucial for the development of an organism, *Drosophila* embryo dorsal closure relies on ROS levels to alter cell shapes during the process (Muliyil et. al. 2012). Mitochondria are not the only source of ROS in the cell; NADH oxidase present on the cell membrane also synthesis ROS in response to signals such as pathogen attack (Nauseef 2008). ROS levels were checked by incubating the ovarioles in dihydroethidium (DHE) and imaging DHE fluorescence in the live tissues. DHE fluoresces on oxidation by superoxide ion and can be used to estimate ROS amount in the cell (Sinenko *et al.* 2012). We also used MitoSOX in order to analyze levels of mitochondria specific ROS. MitoSOX is targeted to the mitochondria and is sensitive only to superoxides (Tang *et al.* 2009).

3.3.3.1 *drp1*^{KG} mutant FCs have increased ROS

Mitochondrial ROS in a cell depends on the mitochondrial morphology. Hyperglycemia induced mitochondrial fission mediates increased ROS production in human cell line (Yu *et al.* 2006; Maimaitijiang *et al.* 2016). The decrease in Drp1 activity reduced mitochondrial ROS production (Röth *et al.* 2014). Mitochondria producing high amounts of ROS are fated for autophagy. Increased ROS due to complex I mutation is shown to cause shortening of mitochondria in MEFs (Valsecchi *et al.* 2013).

We standardised DHE as well as MitoSOX for wild type *Drosophila* ovaries and both seemed to show a basal fluorescence which can overlap with the mitochondrial signal (Figure 3.7A-B). We found a significant increase in nuclear to cytoplasmic ratio of DHE in the *drp1*^{KG} mutant cells. Increased oxidation of DHE leads to its subsequent binding to DNA and increased nuclear signal. Hence *drp1*^{KG} mutant cells have higher ROS than neighbouring control cells (Figure 3.7C-D). This was not in agreement with previous results in which increased fission favored ROS release (Yu et. al., 2006). Incomplete oxidation can be a result complex I and II dysfunction in the *drp1*^{KG} mutant

cells. *pdsw* downregulation also showed increase in ROS as has been shown earlier in eye epithelial cells (Owusu-Ansah et. al., 2008). MitoSOX can help assess the contribution of mitochondrial ROS in *drp1*^{KG} mutant FCs and distinguish if the defects are mediated solely by mitochondrial ROS or cellular ROS contributes as well. Even though the mitochondrial membrane potential is high, *drp1*^{KG} mutant is under both nutrient and oxidative stress.

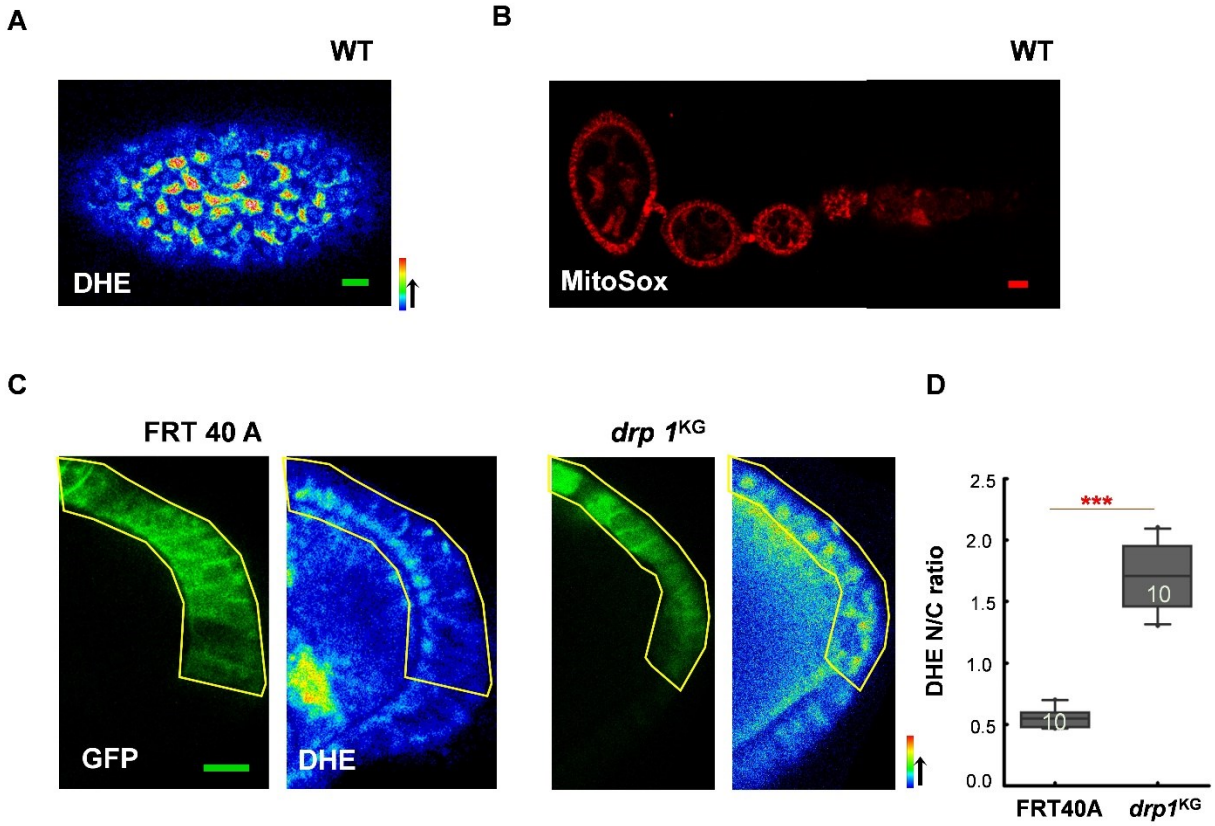

Figure 3.7. *drp1*^{KG} mutants have high ROS. (A-C) DHE is a live probe to detect ROS in a cell. DHE fluorescence shows active ROS in the wild type ovariole chamber (A). MitoSox is another tissue ROS detector. Mitosox enters the mitochondria and on oxidation fluoresces hence reflecting the mitochondrial ROS in the chambers in all stages and cell types (B). DHE fluorescence is increased in *drp1*^{KG} mutant PFCs as compared to FRT 40A. *drp1*^{KG} mutant has higher oxidized DHE as seen by elevated nuclear signal. Quantification of DHE fluorescence in nucleus compared to cytoplasm reveals the relative ROS amount in the cell. This is higher in *drp1*^{KG} (C, n= 10,10, N=3, ***, P≤0.001).

Data is presented as box plots where horizontal bar represents mean, box limits 25th and75th percentiles, whiskers 10th and 90th percentiles and dots are observations outside 10th and 90th percentiles. Numbers within the box represent number of data points (n). Each data point in the box plot is an average from 5-30 cells. ns=not significant, Scale Bar: 10μm. n=FC clones in independent ovarioles, N=Experimental replicates.

3.3.4 Analysis of mitochondrial network in *Drosophila* ovarioles

We attempted to examine exchange of mitochondrial network and its movement in various cell types in the ovarioles. Photoactivatable GFP tagged to mitochondrial matrix protein cytochrome oxidase VIII, Mito-PAGFP driven by *nanos*-Gal4 was used. A region of interest (ROI) was activated in the cell and then change in its fluorescence was monitored in ROI as well neighbouring regions by 4D imaging.

We found mitochondria to be more or less static in nurse cell as well as oocyte. Laser always activated a small region outside the ROI at the same time as ROI, which was a limitation of the donut shaped point spread function of the confocal microscope. On activation, there was no change in mitochondrial intensity during the duration of imaging (Figure 3.8A-B). Similar dynamics were observed for oocyte mitochondria as well (Figure 3.8C-D). There was also no difference in mitochondria in different regions such as close to or further away from the oocyte. This indicated that mitochondria are not travelling large distances and instead of long networks it is possible that short networks or fragmented mitochondria are present in both cell types. There are contrasting electron micrographs (EMs) from studies showing germline mitochondrial architecture. Earlier study suggests nurse cell mitochondria elongate from stage 4-stage 9 chambers (Tourmente *et al.* 1990). Recent EMs show smaller fragmented mitochondria in Stage 8 chamber nurse cells (Sieber *et. al.*, 2016). Mito-PAGFP probe suggests smaller dispersed mitochondria in germline cells in *Drosophila* ovaries. Also, highly dynamic mitochondria observed in cell culture studies and during cell division are seldom found *in-vivo* systems (Mitra *et al.* 2009; Mandal *et al.* 2011b; Nagaraj *et al.* 2012; Ratnaparkhi 2013; Chowdhary *et al.* 2017). Hence, *Drosophila* oocyte and nurse cells maintain a stable pool of small mitochondria in accordance with their functional requirements.

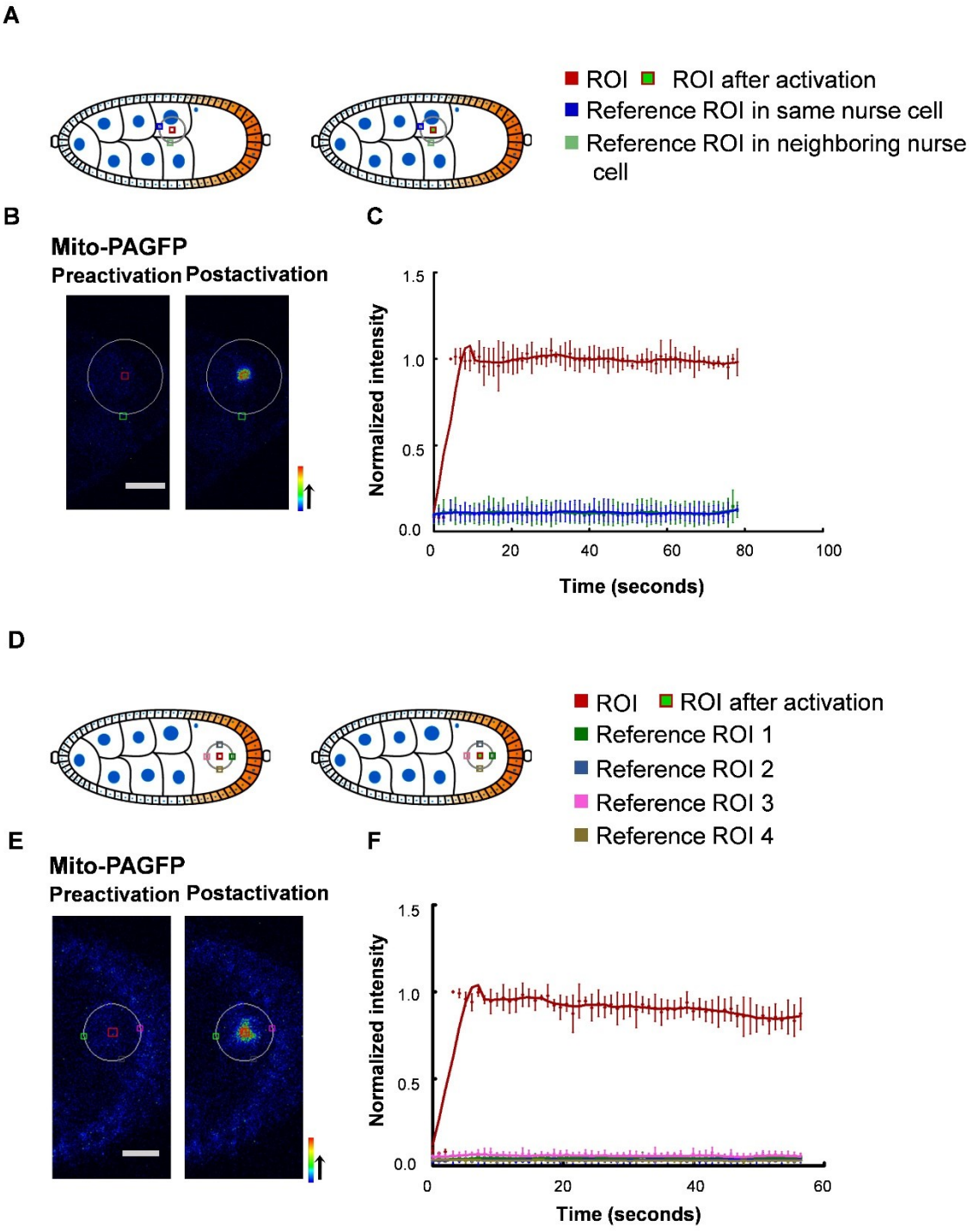

Figure 3.8. Mitochondrial network is immobile in germline cells in *Drosophila* ovariole. (A-C) Photoactivation of mitochondria in nurse cells remains restricted in ROI.

Mitochondrial network is specifically activated in a region of the nurse cell (red box). After activation the change in fluorescence is noted for the ROI as well as reference regions which are region from same nurse cell (blue box) and region from neighboring cell (green box). The two references are equidistant from the ROI (Marked by grey circle) (A). Nurse cell mitochondria in Mito-PAGFP flies is activated and there is a sharp increase in fluorescence in the region (pseudocolored, red depicts highest pixels and blue the lowest) (B). This fluorescence is followed through time. Background subtracted normalized mean intensity with time is depicted here in the form of a curves, where red is ROI, blue is the region in same nurse cell and green is in neighboring nurse cell. There is no change in normalized intensity in any of the regions (C, n=3, N=2). (D-F) Mitochondria in the oocyte region is photoactivated and the fluorescence in monitored for the ROI (red) and equidistant regions in all directions from the ROI (Marked by grey circle) are considered references (D). MitoPAGFP gets activated in the oocyte region, and no change in fluorescence is seen in any of the reference regions. Quantification in (F) shows the constant fluorescence in ROI and reference regions within the time of monitoring the fluorescence (F).
Scale Bar: 10 μm. Bars in (C) and (F) represent standard deviations. n=number of regions activated, N=Experimental replicates.

3.4 Discussion

We have attempted to scrutinize mitochondrial properties such as membrane potential, ROS and AMPK in a quantitative manner so that they can be statistically compared across experiments accurately.

We have shown that fused mitochondria in *drp1*^{KG} mutant FCs have higher mitochondrial membrane potential across the inner membrane and the cells have higher ROS and pAMPK. These results reveal the stressed environment in fission deficient FCs. We discussed aberrant cell cycle in *drp1*^{KG} mutant in Chapter 2. Cell cycle progression is dependent on the cellular state. Stress mediated via ROS can alter phosphorylation of growth factors and hence modulate levels of Cyclins in the cell (Boonstra and Post 2004). Similarly AMPK regulates cell cycle via p21 and mTOR, thus leading to cell cycle defects in high pAMPK conditions (Motoshima *et al.* 2006). MARCM clones for Superoxide dismutase (SOD), a ROS quenching enzyme, in the FCs exhibit

Cyclin E defect (Appendix A1). Increased mitochondrial membrane potential in the mutant can also be the causal agent for cell cycle defects (Mitra et. al., 2009). Hence change in mitochondrial architecture distorts cell equilibrium via the above mitochondrial readouts.

Drosophila embryo is susceptible to acute as well as chronic ETC insult and both lead to AMPK activation. Metaphase furrow formation has been extensively studied and the actin nucleators involved in its dynamics are well understood (Sherlekar and Rikhy 2016). Furrow extension helps in stabilizing the spindle network and subsequent nuclear division. The fast divisions require a lot of ATP and hence can depend on energy reserves in the syncytial embryo. In addition to ATP required by actin dynamics, cell division machinery, cellular movement during gastrulation are also energy intensive processes. LKB1 regulates RhoA and in turn the actin polymerization in *Drosophila* neurons (Cook *et al.* 2014). This suggests that similar LKB1-AMPK-Rho A mediated mechanism can be active in the embryo as well and it is worth checking the interplay to further establish the role of energy stress during embryo development. It would be interesting for example to see the effect of ETC inhibitor drugs on RhoA overexpression. Mitochondria dependent stress is not extensively characterised in the *Drosophila* embryo. For example, it has been shown that 1-2 hour old embryos undergo cell cycle arrest under hypoxia (Fischer *et al.* 2004). Chk2 mediated *pdsw* and *cova* activation has been shown to lead to cell death (Xie and Dubrovsky 2015). In *Drosophila* embryos as well, there were defects in nucleus appearance suggestive of cell death. However, the field lacks literature in the area and the embryo can be used a model system to study stress responses during development.

AMPK, the cellular energy sensor gets activated on decrease in ATP to ADP ratio. In the wild type there is some nuclear pAMPK, this suggests that AMPK is necessary to activate pathways critical to early development. LKB1 is the major AMPK activator by phosphorylation at T172 (Shaw *et al.* 2004). In addition to LKB1, AMPK can be activated downstream of several factors. For example, in human skin fibroblasts ROS activates AMPK and switches on glycolytic metabolism (Wu and Wei 2012). Calcium regulated CAMKK2 is another activator of AMPK, whose role in neurons is understood (Hawley *et al.* 2005). $AMPK^{T172}$ increase is also necessary for calcium

induced tight junction assembly in MDCK cells (Zheng and Cantley 2006). FCCP has been shown to lead to ROS release in mouse myoblasts (Wang *et al.* 2014). In *Drosophila*, role of AMPK is understood in multiple systems. *Drosophila* mature neurons regulate F/G actin ratio via AMPKγ dependent prenylation of RhoA and thus control neuronal outgrowths (Cook *et. al*, 2014). modENCODE data shows that AMPKγ is especially abundant in the 0-4 hour embryo. Cytoskeleton is known to regulate mitochondrial transport and positioning (Saxton and Hollenbeck 2012), however it is interesting to see a converse regulation as well. AMPK null flies have multiple defects like abnormal cell divisions, deformed cuticles and aberrant cell polarity (Lee *et al.* 2007). These results indicate that pAMPK is essential for the *Drosophila* embryo development and it can be activated via multiple pathways.

Nuclear localization of pAMPK is interesting and has been seen earlier in cell lines as well adult brain tissue. It is possible that cytoplasmic targets of AMPK control fast metabolic changes while nuclear targets help in transcriptional changes in the cell (Ramamurthy and Ronnett 2006). Spindler localization of activated AMPK in mammalian cell lines is required for actin mediated spindle orientation (Thaiparambil *et al.* 2012). *Drosophila* embryo requires rapid spindle organisation and orientation changes to coordinate cell division of entire syncytial cell population. We also observed pAMPK puncta on the spindles and believe that pAMPK is required for spindle organisation in *Drosophila* embryo as well. Increased pAMPK can phosphorylate more of MRLC (Lee et. al., 2007), leading to more globular actin rather that filamentous and decrease in actin dynamicity. This can hinder the fast furrow dynamics in each cycle with the furrow not being able to extend fully. Hence it will be interesting to check for MRLC in the drug treated embryos and further crack the factors mediating differential nuclear and cytoplasmic AMPK in the wild type cell.

Using these methods and analysis, we further checked the effect of signaling pathways EGFR and Notch on mitochondria. Let us first discuss EGFR pathway in the next chapter.

CHAPTER 4

Aberrant Ras/ERK signaling in *drp1*^{KG} mutant FCs is responsible for mitochondrial morphology and mitochondrial membrane potential defect

4.1 Introduction

EGFR is a well-studied growth pathway involved in functions such as cell proliferation, patterning, cell differentiation making it one of the versatile signaling pathways (Shilo 2003). Ligands involved in its activation are well understood in fruit flies. It is regulated at multiple steps, such as ligand processing, nature of ligand, feedback from transcription factors, transactivation, endocytosis and localisation within the cell (Gabay *et al.* 1996; Levkowitz *et al.* 1999; Sasamura *et al.* 2013; Tomas *et al.* 2014; Malartre 2016). In flies EGFR interacts with the ligands- Spitz, Keren, Gurken, Vein and Argos. On activation, the internal domain of the receptor dimerises. The downstream signal can be transmitted via the PI3K or Ras/ERK. Ras-MEK-ERK through a series of phosphorylation events eventually lead to regulation of cytoplasmic and/or nuclear substrates and gene expression (Hughes, 1995) (Figure 4.1A). In addition to multiple downstream targets, the output of the pathway is further complicated by its tight spatiotemporal regulation. It is used at various stages of development in the same tissue with completely opposite targets and outcomes (Shilo, 2002).

A number of signaling pathways such as EGFR/MAPK, Notch, NFkB, Hippo and Wnt interact with mitochondrial morphology, biogenesis and metabolism during differentiation. The EGFR and Hippo directly regulate mitochondrial shape. Yorkie, a component of Hippo pathway, transcriptionally increases mitochondrial fusion proteins Marf and Opa to affect proliferation (Nagaraj et. al., 2012). EGFR is required for fragmented mitochondria in PFC (Mitra et. al., 2012). Fusion protein Marf binds and regulates Ras activity (de Brito and Scorrano, 2009). Taken together there is an emerging evidence of interplay between mitochondrial morphology, activity and signaling pathways and the mechanism by which this is regulated is an upcoming area

of investigation.

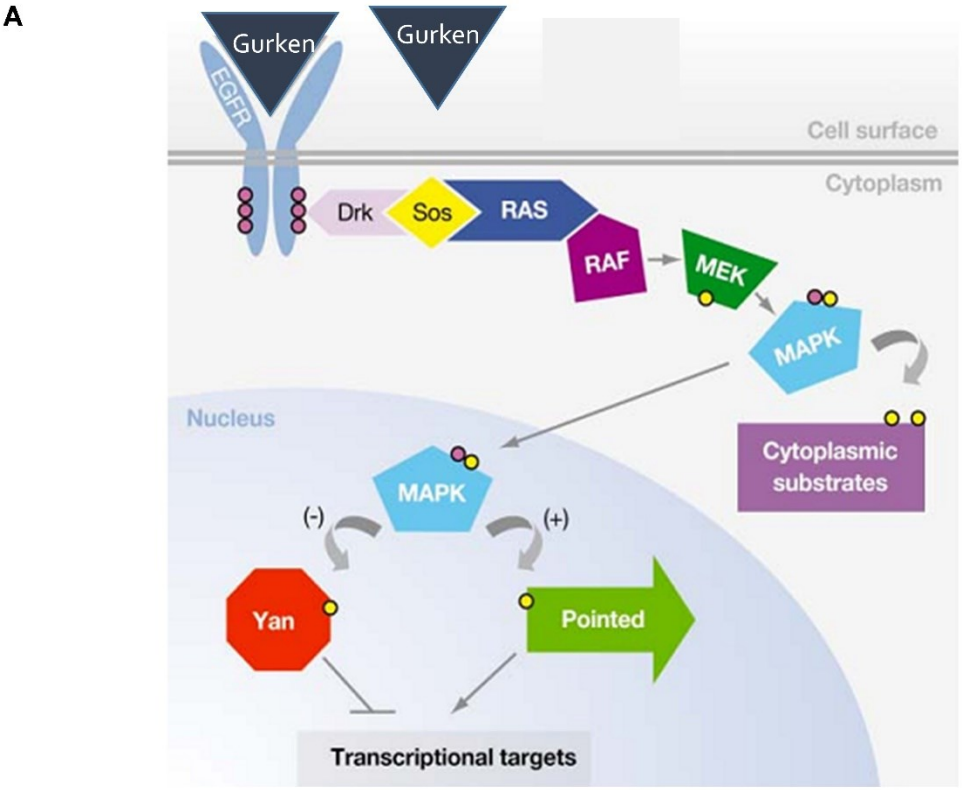

Figure 4.1. Schematic for EGFR and its downstream components. Gurken ligand on the germline activates EGFR on the FCs. On activation, dimerization of the receptor promotes activation of downstream kinase Ras, MEK and ERK (MAPK). MAPK activates nuclear targets such as transcription factor Pointed in the FCs. (Image modified from Vivekanand & Rebay, 2006).

EGFR pathway is activated in two distinct stages in *Drosophila* ovaries. It is required during stage 1 in FSCs to repress apical polarity. As a FSC differentiates to give rise to prefollicle cell, EGF pathway is repressed and as a result aPKC appears (Figure 4.2A). In EGFRAc, aPKC is absent (Castanieto et. al, 2014). In stage 8 *Drosophila* ovariole chamber EGFR is activated by the ligand Gurken (Figure 4.2B). Gurken mRNA is localized in dorso-anterior portion in the oocyte and activates EGFR only in dorsal PFCs. Some studies suggest that Gurken is present in the form of a gradient (Goentoro *et al.* 2006), and hence different levels of EGFR are activated as one moves towards the ventral portion of the ovariole. Activation by Gurken leads to initiation of the EGFR

A

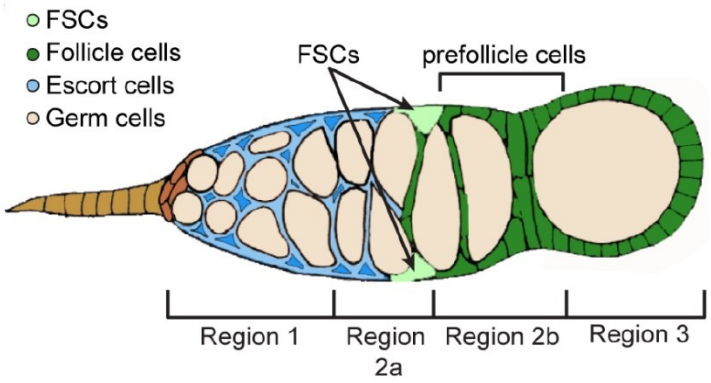

Follicle stem cell	Prefollicle cell
EGFR active, aPKC absent	EGFR inactive, aPKC present

B

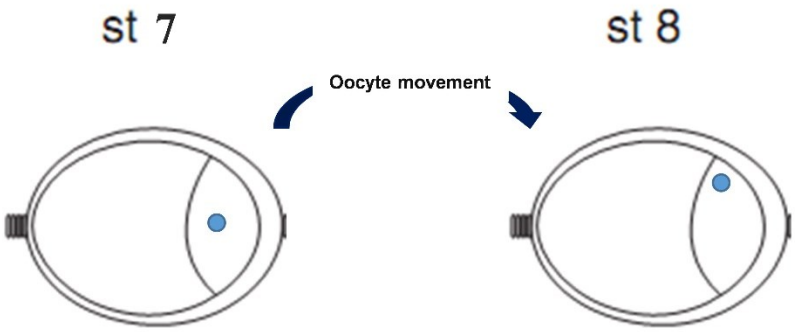

Figure 4.2. Role of EGFR pathway in oogenesis. (A) EGFR is activated in the stage 2a chamber for FSC maintenance. FSCs are present in stage 2a chamber along with germ cells which are held in the niche with the help of cap cells in stage 1. Prefollicle cells arise from FSCs and subsequently, acquire apical polarity with the inactivation of EGFR in them. (B) EGFR is activated in stage 7-8 chambers by the ligand Gurken to direct movement of oocyte (blue cell) to dorso-anterior position. (A) Schematic from Kronen *et. al.*, 2014).

cascade via Ras and ERK and determines dorsal FC fate. This symmetry breaking step establishes the future axis in *Drosophila*. Loss of Gurken leads to loss of polarity along

both dorso-ventral and antero-posterior axis (Roth and Lynch 2009) and ventralized embryo (Sen *et al.* 1998). Active ERK which is the double phosphorylated form is known to activate downstream transcription targets and this leads to oocyte movement in the dorso- anterior direction (Peri *et al.* 1999). The dorso-anterior movement of the oocyte is mediated by microtubules present in the oocyte region (Zhao *et al.* 2012). In addition, a variety of ligands involved in feedback in the pathway such as Kekkon and Argos are also activated (Wasserman and Freeman 1998; Ghiglione *et al.* 1999). Hence maintaining an active regulation of the pathway via multiple mechanisms. In the dorsal midline FCs, EGFR levels lead to formation of dorsal appendages. Loss or misplacement of dorsal appendages is characteristic EGF loss of function phenotype (Wasserman and Freeman, 1998). Hence EGF and its downstream activators are well characterised in the fly ovaries.

The dorsal cell fate assignment by EGFR pathway is mediated by activation of transcription factors such as pointed (Morimoto *et al.* 1996). It is known that abrogation of EGFR using a dominant negative allele, leads to formation of fused mitochondria and activated EGFR allele in the MBCs results in fragmentation of mitochondria (Mitra et. al., 2012). This study further characterized the need for fragmented mitochondria and found that mitochondrial fusion in a wild type background leads to disruption of tissue architecture and status of Notch pathway. However, components downstream of EGFR pathway which interact with mitochondria are not known and why mitochondrial fragmentation is necessary for the pathway. We have used the *Drosophila* FCs differentiation as a paradigm to study the interaction of Ras/ERK with mitochondrial morphology.

Src mediated activation of EGFR leads to its mitochondrial translocation and binding to cytochrome oxidase subunit II enhancing tumorigenesis (Boerner *et al.* 2004). Mitochondrial EGFR supports its fusion by Prohibitin 2 and Opa1 activation (Bollu *et al.* 2014). Activated Ras along with dysfunctional mitochondria leads to metastasis in *Drosophila* eye epithelia (Ohsawa *et al.* 2012) and directly induces mitochondrial fragmentation causing a metabolic switch to glycolysis in cancer cells (Chiaradonna *et al.* 2006). ERK2 inactivates Mfn1 and activates Drp1 by phosphorylation in mammalian cancer cells (Kashatus *et al.* 2015; Pyakurel *et al.* 2015). Taken together the EGFR-

Ras-ERK pathway increases glycolysis and regulates mitochondrial fragmentation for its appropriate activation in cancer cells but the mechanism by which mitochondrial morphology impacts the pathway is unknown.

Fused mitochondrial morphology is correlated with high membrane potential, high calcium sequestration and increased ATP generation (Thayer and Miller 1990; Chen *et al.* 2003; Lodi *et al.* 2004; Zanna *et al.* 2008). Fragmented mitochondrial morphology is associated with lowered electron transport chain (ETC) activity and ATP generating ability (Ashrafian *et al.* 2010; Jheng *et al.* 2012). Fused mitochondrial morphology in *drp1* mutant FCs results in loss of function phenotypes for oocyte patterning and FC differentiation regulated by the EGFR and Notch pathways (Mitra *et al.* 2012) and the mechanism by which this interaction takes place has not been analyzed. It is not known whether the EGFR pathway affects mitochondrial function by altering ROS generation or mitochondrial membrane potential to result in changes in signaling. Here we study the differential interaction of Ras/ERK with mitochondrial morphology and bioenergetics in the form of ETC activity in *Drosophila* FCs.

4.2 Material and Methods

4.2.1 *Drosophila* genetics

All *Drosophila* crosses were performed in standard cornmeal agar medium at 25^{o}C. The *drp1*^{KG03815}, *erk*^{i}, *ras*^{i}, *pdsw*^{i}, FRT40A/CyO lines were obtained from the Bloomington Stock Center. The *drp1*^{KG03815}FRT40A/CyO, *drp1*^{KG03815} FRT40A/CyO; *erk*^{i}/TM6 and *drp1*^{KG03815}FRT40A/CyO; *ras*^{i}/TM6 stocks were generated using standard genetic crosses.

4.2.2 Generation of FC clones

Procedure to generate MARCM clones has been added in Chapter 2, Materials and Methods section 2.2.2.

4.2.3 Immunostaining of FCs

Protocol followed is same as in Chapter 2, Materials and Methods section 2.2.3. The primary antibodies used were: mouse anti-CycB 1:10 (DSHB), rabbit anti-CycE 1:500 (Santacruz), rabbit anti-Ras 1:200 (Cell Signaling), mouse anti-dpERK 1:200 (Cell Signaling), rabbit anti-p38K 1:200 (Cell Signaling).

4.2.4 Mitochondrial membrane potential CMXRos assay

Please refer to Chapter 3 Materials and Methods section 3.2.5.

4.2.5 Image acquisition and phenotypic estimation in FCs

Same as Chapter 2 Materials and Methods section 2.2.4. Percentage values in the figures with aggregated mitochondria, loss of Ras and dpERK immunostaining, multilayering, mitochondrial morphology and oocyte positioning at the dorsal anterior position are representative of percentage of independent clones showing the defective phenotype. Cytoplasm to nuclear ratio of dpERK was measured by creating a thresholded mask for DNA and cytoplasmic signal and intensity was measured using ImageJ.

4.2.6 Quantification of oocyte nuclear position

The oocyte moves to the dorsal anterior position (away from the antero-posterior axis) at stage 7 in response to EGFR signaling. The oocyte remained at the posterior location when PFCs were mutant for *drp1* or EGFR signaling. If the oocyte was positioned between 0°-10° along the antero-posterior axis drawn in the center of the egg chamber it was considered mislocalized. Oocyte mislocalization is represented as the percentage of chambers with posterior FC clone and lack of oocyte at the dorsal anterior position out of total chambers imaged (schematic in Figure 4.2B).

4.2.7 Estimation of cell numbers per FC clone

Clone cell number count was done as described in Chapter 2, Materials and Methods section 2.2.5.

4.2.8 Image analysis for estimation of fluorescence in FCs

Image analysis was done as reported in Chapter 2, Materials and Methods section 2.2.6.

4.2.9 High resolution imaging of mitochondria

Airyscan imaging and processing were done as written in Chapter 2, Materials and Methods section 2.2.7.

4.3 Results

4.3.1 *drp1*^{KG} mutant PFCs have increased Ras and increased cytoplasmic ERK

We checked the status of EGFR signaling pathway in *drp1*^{KG} mutant cells. Antibodies against Ras and dpERK were used to monitor levels of Ras and activated ERK in *drp1*^{KG} FCs respectively. Ras and dpERK immunostaining was significantly increased in stage 8 *drp1*^{KG} PFCs as compared to background control cells while it was similar to non-GFP cells in FRT40A control (Figure 4.3A-D). In the control we found uniform Ras immunostaining in anterior, main body as well as PFCs (Figure 4.3A). dpERK showed a differential immunostaining pattern in wild type (Figure 4.3C). In *drp1*^{KG} FCs, Ras increase was seen on the plasma membrane and this has been correlated previously with increased active GTP bound Ras (Arozarena *et al.* 2000). This is also in accordance with increased dpERK. The activated ERK however was both cytoplasmic and nuclear in localization in *drp1* mutant PFCs at stage 8 in contrast to primarily nuclear in control FRT40A cells (Figure 4.3C, E). The increase in cytoplasmic dpERK as compared to background control cells was also seen at stage 2-5 (Figure 4.3F-G). The increase in dpERK in *drp1* mutant also correlated with depletion of aPKC as compared to Dlg in the clone cells at stage 3 and stage 7 (Figure 2.6A-C, Chapter 2). Depletion of active ERK and EGF signaling is required for stability of apical markers in prefollicle cells (Castanieto *et al.* 2014). Moleskin is the nuclear importer of ERK in *Drosophila* S2 cells. In the *Drosophila* eye, dpERK is restricted in the cytoplasm, thus inhibiting activation of its nuclear targets (Lorenzen *et al.* 2001). Moleskin downregulation can be used to deplete nuclear dpERK and check if it phenocopies *drp1* mutant.

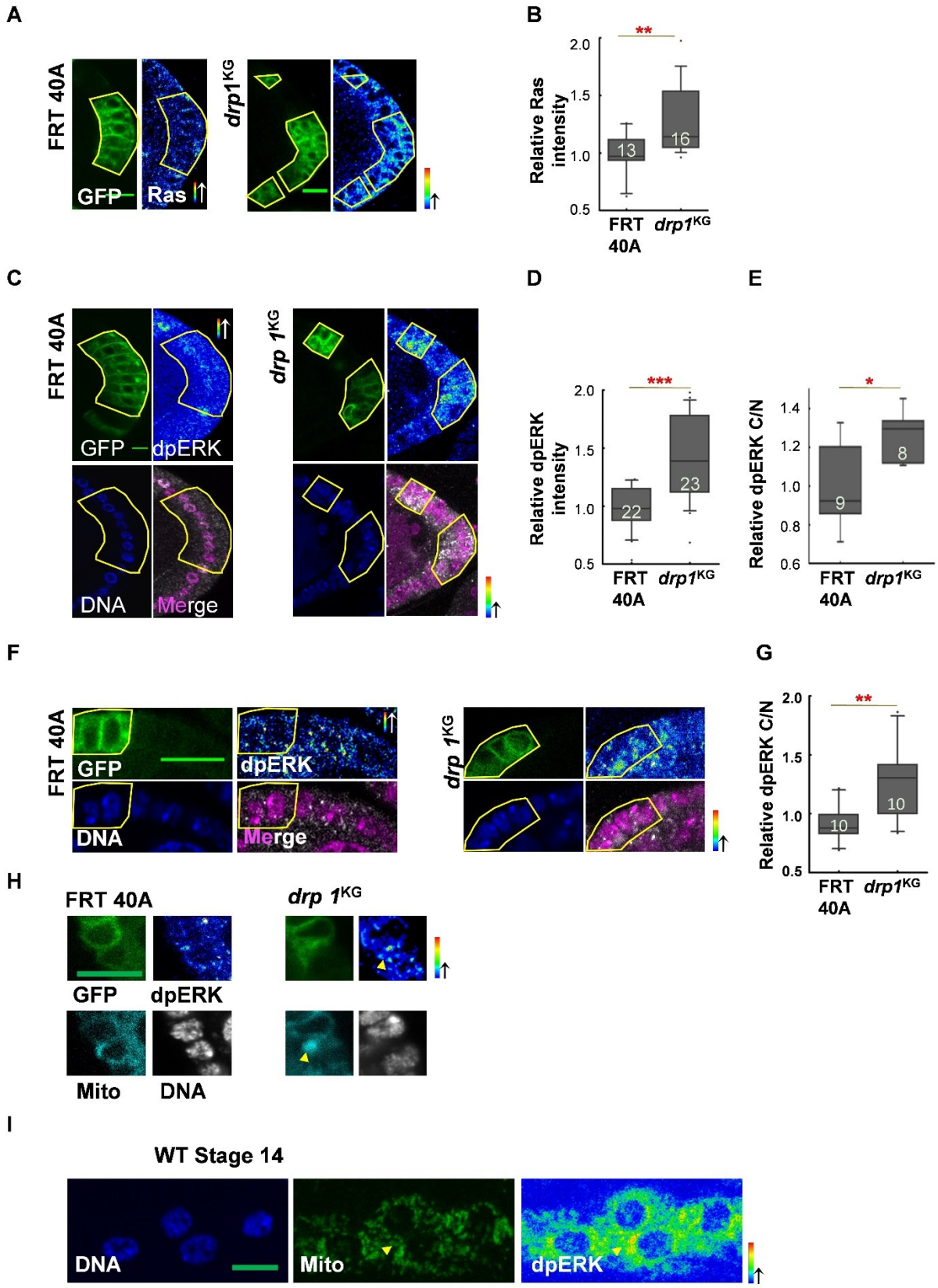
A
FRT 40A
GFP
Ras
drp1KG
B
Relative Ras intensity
**
2.0
1.5
1.0
0.5
13
16
FRT 40A
drp1KG
C
FRT 40A
GFP
dpERK
DNA
Merge
drp 1KG
D
Relative dpERK intensity
***
22
23
E
Relative dpERK C/N
*
9
8
F
G
Relative dpERK C/N
**
10
10
H
FRT 40A
drp 1KG
GFP
dpERK
Mito
DNA
I
WT Stage 14
DNA
Mito
dpERK

Figure 4.3. *drp1*^{KG} cells have increased Ras and activated ERK in the cytoplasm. (A-B) Ras immunostaining (pseudocolour; where red represents highest intensity pixels and blue the lowest) is increased on the membrane in *drp1*^{KG} cells (CD8GFP; green) as compared to neighboring control cells (A). Quantification also shows that FRT 40A has ratio equal to 1, that is GFP and non-GFP are similar, while *drp1*^{KG} cells have ratio higher than 1 (B) (n=13, 16, N=3, **, P≤0.01, two tailed Mann-Whitney test).
(C-E) *drp1*^{KG} PFCs have higher dpERK (pseudocolour; where red represents highest intensity pixels and blue the lowest), and it is concentrated in the cytoplasm, while it is mainly nuclear (DNA; blue, magenta in merge) in FRT 40A cells (C). (D) shows quantification of increased dpERK in *drp1*^{KG} cells in comparison to FRT 40A (n=22,23, N=4, ***, P≤0.001, two tailed Mann-Whitney test) and (E) depicts elevated cytoplasm: nuclear ratio in the *drp1*^{KG} mutant (n= 9,8, N=3, *, P≤0.05, two tailed Mann-Whitney test).
(F-G) Early stages also show dpERK enrichment in the cytoplasm. dpERK is enhanced in the cytoplasm in the *drp1*^{KG} FCs (F), and cytoplasm: nuclear ratio is higher for *drp1*^{KG} cells than FRT 40A (G, n=10,10, N=3, **, P≤0.01, two tailed Mann-Whitney test).
(H-I) dpERK is localized on the mitochondria in *drp1*^{KG} FCs. dpERK signal (pseudocolour; where red represents highest intensity pixels and blue the lowest) overlaps (marked by yellow arrowhead) with mitochondrial signal (cyan) in the *drp1*^{KG} stage 8 mutant (CD8GFP; green, DNA; grey) FRT 40 A does not show dpERK localization on the mitochondrial signal (H). Wild type (DNA; blue) has sharp mitochondrial localization (green) of dpERK (pseudocolour; where red represents highest pixels and blue lowest) (marked by yellow arrow heads) in stage 14 cells (I).
Data is presented as box plots where horizontal bar represents mean, box limits 25th and 75th percentiles, whiskers 10th and 90th percentiles and dots are observations outside 10th and 90th percentiles. Numbers within the box represent number of data points (n). Each data point in the box plot is an average from 5-30 cells. ns= not significant, Scale Bar: 10μm. n=FC clones in independent ovarioles, N=Experimental replicates.

A number of proteins are known to localize on the mitochondria. For example, BARD1 which is an apoptosis inducing factor, binds p53 on mitochondrial membrane (Tembe *et al.* 2015). Localization of apoptotic proteins help in fragmentation and subsequent release of Cytochrome C. Atypical cadherin Fat has been shown to be imported into mitochondria and control metabolism via interaction with Complex I

proteins (Sing *et al.* 2014). EGFR is also known to localize to mitochondrial outer membrane. It binds COXII protein and modulates ETC (Boerner *et al.* 2004). Increased localization of ERK in the cytoplasm in *drp1*^{KG} mutant as opposed to nuclear in WT prompted us to check if even within the cytoplasm, there is an enrichment of ERK on the mitochondria. Indeed there was such an enrichment of ERK on fused mitochondrial fraction (Figure 4.3H-I). Surprisingly while stage 1-10 wild type does not show mitochondrial enrichment of ERK, stage 14 cells have distinct ERK signal overlap with the mitochondria (Figure 4.3J). The mitochondrial fraction of ERK should be further analyzed by isolating mitochondria in suspension and probing for ERK by immunoblotting. Thus, fused mitochondria result in enrichment of Ras on the membrane and ERK in the cytoplasm in *drp1* mutant cells.

4.3.2 *drp1*^{KG} mutation leads to oocyte localization defect

Since we found Ras/ERK enriched in the *drp1*^{KG} we wanted to check the impact of this enrichment on the pathway. EGFR pathway is responsible for oocyte migration to dorso-anterior position in Stage 8 ovariole chamber. Even though the *drp1*^{KG} PFCs had elevated Ras and dpERK levels, the oocyte failed to migrate to the dorso-anterior position by stage 8 showing a loss of EGFR pathway mediated oocyte patterning (Figure 4.4A). A similar phenotype of dpERK accumulation and loss of oocyte patterning is also seen in polarity mutants of *scrib* and *dlg* (Li *et al.* 2009). This can be because of confinement of dpERK in the cytoplasm and subsequent loss of EGFR signaling dependent oocyte migration in *drp1* mutant PFCs. aPKC regulates Lgl and Par-1 proteins to direct microtubule organisation, which in turn is required for proper positioning of the oocyte (Tian and Deng, 2008). Hence loss of aPKC can also be responsible for oocyte mispositioning in the *drp1*^{KG} mutant.

Oocyte positioning is known to be guided by DE-Cadherin levels in the germline and FCs (Godt and Tepass 1998). We overexpressed DE-Cadh in the *drp1*^{KG} mutant background and found that the oocyte always positioned itself adjacent to the clone (Figure 4.4B). This points towards an intact microtubule network in *drp1*^{KG} mutant and

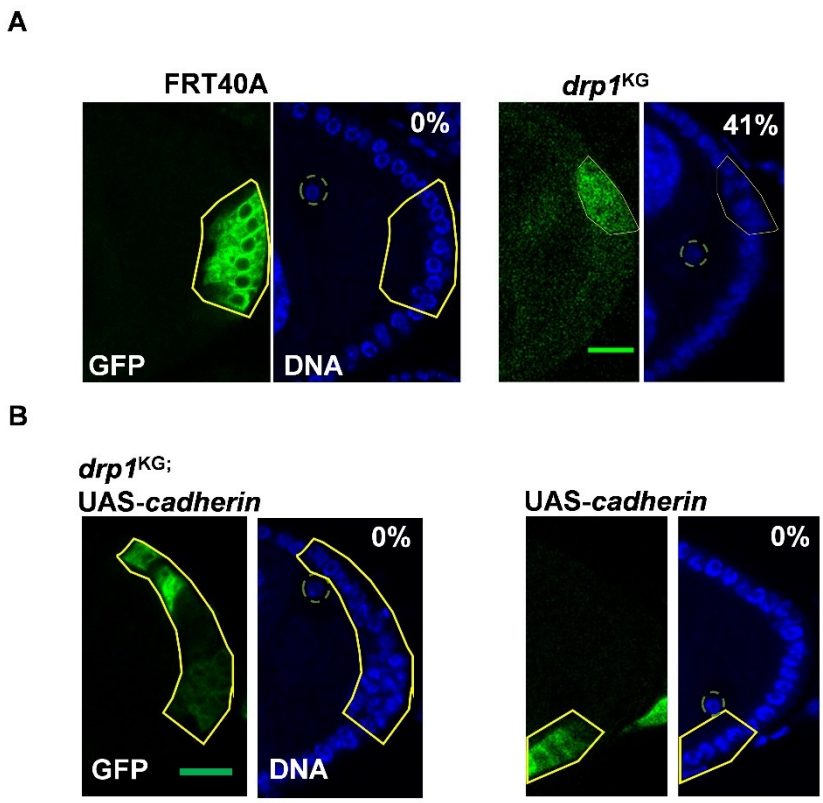

Figure 4.4. Oocyte is mislocalized to center in *drp1*^{KG} mutant. (A-B) Mislocalized oocyte in *drp1*^{KG} chambers is rescued by DE-cadherin overexpression. Oocyte (DNA; blue; marked by orange circle) in the control (FRT 40A, 0% mislocalization, n=40, N=3) is in the dorso-anterior position. *drp1*^{KG} mutant (CD8GFP;green) has oocyte in centre (41% mislocalization, n=47, N=3) (A). Overexpression of DE-cadherin in the *drp1*^{KG} background shifts the oocyte adjacent to the clone (B, 0% oocyte mislocalized, n=25, N=2). DE-cadherin overexpression alone as well positions the oocyte next to the clone (C, 0% oocyte localization defect, n= 12, N=2).
Scale Bar:10μm. n=FC clones in independent ovarioles, N=Experimental replicates.

the lack of ERK nuclear signal is perhaps overcome by overexpression of DE-Cadherin in the PFCs. Consequently positioning the oocyte along the site of increased Cadherin. FC clone for a functional null allele of EGFR show loss of Cadherin in Stage 2 FCs (Castanieto et. al., 2014). However, no defect was seen in Cadherin immunostaining in Stage 8 in *drp1*^{KG} mutant (Chapter 2, Figure 2.6F-G). In summary, increase in ERK levels failed to bring about oocyte positioning and this argued for its nuclear localisation downstream of EGFR being necessary for oocyte patterning.

4.3.3 Increased Ras/ERK are responsible for multilayering and reduced cell number in *drp1*^{KG} mutant cells

Ras/ERK control cell numbers via regulation of cell proliferation (Buchon *et al.* 2010). FC number is mainly controlled by polyhomeotic and hedgehog (Forbes *et al.* 1996; Narbonne *et al.* 2004). ERK1/2 is shown to promote proliferation in mouse FCs under hormonal stimulation (Babu *et al.* 2000).

In order to check if *drp1*^{KG} cell number defects were because of Ras/ERK accumulation, we used RNAi against Ras (*ras*^{i}) and ERK (*erk*^{i}). As expected, Ras and dpERK antibody staining were depleted in PFCs expressing *ras*^{i} and *erk*^{i} respectively (Figure 4.5A). The *ras*^{i} lowered but did not completely deplete Ras antibody. Increased number of PFC clones were in a single layer in the *drp1*^{KG}; *ras*^{i} and *drp1*^{KG}; *erk*^{i} as compared to *drp1*^{KG} (Figure 4.5B). Similar rescue is seen when multilayering induced by loss of polarity in Scribbled mutants is rescued by pharmacological ERK inhibition in mammary duct (Godde *et al.* 2014). In a complementary study, depletion of apical polarity protein, Par-3 enhances tumorigenesis in Ras overexpression (Mccaffrey *et al.* 2012). Hence increased Ras/ERK in *drp1*^{KG} leads to the multilayering defect.

Depletion of *ras* and *erk* alone, like *drp1*^{KG} showed decreased clone cell numbers and this defect was reversed with the clone size returning to control levels in the combination clones (Figure 4.5C). The decrease in cell numbers in *ras*^{i} is similar to Ras null mutant clones observed previously (James *et al.* 2002). The reversal was on account of rescue in mitotic stages as the cell number increased in stage 3-5 *drp1*^{KG}; *ras*^{i} and *drp1*^{KG}; *erk*^{i} clones (Figure 4.5D-E). The loss of cells per clone in *ras*^{i} and *erk*^{i} is consistent with the requirement of the EGFR-Ras-ERK pathway for establishment of polarity in FSCs (Castanieto *et al.* 2014) and the reversal of multilayering suggested that increased Ras/ERK in *drp1*^{KG} PFCs was a possible cause of these phenotypes. Hence activated EGF signaling manifested as increased Ras/ERK in *drp1* mutant PFCs was responsible for decreased numbers.

We next checked for the oocyte mislocalization defect in the combination clones. As expected, loss of oocyte migration was also seen in *erk*^{i} alone and *drp1*^{KG}; *erk*^{i} even though all other mutant phenotypes of *drp1*^{KG} PFCs were reversed (Figure 4.5F).

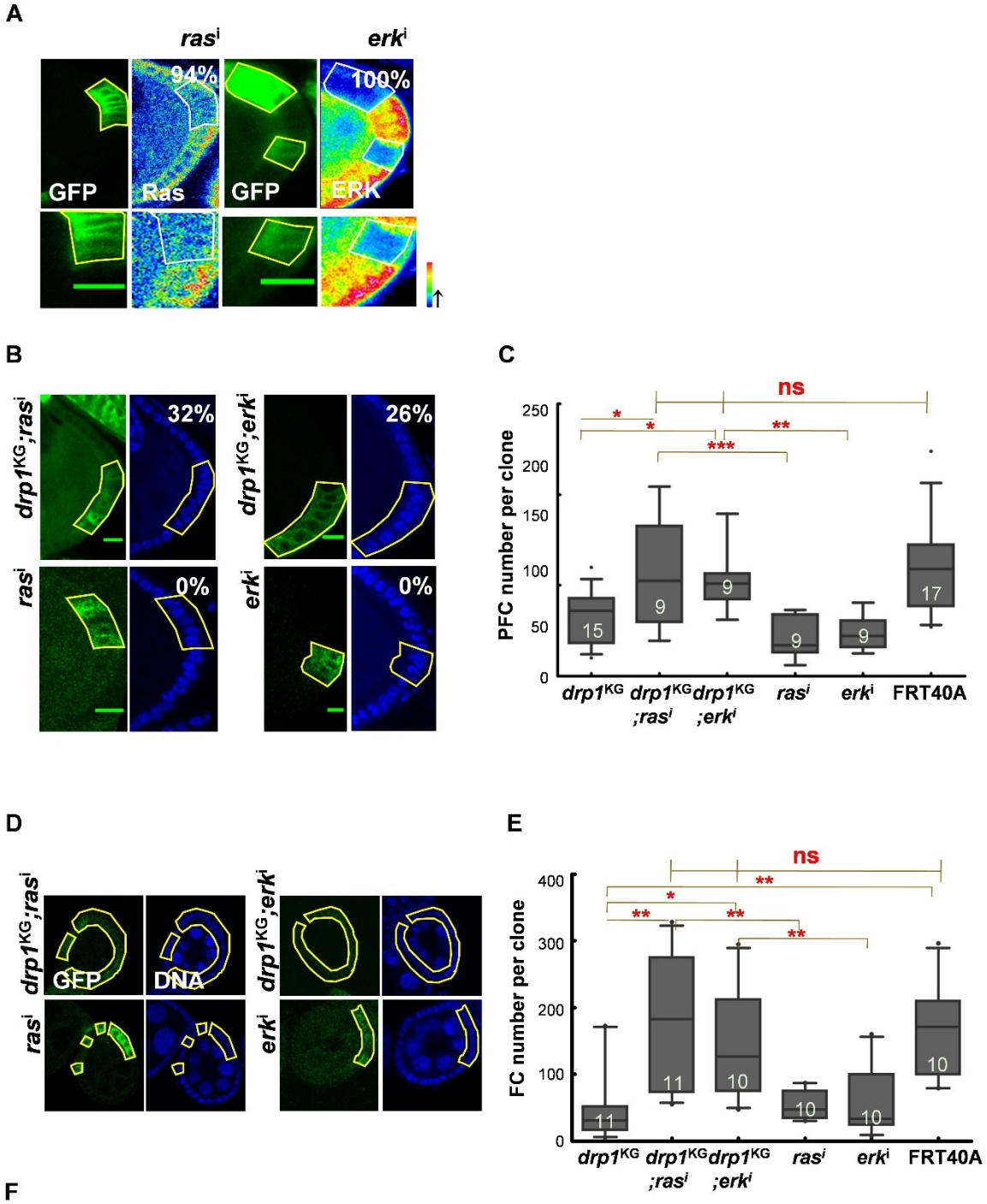
A
ras^i
erk^i
94%
100%
GFP
Ras
GFP
ERK
B
drp1^KG;ras^i
32%
drp1^KG;erk^i
26%
ras^i
0%
erk^i
0%
C
ns
*
*
**
***
PFC number per clone
250
200
150
100
50
0
15
9
9
9
9
17
drp1^KG
drp1^KG ;ras^i
drp1^KG ;erk^i
ras^i
erk^i
FRT40A
D
drp1^KG;ras^i
GFP
DNA
drp1^KG;erk^i
ras^i
erk^i
E
ns
**
*
**
**
**
FC number per clone
400
300
200
100
0
11
11
10
10
10
10
drp1^KG
drp1^KG ;ras^i
drp1^KG ;erk^i
ras^i
erk^i
FRT40A
F
drp1^KG;erk^i
erk^i
39%
31.5%
GFP
DNA

Figure 4.5. Ras/ERK downregulation rescues multilayering and cell number defect but not oocyte localization. (A) *ras*^{i} clone (CD8GFP;green) shows slight depletion of Ras antibody (pseudocolour; where red represents highest intensity pixels and blue the lowest) (94%, n=16, N=2), while *erk*^{i} shows complete loss of pERK antibody (pseudocolour; where red represents highest intensity pixels and blue the lowest) (100%, n=15, N=2) (A).
(B-E) Depletion of Ras/ERK relieves cell number and multilayering defect in *drp1*^{KG} mutant. *drp1*^{KG}; *ras*^{i} (32% multilayered, n=62, N=3) and *drp1*^{KG}; *erk*^{i} mutant (26% multilayered, n=62, N=3) are not multilayered. *ras*^{i} and *erk*^{i} exhibit normal tissue morphology (*ras*^{i} (0% multilayered, n= 21, N=3) and *erk*^{i} (0% multilayered, n=24, N=3)) (B). Cell number (DNA;blue) in clones is comparable to FRT 40A (CD8GFP;green) in *drp1*^{KG} ; *ras*^{i} and *drp1*^{KG} ; *erk*^{i} mutant. *ras*^{i} and *erk*^{i} proliferate less alone and hence the cell number is low (C, n=15,9,9,9,9,17,N=3, *, P≤0.05, **, P≤0.01, ***, P≤0.001, two tailed Kruskal Wallis, Dunn's test). Early stage clones of *ras*^{i} and *erk*^{i} also rescue *drp1* mutant (D). Quantification in (E, n=11, 11, 10, 10, 10, 10, N=3, *, P≤0.05, **, P≤0.01, ***, P≤0.001, two tailed Kruskal Wallis, Dunn's test).
(F) Oocyte mislocalization is not rescued by *erk* depletion. Oocyte (DNA; blue, marked by orange circle) is mislocalized in *drp1*^{KG}; *erk*^{i} and *erk*^{i} alone (F, *drp1*^{KG}*; erk*^{i} (39% mislocalized, n=62, N=3) and *erk*^{i} (31.5% mislocalized, n=24, N=3)).
Data is presented as box plots where horizontal bar represents mean, box limits 25th and 75th percentiles, whiskers 10th and 90th percentiles and dots are observations outside 10th and 90th percentiles. Numbers within the box represent number of data points (n). Each data point in the box plot is an average from 5-30 cells. ns=not significant, Scale Bar: 10µm. n=FC clones in independent ovarioles, N=Experimental replicates.

4.3.4 Ras/ERK depletion reverses mitochondrial morphology in *drp1* mutant FCs

EGFR loss of function causes mitochondrial aggregation in PFCs (Mitra *et al.* 2012) and ERK activates Drp1 by phosphorylation to cause fragmentation in cancer cells (Kashatus *et al.* 2015). ERK depletion in the genetic null *drp1*^{KG} PFCs reversed phenotypes of PFC numbers and organization. Hence we tested if ERK depletion could result in these changes due to an impact on mitochondrial morphology even in the absence of *drp1*. We visualized mitochondrial morphology in *drp1*^{KG} PFCs additionally depleted of ERK. The aggregated mitochondrial phenotype in the *drp1*^{KG}; *ras*^{i} and the

drp1^{KG}; *erk*^{i} combination was reversed as compared to *drp1*^{KG} PFCs with mitochondria present on both sides of the nucleus (Figure 4.6A-E). In order to observe mitochondrial morphology at a higher resolution, we used the super resolution Airyscan detector and saw that the aggregated mitochondrial morphology was reverted and the mitochondrial organization was indistinguishable from the surrounding control cells (Figure 4.6F). Even though *erk*^{i} and *ras*^{i} alone did not have an appreciable impact on mitochondrial organisation in PFCs, mitochondrial organization and morphology were reverted similar to control in cells depleted of both *drp1* and *ras*/*erk.*

4.3.5 ERK depletion decreases mitochondrial membrane potential in *drp1* mutant FCs but does not alter high ROS in *drp1* mutant

We next assessed if ERK depletion also changed the mitochondrial membrane potential in PFCs. PFCs containing the *drp1*^{KG}; *erk*^{i} combination had decreased CMXRos fluorescence as compared to the background control cells (Figure 4.7A-B). *Egfr*^{DN} expression also lowered the membrane potential in *drp1*^{KG} PFCs. Moreover, ERK depletion alone also lowered the mitochondrial membrane potential as compared to control cells (Figure 4.7A-B). Ras depletion did not show a significant change in mitochondrial membrane potential alone or in combination with *drp1*^{KG} (Figure 4.7A-B).

A significant change was not found in DHE fluorescence in *drp1*^{KG}; *erk*^{i} and *drp1*^{KG}; *ras*^{i} combination as compared to *drp1*^{KG} clones (Figure 4.7C-D). Hence increased ROS in *drp1*^{KG} is not interacting with the EGFR pathway kinases in this tissue.

These data together showed that EGFR pathway inhibition by *Egfr*^{DN} and *erk* RNAi reversed the elevated mitochondrial membrane potential in *drp1* mutant PFCs and interestingly *erk* depletion alone also reduced the mitochondrial membrane potential. Since Ras/ERK loss did not change mitochondrial morphology appreciably as compared to EGFR dominant negative (Mitra *et al*. 2012), the EGFR pathway may regulate mitochondrial morphology independent of Ras/ERK. In order to check if EGFR regulates mitochondrial morphology via PI3K, we checked for depletion and activation of PI3K in the FCs using *e22c*-Gal4. However, there was no alteration in morphology (Figure

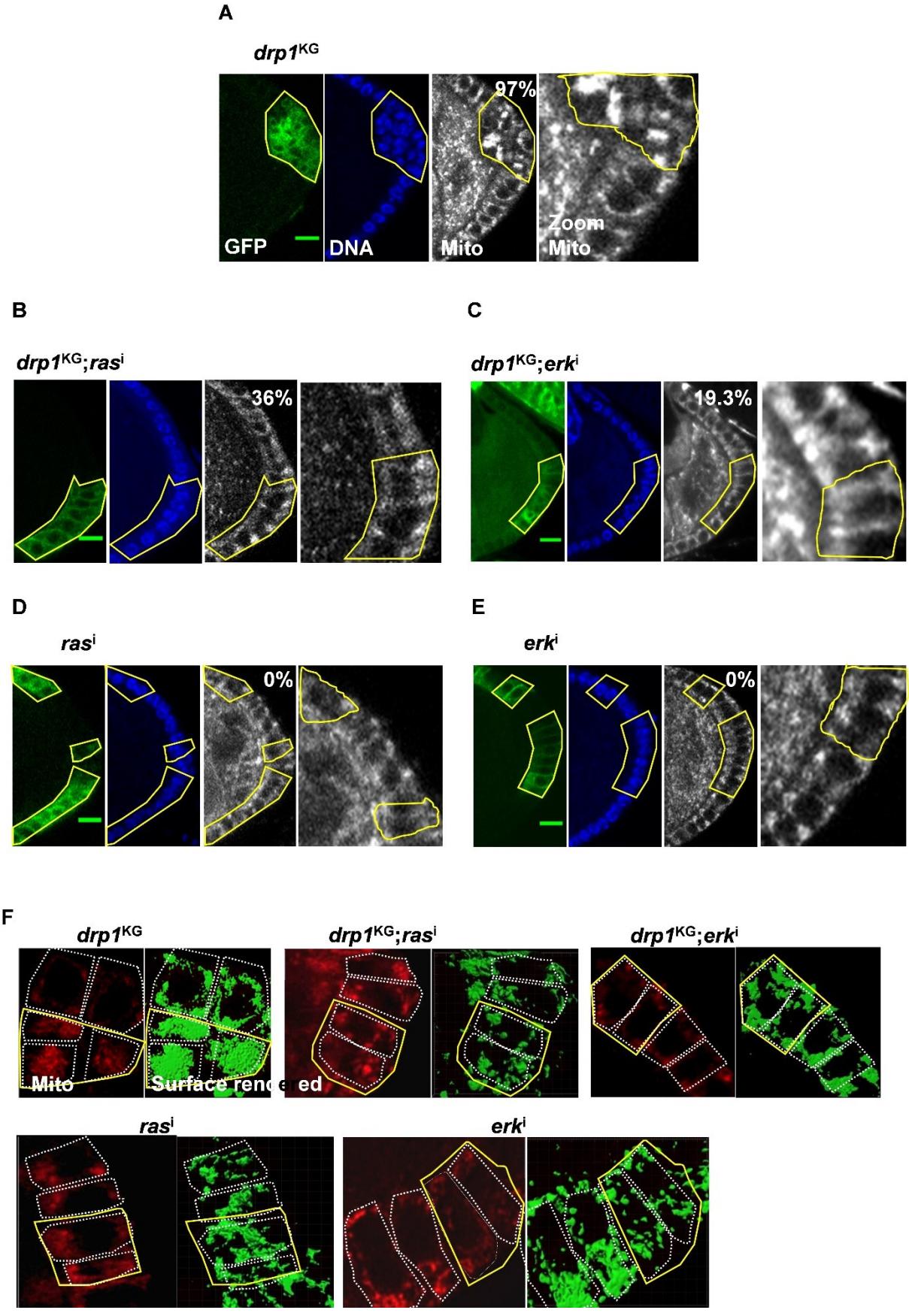
A
drp1KG
97%
GFP
DNA
Mito
Zoom
Mito
B
drp1KG;rasi
36%
C
drp1KG;erki
19.3%
D
rasi
0%
E
erki
0%
F
drp1KG
drp1KG;rasi
drp1KG;erki
Mito
Surface rendered
rasi
erki

Figure 4.6. Aggregated mitochondrial morphology is reverted by *drp1*^{KG}; *ras*^{i} and *drp1*^{KG}; *erk*^{i}. (A-F) Mitochondria (grey) are aggregated in *drp1*^{KG} clones (CD8GFP;green, DNA; blue) (A). Mitochondria recover the dispersed morphology in majority of *drp1*^{KG}; *ras*^{i} and *drp1*^{KG}; *erk*^{i} and appear similar to background control cells (B-C). Mitochondria are dispersed in *ras*^{i} and *erk*^{i} and do not show any difference in distribution from non-GFP control cell mitochondria (D-E) (% aggregation depicted in each panel, n=47, 62, 62, 24, 21, N=3 for all). (F) Airyscan images also show compact mitochondrial network in *drp1*^{KG} and it is dispersed in when Ras/ERK are depleted in the background. *ras*^{i} and *erk*^{i} also show dispersed mitochondria at this resolution (F).
Scale Bar: 10 µm. n=FC clones in independent ovarioles, N=Experimental replicates.

4.7E). It is possible that a combination of PI3K and ERK maintain mitochondrial shape and loss of one compensates for the other. However, we were not able to check PI3K and ERK depletion doubles to test the hypothesis. Also other unknown effectors downstream of EGFR can be involved.

4.3.6 Elevated mitochondrial membrane potential does not affect ERK accumulation and loss of EGF signaling in *drp1* mutant PFCs

Since ERK depletion in *drp*1^{KG} mutant PFCs reduced the mitochondrial membrane potential, we used *pdsw*^{i} and FCCP to assess the effect of membrane potential loss on the EGF pathway. Even though the mitochondrial membrane potential was lowered in *drp*1^{KG}; *pdsw*^{i}, the multilayering phenotype and mitochondrial aggregation phenotype remained unchanged (Figure 4.8A). The *pdsw* mutant reduces cell number in the larval eye imaginal disc due to cell cycle arrest (Owusu-Ansah *et al.* 2008). We observed a similar decrease in PFC numbers in *pdsw*^{i} and the *drp1*^{KG}; *pdsw*^{i} combination (Figure 4.8B).

Further EGFR signaling was analysed in *pdsw*^{i} and *drp1*^{KG}; *pdsw*^{i} PFCs. The oocyte patterning defect was not alleviated in mitochondrial membrane potential depleted *drp1*^{KG}; *pdsw*^{i} combination mutant PFCs (Figure 4.8C). In addition, *drp1*^{KG}; *pdsw*^{i} combination failed to rescue increased dpERK in the *drp1* mutant cells (Figure 4.8D-E) as compared to *drp1*^{KG}. Also an acute FCCP treatment to disrupt

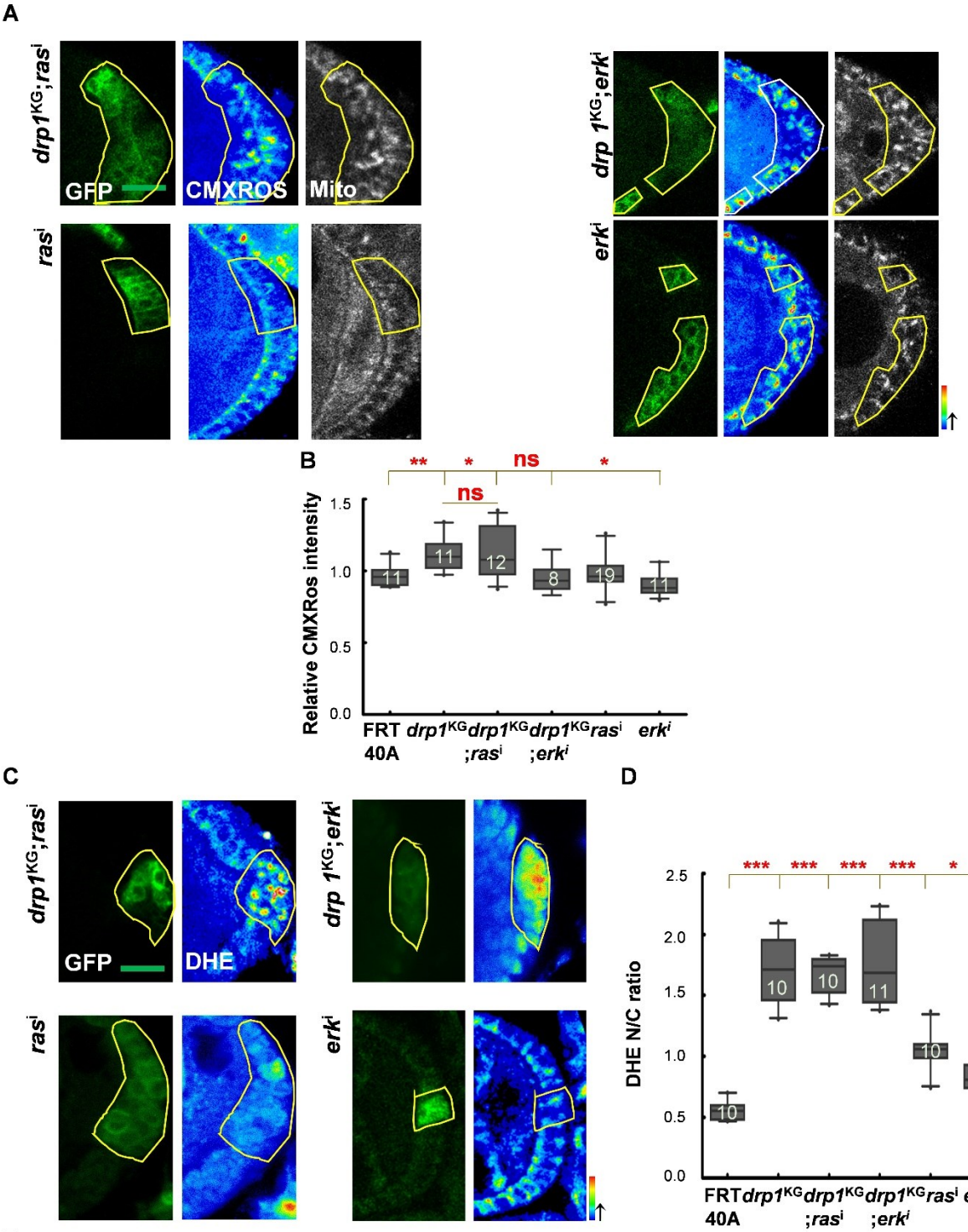
A
drp1KG;rasi
GFP
CMXROS
Mito
rasi
drp 1KG;erki
erki
B
Relative CMXRos intensity
1.5
1.0
0.5
0.0
**
*
ns
ns
*
11
12
8
19
11
FRT 40A
drp1KG ;rasi
drp1KG ;erki
drp1KG rasi
erki
C
drp1KG;rasi
GFP
DHE
drp 1KG;erki
rasi
erki
D
DHE N/C ratio
2.5
2.0
1.5
1.0
0.5
0.0
***
***
***
***
*
10
10
11
10
12
FRT 40A
drp1KG ;rasi
drp1KG ;erki
drp1KG rasi
erki
E
e22c; +
e22c; pi3kDN
e22c; pi3ki
0%
0%
0%
DNA
Mito
Zoom

Figure 4.7. ERK accumulation results in increased mitochondrial membrane potential in *drp1*^{KG}. (A-B) ERK depletion in *drp1*^{KG} background rescues the mitochondrial membrane potential. Increased mitochondrial membrane potential (pseudocolour; where red represents highest intensity pixels and blue lowest) is reverted in *drp1*^{KG}; *erk*^{i}. *erk*^{i} also has lower mitochondrial membrane potential than FRT 40A control cells. Ras downregulation does not rescue the mitochondrial membrane potential in *drp1*^{KG} cells (A). Quantification in (B, n=11, 11, 12, 8, 19, 11, N=3, *, P≤0.05, **, P≤0.01, two tailed Mann-Whitney test).
(C-D) Increased ROS is not rescued by Ras/ERK depletion in *drp1*^{KG} mutant. DHE fluorescence (pseudocolour; where red represents highest intensity pixels and blue the lowest) is higher than background cells in *drp1*^{KG}; *erk*^{i} and *drp1*^{KG}; *ras*^{i}. *erk*^{i} and *ras*^{i} have slightly increased ROS than control cells (C). Quantification shows nuclear: cytoplasm ratio is high in *drp1*^{KG}; *erk*^{i}, *drp1*^{KG}; *ras*^{i}, *erk*^{i} and *ras*^{i} than FRT 40A (D, n=10, 10, 10, 11, 10, 12, N=2, *, P≤0.05, P≤0.001, two tailed Mann-Whitney test).
(E) *pi3k* downregulation does not alter mitochondrial morphology. Mitochondria are dispersed in *pi3k*^{i} and *pi3k*^{DN} driven by *e22c*-Gal4 and do not show any difference in morphology (E, Zoom of yellow inset, 0% defect in mitochondrial morphology, n=25 for all, N=2).
Data is presented as box plots where horizontal bar represents mean, box limits 25th and 75th percentiles, whiskers 10th and 90th percentiles and dots are observations outside 10th and 90th percentiles. Numbers within the box represent number of data points (n). Each data point in the box plot is an average from 5-30 cells. ns=not significant, Scale Bar: 10μm. n=FC clones in independent ovarioles, N=Experimental replicates.

mitochondrial membrane potential in *drp1*^{KG} or wild-type ovarioles at stage 8 did not alter dpERK immunostaining. Thus mitochondrial membrane potential decrease in *pdsw*^{i} was not able to remove dpERK accumulation and change the loss of EGF signaling in *drp1*^{KG} PFCs.

4.4 Discussion

EGFR pathway interacts with mitochondria in *Drosophila* FCs via Ras/ERK (Figure 4.9A). We found that localisation of dpERK determines the function of the protein in FCs. It has already been shown to have differential output depending on its localisation

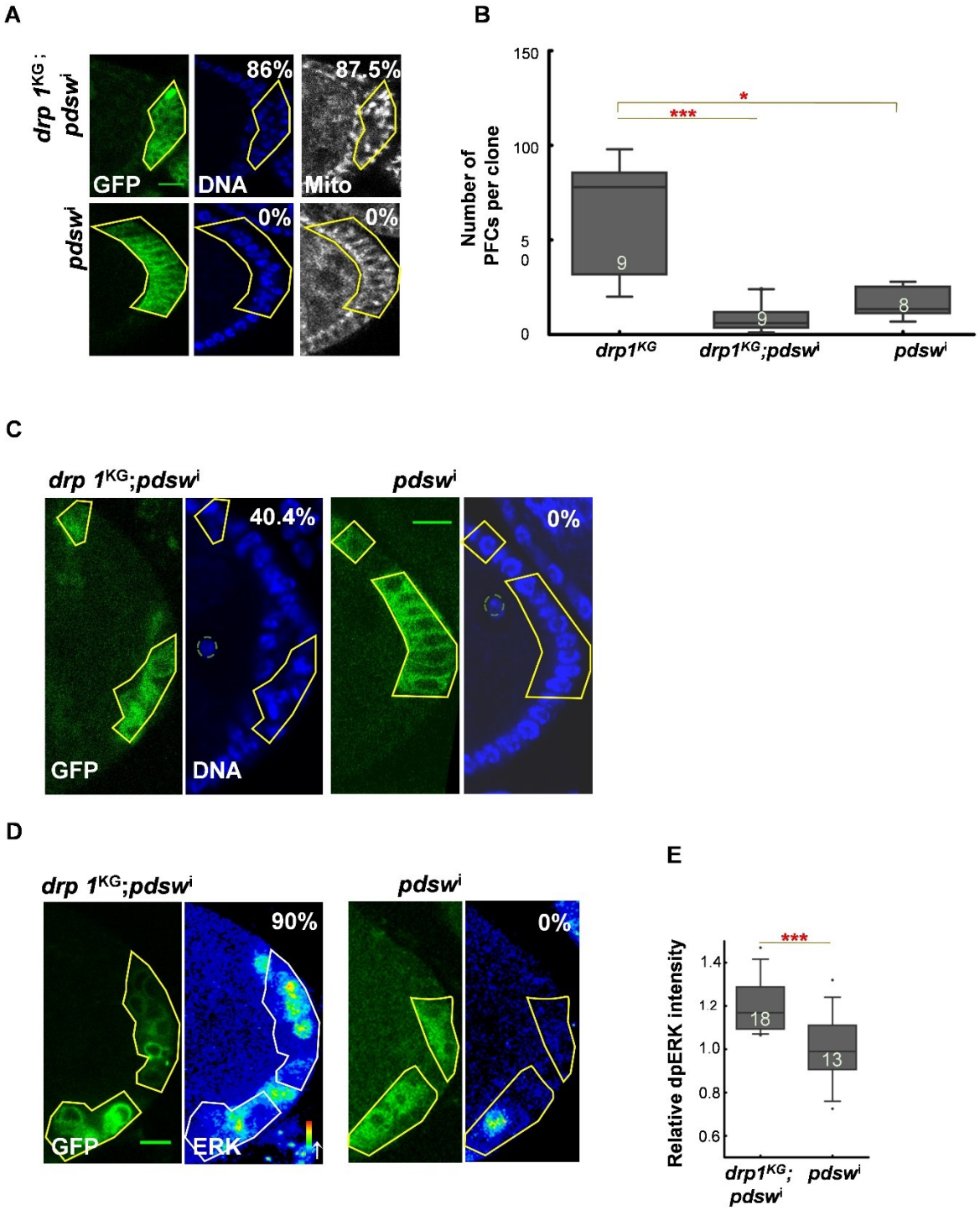

Figure 4.8. Decrease in mitochondrial membrane potential does not affect EGFR pathway. (A-B) Downregulation of *pdsw* does not rescue multilayering, mitochondrial morphology and cell number defect in *drp1*^{KG}. *drp1*^{KG}*; pdsw*^{i} has multilayering (86% multilayered chambers) (DNA;blue) and aggregated mitochondria (grey, 87.5%

aggregated mitochondria, n=47, N=3) similar to *drp1*^{KG}*; pdsw*^{i} does not exhibit change in mitochondrial morphology at this resolution (A). Cell number is further lowered *drp1*^{KG}*; pdsw*^{i} in and *pdsw*^{i} (B, n=9, 9, 8, N=3, *, P≤0.05, ***, P≤0.001, two tailed Kruskal Wallis test and Dunn's test).

(C-E) Oocyte mislocalization and increased dpERK are not reverted in the double *drp1*^{KG}*; pdsw*^{i}. *drp1*^{KG}*; pdsw*^{i} has central oocyte (Orange dashed circle) (40.4% mislocalization, n=47, N=3) while *pdsw*^{i} does not have a defect in the oocyte positioning (0% mislocalization, n=25, N=3) (C). dpERK immunostaining is higher in *drp1*^{KG} *; pdsw*^{i} similar to *drp1*^{KG} while *pdsw*^{i} does not show dpERK accumulation (D). Quantification in (E) shows the increased dpERK immunostaining in *drp1*^{KG}*; pdsw*^{i} as compared to *pdsw*^{i} (n=18, 13, N=3, ***, P<0.001, two tailed Mann- Whitney test).

Data is presented as box plots where horizontal bar represents mean, box limits 25th and 75th percentiles, whiskers 10th and 90th percentiles and dots are observations outside 10th and 90th percentiles. Numbers within the box represent number of data points (n). Each data point in the box plot is an average from 5-30 cells. ns= not significant, Scale Bar: 10µm. n= FC clones in independent ovarioles, N= Experimental replicates.

in the cell during wing development (Marenda *et al.* 2006). dpERK shows a predominant nuclear staining in wild-type as opposed to cytoplasmic in *drp1*^{KG} PFCs and increased cytoplasmic retention is a possible way for failure of signaling and oocyte mislocalization to a posterior position in *drp1*^{KG} mutants. Cytoplasmic ERK can dimerize and activate different cytoplasmic substrates (Ebisuya 2005; Casar *et al.* 2008) and result in modification of the mitochondrial activity (Monick *et al.* 2008). While activated ERK enters the nucleus to promote gene expression, it can also be enriched in the cytoplasm or organelles such as mitochondria (Horbinski and Chu 2005). Activated ERK is seen in mitochondria during brain development (Alonso *et al.* 2004). Fused mitochondria in the *drp1* mutant cells may act as docking platform for activated ERK (Duarte *et al.* 2014) and retain it outside the nucleus. A study to understand if different proteins decorate a fused/fragmented mitochondria is required. This can help in answering what attracts ERK to the mitochondrial surface. We have made point mutants of predicted ERK phosphorylation target sites on Drp1 and Marf. These can help in understanding if ERK interacts with Drp1 and Marf via phosphorylation in the FCs (Appendix A2).

ERK regulates cellular energy demands via insulin pathway in *Drosophila* eye (Zhang *et al.* 2011). We found that EGFR via ERK is upstream of mitochondrial membrane potential in *Drosophila* FCs. Accumulation of activated ERK in the cytoplasm may directly interact with the mitochondrial ETC proteins and increase the mitochondrial membrane potential. On the other hand, an impact of ERK on other signaling molecules can also mediate mitochondrial energetics. Another question which arises is if the control is transcriptional or post translational. In 2008, a study looked at the effect of growth signal on mitochondrial efficiency. They found that increase in membrane potential is higher for region of mitochondrial network closer to site of ligand-receptor binding. This change in mitochondrial membrane potential was abolished on depletion of MAPK signal (Verburg and Hollenbeck, 2008). Drug based experiments can help answer some of these questions and offer insight into how fast and sensitive EGFR-Ras-ERK regulation of mitochondrial attributes is. Thus EGFR can regulate mitochondrial morphology (Mitra *et al.* 2012) and EGFR-Ras-ERK maintain mitochondrial membrane potential in a state of equilibrium in wild type animals.

ROS is known to interact and activate phosphatases in the cell leading to repression of kinases under specific signaling. It is usually suspected as the prime culprit when ERK pathway is abrogated in a mitochondrial mutant. We were not able to find phenotype which can be attributed to the increased ROS. It is possible that the PFCs are robust to changes in ROS levels during development. FSCs respond to increase in ROS due to mitochondrial dysfunction. The FSC number decreases in *pdsw*^{i} due to activation of JNK via ROS (Wang et. al., 2012). Further experiments with drugs such as paraquat can perhaps help understand role of ROS in *Drosophila* ovary development.

EGFR signaling through Ras/MEK/ERK is important for basal polarity in FSCs (Castanieto *et al.* 2014). pERK activates the LKB-pAMPK pathway to induce basal polarity and suppress apical polarity in these cells. It is likely that cytoplasmic increase of pERK and pAMPK in *drp1* depleted FCs decreases apical polarity by reduction of aPKC and results in multilayering. It is also possible that sustained increase of pERK in *drp1* mutant cells and an altered cell cycle along with loss of apical polarity lowers the

A

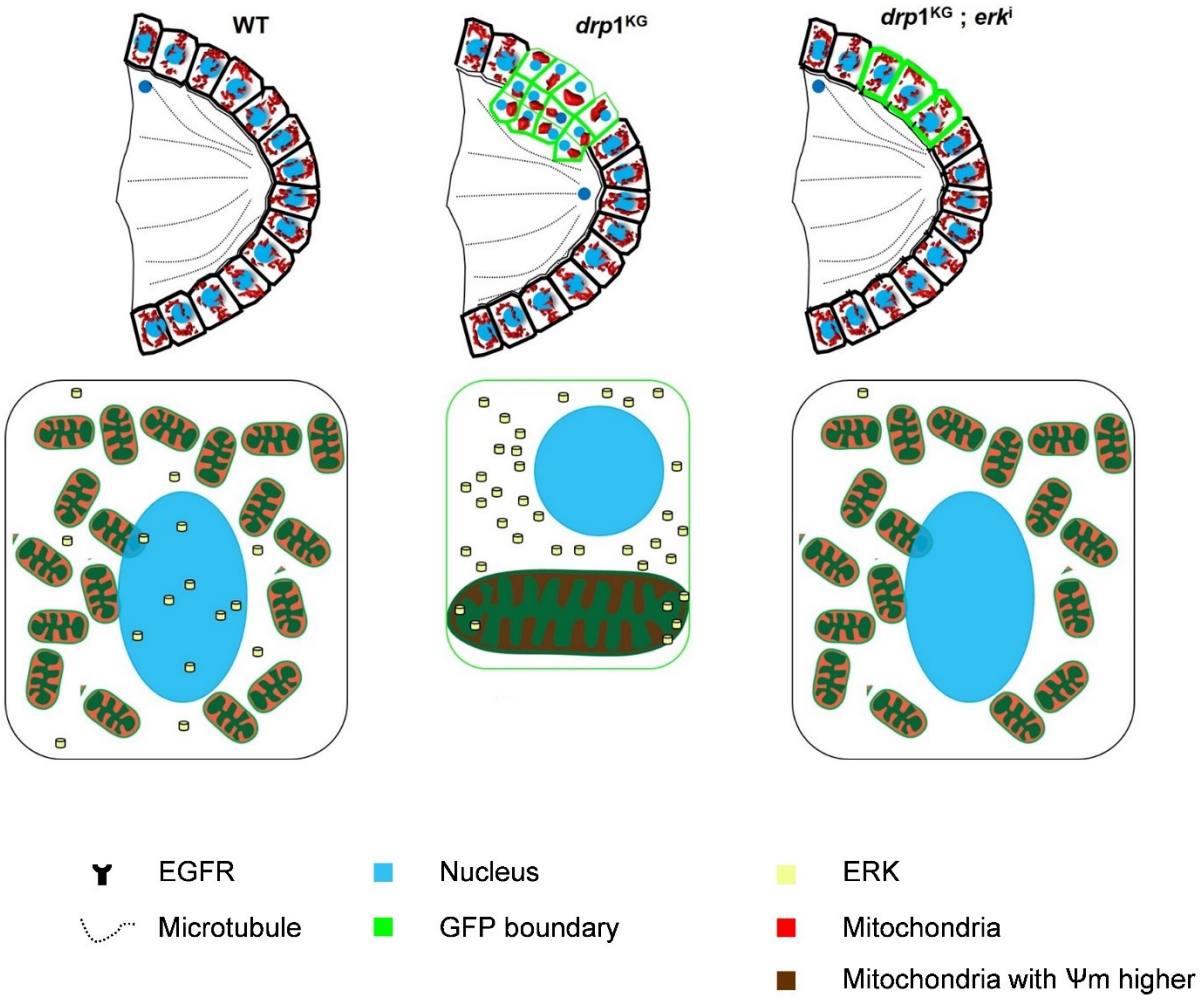

Figure 4.9. Increased ERK is responsible for tissue and cell number defects in *drp1*^{KG} mutant. (A) Schematic depicting PFC arrangement in wild type ovariole in which PFCs are arranged in a single layer and mitochondrial are distributed all around in the cytoplasm. PFCs receive signal from the ligand Gurken and activate the EGFR pathway. EGFR pathway activates downstream signaling to ensure that the oocyte is transported to the dorso-anterior position hence establishing the future adult fly axis. In *drp1*^{KG} this is disrupted and the oocyte is in the center. *drp1*^{KG} cells have multilayered tissue and aggregated mitochondria with high mitochondrial membrane potential. Mitochondrial morphology, membrane potential as well as well as tissue architecture are rescued in *drp1*^{KG}*;erk*^{i} . dpERK is in mainly nuclear in wild type and in the cytoplasm and probably on the mitochondria in the *drp1*^{KG} mutant.

numbers of prefollicle cells. Loss of aPKC results in slower proliferation in neuroblasts and eye epithelia (Rolls *et al.* 2003). Thus, a study of polarity pathways in *drp1* mutant FCs will be the key to understanding the mechanism of its reversal by additionally depleting Ras/ERK.

Mitochondrial morphology in most cells exists as a balance between tubular, fragmented and aggregated. Stem cells undergo a distinct change in both inner and outer mitochondrial membrane shape as they differentiate (Chung *et al.* 2007; Facucho-Oliveira *et al.* 2009; Mandal *et al.* 2011b). PFCs have high EGF signaling and contain relatively fragmented mitochondria (Mitra *et al.* 2012) and this is also in agreement with higher Ras/ERK driven mitochondrial fission activity in mammalian cancer cells (Kashatus *et al.* 2015). Loss of mitochondrial fusion has been previously shown to partly revert mitochondrial morphology and Notch signaling in *drp1* mutant PFCs (Mitra *et al.* 2012). In the study, ERK depletion alone does not change mitochondrial morphology appreciably. While higher resolution live imaging or electron microscopic observations will discern mitochondrial morphology more completely, the aggregated mitochondrial structure is resolved by co-depletion of Drp1 and Ras/ERK. We reason that this rescue of mitochondrial organization could occur by multiple pathways. ERK could directly activate mitochondrial fusion in these cells but this is not in agreement with mammalian literature, which shows reduced mitofusin Mfn1 activity by ERK induced phosphorylation. The residue phosphorylated in Mfn1 by ERK2 is not present in Mfn2 or its *Drosophila* orthologue Marf (Pyakurel et al., 2015), but the residue phosphorylated by stress induced JNK in Mfn2 (Leboucher *et al.* 2012) is conserved in Marf and could result in its inactivation and degradation. The ERK2 induced Drp1 phosphorylation residue is conserved from *Drosophila* to mammals suggesting that it is a key regulator of mitochondrial morphology downstream of ERK (Kashatus *et al.* 2015). Taken together ERK depletion in *drp1* mutant PFCs may inactivate mitochondrial fusion by an unidentified mechanism and *Drosophila* ERK may regulate both Marf and Drp1 activity by phosphorylation such that there are more fragmented mitochondria. A second possibility is that a different p38 based stress induced mechanism results in reversal of fusion in $drp1^{KG}$ and erk^{i} doubly depleted cells. p38K homolog *licorene* regulates Gurken posttranslationally and determines oocyte position (Suzanne *et al.* 1999). We

checked for p38K immunostaining in both *drp1*^{KG} and *drp1*^{KG}; *erk*^{i} and found no significant increase in comparison to neighbouring cells. However it is possible that other stress pathways are activated in these cells and future studies on the activation of stress pathways in *drp1* mutant cells will reveal the mechanism by which they affect mitochondrial morphology in combination with Ras/ERK.

These interactions between mitochondrial architecture, membrane potential and Ras/ERK point to their role in regulating the threshold of signaling in the EGF pathway. This study establishes mitochondrial membrane potential as key interactor of EGF alongside the already known players: ROS and mitochondrial morphology proteins.

CHAPTER 5

ERK regulates Notch via mitochondrial membrane potential in *Drosophila* follicle cells

5.1 Introduction

Notch is a transmembrane receptor activated by the cell bound ligands Delta, Serrate, Scabrous in *Drosophila*. It is mainly a cell fate specification pathway and activates transcription factors such as Suppressor of hairless (Su(H)). On binding of the ligand, extracellular domain is cleaved by metalloprotease ADAM (Brou *et al.* 2000), followed by cleavage in the inner region by the protease Presenilin to generate an intracellular domain (NICD) (Struhl and Greenwald 1999). NICD enters the nucleus, where it activates Su(H). Su(H) triggers a number of targets downstream of it such as the Enhancer of split (E(spl)) complex. Notch is responsible for assigning cell fate in number of *Drosophila* tissues such as eye, muscle and neuroblast development etc by lateral inhibition. In the *Drosophila* ovary, it has a role in both germline and somatic cell development. In the germline, it is required for germ cell niche retention and in the somatic population, it is necessary for regulation of polar cell number (Grammont and Irvine 2001) and it is instrumental in the mitotic to endocycle switch in FCs (Figure 5.1A) (Sun and Deng 2005).

Mitotic to endocycle switch involves inactivation of the transcription factor Cut (Sun and Deng, 2005). Cut is present in all the FCs up to stage 6, and stage 7 onwards it is restricted to the polar cells. It is again activated in all the FCs Stage 10 onwards. Cut is necessary for cyst encapsulation and FCs proliferation (Jackson and Blochlinger 1997). Cut peaks during S phase in cell cycle and suppresses CDK inhibitor p21 WAF transcription (Coqueret and Be 1998). Hence Cut regulates cell cycle and keeps FCs engaged in mitosis. Zinc-finger transcription factor Hnt represses Cut and Hedgehog in association with Tramtrack to bring about the endocytic switch in Stage 6-7 (Sun and Deng 2007). Hnt represses String in addition to Cut to shut down proliferation via Cyclins in the FCs (Schaeffer *et al.* 1998; Shcherbata *et al.* 2004). Thus FCs respond to a tightly timed regime of transcription factors during their development.

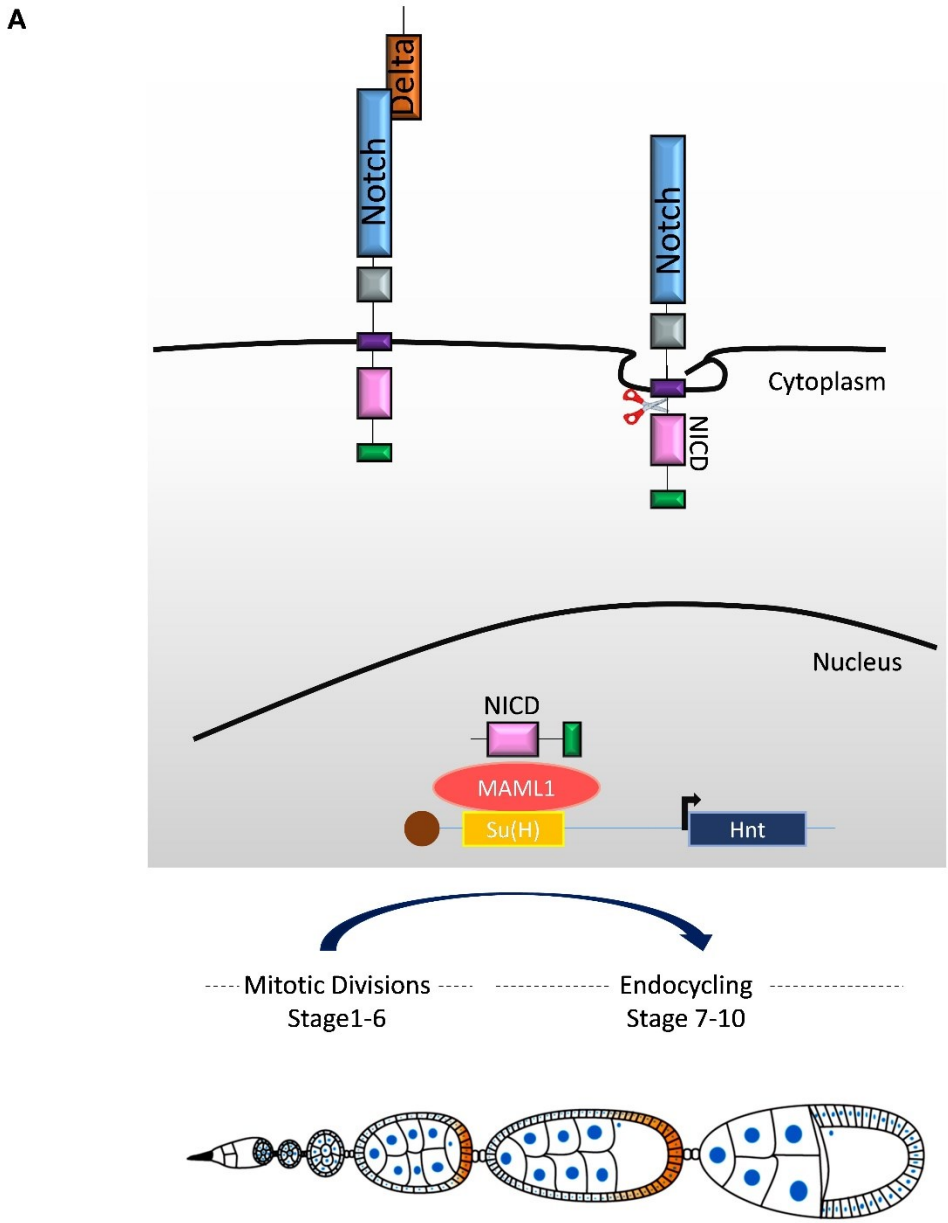

Figure 5.1. Notch pathway activates endocycling in FCs. (A) Notch transmembrane receptor on the FCs is activated by the ligand Delta. On activation the intracellular domain is cleaved and endocytosed. Cleaved and activated Notch intracellular domain (NICD) enters the nucleus to activate transcription factors such as Hnt with the help of proteins such as MAML and Su(H). On activation of Notch, mitotic to endocycle switch occurs in FCs at stage 6-7 leading to FC differentiation.

Among the three differentiated populations in Stage 8 FCs, PFCs are subject to both EGFR and Notch signal. According to the sequential model of activation, first FCs

in posterior acquire terminal identity due to Notch activation and subsequently EGFR is activated to establish PFC fate (Keller *et al.* 1999), thus creating different populations of FCs at the two termini as AFCs and PFCs.

Cellular function and fate is closely interlinked with its metabolic state and as Notch is the primary cell fate regulator in flies, it controls the cell's metabolism as well. Notch regulates metabolic genes involved in glycolysis and represses transcription of proteins which feed into ETC in *Drosophila* wing disc (Slaninova *et al.* 2016). Notch regulates metabolism in cancer cells as well as macrophages under conditions of inflammation (Landor *et al.* 2011; Basak *et al.* 2014; Xu *et al.* 2015). Cytoplasmic NICD inhibits mitochondrial fragmentation by increasing mitochondrial fusion protein Mitofusin2 (Mfn2) by the Akt pathway and protects cancer cells from apoptosis (Perumalsamy *et al.* 2010). Antioxidants responsible for hydrogen peroxide removal are found in a complex with Presenilin and hence oversee Notch processing (Wangler *et al.* 2011). During *Drosophila* hematopoiesis, Notch is required for stem cell maintenance. In response to infection, Notch regulation of lamellocyte differentiation is lifted and ROS spikes specifically in the lymph gland lobes but the anterior lobes are maintained in low ROS condition to preserve stemness in the cells (Sinenko *et al.* 2012; Small *et al.* 2014). Another interesting study points to activation of non-canonical Notch pathway by hypoxia-inducible factor-a (HIF-a) orthologue during crystal cell maintenance and survival (Mukherjee *et al.* 2011). In at least two scenarios in development, Notch signaling increase is consistent with mitochondrial fragmentation: Notch signaling is decreased in oogenesis in *Drosophila drp1* mutant FCs containing fused mitochondria (Mitra et al. 2012) and is increased in mouse embryonic cardiomyocytes mutant for mitochondrial fusion proteins Opa and Mfn (Kasahara et. al. 2013). Elevated cell calcium and increased NICD are possible mechanisms by which fragmented mitochondrial morphology affects Notch signaling in cardiomyocytes (Kasahara et al. 2013). Hence, Notch and mitochondria interact at the level of metabolic gene regulation, ROS and mitochondrial shape.

5.2 Material and Methods

5.2.1 *Drosophila* genetics

Stocks and lines listed in Chapter 4, Material and Methods section were used here as well.

5.2.2 Generation of FC clones

Clones were generated as described in Chapter 2, Materials and Methods section 2.2.2.

5.2.3 Immunostaining of FCs

Protocol delineated in Chapter 2, Materials and Methods section 2.2.3. The primary antibodies used were: mouse anti-CycB 1:10 (DSHB), rabbit anti-CycE 1:500 (Santacruz), mouse anti-NICD 1:100 (DSHB), mouse anti-Hnt 1:10 (DSHB) and mouse anti-Cut 1:10 (DSHB). Fluorescently coupled Streptavidin 633 (Molecular Probes) (1:1000) was used to mark mitochondria in FCs and fluorescently coupled secondary antibodies (Molecular Probes) were used at dilution 1:1000.

5.2.4 Mitochondrial membrane potential CMXRos assay

Same as Chapter 3, Materials and Methods section 3.2.5.

5.2.5 Image acquisition and phenotypic estimation in FCs

Described in Chapter 2, Materials and Methods section 2.2.4.

5.2.6 Image analysis for estimation of fluorescence in FCs and nuclear size

Image analysis done as detailed in Chapter 2, Materials and Methods section 2.2.6. For estimation of nuclear size, an ROI was drawn across the Hoescht stained DNA in the nucleus and the area was measured using ImageJ. The area of 10 nuclei per clone in 5 clones was measured for both mutant and control cells. Each data point in Figure 5.2B, 5.3A, 5.4F is the area of a nucleus from a mutant/control cell in a clone.

5.3 Results

5.3.1 *drp1* mutant PFCs have defective Notch signaling

drp1 mutant clones are multilayered (chapter 2, figure 2.5A). PFC multilayering is strongly associated with defective Notch signaling (Bilder *et al.* 2000; Fernández-Miñán

et al. 2007; Yu *et al.* 2008; Gómez-Lamarca *et al.* 2014). Activation of Notch leads to increase in nuclear size of the FCs on account of shift from mitosis to endocycling. *drp1*^{KG} mutant has previously been shown to have defect in Notch signaling; *drp1*^{KG} PFCs had smaller nuclei (Figure 5.2A-B). Plasma membrane accumulation of NICD can be monitored by a specific antibody and quantified as a ratio to the background control FCs. NICD is enriched on the apical membrane during early stages and as the Notch pathway is activated, its levels on the plasma membrane are decreased. NICD accumulates on the plasma membrane when the germline is mutant for a Notch ligand Delta and this results in a loss of Notch signaling (López-Schier and St. Johnston 2001). The ratio of the plasma membrane NICD fluorescence in *drp1*^{KG} mutant PFCs to the background PFCs was more than 1, consistent with accumulation on the membrane and inactivation of Notch signaling (Figure 5.2C-D). This plasma membrane enrichment of NICD was seen in FCs belonging to all layers in a multilayered clone and not just the ones positioned near the oocyte. This indicates that even the cells in contact with the germline are defective. This can be because of dearth of ligand or inability of Notch receptor to get activated. Consistent with loss of Notch, Hnt was absent in *drp1* mutant PFCs (Figure 5.2E); Cut was present in *drp1* mutant PFCs (Figure 5.2F). Notch pathway markers were identical in GFP and non-GFP cells in FRT40A clones; Hnt and Cut were nuclear and NICD was present on the apical membrane. Hence *drp1* mutant cells do not enter endocycle due to inactivation of Notch pathway.

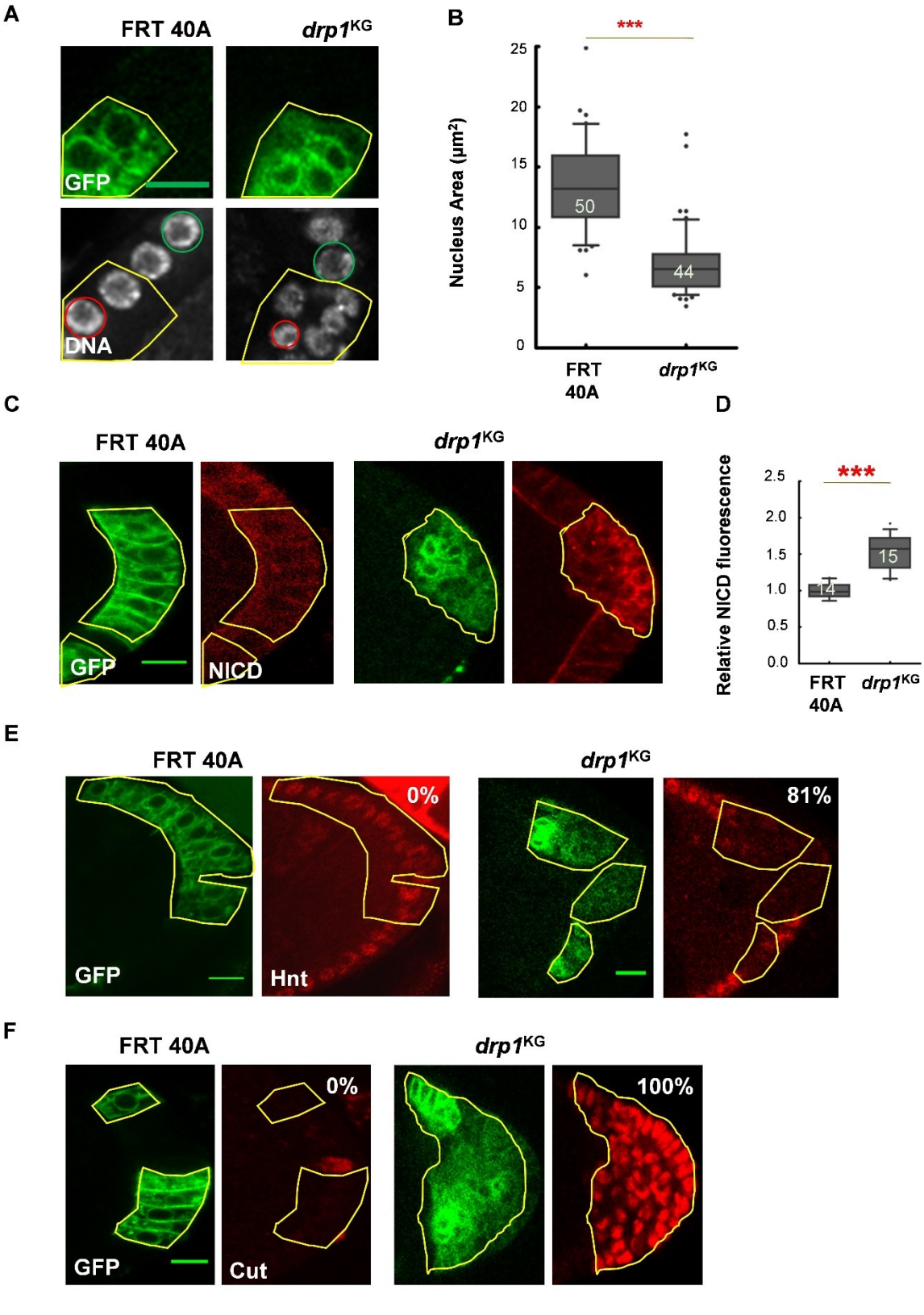
A
FRT 40A
drp1KG
GFP
DNA
B
***
Nucleus Area (µm²)
25
20
15
10
5
0
50
44
FRT 40A
drp1KG
C
FRT 40A
drp1KG
GFP
NICD
D
***
Relative NICD fluorescence
2.5
2.0
1.5
1.0
0.5
0.0
14
15
FRT 40A
drp1KG
E
FRT 40A
drp1KG
GFP
Hnt
0%
81%
F
FRT 40A
drp1KG
GFP
Cut
0%
100%

Figure 5.2. Notch pathway is defective in *drp1*^{KG} mutant cells. (A-B) *drp1*^{KG} nuclei are smaller in size than control. Nuclei are smaller in *drp1*^{KG} (CD8GFP; green circle marks the non-GFP nuclei and red marks GFP positive nuclei) as compared to FRT 40A nuclei (A). Cell area quantification shows that the *drp1*^{KG} nucleus is approximately half in area than control nucleus (B, n=50, 44, from 5 ovarioles, N=3, ***, P≤0.001, two tailed Mann-Whitney test).
(C-D) NICD (red) is higher on plasma membrane in *drp1*^{KG} in contrast to FRT 40A (C). Quantification shows higher GFP: non-GFP ratio in *drp1*^{KG} mutant (D, n=14, 15, N=3, ***, P≤0.001, two tailed Mann-Whitney test).
(E-F) Transcription factors Hnt and Cut are misexpressed in *drp1*^{KG} mutant. Hnt is absent in the *drp1* deficient cells (in 81% clones Hnt absent, n=25, N=3) while it is present in FRT 40A control cells (E). Transcription factor Cut persists in *drp1*^{KG} (Cut absent in 100% clones, n= 25, N=3) while it is removed in FRT 40A cell (F).
Data is presented as box plots where horizontal bar represents mean, box limits 25th and 75th percentiles, whiskers 10th and 90th percentiles and dots are observations outside 10th and 90th percentiles. Numbers within the box represent number of data points (n). Each data point in the box plot is an average from 5-30 cells in (D). Each data point in (B) is area of a nucleus. ns=not significant, Scale Bar: 10μm. n=FC clones in independent ovarioles, N=Experimental replicates.

5.3.2 Increased Ras/ERK leads to loss of Notch mediated differentiation in *drp1* mutant PFCs

EGFR and Notch antagonism is well characterised in *Drosophila* (Sundaram 2005). We assessed if elevated ERK/Ras levels in the *drp1*^{KG} mutant PFCs mediated a Notch signaling defect. The small nuclei size in *drp1*^{KG} alone was rescued in *drp1*^{KG}; *erk*^{i} and *drp1*^{KG}; *ras*^{i} combinations (Figure 5.3A-B). The *drp1*^{KG}; *erk*^{i} combination reversed the NICD accumulation and Hnt depletion and Cut persistence seen in *drp1*^{KG} PFCs (Figure 5.3C-F). The *drp1*^{KG}; *ras*^{i} combination showed a slight reduction in the average NICD fluorescence but this was not statistically significant (Figure 5.3C-D). There was also a weaker reversal of Hnt loss and Cut gain as compared to the *drp1*^{KG}; *erk*^{i} combination. This data was consistent with the previous observation of rescue of *drp1*^{KG} mediated Notch signaling defects on expression of EGFR dominant negative in PFCs (Mitra *et al.* 2012). Depletion of Ras/ERK however, reversed the cell organization in addition to

Notch signaling in *drp1*^{KG} PFCs which *Egfr*^{DN} did not. Hence, EGF acts through Ras/ERK in FCs to rescue Notch defect in the *drp1* mutant. Partial rescue hints at other signaling molecules downstream of EGFR in addition to Ras/ERK.

drp1^{KG} PFCs exhibit Cyclin B and E accumulation (Chapter 2, Figure 2.5N-Q). As mentioned in the introduction in this chapter, Notch regulates cell cycle by regulating levels of Cyclins in the cell. In the *drp1*^{KG}; *erk*^{i} combination ovarioles, there was a rescue of increased Cyclin B and E staining. This rescue was not statistically significant for the *drp1*^{KG}; *ras*^{i} combination, even though there was a decrease in averages (Figure 5.3G-J). We attribute this difference to *ras*^{i} being less efficient in removing Ras/ERK as compared to *erk*^{i} in removing ERK. As mentioned earlier, status of Cyclins in *drp1*^{KG} also allowed us to comment of the status of cell cycle. High Cyclin B and E indicated that the cell cycle is not able to proceed and is slower in the *drp1*^{KG} mutant. In the *drp1*^{KG}; *erk*^{i} rescue of Cyclins leads to rescue of the cell cycle pace and hence rescues the cell numbers (Chapter 4, Figure 4.5B-E). In summary elevated Ras/ERK in *drp1* mutant PFCs was responsible for loss of Notch mediated differentiation and cell cycle defects.

A

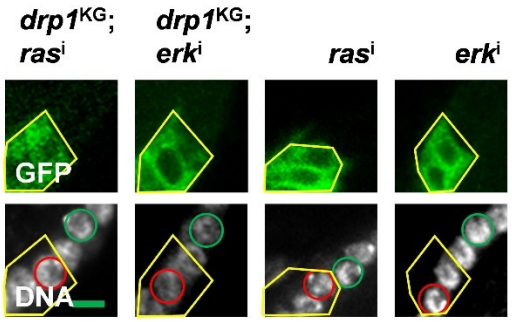
drp1KG; rasi
drp1KG; erki
rasi
erki
GFP
DNA

B

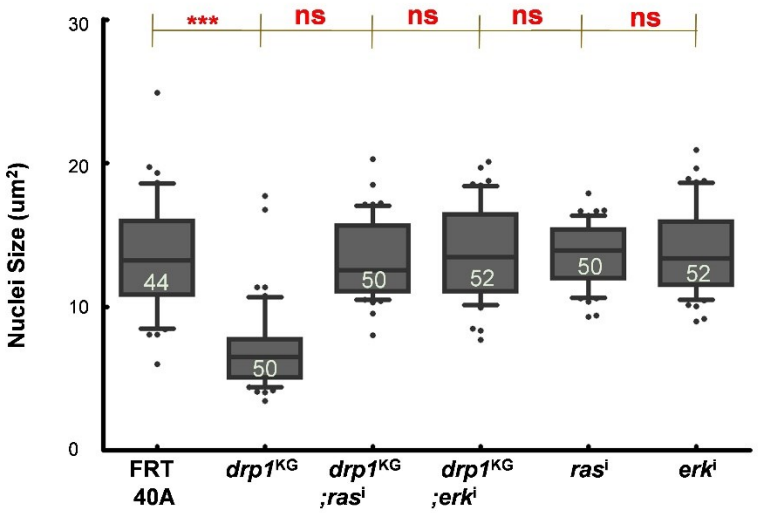
***
ns
ns
ns
ns
Nuclei Size (um2)
30
20
10
0
44
50
50
52
50
52
FRT 40A
drp1KG
drp1KG ;rasi
drp1KG ;erki
rasi
erki

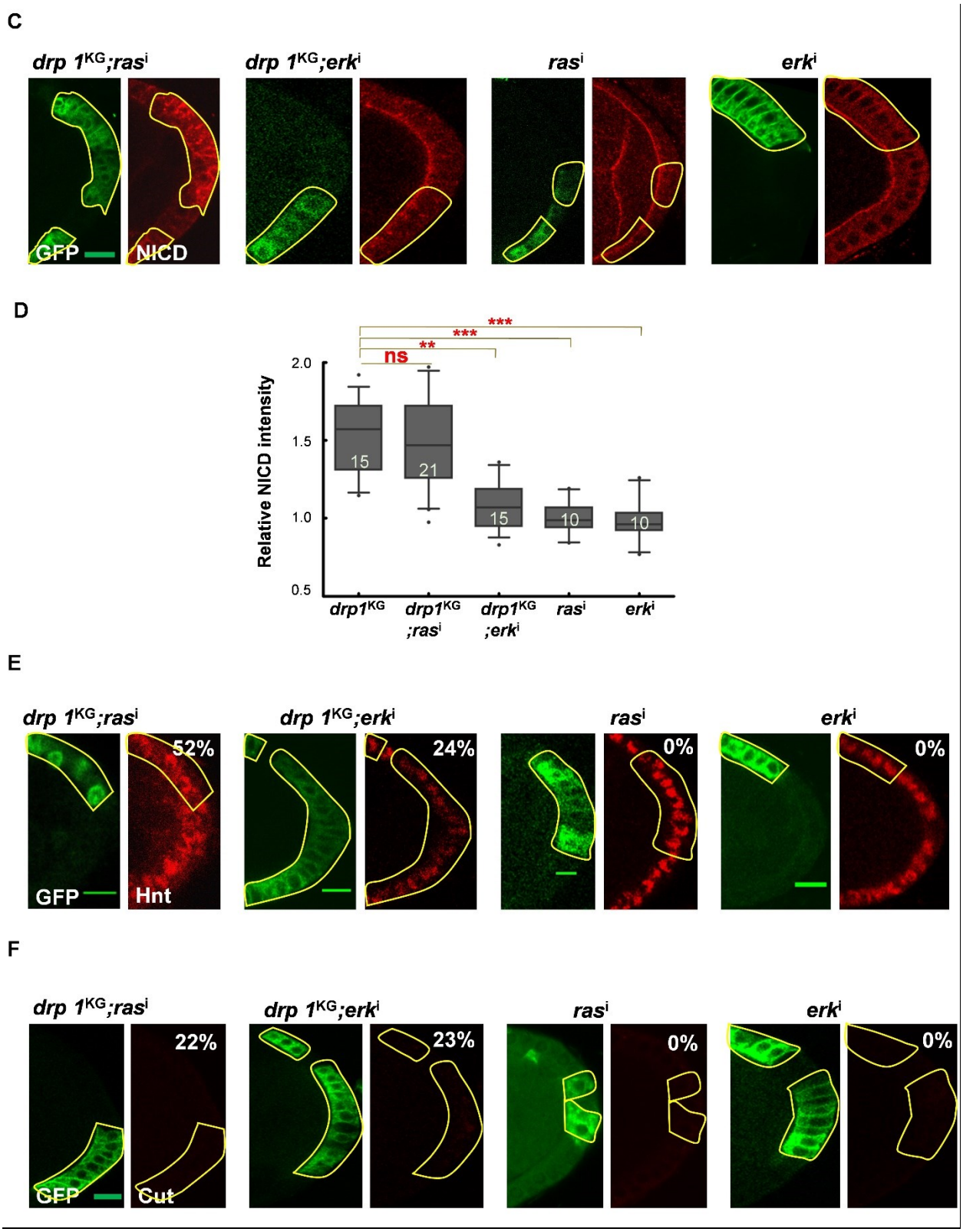
C
drp 1KG;rasi
drp 1KG;erki
rasi
erki
GFP
NICD
D
Relative NICD intensity
2.0
1.5
1.0
0.5
***
***
**
ns
15
21
15
10
10
drp1KG
drp1KG ;rasi
drp1KG ;erki
rasi
erki
E
drp 1KG;rasi
drp 1KG;erki
rasi
erki
52%
24%
0%
0%
GFP
Hnt
F
drp 1KG;rasi
drp 1KG;erki
rasi
erki
22%
23%
0%
0%
GFP
Cut

G

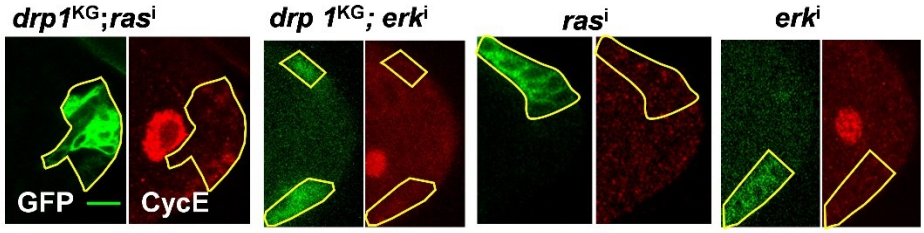
drp1KG;rasi
drp 1KG; erki
rasi
erki
GFP
CycE

H

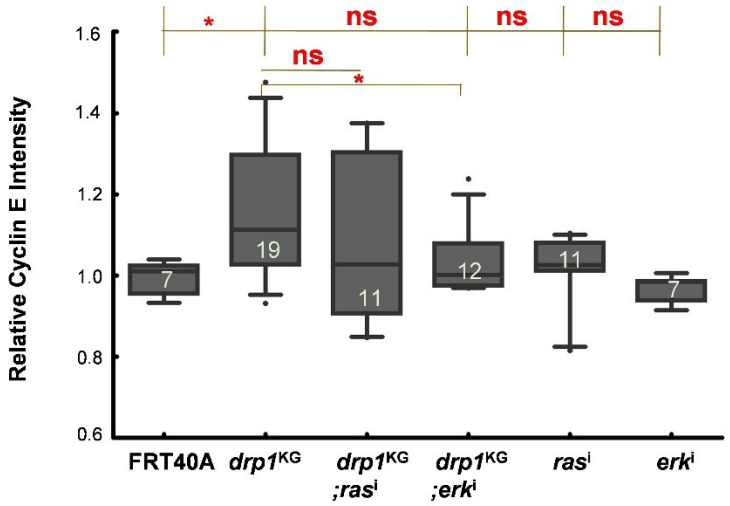
Relative Cyclin E Intensity
1.6
1.4
1.2
1.0
0.8
0.6
*
ns
ns
ns
ns
*
7
19
11
12
11
7
FRT40A
drp1KG
drp1KG ;rasi
drp1KG ;erki
rasi
erki

I

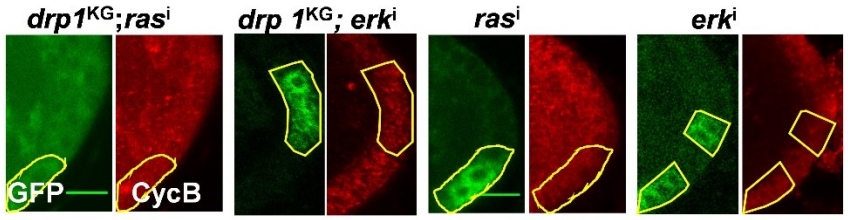
drp1KG;rasi
drp 1KG; erki
rasi
erki
GFP
CycB

J

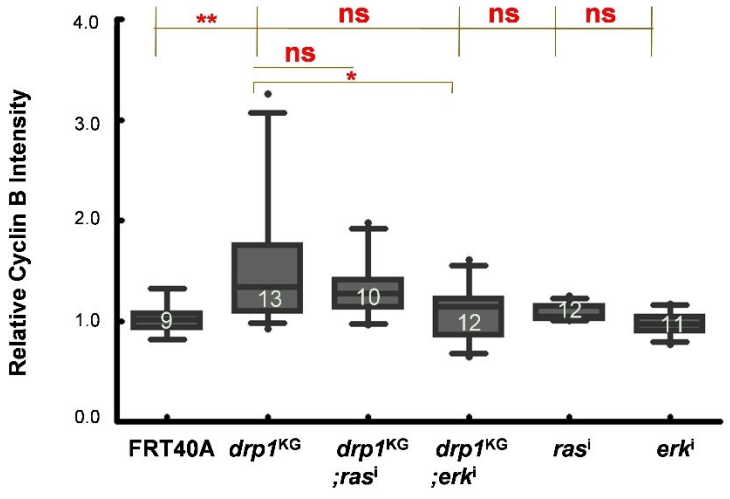
Relative Cyclin B Intensity
4.0
3.0
2.0
1.0
0.0
**
ns
ns
ns
ns
*
9
13
10
12
12
11
FRT40A
drp1KG
drp1KG ;rasi
drp1KG ;erki
rasi
erki

Figure 5.3. Increased Ras/ERK is responsible for Notch pathway defects in *drp1*^{KG} mutant. (A-B) *drp1*^{KG} nucleus size (DNA-grey; GFP positive nucleus marked by red circle and non-GFP by green circle) is comparable on Ras/ERK depletion in its background (A). Quantification of clone nucleus size shows a reversion to control size in *drp1*^{KG} ; *ras*^{i} and *drp1*^{KG} ; *erk*^{i} tissue (B, n=44,50,50,52,50,52, N=3, ***,P≤0.001, two tailed Mann-Whitney test).
(C-F) Notch pathway downstream effectors are rescued on Ras/ERK downregulation in *drp1*^{KG} mutant cells. Prominent membranous NICD immunostaining (red) in *drp1*^{KG} is not present in *drp1*^{KG}; *erk*^{i}. However, *drp1*^{KG}; *ras*^{i} combination does not rescue NICD accumulation. *ras*^{i} and *erk*^{i} do not have defects in NICD (C). Quantification in (D, n=15, 21, 15, 10, 10, N=3, **, P≤0.01, ***, P≤0.001, two tailed Kruskal Wallis test and Dunn's test).
(E-F) Hnt and Cut defects rescued by Ras /ERK downregulation in *drp1*^{KG} background. *ras*^{i} and *erk*^{i} do not have any defect in Hnt (E, 52% for *drp1*^{KG}; *ras*^{i}, 24% for *drp1*^{KG}; *erk*^{i}, 0% for *ras*^{i} and *erk*^{i})/Cut (F, 22% for *drp1*^{KG}; *ras*^{i}, 23% for *drp1*^{KG}; *erk*^{i}, 0% for *ras*^{i} and *erk*^{i}) immunostaining.
(G-H) Cyclin E accumulation is rescued by ERK depletion in *drp1*^{KG}. Increased Cyclin E (red) is absent in the *drp1*^{KG}; *erk*^{i} combination (CD8GFP; green). *drp1*^{KG}; *ras*^{i} however does not rescue the increased Cyclin E (G). Quantification in (H, n=7, 19, 11, 12, 11, 7, N=3, *, P≤0.05, two tailed Kruskal Wallis test and Dunn's test) shows Cyclin E in *drp1*^{KG}, *erk*^{i} and *drp1*^{KG}; *erk*^{i} is similar to control FRT 40A while it is high in *drp1*^{KG}; *ras*^{i} (H).
(I-J) ERK depletion reverts increased Cyclin B in *drp1*^{KG}. Cyclin B immunostaining (red) is comparable in *drp1*^{KG}; *erk*^{i}, however it is high in *drp1*^{KG}; *ras*^{i} (I). Quantification shows rescue of increased Cyclin B GFP: non-GFP ratio in *drp1*^{KG} to control levels in *drp1*^{KG}; *erk*^{i} (J, n=9, 13, 10, 12, 12, 11, N=3, **, P≤0.01, two tailed Kruskal Wallis test and Dunn's test). Data is presented as box plots where horizontal bar represents mean, box limits 25th and 75th percentiles, whiskers 10th and 90th percentiles and dots are observations outside 10th and 90th percentiles. Numbers within the box represent number of data points (n). Each data point in the box plot is an average from 5-30 cells. ns=not significant, Scale Bar: 10μm. n=FC clones in independent ovarioles in (D), (H), (J) and represents individual nuclei in B taken from 5 ovarioles, N=Experimental replicates.

5.3.3 Elevated mitochondrial membrane potential is responsible for loss of Notch mediated differentiation in *drp1* mutant PFCs

ERK depletion reversed the increased mitochondrial membrane potential and Notch

mediated differentiation in *drp1* mutant PFCs. Reduction of mitochondrial membrane potential using *drp1*^{KG}; *pdsw*^{i} combination did not have an effect on EGFR signaling (Chapter 4, Figure 4.8). We finally analyzed the impact of lowering mitochondrial membrane potential on Notch signaling. Interestingly, the *drp1*^{KG}; *pdsw*^{i} combination showed appearance of Hnt in greater number of clones as compared to *drp1*^{KG} alone (Figure 5.4A). NICD membrane accumulation seen in *drp1*^{KG} PFCs was reversed in the *drp1*^{KG}; *pdsw*^{i} combination (Figure 5.4B, E). Cut is not rescued in the *drp1*^{KG}; *pdsw*^{i} combination however (Figure 5.4C). Since *pdsw*^{i} lowered the mitochondrial membrane potential but did not change the mitochondrial organization in *drp1*^{KG} FCs it was possible that lowering of mitochondrial membrane potential specifically brought about the reversal in Notch mediated differentiation. We therefore analyzed Notch phenotypes on acute treatment of FCCP for 30 min in *drp1*^{KG} PFCs and did not find a significant change in Hnt appearance and NICD accumulation (Figure 5.4D-E). Even on varying FCCP concentration to include higher doses, we were never able to rescue the Hnt

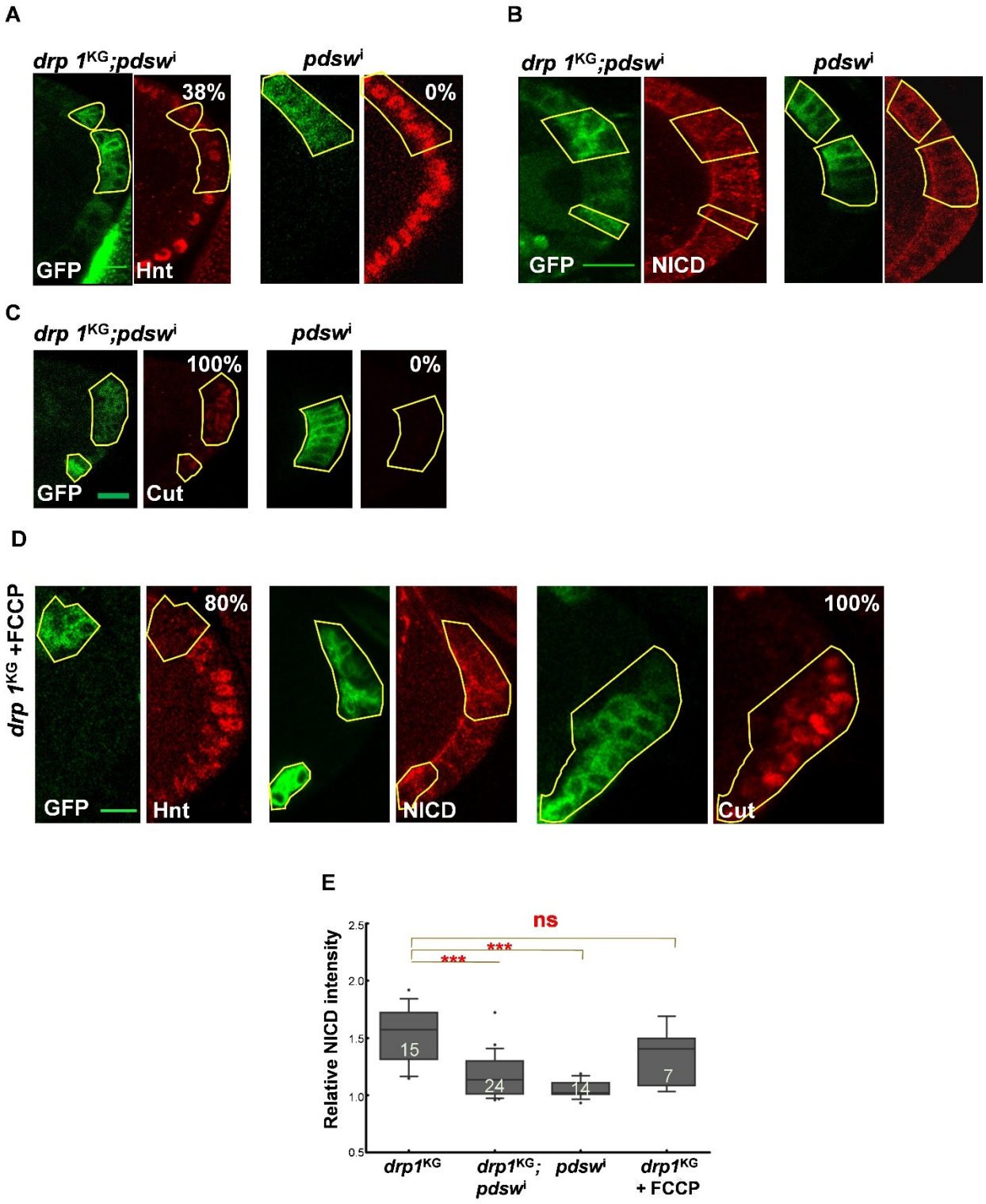
A
drp 1KG;pdswi
38%
GFP
Hnt
pdswi
0%
B
drp 1KG;pdswi
GFP
NICD
pdswi
C
drp 1KG;pdswi
100%
GFP
Cut
pdswi
0%
D
drp 1KG +FCCP
80%
GFP
Hnt
NICD
100%
Cut
E
ns
***
***
Relative NICD intensity
2.5
2.0
1.5
1.0
0.5
15
24
14
7
drp1KG
drp1KG; pdswi
pdswi
drp1KG + FCCP

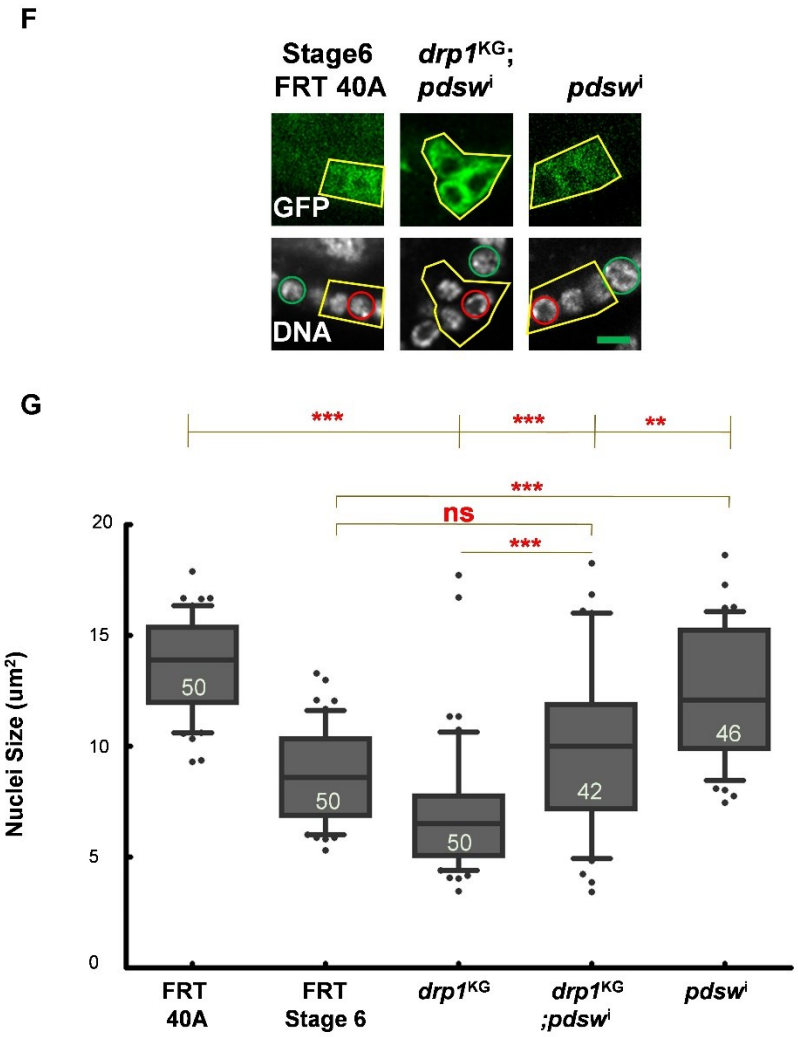

Figure 5.4. *pdsw* knockdown rescues the Notch pathway defect in *drp1*^{KG} . (A-E) EGFR pathway is not rescued on pdsw depletion, however Notch pathway markers are rescued in the *drp1*^{KG}; *pdsw*^{i} . Hnt (red) is present in *drp1*^{KG}; *pdsw*^{i} and *pdsw*^{i} alone as well. Intensity of Hnt is however fainter in some cells of the clone indicating slowness in activation of endocycle (A, 38% show Hnt defect, n= 29, N= 4, 0% for *pdsw*^{i} , n= 18, N=3). NICD is removed from the membrane in the doubles *drp1*^{KG}; *pdsw*^{i} (B, n=15, 24, 14, 7, N= 4, 3, 3, 4, ***, P≤ 0.001, two tailed Kruskal Wallis and Dunn's test). Transcription factor Cut (red) is similarly rescued, it is absent in *drp1*^{KG}; *pdsw*^{i}. There is no defect in Cut immunostaining in *pdsw*^{i} alone (C, 100% cut absent, n=11, N=2, 0% for *pdsw*^{i}, n= 12, N=2).

Quantification of GFP: non-GFP ratio for all the genotypes is shown in (E). FCCP treatment of *drp1*^{KG} still shows absence of Hnt, presence of Cut and NICD accumulation on the membrane (D, quantification of NICD in (E).
(F-G) *pdsw* knockdown reverts the small nuclei size in *drp1*^{KG}. *drp1*^{KG}; *pdsw*^{i} nuclei are larger than *drp1*^{KG} nuclei, however they are still smaller than FRT 40A nuclei. The *drp1*^{KG}; *pdsw*^{i} are comparable to stage 6 FRT 40A cells in line with slower endocycling in them. *pdsw*^{i} are also smaller than FRT 40A nuclei (F). Nucleus size in each genotype is plotted to show the smaller nuclei in *drp1*^{KG} and their rescue in *drp1*^{KG}; *pdsw*^{i} (G, n= 50, 50, 50, 42, 46, 5 ovarioles each, N=3, **, P≤0.01, ***, P≤0.001, two tailed Mann-Whitney test). Data is presented as box plots where horizontal bar represents mean, box limits 25th and 75th percentiles, whiskers 10th and 90th percentiles and dots are observations outside 10th and 90th percentiles. Numbers within the box represent number of data points (n). Each data point in the box plot in (E) is an average from 5-30 cells. Data point in (G) represents number of nuclei whose area is measured for each genotype. ns= not significant, Scale Bar: 10μm. n=FC clones in independent ovarioles in (E)/ number of nucleus in (G), N=Experimental replicates.

defect in *drp1*^{KG} PFCs. We also found that nuclear size defect is reverted in the combination clones (Figure 5.4F-G). *drp1*^{KG}; *pdsw*^{i} however had smaller nuclear size than the FRT40A control clone nuclei. The *pdsw*^{i} also had slightly smaller nuclei than control clones. This might be due to slowing down of the endocycle and hence delay in Notch. Indeed in the *drp1*^{KG}; *pdsw*^{i} clones Hnt is fainter (44%, n=29, N=3) than neighbouring non -GFP cells. This suggests that while *drp1*^{KG} are Notch deficient, it is only slowed down in *drp1*^{KG}; *pdsw*^{i} and *pdsw*^{i} alone. In order to further understand this, we compared the *drp1*^{KG}; *pdsw*^{i} nuclei size with stage 6 FRT40A clone nuclei size as Hnt just starts appearing in this stage, stage 8-9 *drp1*^{KG}; *pdsw*^{i} nuclei are equivalent in size to stage 6 FRT40A clone nuclei (Figure 5.4F-G). Lowering of *pdsw* in *drp1*^{KG} PFCs could partially reverse the *drp1*^{KG} phenotype in loss of Notch mediated differentiation but was not sufficient to change the multilayering phenotype and aggregated mitochondrial morphology.

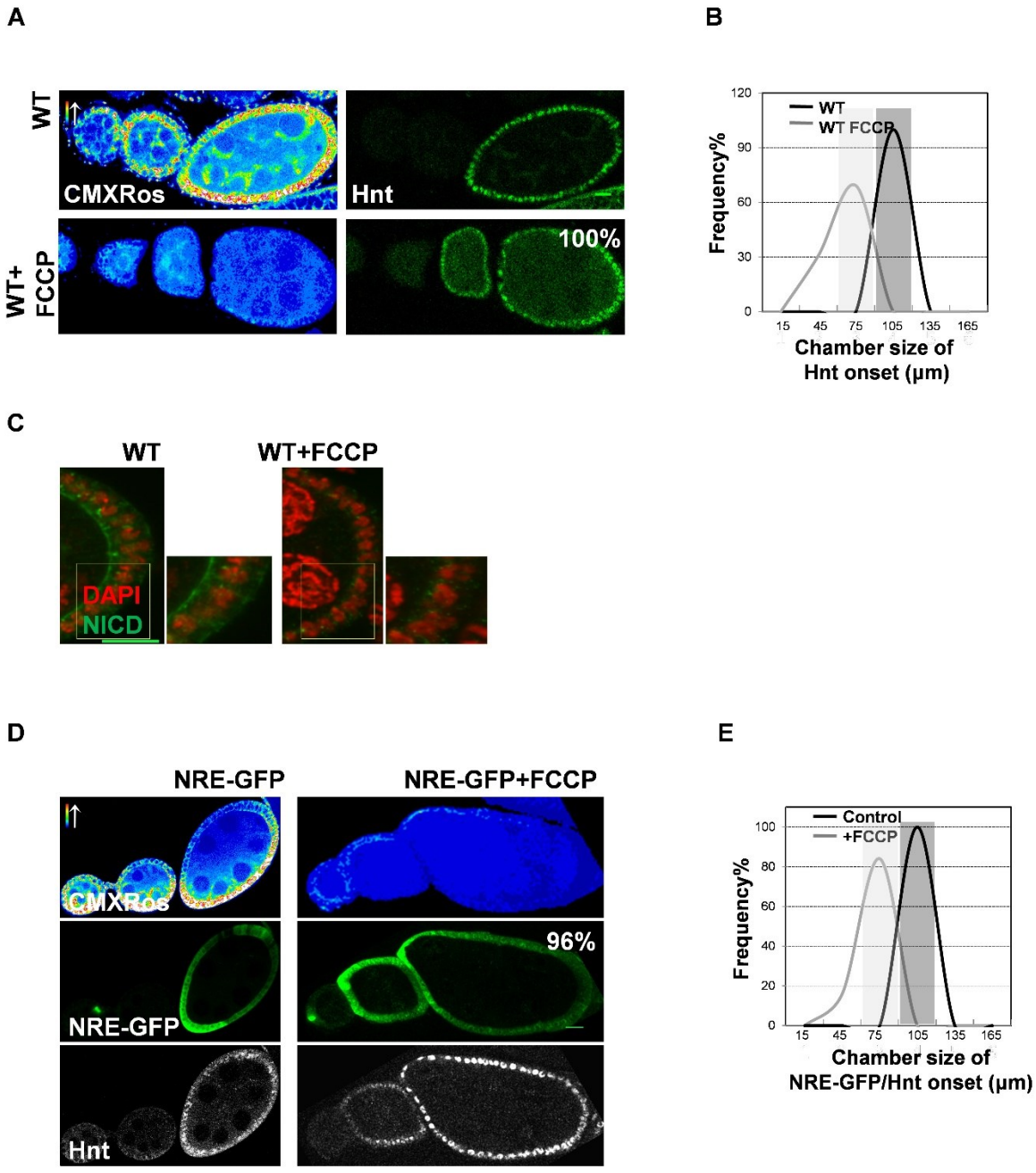

Figure 5.5. Loss of mitochondrial membrane potential activates Notch in stage 5 chambers. (A-B) Hnt appears in stage 5 ovariole chambers on FCCP treatment of wild type. FCCP treatment abolishes CMXRos fluorescence (pseudocolour; where red represents highest intensity pixels and blue the lowest) in the wild type. Hnt (green) is present in all the chambers in which there is a loss of CMXRos (A, 100% show Hnt in stage 5, n= 28, N=3, control n=30, N=2).

Histogram depicting the early appearance of Hnt in wild type on FCCP addition (B). NICD immunostaining disappears from the membrane on FCCP treatment in stage 5 chambers. NICD (green; DNA,red) is dislodged from the membrane in stage 5 chambers after mitochondrial membrane potential goes down in FCCP treated chambers (C, n=7, N=3). Yellow box marks the zoomed area.
(D-E) NRE-GFP expression also shifts to early stages on FCCP treatment. NRE-GFP (green; Hnt, grey) shows a nuclear staining in the FCs stage 6 onwards. NRE-GFP positive cells appear in stage 5 on FCCP treatment as CMXRos (pseudocolour; where red represents highest intensity pixels and blue the lowest) fluorescence is reduced (D, n= 26, N=2, control n=30, N=2). Shift in histogram seen on FCCP treatment (E).
Scale bar: 10 μm. n= independent ovarioles, N=Experimental replicates.

5.3.4 Lowering of mitochondrial membrane potential activates Notch precociously at Stage 5

drp1^{KG}; *pdsw*^{i} combination rescued the Notch defect, hence, is the Notch pathway dependent on mitochondrial membrane potential lowering in a wild type background as well? FCCP treatment resulted in Notch activation at an earlier stage in wild-type ovarioles (Figure 5.5A). A distribution of chamber sizes showed the onset of Hnt in smaller sized chambers corresponding to stage 5 as compared to Hnt onset at stage 6-7 in controls (Figure 5.5B). NICD is higher on the plasma membrane in early stages than late stages as the Notch pathway is inactive until stage 5. NICD depletion was seen from the plasma membrane on FCCP treatment (Figure 5.5C). Further the Notch response element construct NRE-GFP (Jouandin *et al.* 2014; Jia *et al.* 2015) showed an early appearance at stage 5 instead of stage 6 in wild type controls along with Hnt, when treated with FCCP for 30 min (Figure 5.5D-E). This suggested that lowering of mitochondrial membrane potential in wild-type chambers in the presence of Drp1 could prepone Notch signaling.

In summary, Ras-dpERK accumulation in *drp1*^{KG} PFCs with aggregated mitochondria increased mitochondrial membrane potential, thus leading to loss of Notch mediated differentiation. Decrease of mitochondrial membrane potential in wild-type

ovarioles was sufficient to activate the Notch pathway (Figure 5.6A).

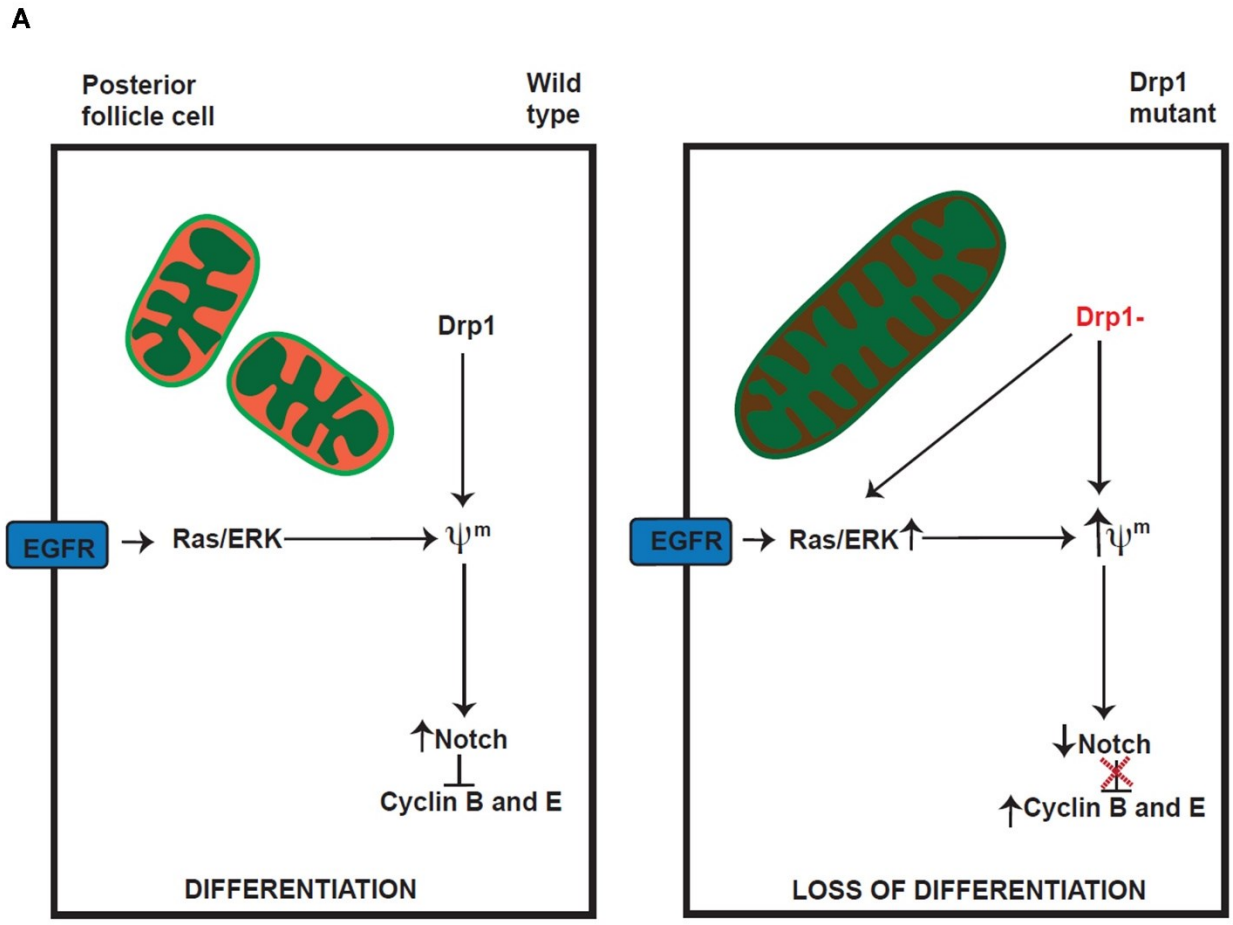

Figure 5.6. Notch pathway mediated FC differentiation is regulated by EGFR and mitochondrial shape as well as membrane potential. (A) In a wild type PFC, EGFR pathway regulates mitochondrial architecture and maintains its membrane potential at an equilibrium level. This activates Notch pathway and cell cycle regulators. In *drp1* mutant mitochondria are fused and mitochondrial membrane potential is elevated with Ras and dpERK increasing in the cell. Increase in mitochondrial membrane potential leads to inactivation of Notch and aberrant cell cycle.

5.4 Discussion

Developmental signaling pathways integrate cues at the cellular level by coordinating activities of various subcellular organelles to determine cell fate. We found that coregulation of two well characterized developmental pathways, EGFR and Notch, can

occur through mitochondrial morphology and activity during FC differentiation and oocyte patterning in oogenesis (Figure 5.6A). EGFR and Notch pathways work antagonistically in regulation of *Drosophila* eye cell fate (Rohrbaugh *et al.* 2002) and together in cell fate determination of photoreceptor R7 (Tomlinson and Struhl 2001). Recently EGFR has been shown to regulate Notch via the transcription factor Groucho in FCs (Johnston *et al.* 2016). While we could not find any effect on tissue organisation on ERK lowering other than decrease in cell number (summarised in Chapter 4), we did find that increased mitochondrial membrane potential mediated by higher cytoplasmic ERK in mitochondrial fission mutant inactivates Notch pathway. Hence, we show that increased Ras/ERK in *drp1* mutant PFCs with aggregated mitochondria and elevated mitochondrial membrane potential results in the loss of both EGFR signaling driven oocyte patterning and Notch driven PFC differentiation.

FCCP treatment causes mitochondrial fragmentation in presence of Drp1 in HeLa cells (Cereghetti *et al.* 2008) and mitofusin, Marf depletion leads to mitochondrial fragmentation and shows earlier onset of Hnt (Mitra *et al.* 2012) similar to FCCP in our study. Depleting *drp1* mutant PFCs of ETC activity with *pdsw* RNAi results in a partial reversion of the Notch loss of function phenotype. Hence mitochondrial fragmentation and membrane potential decrease are closely correlated with Notch activation. The impact of membrane potential increase on Notch deactivation can be through calcium or ROS levels or activation of PARL family of proteases resulting in NICD cleavage. Membrane potential difference across the mitochondrial inner membrane allows calcium influx (Gunter and Pfeiffer 1990). Lowering of mitochondrial membrane potential using an uncoupler releases stored calcium (Thayer and Miller 1990). Released calcium can be involved in Notch activation as shown in cardiomyocyte differentiation (Kasahara *et al.* 2013). It has been shown that NICD is cleaved by mitochondrial outer membrane peptidase to generate an active form of NICD in HeLa cells (Lee *et al.* 2011). It is possible that low mitochondrial membrane potential scenario created by FCCP prevents entry of NICD in the mitochondria and subsequently it is free to enter the nucleus and activate Hnt. Further support to this hypothesis is lent by two studies. A study in T-cells shows that processed Notch is found in mitochondrial fractions in Mfn1/2 containing cells but not Mfn1/2 mutant cells (Perumalsamy et. al., 2010). NICD localization in

mitochondria is required to activate mitochondrial genes (Xu *et al.* 2015). Hence more careful analysis can reveal if indeed Notch interacts directly with mitochondria or via calcium regulation. ROS has been shown to crosstalk with Notch. In our study, *drp1*^{KG} mutant PFCs also showed an increased ROS content but it was not reversed by ERK depletion, showing that it was not a possible mechanism in which the Ras-ERK pathway interacts with Notch.

The mid oogenesis stage is especially susceptible to any changes, as it is a transition stage. It also has the highest rate of apoptosis in response to starvation as a lot of active remodelling of the whole machinery occurs at this stage (Drummond-barbosa and Spradling 2001). It is a relatively short stage and takes about 2 hours to develop into Stage 6. Hence it seems that one of the factors that control the switch for Notch activation from stage 5 to stage 6 is mitochondrial membrane potential. It is interesting to ask if there are slight changes in mitochondrial membrane potential in each stage of the ovariole. A careful analysis using TMRE or JC1 dye can answer these questions.

To summarize we found that Notch pathway is sensitive to changes in mitochondrial membrane potential in FCs and ERK regulates Notch via regulation of mitochondria in the FCs.

CHAPTER 6

Mitochondrial proteins interact with EGFR pathway during *Drosophila* wing development

6.1 Introduction

Mitochondrial morphology varies between various cells and tissues (Collins and Bootman 2003; Mitra *et al.* 2012). We had found mitochondrial contribution to FC differentiation; mitochondria interact with the EGFR and Notch signaling pathways via their shape and activity. The EGFR pathway is a major pathway controlling wing vein development. The results in FCs (Chapter 4 and 5) found that there is increased dpERK in the cytoplasm in mitochondrial fission deficient *drp1* mutant cells. pERK depletion in the nucleus presumably results in lack of oocyte movement to the dorso-anterior position. Epistasis experiments were further performed in *Drosophila* wing to establish if the EGFR pathway interacts with mitochondrial morphology proteins in a similar manner. Mitochondrial manipulation is known to affect wing development. Marf knockdown in posterior wing compartment is known to cause cell death in the developing wing discs (Thomenius *et al.* 2011). In contrast inhibition of fusion in the dorsal region of wing pouch causes cell hyperproliferation (Gupte 2015). These two studies already highlight the differential role of the mitochondrial morphology in the fly wing. However, most other studies concentrate only on the apoptotic function of the organelle. A *vg*-Gal4 (expression in proximal and distal hinge region) based screen showed that inhibition of mitochondrially localized apoptotic proteins hid and reaper leads to notching of the wing blade and loss of wing fusion. The phenotype was attributed to drop in mitochondrial membrane potential induced by Hid and Reaper, which Bcl2 is able to rescue (Brun *et. al*., 2002). Thus it would be interesting to understand the role of mitochondria in EGFR during wing development.

6.1.1 Understanding the model system; *Drosophila* wing

Drosophila adult wing develops from a flattened disc of epithelial cells known as wing imaginal disc in the 3rd instar larvae. The wing disc can be divided into 2 main portions, the adult wing blade and the hinge. During the pupal stage, the wing disc forms two separate layers by eversion followed by apposition (Figure 6.1A-F). The separate layer of cells facing each other on basal side grow in size, until finally the adult wing flattened structure arises after fluid fills the veins (Milner 1977; Aldaz *et al.* 2010). A precise interplay of number of signaling pathways results in framework of adult wing. These signaling molecules define boundaries, rates of cell divisions and in turn pattern the wing shape (Loza and Thompson 2017).

Role of EGFR pathway is very well studied in the wing and is induced in two distinct waves. EGF is upregulated during larval and downregulated during pupal stages giving it a unique spatio temporal nature (Martín-Blanco *et al.* 1999). During early wing disc development it is shown to specify notum and wing disc identity through activation of the transcription factor Apterous (Wang 2000). In the pupal stage it is responsible for adult vein patterning. Wing veins are epidermal sclerotizations which enclose trachea and nerves (Garcia-Bellido and de Celis 1992). *Drosophila* wing has five veins (L1-5) and two cross veins, posterior crossvein between L4 and L5 and anterior cross vein between L3 and L4 (Figure 6.1F). Clones with loss of EGFR exhibit lack of proliferation in early stages and loss of vein phenotype in later (Diaz-Benjumea and Hafen 1994; Sturtevant and Bier 1995). EGFR interacts with pathways such as Hedgehog, Dpp, Notch and Wingless signaling to induce adult vein pattern. Like FSCs, where EGFR maintains apico-basal polarity, in the wing it restricts E-cadherin to the apical surface in vein cells as opposed to basal in intervein cells. This drives unique cell-cell contact in only the vein region and determines vein architecture (Keefe *et al.* 2007). Blistered is known to regulate Dpp, Hh and EGF and Notch signaling and all these pathways also signal back to the serum growth factor during vein formation (Loza and Thompson 2017). EGFR is activated by the ligands Vein and Rhomboid in the wing (Martín-Blanco *et al.* 1999). Entry of MAPK into the nucleus, downstream effector of EGFR is regulated in the wing. It is sequestered in the cytoplasm for the pro-vein fate (Marenda et. al., 2006). Thus in addition to its differential role in specific stage and cell type (Shilo 2003), it is also regulated in terms of its intracellular localization. We have already listed a few

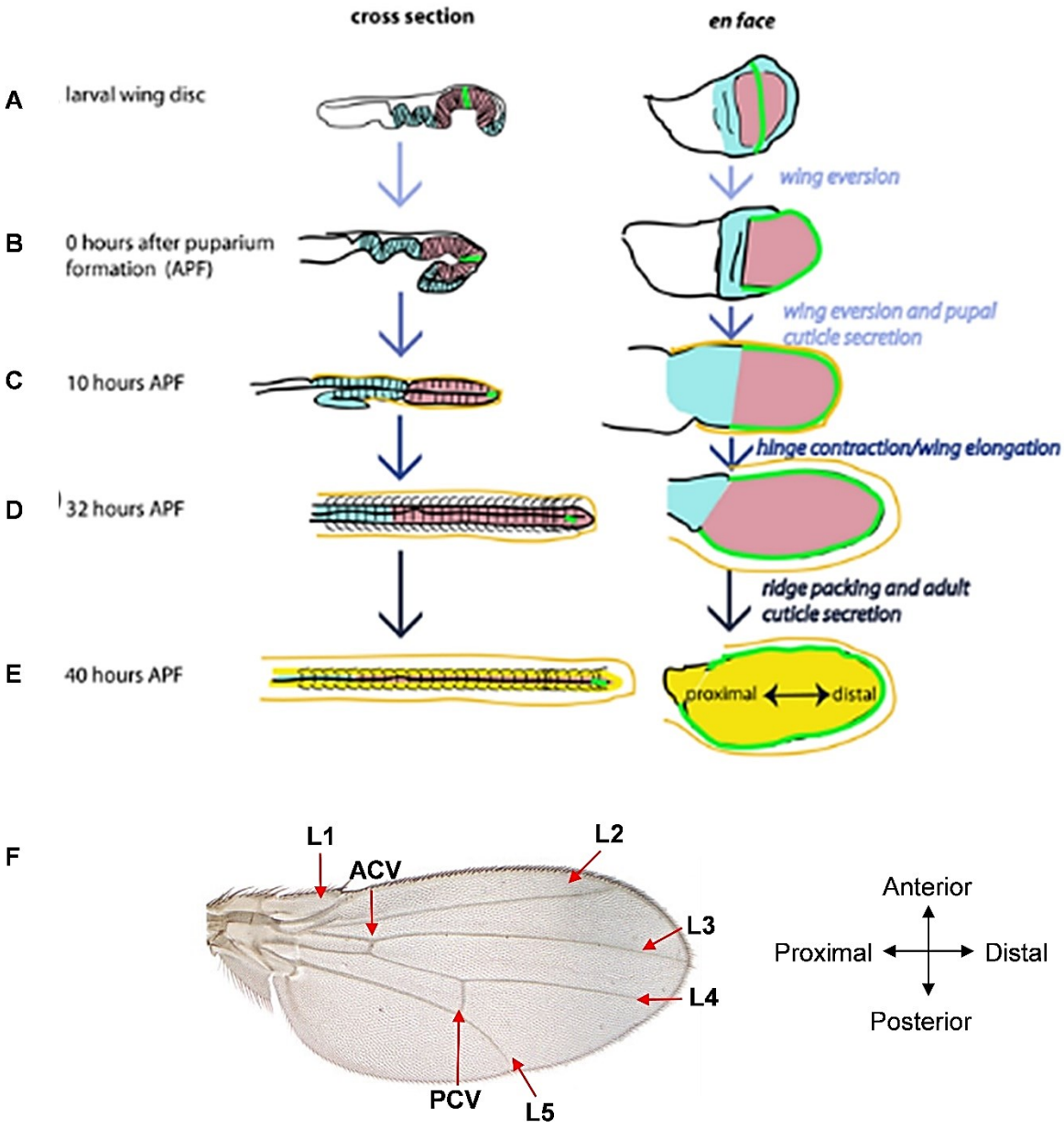

Figure 6.1. *Drosophila* wing disc undergoes series of modifications in order to form adult wing. (A-E) Transition of larval wing disc to pupal wing. *Drosophila* larval wing disc is a folded sheet of epithelial cells, assembled into distinct regions namely; dorsal pouch (pink), hinge region (blue). Green band depicts the band of cells expressing the morphogen wingless in the disc and it divides the disc into dorsal and ventral halves (A). As the pupa forms the sac of cells move inward (B) and subsequently from a double layered structure (C). This process is referred to as wing eversion and it is required to

bring the dorsal and ventral surfaces to align in a vertical direction. This is followed by wing extension and hinge region recedes (D). Lastly the fully formed wing is extended as fluid fills the veins (E) (Image modified from Dr. Suzanne Eaton group web page).
(F) Adult *Drosophila* wing is marked by five veins (L1-5) and two crossveins (anterior crossvein (ACV) and posterior cross vein (PCV)).

known roles of mitochondrial morphology as well as its impact due to its role in apoptosis during wing development. An *in silico* study using proteome association showed that wing size is determined more greatly by glucose metabolism as compared to ETC mediated activity (Okada *et al.* 2016). The interaction of mitochondrial morphology proteins with wing development pathways has otherwise been largely undetermined. This chapter summarizes preliminary results pointing towards requirement of fragmented mitochondria for proper EGFR pathway function in *Drosophila* wing development.

6.2 Materials and Methods

6.2.1 *Drosophila* genetics

All *Drosophila* crosses were performed in standard cornmeal agar medium at 25^{o}C. The *drp1*^{i}, *marf*^{i}, *opa*^{i}, *erk*^{i}, *ras*^{i}, *pdsw*^{i}, *cova*^{i}, UAS-*drp1*, UAS-*marf*, UAS-*Egfr*, UAS-*Egfr*^{DN}, *ras*^{V12}, *ms1096*-Gal4 lines were obtained from the Bloomington Stock Center. The *marf*$^{i(MG)}$ and *opa*$^{i(MG)}$ lines were a gift from Ming Guo lab. *ms1096*-Gal4/FM7a; UAS-*Egfr*^{DN}/TM6 Tb, *ms1096*/FM7a; UAS-*Egfr*/TM6 Tb stocks were generated using standard genetic crosses.

6.2.2 Imaging and estimation of wing defect phenotype

Wings were detached carefully from the flies and mounted in clove oil. Imaging was done on Olympus MVX10 1X. Vein pattern was compared in the wings and percent phenotype was calculated using Microsoft Excel.

6.3 Results

6.3.1 Manipulation of mitochondrial morphology proteins abrogates wing development

We first looked for effects of manipulation of mitochondrial shape regulator proteins in the dorsal wing pouch. *ms1096*-Gal4 was used to drive the expression of RNAi lines against mitochondrial morphology proteins. Downregulation of fission protein Drp1 (*drp*^{i}) gave a mild phenotype of crumpled wings (Figure 6.2B, control in Figure 6.2A). Upregulation of *drp1* did not alter wing morphology (Figure 6.2B). Mild downregulation of Marf, the outer membrane fusion protein did not cause any wing defect. However very few *ms1096*; *marf*$^{i(MG)}$ flies emerged and they had severe wing crumpling and blackening defects. Marf overexpression resulted in male lethality and females had crumpled wings (Figure 6.2C). We used two trangenes to downregulate inner membrane fusion protein Opa. *opa*^{i} is pupal lethal and *opa*$^{i(MG)}$ leads to crumpling of wings. Table 1 contains summary of the results mentioned above. Marf downregulation in the wing using *scalloped*-Gal4 (which expresses in the posterior wing margin) shows increase in pH3 staining. In third instar larvae using *dpp*-Gal4 (A-P axis), Opa and/or Marf downregulation does not lead to change in EdU immunostaining (Nagaraj et. al., 2012). Our results indicate that modification of mitochondrial network in the dorsal pouch triggers cell death pathways.

Hence modification of prime mitochondrial shape regulators alters adult wing shape and they are crucial for fly survival.

6.3.2 Downregulation of metabolism regulating proteins causes curling of wing

We used RNAi against *pdsw*, an ETC complex I subunit and observed curling of wing blade (Figure 6.2D). This curling phenotype is reminiscent of complex II and TCA cycle mutants (Sereda,*et.al*. 2007). We also downregulated complex IV protein *cova* and found two degrees of defect; pupal lethality and if emerged 100% wingless progeny (Figure 6.2D). Superoxide dismutase (SOD) downregulation also induced wing curling (Figure 6.2D), similar to that of *pdsw*^{i}, hinting that ROS is a causal factor triggering cell

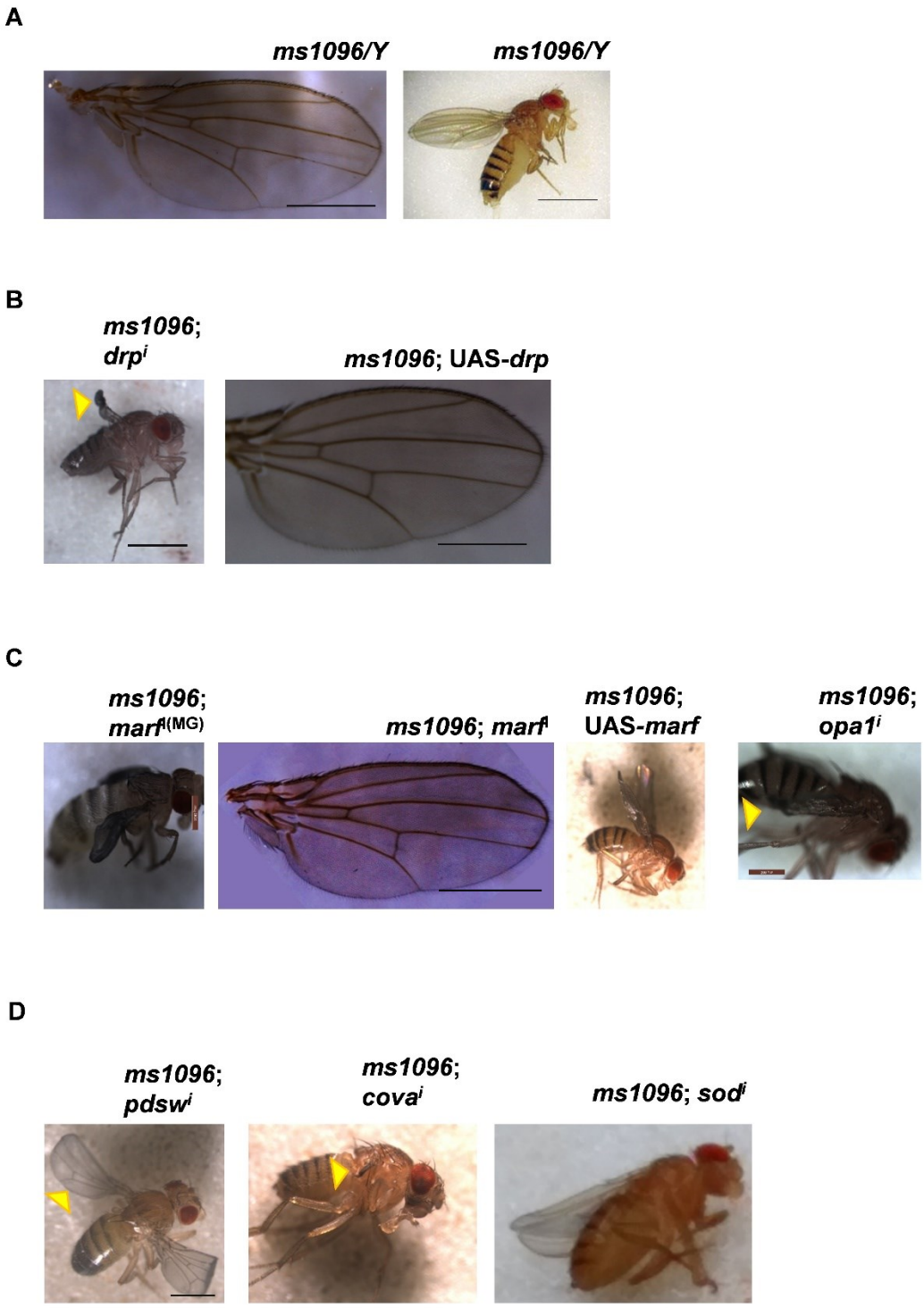

Figure 6.2. Modulation of mitochondrial proteins impairs the *Drosophila* adult wing structure. (A) Control wing morphology. Wild type *Drosophila* wing blade are straight in adult flies (A).

(B-C) Manipulation of mitochondrial shape regulating proteins leads to defect in wings. Downregulation of *drp1* causes severe wing crumpling (marked by yellow arrow head, first panel). However *drp1* overexpression has no effect on wing development (second panel) (B). Severe depletion of fusion protein *marf* causes defect in wing extension. The process of fluid filling appears to be impaired in $marf^{1(MG)}$ (first panel). Mild depletion of *marf* does not have a phenotype. Increase in Marf in UAS-*marf* leads to wing crumpling. Downregulation of *opa1* also causes similar wing crumpling (marked by yellow arrow head) (C).
(D) Mitochondrial ETC proteins are crucial for *Drosophila* wing development. Knockdown of *pdsw* causes wing curling phenotype (first panel, curled wing marked by yellow arrow head). *cova* knockdown causes wing crumpling similar to downregulation of fusion-fission proteins (yellow arrow head marks the small wing remnant). Increased ROS in developing wing on *sod* knockdown also induces curled wing phenotype.
Scale bar: 100mm.

death or change in rate of proliferation. Results are summarized in Table 6.1. *pdsw* loss has been shown earlier to increase ROS in eye epithelium via JNK pathway (Owusu-Ansah et. al., 2008). Both $pdsw^{i}$ and sod^{i} induce identical phenotype of wing curling. This can be because the cell cycle is effected in these genotypes. As a result there might be a decrease in cell number and subsequent change in wing shape.

	Genotype	Phenotype	%age defect, Number of flies
Mitochondrial shape regulators	*drp1*^{i}	Wing crumpled	33%, 66
	UAS- drp1	No defect	0%, 121
	marf^{i}	No defect	0%, 100
	marf$^{i(MG)}$	Wing crumpled	100%, 22
	UAS- *marf*	Male lethality, wing crumpled in females	100%, 106
	opa^{i}	Pupal lethal	100%
	opa$^{i(MG)}$	Wing crumpled	66%, 77
Mitochondrial ETC proteins	*pdsw*^{i}	Wing curly	100%, 100
	cova^{i}	Pupal lethal, escapers wingless	100%, 20
	sod^{i}	Wing curly	100%, 79

Table 6.1. *Drosophila* wing development is impaired on manipulation of mitochondrial proteins. The table summarizes the effect of alteration of mitochondrial shape regulators, ETC and ROS proteins. All the genotypes are in the background of *ms1096*-Gal4. Last column shows the percentage of flies with defects and the total number of flies counted.

6.3.3 EGFR mediated loss of vein defect is rescued by increased mitochondrial fission

In order to comprehend EGFR-Mitochondria interaction during *Drosophila* wing development, we first wanted to assess EGFR and its pathway components alone with the *ms1096*-Gal4. EGFR overexpression (UAS-*Egfr*) leads to increase in number of veins (Figure 6.3A) as reported previously (Schnepp *et al.* 1998). We also checked dominant negative (DN) allele of EGFR and on expressing it with *ms1096*-Gal4 as

Genotype	Phenotype	%age defect, Number of flies
UAS-*Egfr*	Veins increased	92%, 101
Ras^{V12}	Larval lethal	100%
UAS-$Egfr^{DN}$	Vein 3rd and 4th absent	98.5%, 100
ras^{i}	Wing crumpled	30%, 148
erk^{i}	Wing crumpled	100%, 70

Table 6.2. Table summarizes defect in wing on EGFR pathway components knockdown.

expected, found a loss of 3rd and 4th vein (Figure 6.3A). Activated Ras (Ras^{V12}) was 100% larval lethal with *ms1096*-Gal4. Ras DN (Ras^{N17}) on the other hand had no effect. Prober and Edgar 2000 have shown that Ras^{N17} leads to loss of veins, we speculate that the allele we had was not working. Ras RNAi being a weaker transgene gave crumpled wing blade phenotype in few flies (Figure 6.3A). ERK downregulation gave crumpled wings which can be a result of apoptosis. (Figure 6.3A, summary and quantification of the above results is in Table 6.2).

Stable double balanced lines were made for *ms1096*-Gal4 with EGFR overexpression (UAS-*Egfr*) and DN (UAS-$Egfr^{DN}$). We then combined mitochondrial proteins with the lines and looked for suppression or enhancement of the phenotypes in adult wing blade. A summary of the results can be found in Table 6.3. Significant findings are discussed here. UAS-$Egfr^{DN}$ /opa^{i} flies survive till adult stage in contrast to opa^{i} alone which exhibited pupal lethality. However wing is completely crumpled and blackened in the flies (Figure 6.3B). $Egfr^{DN}$ in combination with $marf^{i(MG)}$ also has crumpled wings but the number of flies which emerge is higher than $marf^{i(MG)}$ alone hence lethality is reduced in this scenario as well. EGFR overexpression also similarly rescues the opa^{i} pupal lethality (Figure 6.3B).

$marf^{i}$ which did not have any phenotype alone with *ms1096*-Gal4, rescues the $Egfr^{DN}$ wing and the 3rd and 4th veins are present. Significantly UAS-*drp1* also reverts the vein loss phenotype of $Egfr^{DN}$. In addition $marf^{i}$ worsens the UAS-*Egfr* phenotype (Figure 6.3B). Thus fragmented mitochondrial function seems to be downstream of

EGFR in the *Drosophila* wing as well and loss of EGFR is compensated by downstream fragmentation of the mitochondria. Loss of fusion proteins was rescued both by DN and overexpression of EGFR.

Figure 6.3. Increased mitochondrial fusion is responsible for the loss of vein in UAS-*Egfr^{DN}* flies. (A) EGFR pathway regulates wing vein formation. Increased vein formation is seen in EGFR overexpression and downregulation leads to loss of vein. Ras and ERK downregulation is known to cause severe wing defects and wing crumpling (yellow arrow head) (A). (B-C) *Egfr*^{DN} rescues *opa*^{i} lethality, however the few wings are still crumpled (yellow arrow head). EGFR overexpression also rescues Opa loss mediated lethality and increased vein like structures are present on the wing (yellow arrow head). Marf downregulation in *Egfr*^{DN} rescues the loss of veins and in EGFR overexpression increased vein phenotype is not rescued (B). Downregulation of fission in *Egfr*^{DN} worsens the phenotype and causes wing crumpling. It also does not alter EGFR overexpression phenotype. *drp1* overexpression rescues the *Egfr*^{DN} vein loss (C).
Scale bar: 100mm

This hints at a state of equilibrium of EGF signaling which needs to be readjusted in fragmented mitochondria scenario. However further experiments are required to prove the same.

In order to analyze this more whether the interaction between mitochondria and EGF is solely because of morphology or metabolism as well, we also combined energy mutant proteins and EGF. *pdsw*^{i} modified the UAS-*Egfr* gain of vein phenotype and the wing blade curled up (Table 6.3). Hence it is possible that fragmented mitochondria, with abrogated ETC can compensate loss of EGFR in the wing. However, this requires analysis of mitochondrial morphology on *pdsw* depletion in the *Drosophila* wing. *cova*^{i} in *Egfr*^{DN} background was mostly lethal and only a few flies emerged. *cova* downregulation in UAS-*Egfr* background however was 100% lethal at pupal stage. Here again EGFR loss is able to compensate for ETC defect. Hence mitochondrial morphology and function are closely interlinked with the EGF mediated signaling during *Drosophila* wing development.

	Genotype	Phenotype	%age defect (Number of flies)
UAS-*Egfr* +	*drp1*^{i}	Veins increased	100%, 75
	UAS-*drp1*	Veins increased	100%, 10
	marf^{i}	Veins increased	100%, 116
	UAS-*marf*	Veins increased, Wing curly	100%, 40
	marf$^{i(MG)}$	ND	ND
	opa^{i}	Pupal lethal	100%
	Opa$^{i(MG)}$	Veins increased	100%, 73
	pdsw^{i}	Veins increased, Wing curled	100%, 62
UAS-*Egfr*^{DN} +	*drp1*^{i}	Wing crumpled	64%, 94
	UAS-*drp1*	**Rescue**; Vein 3rd and 4th absent	34%, 60
	marf^{i}	**Rescue**; Vein 3rd and 4th absent	19.4%, 121
	UAS-*marf*	Wing crumpled	91%, 75
	marf$^{i(MG)}$	Wing crumpled	100%, 89
	opa^{i}	Wing crumpled	100%, 70
	opa$^{i(MG)}$	Wing crumpled	22%, 122
	pdsw^{i}	ND	ND

Table 6.3. Epistatic relationship between mitochondria proteins and EGFR in the wing. Manipulation of mitochondrial proteins in the background of EGFR overexpression shows the above phenotypes.

6.3.4 Downregulation of mitochondrial fusion proteins in spatial domains different from *ms1096*-Gal4 also result in larval/pupal lethality

Specific Gal4s were used to try and pinpoint the exact region and stage at which mitochondrial architecture plays a crucial role. *armadillo*-Gal4 which expresses specifically in the region of wingless expression was used with *opa*$^{i(MG)}$ and *opa*^{i} lines. Here as well *opa*^{i} gave pupal lethality; *opa*$^{i(MG)}$ however gave crumpled wings in only 20% (n=100, N=2) of the flies in contrast to 66% with *ms1096*-Gal4. *69b*-Gal4 which expresses early in the notum had very thin larvae with *opa*^{i} and the wing disc was completely absent in the larvae. *sal*-Gal4 is expressed in specifically in the L3 L4 vein region. *sal*-Gal4 expressing *opa*^{i} had huge larvae with abnormally shaped wing discs.

Hence the loss of fusion proteins manifests in various ways depending on the zone of inactivation and the stage of wing development. This hints at variable interaction with other signaling molecules. It again points to differential requirement of mitochondrial shape and energy during development.

6.4 Discussion

EGFR pathway is known to be upstream of mitochondrial morphology in the FC system (Mitra et. al, 2012). It is also known that ERK phosphorylates Drp1 at S616 to activate the fission protein in cell lines (Kashatus et. al., 2015). We also see a crosstalk between mitochondria and ERK as discussed in chapter 4. We wanted to see if a similar relationship holds true in *Drosophila* wing as well. These results suggest a feedback loop from the mitochondria to the EGFR signaling pathway. This again strengthens the hypothesis that signaling pathways integrate the signals from a number of organelles in order to process their function. This feedback loop can be because of regulation of ATP generation by mitochondria as mitochondrial shape dictates its energy output.

It has been shown earlier that Mfn1 down regulation using *engrailed*-Gal4 (posterior compartment) shows higher Caspase immunostaining (Thomenius et. al., 2011). This indicates how *opa* and *marf* downregulation can lead to blistered and crumpled wings. EGFR represses apoptosis mediator Hid in eye imaginal disc via Ras

(Bergmann *et al.* 1998). Is it via Hid that EGFR is able to rescue flies mutant for fusion proteins? Blistered wing can also be a result of improper unfolding during pupal eclosion (Lee *et al.* 2003). It has been postulated that overexpression of Ras leads to cell cycle arrest at G1 phase, and triggers apoptosis (Sotillos and Campuzano 2000). Rescue of *opa*^{i} and *marf*$^{f(MG)}$ lethality can also be because of expression of *ms1096*-Gal4 early and late. Early downregulation of Opa and Marf can be responsible for larval death while EGFR is able to rescue this, cell death later is not rescued as apoptotic factors are active. This is evident by the phenotypes with specific Gal4s such as *sal* and *vg*-Gal4.

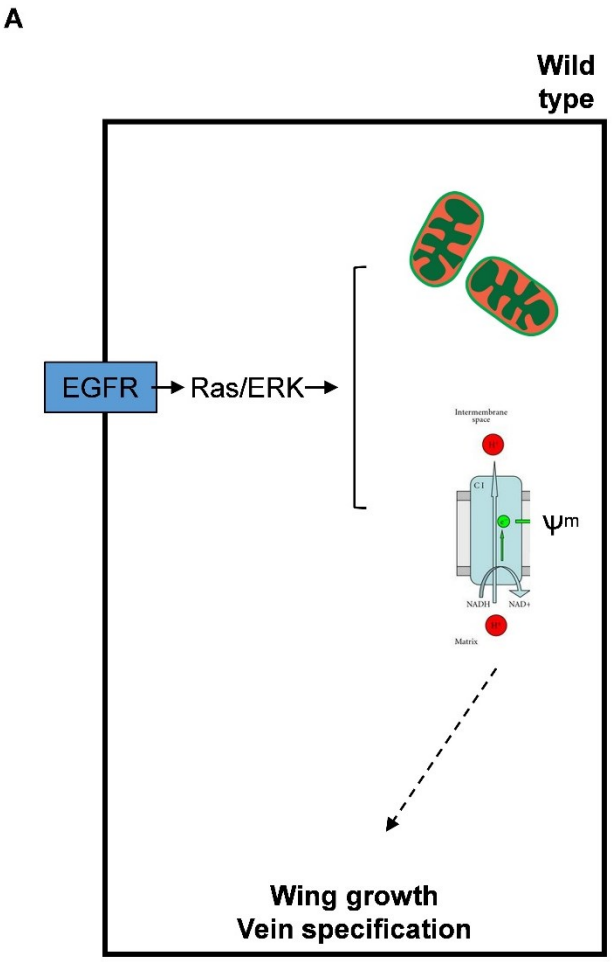

Figure 6.4. EGFR mediated wing growth and vein formation is dependent on mitochondrial fragmentation. EGFR pathway is activated in the *Drosophila* wing, facilitating appropriate wing cell proliferation and differentiation. In case of loss of EGFR, increase in mitochondrial fission rescues the decreased vein formation.

There are not many studies which explain the role of mitochondrial energy and shape during wing formation. Mutants of Enigma, a mitochondrial protein involved in lipid homeostasis have small wing imaginal discs (Mourikis *et al.* 2006). ROS and EGFR connection is fairly well understood, In cardiac fibroblast cells, ROS inhibits SHP2 by catalytic oxidation to activate EGFR (Chen *et al.* 2006). *Drosophila* hemocytes on

encountering challenge activate EGFR pathway via ROS. ROS activates the ligand Spitz via Rho1, hence it is an indirect activation of the pathway (Sinenko et. al., 2012). Tyrosine phosphorylation of EGF receptor is a direct method by which ROS interacts with the pathway. This activation however, requires very high levels of ROS to counter the activity of phosphatases. ROS can also oxidize the phosphatase to inactivate them (Bae *et al.* 1997). Net result of ROS induced EGFR activation is MAPK mediated cellular proliferation (Schieber and Chandel 2014). Hydrogen peroxide has been shown to activate ERK2 within 10 min followed by its inactivation (Guyton *et al.* 1996). They, as well as others, suggest interaction at the transcriptional level (Allen and Tresini 2000). As mentioned earlier *pdsw*^{i} has been shown to increase ROS in wing epithelium (Owusu-Ansah et. al, 2008), However, if the same is true for the wing as well is not known. A study shows that ROS is required for wing regeneration after tissue damage in order to illicit JNK pathway (Ruiz *et al.* 2015). *pdsw* alone interestingly gives a curling wing phenotype. The curly balancer has been found to encode for dual oxidase, a ROS generating enzyme (Hurd *et al.* 2015). Duox defective fly wings curl because the cuticles do not adhere properly. Mutant for Duox in the posterior compartment reduces ROS content as well as increase apoptotic cell population as seen by Caspase immunostaining (Anh *et al.* 2011). Also there is huge diversity in the manner and intensity of ROS interaction with the EGFR pathway and its components. Our results in *pdsw*^{i} and *sod*^{i} warrant a thorough study of stage wise interaction of ROS with EGF signaling in *Drosophila* wing. In addition to complex I and IV, we depleted a number of ETC proteins and metabolism related proteins in the wing as part of a screen to identify if wing development is dependent on mitochondria related genes (Appendix A3).
A lot of defects that we see appear to be a limitation at the unfolding stage of the wing. duox is active during the same phase as it allows the dorsal and ventricular surfaces to adhere (Hurd et. al., 2015). It is possible that the phenotypes that we see are because of increased ROS in the system.

We were not able to dissect and image to show mitochondrial morphology in the wing disc as the cells are much smaller in size. It would be interesting to observe that to completely understand the phenotypes. Hence we were able to show a genetic interaction between EGFR and mitochondrial morphology in wings as well, similar to the

ovary. Our experiments suggest that fragmented mitochondria are required downstream of EGFR and fused mitochondria lead to abrogation of pathway function (Figure 6.4A).

7 THESIS SUMMARY AND FUTURE DIRECTIONS

The textbook diagrams of the organelle mitochondria are known to be limited for the last 80 years or so as dynamic nature of the mitochondria was discovered. The simple representation of an isolated double membrane bound mitochondria has been replaced by a complex dynamic tubular network. The field has been able to establish the key players involved in the dynamics of the network, diseases arising due to defects in the dynamics and their regulation. What is relatively unknown, is functional significance of the architecture itself and the impact it has on organism's development and function. How does the shape change fit into the general scheme of patterning by developmental pathways? Studies till now have proved that there is a lot of variation in the shapes across species, cell types and cell status and alteration in these affects the cellular development (Bourges *et al.* 2004; Zick *et al.* 2009). Is the architecture only a manifestation of the ATP output or it has independent tasks as well.

A number of studies in the field are attempting to unravel the significance of mitochondrial architecture in using cell lines as well as model organisms (Quintero *et al.* 2006; Mitra *et al.* 2012). More and more people believe that mitochondria have an instructional rather than a supporting role in an organism's development (Mcbride and Neuspiel 2006; Soubannier and McBride 2009; Aon and Camara 2015; Chandel 2015). Role of mitochondria in signaling also adds a new dimension to developmental and disease scenarios.

7.1 *drp1*^{KG} cells have high mitochondrial membrane potential, increased ROS and pAMPK

We characterized and quantified the outcome of mitochondrial fission defect in PFCs. The fused mitochondria in the *drp1*^{KG} mutant have high mitochondrial membrane potential as expected however the cells have elevated ROS and pAMPK stress. *drp1*^{KG} cells lack apical polarity marker and aberrantly arrange in multiple layers characteristic of loss of polarity in the FC population. *drp1*^{KG} cells have increased Cyclins B and E, and slower mitoses resulting in fewer cell number than FRT 40A controls. Fused mitochondria have been shown to be better energy factories in a number of cell types

(Westermann 2010; Wai and Langer 2016). However here we find that high mitochondrial membrane potential does not necessarily result in a healthier cell. Mitochondrial shape and ATP output are dependent on cellular functions.

7.2 Increased Ras/dpERK in *drp1*^{KG} mutant FCs result in decreased proliferation and aberrant tissue organisation

EGFR signal is activated in PFCs via the ligand Gurken released by the germline cells. We checked for downstream effectors of EGFR pathway Ras and dpERK and found them to be augmented in *drp1*^{KG} cells. dpERK was mostly nuclear in the control but was restricted to the cytoplasm in the *drp1*^{KG} mutant. Probably as a result of inadequate dpERK in the nucleus, oocyte remains in the central position in the chamber containing *drp1*^{KG} mutant clone. Hence we find that dpERK has differential targets in FC cytoplasm versus nucleus. Increased cytoplasmic versus nuclear ERK localization was earlier shown during *Drosophila* wing vein specification (Marenda *et al.* 2006). An experiment to pull down cytoplasmic and mitochondrial targets of ERK in FCs will shed more light on the protein's function. Downregulation of Ras/ERK in the *drp1*^{KG} mutant background rescued the cell number and multilayering. This result in combination with the dpERK cytoplasmic localization tells us that EGFR via Ras/ERK maintains cell cycle and polarity in the FCs.

7.3 ERK regulates Notch via mitochondrial membrane potential in PFCs

Ras/ERK downregulation in *drp1*^{KG} cells rescues the mitochondrial architecture as well elevated mitochondrial membrane potential. Dependence of mitochondrial architecture on EGFR/ERK was known however the control on mitochondrial membrane potential was novel in this tissue. How do EGFR/ERK exert control on mitochondrial membrane potential? Is it is a direct result of slight changes in morphology or is it ETC manipulation. *drp1*^{KG} cells were known to be Notch negative hence did not enter endocycle. We found that increased Ras/ERK lead to Notch defect as *ras*^{i}*/erk*^{i} in *drp1*^{KG} background rescued the Notch markers. In order to further address if the rescue was result of EGF mediated salvage of mitochondrial membrane potential defect we lowered ETC complex I, *pdsw*^{i} in *drp1*^{KG} cells and were able to partially rescue endocycling.

Most importantly, we found that the stage 5 chambers in FCCP treated wild type ovariole expressed Notch. Hence mitochondrial membrane potential can be a switch for the Notch mediated endocycling in *Drosophila* FCs. This paves the way for intriguing questions such as how does mitochondrial membrane potential activate Notch, what is the sensitivity of this switch, if the switch is universal or confined to a cell type etc. Mitochondrial morphology mutants are most studied in neuronal disorders, where both EGFR and Notch signaling play crucial roles. Most of these diseases are studied from the lack of energy perspective. However, the status of cell growth and differentiation pathways can also be checked in them.

It is intriguing to note that lowering the of ETC complex I protein Pdsw, which maintains the FCs in a low mitochondrial membrane potential scenario from stem cell stage, does not bring about early activation of Hnt as FCCP does. This indicates that the cells respond to a spike in mitochondrial membrane potential at stage 5 when the raw materials for Notch activation are ready. This can also mean that cells maintained continuously in a state of low mitochondrial membrane potential are acclimatised to it during development or *pdsw*^{i} is not able to lower the mitochondrial membrane sufficiently.

The study was able to show that perhaps a similar relationship between EGFR and mitochondria holds true for other *Drosophila* tissues as well. In two different epithelial cell types (FCs and wing cells) EGFR pathway prefers fragmented mitochondria for proper functioning of cell. EGFR loss was rescued by overexpressing *drp1* or depleting *marf*. Further characterization of the rescue is required through immunostaining for cell cycle markers and EGF pathway proteins in the wing.

Drosophila embryo acquires its mitochondrial pool from the oocyte and nurse cells. Photoactivated mitochondria did not travel within the nurse cell and the oocyte cytoplasm indicating that mitochondria are small and distinct in the germline cells. The oocyte obtains metabolites from nurse cells; which can explain why their mitochondria can be small and isolated as they have to be relatively inactive in terms of ATP synthesis. However as this oocyte matures to form an embryo, its mitochondrial content is activated and it is now a primary source of ATP as we have seen with the help of ETC

inhibition experiments. Experiments in the jelly fish, *Aurelia aurita* have shown that oocyte mitochondria are less active than sperm mitochondria in order to prevent accumulation of mutations and ROS. Thus not impacting mitochondrial DNA replication fidelity and providing more accurate genetic templates for the next generation (Paula *et al.* 2013). Another study shows the progressive decrease in mitochondrial ETC content as the oocyte progresses towards stage 14 and subsequently these complexes reenter the mitochondria in the embryo (Seiber et. al., 2016). It is possible that calcium waves are responsible for the activation of mitochondria in *Drosophila* embryo as has been shown for ascidian embryos (Cox and Spradling 2003).

Along with a role in proliferation alluded to by a number of studies, the work attempts to characterize role of mitochondria during development. This piece of work has added a new dimension to the EGFR-Notch interaction, by introducing mitochondria as a key mediator.

7.4 Future perspectives

This thesis hopes to contribute the mechanism of interaction between signalling molecules and mitochondrial shape to the field of mitochondrial biology. It is interesting to ask if these interactions hold true for other species as well and when during the course of evolution they first arose. Mitochondrial morphology regulating proteins are pretty well conserved from yeast to humans. So are their interactors also conserved or they were tailored to fit each organism's development cycle? The interactions would have become more complex in multicellular versus unicellular eukaryotes. Did mitochondrial role in cell fate arise with multicellularity is another fascinating question. An evolution based study can tell us the point at which mitochondria switched from being an ATP producing endosymbiont to a signaling regulator in the cell.

Mitochondrial architecture and function are intimately coordinated with the ER. Their interactions impact calcium signaling, mitochondria fission-fusion and stress pathways such as UPR pathway (Marchi *et al.* 2014). It will be exciting to look at the impact on ER network in *Drosophila* tissues during development and Mito-ER interaction can be studied to understand the contribution of stress to the *drp1*^{KG} mutant phenotypes.

Drp1 is the only mitochondrial fission protein understood well till date. Dynamin2 has recently been shown to participate in the final scission step along with Drp1 (Lee *et al.* 2016a). A lot of adaptor proteins such as Mdv, Caf, Fis1 are known (Shaw and Nunnari 2002; Okamoto and Shaw 2005). It is possible that other unknown players are involved in mitochondrial fission. *Drosophila* wing can be used as an assay to identify such players alone and in the EGFRDN background. The screen can quickly help identify any modifiers of the missing vein defect of EGFRDN.

To summarize, mitochondria is an upcoming signaling modulator in the cell during development. A better understanding of this organelle with diverse functions can aid cancer, growth related diseases and unravel new knowledge about this endosymbiont in the field.

8 APPENDICES

Appendix A1

Differential impact of Superoxide dismutase manipulation on *Drosophila* follicle cell development

A.1.1 SOD overexpression results in increased Cyclin E levels in the posterior FCs

Mitochondrial fission mutant cells have high ROS (chapter 3, section 3.3.3). However Ras/ERK increase was not responsible for the spike in oxidants in the mutant cells. In order to gauge role of ROS, we overexpressed and downregulated superoxide dismutase (SOD) using the MARCM strategy. SOD is the enzyme responsible for quenching superoxide ions from the cell. In *sod* overexpression we did not find appreciable change in mitochondrial arrangement in GFP positive cells compared to the background control cells (Figure A1.1A). Misfolded SOD is known to enter mitochondria and lead to increased fusion (Vande Velde *et al.* 2011). However we were not able to test if the mitochondria were indeed more continuous in SOD overexpression clones. We checked for mitochondrial membrane potential using CMXRos and found that there is no difference in the fluorescence (Figure A1.1B-C).

Notch markers, Hnt and Cut were similar to background control cells (Figure A1.1D-E). However, cell cycle protein, Cyclin E was higher in SOD overexpression clones (Figure A1.1F-G). The hike in Cyclin E levels was similar to *drp1* mutant cells. Cell cycle stalling is well known on alteration of ROS levels (Turley *et al.* 1997; Menon *et al.* 2003). However in some cell lines SOD administration, lead to decrease in Cyclin E and cell cycle halt (Liu and Liu 2013). In Jurkat cells, ROS increases during G1-S and is decreased during M-G1 phase. Treating these cells with antioxidants halted the cell cycle at late G1 and Cyclin E was high in them (Havens *et al.* 2006). We were puzzled by the increased Cyclin E in SOD overexpression. In rat fibroblasts increased Cyclin E correlates with increased ROS in resistance to doxorubicin (Sgambato *et al.* 2003), however how one affects the other is not understood. Hence both increase and

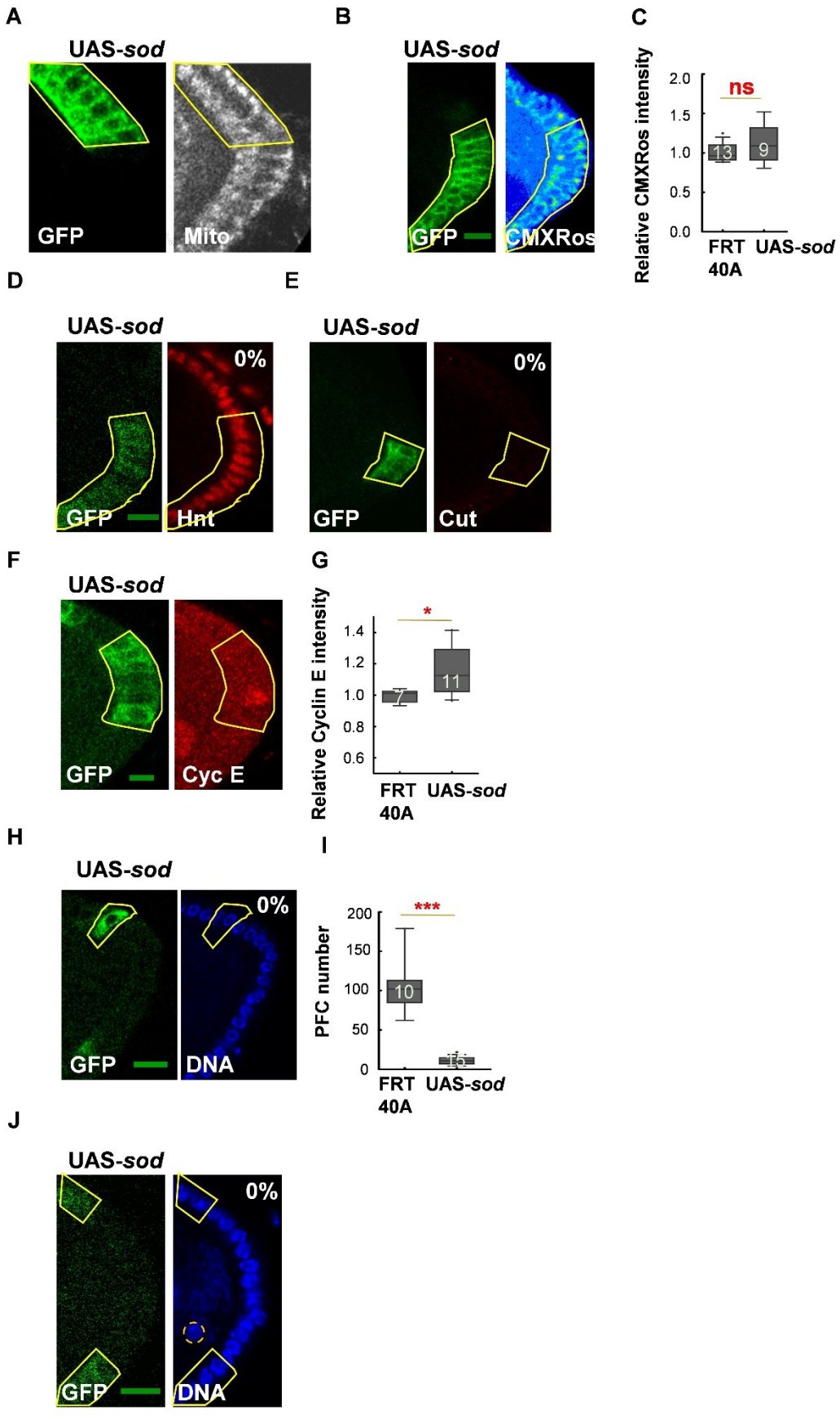
A
UAS-sod
GFP
Mito
B
UAS-sod
GFP
CMXRos
C
Relative CMXRos intensity
2.0
1.5
1.0
0.5
0.0
ns
13
9
FRT 40A
UAS-sod
D
UAS-sod
0%
GFP
Hnt
E
UAS-sod
0%
GFP
Cut
F
UAS-sod
GFP
Cyc E
G
Relative Cyclin E intensity
1.4
1.2
1.0
0.8
0.6
*
7
11
FRT 40A
UAS-sod
H
UAS-sod
0%
GFP
DNA
I
PFC number
200
150
100
50
0
***
10
FRT 40A
UAS-sod
J
UAS-sod
0%
GFP
DNA

Figure A1.1. *sod* overexpression leads to cell cycle defects in PFCs. (A-C) Mitochondria are not aberrant in pUASP-*sod*, mitochondrial architecture (A, grey, 0% exhibit defective mitochondria, n=33, N=3) as well as membrane potential difference across its inner membrane is intact and comparable to the neighboring cells (B, pseudocolor where red is highest intensity and blue is the lowest intensity pixel) as depicted by the ratio being close to 1 in pUASP-*sod* clones (C, n=13,9, N=2, two tailed Mann-whitney test).
(D-E) Notch pathway markers are same as control cells (D-E, Hnt- 0% defect, n=8, N=2, Cut, 0% defect, n=14, N=2).
(F-G) pUASP-*sod* clones have higher levels of Cyclin E than control cells (F, quantification in (G) (n=7, 11, N=2, *, $P \leq 0.05$, two tailed Mann-Whitney test).
(H-J) There is no multilayering (DNA; blue) and the clones have fewer cells than FRT 40A clones (CD8GFP; green) (H). Cell number comparison in (I), shows statistically significant lowering in cell number (n=10, 15, N=3, ***, $P<0.001$, two tailed Mann-Whitney test). (J) Oocyte positioned in dorso-anterior in all the pUASP-*sod* clones (0% oocyte defect, n=33, N=3).
Data is presented as box plots where horizontal bar represents mean, box limits 25th and 75th percentiles, whiskers 10th and 90th percentiles and dots are observations outside 10th and 90th percentiles. Numbers within the box represent number of data points (n). Each data point in the box plot is an average from 5-30 cells. ns=not significant, Scale Bar: 10μm. n=FC clones in independent ovarioles, N=Experimental replicates.

decrease in ROS seems to induce a cell cycle halting phenotype. When we checked the clonal cell number, we found a decrease in PFC number (Figure A1.1H-I), however we need to still check early stage clones. In addition, analysis of status of BrdU, Cyclin A and B will also shed light on the stage of cell cycle the cells are in.

A.1.2 SOD depletion does not alter the mitochondria and FC growth and development

We found that the ovarioles were largely unaffected in *sod*^{i}. There was no defect in tissue organisation. Mitochondrial morphology was identical to control clones (Figure A1.2A), Mitochondrial membrane potential was also similar to controls (Figure A1.2B-

C). Notch pathway markers, Hnt and Cut as well Cyclin E were same as the neighbouring cells (Figure A1.2D-G). The number of cells in the clone however were much smaller than control clones (Figure A1.2H-I). This can be a direct effect of increase in ROS in the system and the cell division is slowed down. A more thorough examination of other cell cycle markers as well as early clone cell number can shed light on this observation. We found slight oocyte mislocalization as well (Figure A1.2J), which was not present in UAS-*sod* overexpression (Figure A1.1J). It is not known if oocyte positioning is dependent on ROS levels, it is possible that the microtubule network is indirectly affected via LKB1 which is a target of ROS mediated activation in the cell (Soares *et al.* 2014). A more direct control can be inactivation of ERK and subsequent loss of oocyte movement (Dröge 2002; Poulton and Deng 2007). Further analysis of EGFR pathway components will be able to help in answering these questions. To summarize, depletion and overexpression of *sod* alone gave mild phenotype of cell number defect indicating availability of multiple alternate pathways in the *Drosophila* ovary to compensate for *sod* alteration.

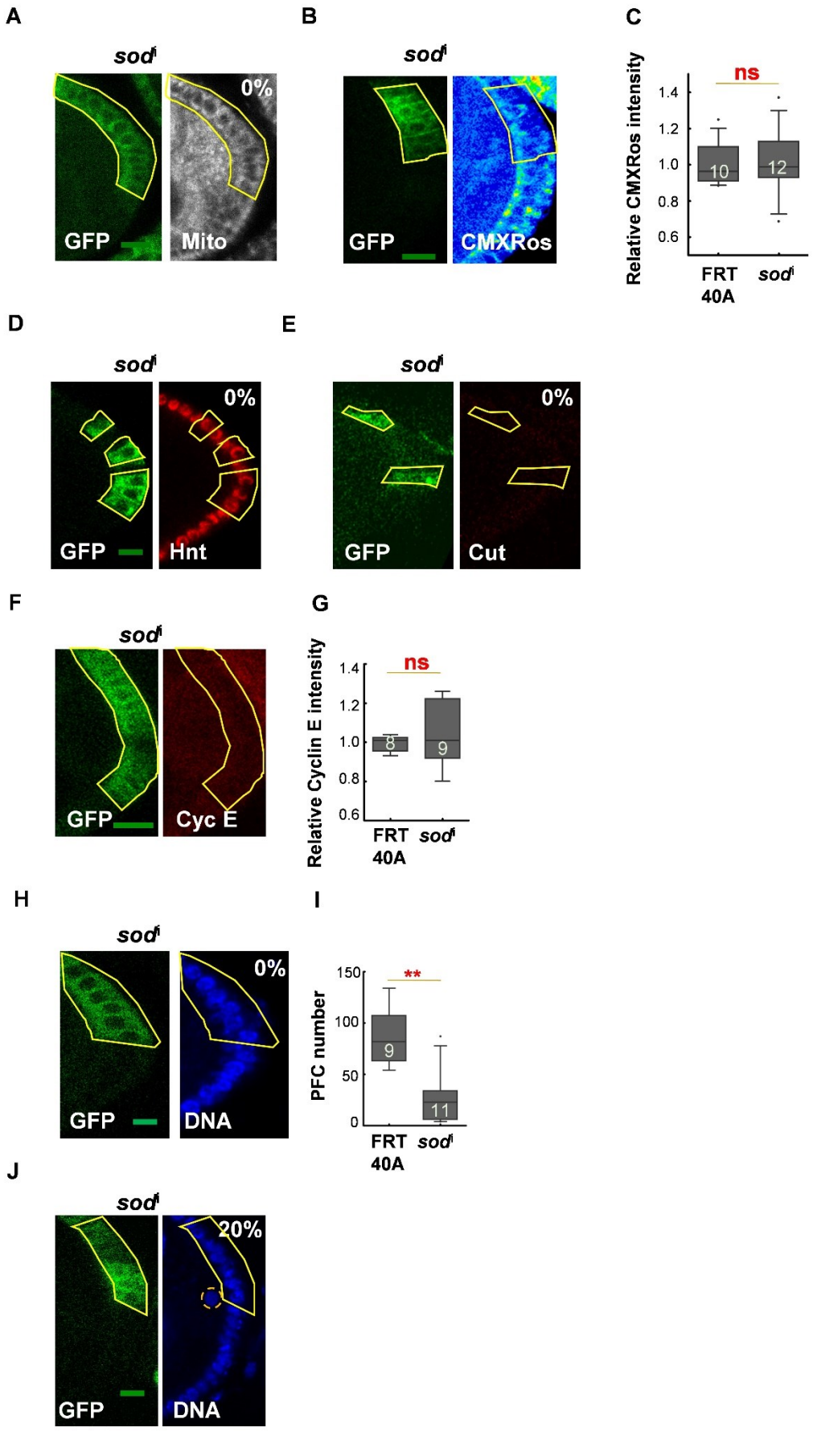
A
sod^i
0%
GFP
Mito
B
sod^i
GFP
CMXRos
C
Relative CMXRos intensity
ns
1.4
1.2
1.0
0.8
0.6
10
12
FRT 40A
sod^i
D
sod^i
0%
GFP
Hnt
E
sod^i
0%
GFP
Cut
F
sod^i
GFP
Cyc E
G
Relative Cyclin E intensity
ns
1.4
1.2
1.0
0.8
0.6
8
9
FRT 40A
sod^i
H
sod^i
0%
GFP
DNA
I
PFC number
**
150
100
50
0
9
11
FRT 40A
sod^i
J
sod^i
20%
GFP
DNA

Figure A1.2. *sod* depletion effects cell number and oocyte positioning in the *Drosophila* ovaries. (A-C) Mitochondrial distribution and activity not effected in *sod* knockdown. Mitochondria (grey) are dispersed (A, 0% defect, n=35, N=4) and the mitochondrial membrane potential (pseudocolor, red is the highest intensity pixel and blue represents lowest intensity pixels) is at the same level as control cells in *sod*^{i} clones (B) (CD8GFP; green). Quantification of mitochondrial membrane potential in (C).
(D-E) Notch transcription factor Hnt is present in *sod* clones as in control cells (D, 0% defect, n=10, N=2). Similarly Cut is absent in clones as well as the control PFCs (E, 0% defect, n=13, N=2).
(F-G) Cyclin E (red) is also similar to control cells in *sod*^{i} clones (F, quantification in G, two tailed Mann-Whitney test).
(H-I) There is no multilayering (H, 0%, n=35, N=4) however the clones are smaller and PFCs number is less than FRT 40A clones (I, n=9, 11, N=3, **, two tailed Mann-Whitney test). (J) Oocyte is in a central position in few *sod*^{i} clones (20%, n=35, N=4).
Data is presented as box plots where horizontal bar represents mean, box limits 25th and 75th percentiles, whiskers 10th and 90th percentiles and dots are observations outside 10th and 90th percentiles. Numbers within the box represent number of data points (n). Each data point in the box plot is an average from 5-30 cells. ns=not significant, Scale Bar: 10μm. n=FC clones in independent ovarioles, N=Experimental replicates.

Appendix A2

Generation and analysis of point mutants of morphology proteins

Drp1 is known to undergo a number of posttranslational modifications such as phosphorylation and ubiquitination. In order to further study the ERK interactors on the mitochondria, we looked for dpERK target sites in all the morphology proteins. We used the prediction software GPS 2.0 (group prediction site). GPS uses computational prediction on the basis of consensus sequence as well as known interactions. It predicted the sites listed in Figure A2.1A. Out of the sites against Drp1, S193 had probability high score and the site is also very well conserved across species (Figure A2.1B). Similarly sites were predicted for Marf and we decided to mutate S37 because of high phosphorylation score and conserved nature of the residue (Figure A2.1C-D). In order to assess the importance and impact of ERK mediated phosphorylation of Drp1 and Marf, we made point mutations in the sequence.

We ordered specific primers against Drp1 with mutation at 193rd Serine to mutate it to Aspartate or Glycine i.e phosphomimetic and phosphodeficient respectively. The primers contained flanking sequences for restriction enzymes. We used these primers to extract the sequence from the vector pOTB7. On obtaining the desired PCR product we treated it with Dpn1 to get rid of the methylated strand. We further used this reaction product to transform DH5α cells. Colonies obtained on transformation were sent for sequencing to allow correct identification of point mutation. Correct sequences with the point mutation were further cloned into the pUASP vector and sent for injections to fly facility in NCBS. The lines we obtained are listed in Table A2.1.

A

Position	Code	Kinase	Peptide	Score	Cutoff
578	T	CMGC/MAPK	NHVAENSTPSMASTW	3.96	3.757
615	S	CMGC/MAPK	PVHNNIVSPVKPVNL	3.887	3.757
536	S	CMGC/MAPK/ERK	NTPRNHMSPQISSHS	5.91	5.91
578	T	CMGC/MAPK/ERK	NHVAENSTPSMASTW	5.958	5.91
578	T	CMGC/MAPK/ERK/MAPK1	NHVAENSTPSMASTW	7.096	6.557
530	T	CMGC/MAPK/ERK/MAPK3	LGQRRANTPRNHMSP	7.828	7.747
578	T	CMGC/MAPK/ERK/MAPK3	NHVAENSTPSMASTW	7.885	7.747
193	S	CMGC/MAPK/ERK/MAPK7	ANTDMATSEALKLAK	4.786	3.214
536	S	CMGC/MAPK/ERK/MAPK7	NTPRNHMSPQISSHS	4.5	3.214
559	S	CMGC/MAPK/ERK/MAPK7	QQPPQPNSSQQQYSQ	3.571	3.214
578	T	CMGC/MAPK/ERK/MAPK7	NHVAENSTPSMASTW	3.286	3.214
599	S	CMGC/MAPK/ERK/MAPK7	PAPTRPDSIENSTNN	3.429	3.214
615	S	CMGC/MAPK/ERK/MAPK7	PVHNNIVSPVKPVNL	3.286	3.214

B

```
FBpp0077424          ENPNSIILAVTAANTDMATSEALKLAKDVDPDGRRTLAVVTKLDLMDAGTDAIDILCGRV
sp|O00429|DNM1L_HUMAN SNPNSIILAVTAANTDMATSEALKISREVDPDGRRTLAVITKLDLMDAGTDAMDVLMGRV
sp|Q8K1M6|DNM1L_MOUSE SNPNSIILAVTAANTDMATSEALKISREVDPDGRRTLAVITKLDLMDAGTDAMDVLMGRV
                     .**********************::::**********:**********:*:* ***
```

C

Position	Code	Kinase	Peptide	Score	Cutoff
38	S	CMGC/MAPK/ERK	VDKSGPGSPLSRFNS	7.749	5.91
626	T	CMGC/MAPK/ERK	SIGHSVSTPTTTPVE	6.359	5.91
630	T	CMGC/MAPK/ERK	SVSTPTTTPVEATPV	6.293	5.91
38	S	CMGC/MAPK/ERK/MAPK1	VDKSGPGSPLSRFNS	10.73	6.557
71	S	CMGC/MAPK/ERK/MAPK1	LYQSNDKSPLQIFVR	6.896	6.557
626	T	CMGC/MAPK/ERK/MAPK1	SIGHSVSTPTTTPVE	6.765	6.557
630	T	CMGC/MAPK/ERK/MAPK1	SVSTPTTTPVEATPV	7.687	6.557
38	S	CMGC/MAPK/ERK/MAPK3	VDKSGPGSPLSRFNS	10.126	7.747
626	T	CMGC/MAPK/ERK/MAPK3	SIGHSVSTPTTTPVE	8.391	7.747
630	T	CMGC/MAPK/ERK/MAPK3	SVSTPTTTPVEATPV	9.253	7.747
635	T	CMGC/MAPK/ERK/MAPK3	TTTPVEATPVCLLPA	8.736	7.747
38	S	CMGC/MAPK/ERK/MAPK7	VDKSGPGSPLSRFNS	3.286	3.214
41	S	CMGC/MAPK/ERK/MAPK7	SGPGSPLSRFNSSLQ	3.786	3.214
630	T	CMGC/MAPK/ERK/MAPK7	SVSTPTTTPVEATPV	4.786	3.214

D

```
FBpp0089222          ESRLYQSNDKSPLQIFVRAKKKINDIYGEIEEYVHETTTFINALHAEAEIVDKA---ERE
sp|O95140|MFN2_HUMAN NKRHMAEVNASPLKHFVTAKKKINGIFEQLGAYIQESATFLEDTYRNAELDPVTTEEQVL
sp|Q80U63|MFN2_MOUSE DKRHMAEVNASPLKHFVTAKKKINGIFEQLGAYIQESASFLEDTHRNTELDPVTTEEQVL
                     :.*   . : ***: ** ******.*: ::  *::*:::*::  : ::*:   :   :
```

Figure A2.1. Putative ERK phosphorylation target sites on Drp1 and Marf. (A-B) GPS software predicted the given list of serine and threonine residues as targets for phosphorylation by ERK (A). Out of the list, S193 (red box in (A)) was found to conserved in mouse and humans as well (red marks the residue of interest) (B). (C-D) Predicted sites on Marf for phosphorylation by ERK and S38 has the highest probability (A). S38 was also conserved across species (B).

Phosphorylation site prediction: GPS2.0. Sequence alignment: ClustalW

We next tested the lines by crossing them to Gal4s in three different tissues, *nanos*-Gal4 to look for expression in early embryo, *e22c*-Gal4 and *gr1*-Gal4 to check for phenotype in the ovaries and *ms1096*-Gal4 for the wing. We tested for lethality with *nanos*-Gal4 to compare severity of the lines (Method followed for checking lethality in Chapter 3, Section). We took a 3 hour embryo collection and the number of dead embryos compared to control were counted after 24 and 48 hour (Table A2.1).

e22c-Gal4 lead to larval lethality and no F1 was obtained suggesting *e22c* expresses in the larval stages as well when ovaries are formed. We did not get any striking change in mitochondrial morphology with the *gr1*-Gal4 which expresses in the PFCs and AFCs stage 7 onwards (Figure A2.2A-B). All in all we did not find ovary specific Gal4s useful. In the wing we used *ms1096*-Gal4 which expresses in dorsal pouch. Out of the lines, UAS-*drp1*^{SD} (Line1) showed crumpling of wings (100%, n=57, N=2). UAS- *drp1*^{SG} (Line4) exhibited slight wing defects (50%, n=40, N=2) (Figure A2.3A-B). This analysis helped us in selecting the strongest knockdown lines. Currently we are combining the strongest lines for both the phosphomimetic and phosphodeficient lines with FRT in order to generate clones and check for effect on EGFR and dpERK localization.

It has been shown that ERK phosphorylates drp1 at S616 in xenografts and this phosphorylation is important for Ras mediated increase in proliferation. S193 which we choose for the mutation lies in the GTPase domain. The mutation shows differential phenotypes using different Gal4s suggestive of the differential requirement of this residue. Expression of pUASP-*drp1*^{SG} in the *Drosophila* embryo gave extremely fused mitochondrial network during cellularization (Figure A2.4A-B, data contributed by Sayali Chowdhary). Mitochondria in neuroblast population of third instar larvae also become

A

	Genotype	**% Lethality with *nanos*-Gal4, n=300, N=3 for each**
Phosphomimetic Overexpression	pUASp*drp1*^{SD} Line1/SM6a	84%
	pUASp*drp1*^{SD} Line2/SM6a	20%
	pUASp*drp1*^{SD} Line3/SM6a	50%
	pUASp*drp1*^{SD} Line4/SM6a	57%
Phosphodeficient overexpression	pUASp*drp1*^{SG} Line1/SM6a	67%
	pUASp*drp1*^{SG} Line2/TM6Tb	46%
	pUASp*drp1*^{SG} Line3/SM6a	55%
	pUASp*drp1*^{SG} Line4/FM7a	ND
Wildtype Drp1 overexpression	pUASp*drp1* Line1/SM6a	2%
	pUASp*drp1* Line2/FM7a	3%
	pUASp*drp1* Line3/TM3Sb	6%
	pUASp*drp1* Line4/SM6a	1%
	pUASp*drp1* Line5/SM6a	8%

Table A2.1. High embryonic lethality in *nanos*-Gal4 driven *drp1* point mutants. The table summarizes the lethality statistics for all the transgenic lines for overexpression of phosphomimetic, phosphodeficient and wild type *drp1* fly lines. Both phosphomimetic and phosphodeficient lines are lethal to varying degrees. Most severe lines in case of point mutants and least severe in case of wild type *drp1* were chosen out of these (marked by red box) for further experiments.

fused in pUASP-*drp1*^{SG} driven by *worniu*-Gal4 (Figure A2.4B-C, data contributed by Dnyanesh Dubal). The degree of fusion differed in both the cell types (compare figure A2.4B to A2.4D). This offered us a nice gradation in the phenotype of pUASP-*drp1*^{SG} in four different systems in *Drosophila*, namely ovaries where there was no defect, neuroblast, which have mild fusion and embryo has completely aggregated network and wing where cells are probably dying. These results point towards tissue specific importance of the residue. It is intriguing to ask if ERK interaction differs in the tissues on account of this amino acid and this is the next experiment in line. We also tried to mutate Marf target sites. JNK is known to phosphorylate Mfn2 (Human homologue of Marf) at S27 (S37 in *Drosophila*) (Leboucher et. al., 2012). We do not have any positive hits till now for both phospohomimetic and deficient. It will be interesting to perturb the role of these specific sites in mitochondrial morphology as well as EGFR pathway. These mutations will also give an insight into tissue and cell specific interaction of EGFR pathway with mitochondrial morphology proteins.

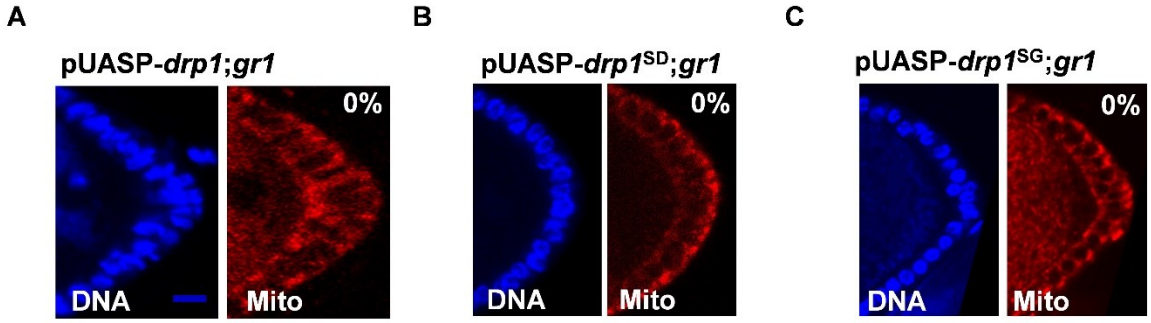

Figure A2.2. Point mutations of *drp1* does not alter mitochondrial morphology in the FCs. (A) Mitochondrial morphology (red) is dispersed in pUASP-*drp1*^{SD} similar to control cells (0% show defect in mitochondrial morphology, n=17, N=3). (B) Mitochondria are similar to control cells in pUASP-*drp1*^{SG} as well (0% show defect in mitochondrial morphology, n=20, N=3) (B).
Scale bar: 10µm. n= number of independent ovarioles. N= Experimental replicates.

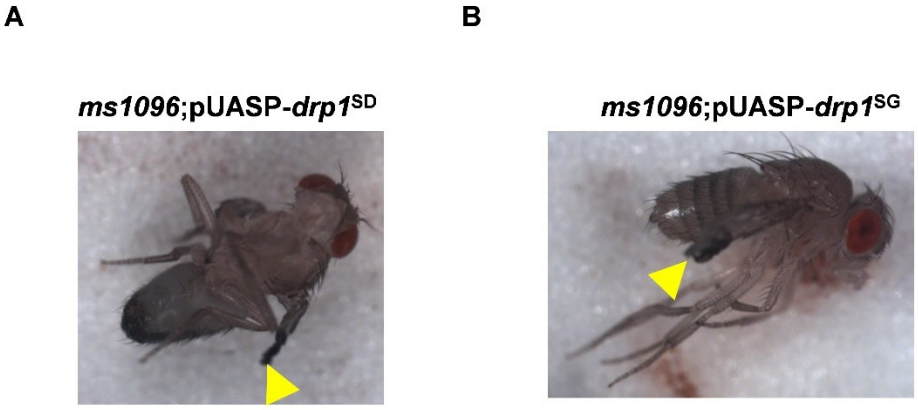

Figure A2.3. Wing morphology is severely compromised in phosphomimetic and phosphodeficient forms of *drp1*. (A) pUASP-*drp1*^{SD} wing is crumpled in 100% F1 progeny and the number of F1 is also less (100% have wing defect, n=32, N=2) (A). Phosphodeficient pUASP-*drp1*^{SG} also exhibit crumpling of wing in F1 (50% have wing defect, n=46, N=2) (B).
Scale bar: 1mm.

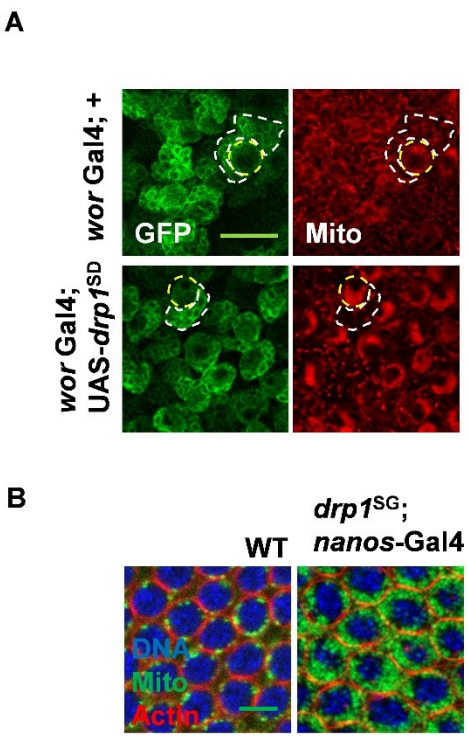

Figure A2.4. *drp1* point mutant cells exhibit aggregated mitochondrial morphology in *Drosophila* embryo and neuroblasts. (A) Mitochondria (red) network in neuroblasts (CD8GFP, green) (marked by yellow dashed outline) and the glia cells (marked by white dashed outline) is more aggregated in $drp1^{SD}$ in comparison to the Gal4 control cells. (B) *Drosophila* embryo in cellularization has sparse small mitochondria (green, DNA; blue, actin; red) in wild type and dense network in the $drp1^{SG}$ mutant.
Scale Bar: 5 μm.

Appendix A3

Screen to identify mitochondrial proteins essential for adult *Drosophila* wing development

In order to establish if the mitochondrial perturbations independently are capable of altering wing vein morphology, we devised a simple adult wing screen. We crossed RNAi lines against various mitochondrial proteins with the dorsal wing Gal4, *ms1096* and scored the F1 for defects in adult wing. The screen was carried out at 29°C. The lines lethal at 29° were repeated at 25°C as well. The table (Table A3.1) below presents the result for the screen followed by a brief discussion on key results which were obtained from it.

Dorsal compartment seems to be most sensitive to alteration in mitochondrial ETC components. Complex V depletion had the most severe impact and most of the RNAi lines were lethal. We were not able to test a number of lines from complex II, III and IV however because their unavailability or the lines did not survive. These results indicate the usage of ETC in the wing pouch. Results for primary morphology regulating proteins are discussed in Chapter 6, and loss of fusion proteins leads to lethality at pupal stage or absence of properly formed wings. We found that the most of the cofactors such as Zucchini and MitoPLD did not transfigure the adult wing. Zucchini, fly homologue of MitoPLD, a transmembrane protein is involved in generating signaling molecule Phosphatidic acid. Lipids have been shown to play significant role in mitochondrial manipulation and signaling (Ha and Frohman 2014). There are reports suggesting role of zucchini in regulation of mitochondrial fusion in *Drosophila* as well as mammalian cells (Choi *et al.* 2006; Muliyil *et al.* 2011). However downregulation of MitoPLD did not show any phenotypic change in the adult wing blade. Only Miro, involved in mitochondrial transport (Frederick *et al.* 2004) was found to display wing curling phenotype indicating an alteration in cell number. In H9c2 cells, Miro depletion lead to fragmented, condensed mitochondria (Saotome *et al.* 2008). Visualization of

mitochondria in wing disc in Miro mutant can further shed light on the genesis of wing curling phenotype.

Protein (Stock number)	%age defect (males);n	%age defect (females);n	Nature of defect	Comment
Complex I				
Cyt B5 Valium 20 (53950)	6%, 52	0%,44	wing crumpled	
Nox Valium 22 (38906)	100%,59	100%,57	wing curly	few flies dead on media
Nox Valium 22 (38921)	0%, 50	0%,46		
Nox Valium 20 (32433)	0%,86	0%,124		
Nox Valium 20 (32902)	0%,47	0%,45		
NDUFA8 Valium 22 (50577)	ND	ND		
NDUFA8 Valium 10 (42487)	0%,50	0%,40		
l(3) neo 18 Valium 22 (43278)	0%,50	0%,49		
CG15434 Valium 20 (52913)	72%,18	15%,26	wing crumpled	
CG8680 Valium 20 (51860)	0%,35	0%,32		few flies dead while eclosing
CG8680 Valium 10 (28576)	0%,84	0%,83		
CG12203 Valium 20 (53325)	No flies	100%,6	wing crumpled	flies dead while eclosing, dead pupae
CG5703 Valium 20 (51855)	Pupal lethal	Pupal lethal		
CG3214 Valium 20 (36695)	0%,82	0%,80		
CG12079 Valium 20 (51425)	0%,66	0%,80		

CG12079 Valium 20 (44535)	0%,50	0%,46		
CG5548 Valium10 (30511)	47%,48	69%,53	wing curly	
CG6020 Valium 20 (52922)	0%,50	0%,42		
CG1970 Valium 10 (28573)	0%,59	0%,57		
CG9140 Valium 20 (52939)	No flies	100%,15	wing crumpled	few flies dead while eclosing, males probably dead at larval stage as not a lot of pupae
CG9140 Valium 20 (36701)	0%,57	0%,72		
Complex II				
Scsalpha Valium 20 (51807)	No flies	No flies	larval lethal	
SdhC Valium 20 (53281)	0%,50	0%,43		
Complex III				
CG7580 Valium 20 (51357)	Pupal lethal	Pupal lethal		
Complex IV				
Surf1 Valium 20 (51783)	ND	ND		
CG3803 Valium 20 (35731)	0%,50	0%,41		
CG3803 Valium 20 (42948)	100%, 25	100%,20	wing crumpled, extra bristles	
Complex V ATP Synthase				
blw Valium 10 (28059)	Pupal lethal	Pupal lethal		
CG1746 Valium 22 (35464)	0%,50	0%,40		
ATP Synthase B Valium 10 (28062)	Pupal lethal	Pupal lethal		

ATP Synthase Beta Valium 10 (27712)	Pupal lethal	Pupal lethal		
ATP Synthase Beta Valium 10 (28056)	Pupal lethal	Pupal lethal		
ATP Synthase Cf6 Valium 20 (51714)	0%,47	0%,38		
ATP Synthase D Valium 20 (33740)	0%,111	0%,122		
ATP Synthase gamma Valium 22 (50543)	No flies	0%,4	wing curly	
Mitochondrial morphology				
Phospholipase D Valium (32839)	0%,77	0%,86		
Zucchini Valium 22 (35228)	0%,48	0%,45		
Zucchini Valium 20 (36742)				
PMI Valium 20 (34892)	0%,57	0%,77		
Miro Valium 22 (43973)	100%,28	100%,30	wing curly	
Miro Valium 10 (27695)	0%,76	0%,75		
Mitochondrial calcium regulation				
Pkc 53E Valium 20 (34716)	0%,44	0%,67		
Pkc 98E Valium 22 (34275)	0%,30	0%,40		
CamKII Valium 22 (35330)	0%,54	0%,79		

CamKI Valium 22 (35362)	0%,66	0%,44		
Camta Valium 21 (35683)	0%,45	0%,49		
Camta Valium 20 (40849)	0%,69	0%,74		
Cam Valium 20 (34609)	100%,25	100%,23	inward bent wings	few flies dead while eclosing, animals exhibit inability to fly
Trpm Valium 22 (35581)	0%,27	0%,27		
Trpy Valium 20 (53313)	0%,59	0%,44		
TrpA1 Valium 20 (36780)	ND	ND		
Trpml Valium 20 (44098)	0%,78	0%,82		
ROS				
SOD2 Valium 22(36871)	Pupal lethal	Pupal lethal		
SOD2 Valium 20 (32496)	0%,54	0%,46		few flies dead while eclosing
SOD2 Valium 20 (32983)	0%,104	0%,129		
SOD2 Valium 10 (25969)	0%,92	0%,80		
Catalase Valium 20 (43197)	100%,20	100%,25	wing crumpled	few flies dead while eclosing
Catalase Valium 20 (34020)	0%,61	0%,89		
PHGPx Valium 22 (41879)	100%,40	100%,57	wing curly	
GSTD1 Valium 22 (36818)	0%,47	0%,60		
GSTD5 Valium 20 (42842)	20%, 54	0%,46	wing crumpled	
GSTE1 Valium 22 (36878)	0%,45	0%,55		
GSTS1 Valium 22 (53238)	Larval lethal	Larval lethal		
Glucose metabolism				
Glut 1 Valium 20 (40904)	0%,44	0%,46		

Glycogen metabolism CG9485 Valium 20 (34333)	0%,35	0%,49		
GlyP Valium 20 (33634)	0%,71	0%,81		few flies dead while eclosing
Pgm Valium 20 (34345)	64%,42	47%,47	wing curly	
Insulin receptor InR Valium 20 (51518)	0%,57	0%,76		
Trancription				
Tfam 26744 Val10	15%,44	0%,40	wing curly	

Table A3.1. Table summerising effect of depletion of mitochondria and metabolism related proteins in the wing dorsal pouch.

Manipulation of calcium signaling machinery in *Drosophila* wing has been shown earlier with *apterous*-Gal4. Knockdown of CamKII causes increased nuclear fragmentation, CamKI depletion causes defects in scutellar structure (Balaji *et al.* 2017). *ms1096*-Gal4 did not show any morphological defect in the wing with calcium machinery knockdown. Trp channel protein depletion had few F1 flies, hinting at lethality at an early stage. Cam knockdown resulted in death during eclosion and inwardly bent wings. *apterous*-Gal4 has a larger expression domain than *ms1096*-Gal4. This might explain the difference in severity of the knockdown in our study and theirs. Immunostaining of wing discs can reveal defects not visible at adult wing level. In addition, the intercellular calcium waves (Restrepo and Basler 2016), are waves propagating in the anterio-posterior direction in the wing disc. It will be interesting to observe these waves using GCAMP, in mitochondrial mutants for ETC and shape regulating proteins.

Knockdown of mitochondrial SOD, SOD2 was lethal at pupal stage and another transgene of SOD2 gave fewer F1 flies. Severe wing crumpling and curling was seen with depletion of other ROS quenchers as well. Role of ROS in wing regeneration via JNK is well studied (Ruiz *et al.* 2015; Brock *et al.* 2017). Excess ROS can trigger apoptotic cell death (Colin *et al.* 2015) resulting in wing crumpling and lethality. EGFR overexpression in *Drosophila* eye and wing is suppressed by increase in ROS (Morey *et*

al. 2001). Excess ROS can affect cell division in developing wing disc, thereby decreasing the cell number and, subsequently wing curling. Phosphoglucomutase (Pgm) contributes to glycogen synthesis by mutating position of phosphate in glucose (Verrelli and Eanes 2001). In *Drosophila* notum, Pgm depletion caused loss of bristles (Mummery-Widmer *et al.* 2009). This paper postulated role of Pgm in Notch mediated lateral inhibition. Wing notching phenotype was not found, however, wing curling indicating deregulation of cell number or shape was documented. Loss of any other glucose or glycogen related protein did not alter adult wing morphology. Tfam is a mitochondrial transcription factor, its loss in *Drosophila* and mice reduces mitochondrial DNA (Larsson *et al.* 1998; Goto *et al.* 2001). Tfam safeguards against increase in ROS (Matsuda *et al.* 2013), its depletion can mimic SOD downregulation, probably that's why we observe the wing curling phenotype.

The preliminary results from the screen hence point towards ETC playing key role in *Drosophila* wing development, probably due to its role in cell cycle regulation. ROS levels are also crucial to the wing morphology due to their role in cell death induction. The screen lines can be combined with EGFR overexpression and knockdown to pick up interactors.

9 REFERENCES

1. Abele D., Heise K., Pörtner H. O., Puntarulo S., **2002** Temperature-dependence of mitochondrial function and production of reactive oxygen species in the intertidal mud clam Mya arenaria. J. Exp. Biol. **205**.
2. Afshar K., Stuart B., Wasserman S. A., **2000** Functional analysis of the *Drosophila* diaphanous FH protein in early embryonic development. Development **127**: 1887 LP-1897.
3. Ahmad T., Aggarwal K., Pattnaik B., Mukherjee S., Sethi T., Tiwari B. K., Kumar M., Micheal A., Mabalirajan U., Ghosh B., Sinha Roy S., Agrawal A., **2013** Computational classification of mitochondrial shapes reflects stress and redox state. Cell Death Dis. **4**: e461.
4. Al-Mehdi A.-B., Pastukh V. M., Swiger B. M., Reed D. J., Patel M. R., Bardwell G. C., Pastukh V. V, Alexeyev M. F., Gillespie M. N., **2012** Perinuclear Mitochondrial Clustering Creates an Oxidant-Rich Nuclear Domain Required for Hypoxia-Induced Transcription. Sci. Signal. **5**: ra47-ra47.
5. Aldaz S., Escudero L. M., Freeman M., **2010** Live imaging of *Drosophila* imaginal disc development. **107**: 14217–14222.
6. Allen R. ., Tresini M., **2000** Oxidative stress and gene regulation. Free Radic. Biol. Med. **28**: 463–499.
7. Alonso M., Melani M., Converso D., Jaitovich A., Paz C., Carreras M. C., Medina J. H., Poderoso J. J., **2004** Mitochondrial extracellular signal-regulated kinases 1/2 (ERK1/2) are modulated during brain development. J. Neurochem. **89**: 248–256.
8. Alto N. M., Soderling J., Scott J. D., **2002** Rab32 is an A-kinase anchoring protein and participates in mitochondrial dynamics. J. Cell Biol. **158**: 659–68.
9. Anderson C. a., Blackstone C., **2013** SUMO wrestling with Drp1 at mitochondria. EMBO J. **32**: 1496–1498.
10. Anh N. T. T., Nishitani M., Harada S., Yamaguchi M., Kamei K., **2011** Essential Role of Duox in Stabilization of *Drosophila* Wing. J. Biol. Chem. **286**: 33244–33251.
11. Aon M. A., Camara A. K. S., **2015** Mitochondria : hubs of cellular signaling ,

energetics and redox balance . A rich , vibrant , and diverse landscape of mitochondrial research. **6**: 2014–2016.

12. Armstrong A. R., Laws K. M., Barbosa D. D., **2014** Adipocyte amino acid sensing controls adult germline stem cell number via the amino acid response pathway and independently of Target of Rapamycin signaling in *Drosophila*. Development **141**: 4479–4488.
13. Arozarena I., Aaronson D. S., Matallanas D., Sanz V., Ajenjo N., Tenbaum S. P., Teramoto H., Ighishi T., Zabala J. C., Silvio Gutkind J., Crespo P., **2000** The Rho family GTPase Cdc42 regulates the activation of Ras/MAP kinase by the exchange factor Ras-GRF. J. Biol. Chem. **275**: 26441–26448.
14. Ashrafian H., Docherty L., Leo V., Towlson C., Neilan M., Lygate C. A., Hough T., Townsend S., Williams D., Wells S., Glyn-jones S., Land J., Barbaric I., Lalanne Z., Denny P., Bhattacharya S., Griffin J. L., Hargreaves I., Fernandez-fuentes N., Cheeseman M., Watkins H., Dear T. N., **2010** A Mutation in the Mitochondrial Fission Gene Dnm1l Leads to Cardiomyopathy. **6**: 1–18.
15. Atsuko Kasahara, Sara Cipolat, Yun Chen, Gerald W. Dorn II L. S., **2013** Mitochondrial Fusion Directs Cardiomyocyte Differentiation via Calcineurin and Notch Signaling. Science (80-.). **342**: 734–737.
16. Babayev E., Seli E., **2015** Oocyte mitochondrial function and reproduction. Curr. Opin. Obstet. Gynecol. **27**: 175–181.
17. Babu P. S., Krishnamurthy H., Chedrese P. J., Sairam M. R., **2000** Activation of Extracellular-regulated Kinase Pathways in Ovarian Granulosa Cells by the Novel Growth Factor Type 1 Follicle-stimulating Hormone Receptor. **275**: 27615–27626.
18. Bach D., Pich S., Soriano F. X., Vega N., Baumgartner B., Oriola J., Daugaard J. R., Lloberas J., Camps M., Zierath J. R., Rabasa-Lhoret R., Wallberg-Henriksson H., Laville M., Palacín M., Vidal H., Rivera F., Brand M., Zorzano A., **2003** Mitofusin-2 determines mitochondrial network architecture and mitochondrial metabolism. A novel regulatory mechanism altered in obesity. J. Biol. Chem. **278**: 17190–7.
19. Balaji R., Bielmeier C., Harz H., Bates J., Stadler C., Hildebrand A., Classen A.,

2017 Calcium spikes , waves and oscillations in a large , patterned epithelial tissue. Nat. Publ. Gr.: 1–14.

20. Banerjee E. O.-A. and U., **2009** Reactive Oxygen Species prime *Drosophila* haematopoietic progenitors for differentiation. Nature **461**: 537–541.
21. Basak N. P., Roy A., Banerjee S., **2014** Alteration of mitochondrial proteome due to activation of Notch1 signaling pathway. J Biol Chem **289**: 7320–7334.
22. Bergmann A., Agapite J., McCall K., Steller H., **1998** The *Drosophila* Gene hid Is a Direct Molecular Target of Ras-Dependent Survival Signaling. Cell **95**: 331–341.
23. Bilder D., Li M., Perrimon N., **2000** Cooperative regulation of cell polarity and growth by *Drosophila* tumor suppressors. Science **289**: 113–116.
24. Biswas G., Adebanjo O. A., Freedman B. D., Anandatheerthavarada H. K., Vijayasarathy C., Zaidi M., Kotlikoff M., Avadhani N. G., **1999** Retrograde Ca2+ signaling in C2C12 skeletal myocytes in response to mitochondrial genetic and metabolic stress: a novel mode of inter-organelle crosstalk. EMBO J. **18**: 522–533.
25. Bliek S. G.-B. and A. M. van der, **2008** The Novel Tail-anchored Membrane Protein Mff Controls Mitochondrial and Peroxisomal Fission in Mammalian Cells. Mol. Biol. Cell **19**: 308–317.
26. Boerner J. L., Demory M. L., Silva C., Parsons S. J., **2004** Phosphorylation of Y845 on the Epidermal Growth Factor Receptor Mediates Binding to the Mitochondrial Protein Cytochrome c Oxidase Subunit II. Mol. Cell. Biol. **24**: 7059–7071.
27. Bollu L. R., Ren J., Blessing A. M., Katreddy R. R., Gao G., Xu L., Wang J., Su F., Weihua Z., **2014** Involvement of de novo synthesized palmitate and mitochondrial EGFR in EGF induced mitochondrial fusion of cancer cells. Cell Cycle **13**: 2415–30.
28. Boonstra J., Post J. A., **2004** Molecular events associated with reactive oxygen species and cell cycle progression in mammalian cells. Gene **337**: 1–13.
29. Bourges I., Ramus C., Mousson de Camaret B., Beugnot R., Remacle C., Cardol P., Hofhaus G., Issartel J.-P., **2004** Structural organization of mitochondrial

human complex I: role of the ND4 and ND5 mitochondria-encoded subunits and interaction with prohibitin. Biochem. J. **383**: 491–499.

30. Boussau B., Karlberg E. O., Frank A. C., Legault B., Andersson S. G. E., **2004** Computational inference of scenarios for proteobacterial genome evolution. **2004**.
31. Brito O. M. de, Scorrano L., **2009** Mitofusin-2 regulates mitochondrial and endoplasmic reticulum morphology and tethering: the role of Ras. Mitochondrion **9**: 222–6.
32. Brock A. R., Seto M., Smith-Bolton R. K., **2017** Cap-n-collar Promotes Tissue Regeneration by Regulating ROS and JNK Signaling in the *Drosophila* Wing Imaginal Disc. Genetics.
33. Brou C., Logeat F., Gupta N., Bessia C., LeBail O., Doedens J. R., Cumano A., Roux P., Black R. A., Israël A., **2000** A Novel Proteolytic Cleavage Involved in Notch Signaling. Mol. Cell **5**: 207–216.
34. Buchon N., Broderick N. A., Kuraishi T., Lemaitre B., **2010** Drosophila EGFR pathway coordinates stem cell proliferation and gut remodeling following infection. BMC Biol. **8**: 152.
35. Burgess S. M., Delannoy M., Jensen R. E., **1994** MMM1 encodes a mitochondrial outer membrane protein essential for establishing and maintaining the structure of yeast mitochondria. J. Cell Biol. **126**: 1375–91.
36. Casar B., Pinto A., Crespo P., **2008** Essential Role of ERK Dimers in the Activation of Cytoplasmic but Not Nuclear Substrates by ERK-Scaffold Complexes. Mol. Cell **31**: 708–721.
37. Castanieto A., Johnston M. J., Nystul T. G., **2014** EGFR signaling promotes self-renewal through the establishment of cell polarity in *Drosophila* follicle stem cells. Elife **3**: 1–18.
38. Cereghetti G. M., Stangherlin a, Martins de Brito O., Chang C. R., Blackstone C., Bernardi P., Scorrano L., **2008** Dephosphorylation by calcineurin regulates translocation of Drp1 to mitochondria. Proc. Natl. Acad. Sci. U. S. A. **105**: 15803–8.
39. Chandel N. S., Schumacker P. T., **1999** Cells depleted of mitochondrial DNA

(rho0) yield insight into physiological mechanisms. FEBS Lett. **454**: 173–6.

40. Chandel N. S., **2015** Essay Evolution of Mitochondria as Signaling Organelles. Cell Metab. **22**: 204–206.
41. Chen H., Detmer S. a., Ewald A. J., Griffin E. E., Fraser S. E., Chan D. C., **2003** Mitofusins Mfn1 and Mfn2 coordinately regulate mitochondrial fusion and are essential for embryonic development. J. Cell Biol. **160**: 189–200.
42. Chen K., Guo X., Ma D., Guo Y., Li Q., Yang D., Li P., Wen S., Xiao R., Tang J., **2004** Dysregulation of HSG triggers vascular proliferative disorders. Nat. Cell Biol. **6**.
43. Chen C., Cheng T., Lin H., Shih N., Chen Y., Chen Y., Cheng C., Lian W., Meng T., Chiu W., Chen J., **2006** Reactive Oxygen Species Generation Is Involved in Epidermal Growth Factor Receptor Transactivation through the Transient Oxidization of Src Homology 2-Containing Tyrosine Phosphatase in Endothelin-1 Signaling Pathway in Rat Cardiac Fibroblasts. **69**: 1347–1355.
44. Chen J., Krasnow M. A., **2012** Integrin Beta 1 Suppresses Multilayering of a Simple Epithelium. **7**.
45. Chiaradonna F., Gaglio D., Vanoni M., Alberghina L., **2006** Expression of transforming K-Ras oncogene affects mitochondrial function and morphology in mouse fibroblasts. Biochim. Biophys. Acta **1757**: 1338–56.
46. Chiche J., Rouleau M., Gounon P., Brahimi-Horn M. C., Pouysségur J., Mazure N. M., **2010** Hypoxic enlarged mitochondria protect cancer cells from apoptotic stimuli. J. Cell. Physiol. **222**: 648–57.
47. Choi S., Huang P., Jenkins G. M., Chan D. C., Schiller J., Frohman M. A., **2006** A common lipid links Mfn-mediated mitochondrial fusion and SNARE-regulated exocytosis. **8**.
48. Chowdhary S., Tomer D., Dubal D., Sambre D., Rikhy R., **2017** Analysis of mitochondrial organization and function in the Drosophila blastoderm embryo. Sci. Rep.: 1–17.
49. Chung S., Dzeja P. P., Faustino R. S., Perez-terzic C., Behfar A., Terzic A., **2007** Mitochondrial oxidative metabolism is required for the cardiac differentiation of stem cells. Nat Clin Pr. Cardiovasc Med. **4**: 1–12.

50. Clancy D. J., **2001** Extension of Life-Span by Loss of CHICO, a *Drosophila* Insulin Receptor Substrate Protein. Science (80-.). **292**: 104–106.
51. Cohen M. M., Amiott E. a, Day A. R., Leboucher G. P., Pryce E. N., Glickman M. H., McCaffery J. M., Shaw J. M., Weissman A. M., **2011** Sequential requirements for the GTPase domain of the mitofusin Fzo1 and the ubiquitin ligase SCFMdm30 in mitochondrial outer membrane fusion. J. Cell Sci. **124**: 1403–10.
52. Colin J., Garibal J., Clavier A., Szuplewski S., **2015** Screening of suppressors of bax -induced cell death identifies glycerophosphate oxidase-1 as a mediator of debcl -induced apoptosis in Drosophila. **6**.
53. Collins T. J., Bootman M. D., **2003** Review Mitochondria are morphologically heterogeneous within cells. : 1993–2000.
54. Cook M., Bolkan B. J., Kretzschmar D., **2014** Increased Actin Polymerization and Stabilization Interferes with Neuronal Function and Survival in the AMPKγ Mutant Loechrig. PLoS One **9**: e89847.
55. Coqueret O., Be G., **1998** The mammalian Cut homeodomain protein functions as a cell-cycle-dependent transcriptional repressor which downmodulates p21 WAF1 / CIP1 / SDI1 in S phase. **17**: 4680–4694.
56. Cosson P., Marchetti A., Ravazzola M., Orci L., **2012** Mitofusin-2 Independent Juxtaposition of Endoplasmic Reticulum and Mitochondria: An Ultrastructural Study. PLoS One **7**: 1–5.
57. Cottet-Rousselle C., Ronot X., Leverve X., Mayol J. F., **2011** Cytometric assessment of mitochondria using fluorescent probes. Cytom. Part A **79 A**: 405–425.
58. Coulom H., Birman S., **2004** Chronic Exposure to Rotenone Models Sporadic Parkinson's Disease in Drosophila melanogaster. J. Neurosci. **24**.
59. Cox R. T., Spradling A. C., **2003** A Balbiani body and the fusome mediate mitochondrial inheritance during *Drosophila* oogenesis. Development **130**: 1579–1590.
60. Cribbs J. T., Strack S., **2007** Reversible phosphorylation of Drp1 by cyclic AMP-dependent protein kinase and calcineurin regulates mitochondrial fission and cell death. EMBO Rep. **8**: 939–44.

61. Cycle C., Menon S. G., Sarsour E. H., Spitz D. R., Higashikubo R., Sturm M., Zhang H., Goswami P. C., **2003** Redox Regulation of the G 1 to S Phase Transition in the Mouse Embryo Fibroblast. : 2109–2117.
62. DeVay R. M., Dominguez-Ramirez L., Lackner L. L., Hoppins S., Stahlberg H., Nunnari J., **2009** Coassembly of Mgm1 isoforms requires cardiolipin and mediates mitochondrial inner membrane fusion. J. Cell Biol. **186**: 793–803.
63. Diaz-Benjumea F. J., Hafen E., **1994** The sevenless signalling cassette mediates Drosophila EGF receptor function during epidermal development. Development **120**: 569 LP-578.
64. Dröge W., **2002** Free radicals in the physiological control of cell function. Physiol. Rev. **82**: 47–95.
65. Drummond-barbosa D., Spradling A. C., **2001** Stem Cells and Their Progeny Respond to Nutritional Changes during *Drosophila* Oogenesis. **278**: 265–278.
66. Duarte A., Castillo A. F., Podestá E. J., Poderoso C., **2014** Mitochondrial fusion and ERK activity regulate steroidogenic acute regulatory protein localization in mitochondria. PLoS One **9**: 1–12.
67. Duve C. de, **2007** The origin of eukaryotes: a reappraisal. Nat Rev Genet **8**: 395–403.
68. Ebisuya M., **2005** The duration, magnitude and compartmentalization of ERK MAP kinase activity: mechanisms for providing signaling specificity. J. Cell Sci. **118**: 2997–3002.
69. Egan D. F., Shackelford D. B., Mihaylova M. M., Gelino S. R., Rebecca A., Mair W., Vasquez D. S., Joshi A., Gwinn D. M., Asara J. M., Fitzpatrick J., Dillin A., Viollet B., Hansen M., Shaw R. J., **2011** Phosphorylation of ULK1 (hATG1) by AMP-activated protein kinase connects energy sensing to mitophagy. Science (80-.). **331**: 456–461.
70. Embley T. M., **2006** Multiple secondary origins of the anaerobic lifestyle in eukaryotes. : 1055–1067.
71. Engelmann R., Weisshart K., **2014** Airyscanning. G.I.T Imaging Microsc.: 20–21.
72. Ernster L S. G., **1981** Mitochondria : a historical review. J. Cell Biol. **91**: 2112799.
73. Eura Y., Ishihara N., Oka T., Mihara K., **2006** Identification of a novel protein that

regulates mitochondrial fusion by modulating mitofusin (Mfn) protein function. J. Cell Sci. **119**: 4913–25.

74. Facucho-Oliveira J. M., Facucho-Oliveira J. M., St John J. C., St John J. C., **2009** The relationship between pluripotency and mitochondrial DNA proliferation during early embryo development and embryonic stem cell differentiation. Stem cell Rev. reports **5**: 140–58.
75. Farida Korobova, Vinay Ramabhadran and H. N. H., **2013** An Actin-Dependent Step in Mitochondrial Fission Mediated by the ER-Associated Formin INF2. Science (80-.). **76**: 211–220.
76. Felipe K. Teixeira, Carlos G. Sanchez, Thomas R. Hurd J. R. K. S., Benjamin Czech, Jonathan B. Preall, Gregory J. Hannon and R. L., **2015** ATP synthase promotes germ cell differentiation independent of oxidative phosphorylation. Nat. Cell Biol. **6**: 300–308.
77. Fernández-Miñán A., Martín-Bermudo M. D., González-Reyes A., **2007** Integrin signaling regulates spindle orientation in *Drosophila* to preserve the follicular-epithelium monolayer. Curr. Biol. **17**: 683–688.
78. Fernández-Mosquera L., Diogo C. V, Yambire K. F., Santos G. L., Luna Sánchez M., Bénit P., Rustin P., Lopez L. C., Milosevic I., Raimundo N., **2017** Acute and chronic mitochondrial respiratory chain deficiency differentially regulate lysosomal biogenesis. Sci. Rep. **7**: 45076.
79. Fischer M. G., Heeger S., Häcker U., Lehner C. F., **2004** The Mitotic Arrest in Response to Hypoxia and of Polar Bodies during Early Embryogenesis Requires Drosophila Mps1. Curr. Biol. **14**: 2019–2024.
80. Forbes A. J., Lin H., Ingham P. W., Spradling A. C., **1996** hedgehog is required for the proliferation and specification of ovarian somatic cells prior to egg chamber formation in Drosophila. **1135**: 1125–1135.
81. Frank S., Gaume B., Bergmann-Leitner E. S., Leitner W. W., Robert E. G., Catez F., Smith C. L., Youle R. J., **2001** The Role of Dynamin-Related Protein 1, a Mediator of Mitochondrial Fission, in Apoptosis. Dev. Cell **1**: 515–525.
82. Frederick R. L., Mccaffery J. M., Cunningham K. W., Okamoto K., Shaw J. M., Yeast Miro GTPase, Gem1p, regulates mitochondrial morphology via a novel

pathway. : 87–98.

83. Fujii N., Hayashi T., Hirshman M. F., Smith J. T., Habinowski S. A., Kaijser L., Mu J., Ljungqvist O., Birnbaum M. J., Witters L. A., Thorell A., Goodyear L. J., **2000** Exercise Induces Isoform-Specific Increase in 5 J AMP-Activated Protein Kinase Activity in Human Skeletal Muscle. **1155**: 1150–1155.
84. Gabay L., Scholz H., Golembo M., Klaes A., Shilo B. Z., Klambt C., **1996** EGF receptor signaling induces pointed P1 transcription and inactivates Yan protein in the Drosophila embryonic ventral ectoderm. Development **122**: 3355 LP-3362.
85. Gao H., Wu X., Simon L., Fossett N., **2014** Antioxidants Maintain E-Cadherin Levels to Limit Drosophila Prohemocyte Differentiation. **9**: 31–33.
86. Garcia-Bellido A., Celis J. F. de, **1992** Developmental Genetics of the Venation Pattern of *Drosophila*. Annu. Rev. Genet. **26**: 277–304.
87. Gegg M. E., Cooper J. M., Chau K. Y., Rojo M., Schapira A. H. V., Taanman J. W., **2010** Mitofusin 1 and mitofusin 2 are ubiquitinated in a PINK1/parkin-dependent manner upon induction of mitophagy. Hum. Mol. Genet. **19**: 4861–4870.
88. Ghiglione C., Iii K. L. C., Amundadottir L. T., Boswell R. E., Perrimon N., Duffy J. B., **1999** The Transmembrane Molecule Kekkon 1 Acts in a Feedback Loop to Negatively Regulate the Activity of the *Drosophila* EGF Receptor during Oogenesis. **96**: 847–856.
89. Godde N. J., Sheridan J. M., Smith L. K., Pearson H. B., Britt K. L., Galea R. C., Yates L. L., Visvader J. E., Humbert P. O., **2014** Scribble Modulates the MAPK / Fra1 Pathway to Disrupt Luminal and Ductal Integrity and Suppress Tumour Formation in the Mammary Gland. **10**.
90. Godt D., Tepass U., **1998** *Drosophila* oocyte localization is mediated by differential cadherin-based adhesion. Nature **395**: 387–391.
91. Goentoro L. A., Reeves G. T., Kowal C. P., Martinelli L., Schüpbach T., Shvartsman S. Y., **2006** Quantifying the Gurken Morphogen Gradient in *Drosophila* Oogenesis. Dev. Cell **11**: 263–272.
92. Golic K. G., Lindquist S., **1989** The FLP recombinase of yeast catalyzes site-specific recombination in the *Drosophila* genome. Cell **59**: 499–509.

93. Gómez-Lamarca M. J., Cobreros-Reguera L., Ibáñez-Jiménez B., Palacios I. M., Martín-Bermudo M. D., **2014** Integrins regulate epithelial cell differentiation by modulating Notch activity. J. Cell Sci.: 4667–4678.
94. Goode S., Melnick M., Chou T., Perrimon N., **1996** The neurogenic genes egghead and brainiac define a novel signaling pathway essential for epithelial morphogenesis during *Drosophila* oogenesis. **3879**: 3863–3879.
95. Goto A., Matsushima Y., Kadowaki T., Kitagawa Y., **2001** *Drosophila* mitochondrial transcription factor A (d -TFAM) is dispensable for the transcription of mitochondrial DNA in Kc167 cells. **248**: 243–248.
96. Gouin E., Welch M. D., Cossart P., **2005** Actin-based motility of intracellular pathogens. Curr. Opin. Microbiol. **8**: 35–45.
97. Grammont M., Irvine K. D., **2001** fringe and Notch specify polar cell fate during Drosophila oogenesis. **2253**: 2243–2253.
98. Gray M. W., **2012** Mitochondrial Evolution. : 1–16.
99. Griffin R., Sustar A., Bonvin M., Binari R., Valle A., Bakal C., Hohl A. M., Bateman J. R., Villalta C., Heffern E., Grunwald D., Desplan C., Schubiger G., Wu C., Perrimon N., **2009** Analysis. Nat. Methods **6**: 600–602.
100. Griparic L., Kanazawa T., Bliek A. M. Van Der, **2007** Regulation of the mitochondrial dynamin-like protein Opa1 by proteolytic cleavage. J. Cell Biol. **178**: 757–764.
101. Grol M. W., Zelner I., Dixon S. J., **2012** mediated calcium influx triggers a sustained, PI3K-dependent increase in metabolic acid production by osteoblast-like cells. Am. J. Physiol. - Endocrinol. Metab. **302**: E561 LP-E575.
102. Gui D. Y., Sullivan L. B., Luengo A., Hosios A. M., Bush L. N., Gitego N., Davidson S. M., Freinkman E., Thomas C. J., Vander Heiden M. G., **2016** Environment Dictates Dependence on Mitochondrial Complex I for NAD+ and Aspartate Production and Determines Cancer Cell Sensitivity to Metformin. Cell Metab. **24**: 716–727.
103. Gunter T. E., Pfeiffer D. R., **1990** Mechanisms by which mitochondria transport calcium. Am. J. Physiol. **258**: C755–C786.
104. Gupte T. M., **2015** Mitochondrial Fragmentation Due to Inhibition of Fusion

Increases Cyclin B through Mitochondrial Superoxide Radicals. : 1–19.

105. Guyton K. Z., Liu Y., Gorospe M., Xu Q., Holbrook N. J., **1996** Activation of Mitogen-activated Protein Kinase by H 2 O 2. **271**: 4138–4142.

106. Ha E. E., Frohman M. A., **2014** Regulation of Mitochondrial Morphology by Lipids. Biofactors **40**: 419–424.

107. Hales K. G., Fuller M. T., **1997** Fusion Mediated by a Conserved , Novel , Predicted GTPase. **90**: 121–129.

108. Hardie D. G., Carling D., **1997** The AMP-activated protein kinase--fuel gauge of the mammalian cell? Eur. J. Biochem. **246**: 259–73.

109. Havens C. G., Ho A., Yoshioka N., Dowdy S. F., **2006** Regulation of Late G 1 / S Phase Transition and APC Cdh1 by Reactive Oxygen Species †. **26**: 4701–4711.

110. Hawley S. A., Pan D. A., Mustard K. J., Ross L., Bain J., Edelman A. M., Frenguelli B. G., Hardie D. G., **2005** Calmodulin-dependent protein kinase kinase-β is an alternative upstream kinase for AMP-activated protein kinase. Cell Metab. **2**: 9–19.

111. Haynes C. M., Petrova K., Benedetti C., Yang Y., Ron D., **2007** ClpP mediates activation of a mitochondrial unfolded protein response in C. elegans. Dev. Cell **13**: 467–80.

112. Hermann G. J., Thatcher J. W., Mills J. P., Hales K. G., Fuller M. T., Nunnari J., Shaw J. M., **1998** Mitochondrial fusion in yeast requires the transmembrane GTPase Fzo1p. J. Cell Biol. **143**: 359–73.

113. Heymann J. a W., Hinshaw J. E., **2009** Dynamins at a glance. J. Cell Sci. **122**: 3427–3431.

114. Hill J. H., Chen Z., Xu H., **2014** Selective propagation of functional mitochondrial DNA during oogenesis restricts the transmission of a deleterious mitochondrial variant. Nat Genet **46**: 389–392.

115. Hoppins S., Lackner L., Nunnari J., **2007** The Machines that Divide and Fuse Mitochondria. Annu. Rev. Biochem. **76**: 751–780.

116. Horbinski C., Chu C. T., **2005** Kinase signaling cascades in the mitochondrion: a matter of life or death. Free Radic. Biol. Med. **38**: 2–11.

117. Horibe T., Hoogenraad N. J., **2007** The Chop Gene Contains an Element for the Positive Regulation of the Mitochondrial Unfolded Protein Response. PLoS One **2**: e835.

118. Hou Y. C., Chittaranjan S., Gonz S., Mccall K., Gorski S. M., **2008** JCB . **182**: 1127–1139.

119. Houghton F. D., Christopher G. T., Leese H. J., **1996** Oxygen Consumption and Energy Metabolism of the Early Mouse Embryo. Mol. Reprod. Dev. **485**: 476–485.

120. Houghton1 F. D., Hawkhead J. A., Humpherson P. G., Hogg J. E., Balen A. H., Rutherford A. J., Leese H. J., **2002** Non-invasive amino acid turnover predicts human embryo developmental capacity. Hum. Reprod. **17**: 999–1005.

121. Hurd T. R., Liang F., Lehmann R., **2011** Curly Encodes Dual Oxidase , Which Acts with Heme Peroxidase Curly Su to Shape the Adult Drosophila Wing. J. Biol. Chem.: 1–15.

122. In R., Tyrosine E. G. F. R., Bae Y. S., Kang S. W., Seo M. S., Baines I. C., Tekle E., Chock P. B., Rhee S. G., **1997** Epidermal Growth Factor (EGF) - induced Generation of. **272**: 217–221.

123. Ishihara N., Nomura M., Jofuku A., Kato H., Suzuki S. O., Masuda K., Otera H., Nakanishi Y., Nonaka I., Goto Y.-I., Taguchi N., Morinaga H., Maeda M., Takayanagi R., Yokota S., Mihara K., **2009** Mitochondrial fission factor Drp1 is essential for embryonic development and synapse formation in mice. Nat. Cell Biol. **11**: 958–966.

124. Jackson S. M., Blochlinger K., **1997** cut interacts with Notch and Protein kinase A to regulate egg chamber formation and to maintain germline cyst integrity during Drosophila oogenesis. **3672**: 3663–3672.

125. James K. E., Dorman J. B., Berg C. a, **2002** Mosaic analyses reveal the function of Drosophila Ras in embryonic dorsoventral patterning and dorsal follicle cell morphogenesis. Development **129**: 2209–2222.

126. Jendrach M., Mai S., Pohl S., Vöth M., Bereiter-Hahn J., **2008** Short- and long-term alterations of mitochondrial morphology, dynamics and mtDNA after transient oxidative stress. Mitochondrion **8**: 293–304.

127. Jheng H.-F., Tsai P.-J., Guo S.-M., Kuo L.-H., Chang C.-S., Su I.-J., Chang C.-R., Tsai Y.-S., **2012** Mitochondrial Fission Contributes to Mitochondrial Dysfunction and Insulin Resistance in Skeletal Muscle. Mol. Cell. Biol. **32**: 309–319.

128. Jia D., Soylemez M., Calvin G., Bornmann R., Bryant J., Hanna C., Huang Y.-C., Deng W.-M., **2015** A large-scale in vivo RNAi screen to identify genes involved in Notch-mediated follicle cell differentiation and cell cycle switches. Sci. Rep. **5**: 12328.

129. Johnston M. J., Bar-Cohen S., Paroush Z., Nystul T. G., **2016** Phosphorylated Groucho delays differentiation in the follicle stem cell lineage by providing a molecular memory of EGFR signaling in the niche. Development: dev.143263.

130. Jouandin P., Ghiglione C., Noselli S., **2014** Starvation induces FoxO-dependent mitotic-to-endocycle switch pausing during Drosophila oogenesis. : 3013–3021.

131. Ju T., Chen H., Lin J., Chang C., Chang W., Kang J., Sun C., Tao M., Tu P., Chang C., Dickson D. W., Chern Y., Nuclear translocation of AMPK- □ 1 potentiates striatal neurodegeneration in Huntington's disease. **194**: 209–227.

132. Karbowski M., Lee Y. J., Gaume B., Jeong S. Y., Frank S., Nechushtan A., Santel A., Fuller M., Smith C. L., Youle R. J., **2002** Spatial and temporal association of Bax with mitochondrial fission sites, Drp1, and Mfn2 during apoptosis. J. Cell Biol. **159**: 931–938.

133. Karbowski M., Jeong S. Y., Youle R. J., **2004** Endophilin B1 is required for the maintenance of mitochondrial morphology. J. Cell Biol. **166**: 1027–1039.

134. Kashatus J. A., Nascimento A., Myers L. J., Sher A., Byrne F. L., Hoehn K. L., Counter C. M., Kashatus D. F., **2015** Erk2 Phosphorylation of Drp1 Promotes Mitochondrial Fission and MAPK-Driven Tumor Growth. Mol. Cell **57**: 537–551.

135. Kazgan N., Williams T., Forsberg L. J., Brenman J. E., **2010** Identification of a Nuclear Export Signal in the Catalytic Subunit of AMP-activated Protein Kinase. **21**: 3433–3442.

136. Keefe D. D. O., Prober D. A., Moyle P. S., Rickoll W. L., Bruce A., **2007** EGFR/Ras signaling regulates DE-cadherin/Shotgun localization to control vein morphogenesis in the Drosophila wing. Dev. Biol. **311**: 25–39.

137. Keller M., Deng L. W., Holder K., Tworoger M., Clegg N., **1999** Role of Notch pathway in terminal follicle cell differentiation during Drosophila oogenesis. : 1995–1996.

138. Kim H. J., Shaker M. R., Cho B., Cho H. M., Kim H., Kim J. Y., Sun W., **2015** Dynamin-related protein 1 controls the migration and neuronal differentiation of subventricular zone-derived neural progenitor cells. Nat. Publ. Gr.: 1–13.

139. Korwitz A., Merkwirth C., Richter-Dennerlein R., Tröder S. E., Sprenger H. G., Quirós P. M., López-Otín C., Rugarli E. I., Langer T., **2016** Loss of OMA1 delays neurodegeneration by preventing stress-induced OPA1 processing in mitochondria. J. Cell Biol. **212**: 157–166.

140. Koshiba T., Detmer S. A., Kaiser J. T., Chen H., McCaffery J. M., Chan D. C., **2004** Structural basis of mitochondrial tethering by mitofusin complexes. Science (80-.). **305**: 858–862.

141. Kowno M., Watanabe-susaki K., Ishimine H., Komazaki S., Enomoto K., **2014** Prohibitin 2 Regulates the Proliferation and Lineage- Specific Differentiation of Mouse Embryonic Stem Cells in Mitochondria. **9**.

142. Lan F., Cacicedo J. M., Ruderman N., Ido Y., **2008** SIRT1 Modulation of the Acetylation Status , Cytosolic Localization , and Activity of LKB1. **283**: 27628–27635.

143. Landor S. K.-J., Mutvei a. P., Mamaeva V., Jin S., Busk M., Borra R., Gronroos T. J., Kronqvist P., Lendahl U., Sahlgren C. M., **2011** Hypo- and hyperactivated Notch signaling induce a glycolytic switch through distinct mechanisms. Proc. Natl. Acad. Sci. **108**: 18814–18819.

144. Larsson N.-G., Wang J., Wilhelmsson H., Oldfors A., Rustin P., Lewandoski M., Barsh G. S., Clayton D. A., **1998** Mitochondrial transcription factor A is necessary for mtDNA maintance and embryogenesis in mice. Nat Genet **18**: 231–236.

145. Leboucher G. P., Tsai Y. C., Yang M., Shaw K. C., Zhou M., Veenstra T. D., Glickman M. H., Weissman A. M., **2012** Stress-Induced Phosphorylation and Proteasomal Degradation of Mitofusin 2 Facilitates Mitochondrial Fragmentation and Apoptosis. Mol. Cell **47**: 547–557.

146. Lee S. B., Cho K. S., Kim E., Chung J., **2003** blistery encodes *Drosophila* tensin protein and interacts with integrin and the JNK signaling pathway during wing development. Development **130**: 4001 LP-4010.

147. Lee J. H., Koh H., Kim M., Kim Y., Lee S. Y., Karess R. E., Lee S., Shong M., Kim J., Kim J., Chung J., **2007** Energy-dependent regulation of cell structure by AMP-activated protein kinase. **447**.

148. Lee S. F., Srinivasan B., Sephton C. F., Dries D. R., Wang B., Yu C., Wang Y., Dewey C. M., Shah S., Jiang J., Yu G., **2011** Γ-Secretase-Regulated Proteolysis of the Notch Receptor By Mitochondrial Intermediate Peptidase. J. Biol. Chem. **286**: 27447–27453.

149. Lee J. E., Westrate L. M., Wu H., Page C., Voeltz G. K., **2016a** Multiple dynamin family members collaborate to drive mitochondrial division. Nature **54o**: 139–143.

150. Lee S., Lee K., Huh S., Hong S. H., Lee S., Lee K., Huh S., Liu S., Lee D., Hong S. H., Yu K., **2016b** Polo Kinase Phosphorylates Miro to Control ER-Mitochondria Contact Sites and Mitochondrial Ca 2 + Homeostasis in Neural Stem Cell Development Article Polo Kinase Phosphorylates Miro to Control ER-Mitochondria Contact Sites and Mitochondrial Ca 2 + Homeos. Dev. Cell **37**: 174–189.

151. Leese H. J., Metabolism of the preimplantation embryo : 40 years on.

152. Lehtinen M. K., Yuan Z., Boag P. R., Yang Y., Villén J., Becker E. B. E., DiBacco S., la Iglesia N. de, Gygi S., Blackwell T. K., Bonni A., **2006** A conserved MST-FOXO signaling pathway mediates oxidative-stress responses and extends life span. Cell **125**: 987–1001.

153. Levkowitz G., Waterman H., Ettenberg S. A., Katz M., Tsygankov A. Y., Alroy I., Lavi S., Iwai K., Reiss Y., Ciechanover A., Lipkowitz S., Yarden Y., **1999** Ubiquitin Ligase Activity and Tyrosine Phosphorylation Underlie Suppression of

Growth Factor Signaling by c-Cbl/Sli-1. Mol. Cell **4**: 1029–1040.

154. Li Q., Shen L., Xin T., Xiang W., Chen W., Gao Y., Zhu M., Yu L., Li M., **2009** Role of Scrib and Dlg in anterior-posterior patterning of the follicular epithelium during Drosophila oogenesis. BMC Dev. Biol. **9**: 60.

155. Li S., Xu S., Roelofs B. A., Boyman L., Lederer W. J., Sesaki H., Karbowski M., **2015** Transient assembly of F-actin on the outer mitochondrial membrane contributes to mitochondrial fission. **208**: 109–123.

156. Liesa M., Shirihai O. S., **2013** Mitochondrial dynamics in the regulation of nutrient utilization and energy expenditure. Cell Metab. **17**: 491–506.

157. Liu D., Liu A., **2013** Superoxide dismutase induces G1-phase cell cycle arrest by down-regulated expression of Cdk-2 and cyclin-E in murine sarcoma S180 tumor cells. Cell Biochem. Funct. **31**: 352–359.

158. Lodi R., Tonon C., Clementi V., Malucelli E., **2004** Deficit of In Vivo Mitochondrial ATP Production in OPA1-Related Dominant Optic Atrophy. : 719–723.

159. Lopez-Mejia I. C., Fajas L., **2015** Cell cycle regulation of mitochondrial function. Curr. Opin. Cell Biol. **33**: 19–25.

160. López-Schier H., Johnston D. St., **2001** Delta signaling from the germ line controls the proliferation and differentiation of the somatic follicle cells during Drosophila oogenesis. Genes Dev. **15**: 1393–1405.

161. Lorenzen J. A., Baker S. E., Denhez F., Melnick M. B., Brower D. L., Perkins L. A., **2001** Nuclear import of activated D-ERK by DIM-7 , an importin family member encoded by the gene moleskin. **1414**: 1403–1414.

162. Loza M. C. D. De, Thompson B. J., **2017** Mechanisms of Development Forces shaping the *Drosophila* wing. Mech. Dev. **144**: 23–32.

163. Maeda Y., Chida J., **2013** Control of cell differentiation by mitochondria, typically evidenced in dictyostelium development. Biomolecules **3**: 943–66.

164. Maimaitijiang A., Zhuang X., Jiang X., Li Y., **2016** Biochemical and Biophysical Research Communications Dynamin-related protein inhibitor downregulates reactive oxygen species levels to indirectly suppress high glucose-induced hyperproliferation of vascular smooth muscle cells. Biochem.

Biophys. Res. Commun. **471**: 474–478.

165. Malartre M., **2016** Regulatory mechanisms of EGFR signalling during Drosophila eye development. Cell. Mol. Life Sci. **73**: 1825–1843.

166. Mandal S., Lindgren A. G., Srivastava A. S., Clark A. T., Banerjee U., Angeles C. L., **2011a** Mitochondrial function controls proliferation and early differentiation potential of embryonic stem cells. Stem Cells **29**: 486–495.

167. Mandal S., Lindgren A. G., Srivastava A. S., Clark A. T., Banerjee U., **2011b** Mitochondrial function controls proliferation and early differentiation potential of embryonic stem cells. Stem Cells **29**: 486–95.

168. Marchi S., Patergnani S., Pinton P., **2014** The endoplasmic reticulum–mitochondria connection: One touch, multiple functions. Biochim. Biophys. Acta - Bioenerg. **1837**: 461–469.

169. Marenda D. R., Vrailas A. D., Rodrigues A. B., Cook S., Maureen A., Lorenzen J. a, Perkins L. a, Moses K., **2006** MAP kinase subcellular localization controls both pattern and proliferation in the developing Drosophila wing. Development **133**: 43–51.

170. Martens S., McMahon H. T., **2008** Mechanisms of membrane fusion: disparate players and common principles. Nat. Rev. Mol. Cell Biol. **9**: 543–556.

171. Martin P. M., Sutherland A. E., Winkle L. J. Van, **2003** Amino Acid Transport Regulates Blastocyst Implantation1. Biol. Reprod. **69**: 1101–1108.

172. Martín-Blanco E., Roch F., Noll E., Baonza a, Duffy J. B., Perrimon N., **1999** A temporal switch in DER signaling controls the specification and differentiation of veins and interveins in the *Drosophila* wing. Development **126**: 5739–47.

173. Martinou J.-C., **1999** Apoptosis. Key to the mitochondrial gate. Nature **399**: 411–412.

174. Martinou J.-C., Youle R. J., 2006 Which came first, the cytochrome c release or the mitochondrial fission? Cell Death Differ. **13**: 1291–1295.

175. Martinus R. D., Garth G. P., Webster T. L., Cartwright P., Naylor D. J., Høj P. B., Hoogenraad N. J., **1996** Selective Induction of Mitochondrial Chaperones in Response to Loss of the Mitochondrial Genome. Eur. J. Biochem. **240**: 98–

103.

176. Matsuda N., Sato S., Shiba K., Okatsu K., Saisho K., Gautier C. A., Sou Y. S., Saiki S., Kawajiri S., Sato F., Kimura M., Komatsu M., Hattori N., Tanaka K., **2010** PINK1 stabilized by mitochondrial depolarization recruits Parkin to damaged mitochondria and activates latent Parkin for mitophagy. J. Cell Biol. **189**: 211–221.

177. Matsuda T., Kanki T., Tanimura T., Kang D., Matsuura E. T., **2013** Biochemical and Biophysical Research Communications Effects of overexpression of mitochondrial transcription factor A on lifespan and oxidative stress response in *Drosophila* melanogaster. Biochem. Biophys. Res. Commun. **430**: 717–721.

178. Mcbride H. M., Neuspiel M., **2006** Mitochondria : More Than Just a Powerhouse. : 551–560.

179. Mccaffrey L. M., Montalbano J., Mihai C., Macara I. G., **2012** Article Loss of the Par3 Polarity Protein Promotes Breast Tumorigenesis and Metastasis. Cell **22**: 601–614.

180. Mears J. A., Lackner L. L., Fang S., Ingerman E., Nunnari J., Hinshaw J. E., **2011** Conformational changes in Dnm1 support a contractile mechanism for mitochondrial fission. Nat. Struct. Mol. Biol. **18**: 20–6.

181. Mihaylova M. M., Shaw R. J., **2011** The AMPK signalling pathway coordinates cell growth , autophagy and metabolism. Nat. Publ. Gr. **13**: 1016–1023.

182. Milner B. M. J., **1977** The eversion and differentiation of *Drosophila* melanogaster leg and wing imaginal discs cultured in vitro with an optimal concentration of (3-ecdysone. **31**: 105–117.

183. Mishra P., Chan D. C., **2016** Metabolic regulation of mitochondrial dynamics. J. Cell Biol. **212**: 379–387.

184. Mitra K., Wunder C., Roysam B., Lin G., Lippincott-Schwartz J., **2009** A hyperfused mitochondrial state achieved at G1-S regulates cyclin E buildup and entry into S phase. Proc. Natl. Acad. Sci. U. S. A. **106**: 11960–5.

185. Mitra K., Rikhy R., Lilly M., Lippincott-Schwartz J., **2012** DRP1-dependent

mitochondrial fission initiates follicle cell differentiation during *Drosophila* oogenesis. J. Cell Biol. **197**: 487–97.

186. Monick M. M., Powers L. S., Barrett C. W., Hinde S., Ashare A., Groskreutz D. J., Nyunoya T., Coleman M., Spitz D. R., Hunninghake G. W., **2008** Constitutive ERK MAPK activity regulates macrophage ATP production and mitochondrial integrity. J. Immunol. **180**: 7485–7496.

187. Morey M., Serras F., Baguñà J., Hafen E., Corominas M., **2001** Modulation of the Ras/MAPK signalling pathway by the redox function of selenoproteins in *Drosophila* melanogaster. Dev. Biol. **238**: 145–156.

188. Morimoto A. M., Jordan K. C., Tietze K., Britton J. S., Neill E. M., Ruohola-Baker H., **1996** Pointed, an ETS domain transcription factor, negatively regulates the EGF receptor pathway in *Drosophila* oogenesis. Development **122**: 3745 LP-3754.

189. Morlino G., Barreiro O., Baixauli F., Robles-Valero J., González-Granado J. M., Villa-Bellosta R., Cuenca J., Sánchez-Sorzano C. O., Veiga E., Martín-Cófreces N. B., Sánchez-Madrid F., **2014** Miro-1 links mitochondria and microtubule Dynein motors to control lymphocyte migration and polarity. Mol. Cell. Biol. **34**: 1412–26.

190. Motoshima H., Goldstein B. J., Igata M., Araki E., **2006** AMPK and cell proliferation – AMPK as a therapeutic target for atherosclerosis and cancer. J. Physiol. **574**: 63–71.

191. Mourikis P., Hurlbut G. D., Artavanis-tsakonas S., **2006** Enigma , a mitochondrial protein affecting lifespan and oxidative stress response in *Drosophila*. **103**: 1307–1312.

192. Mozdy A. D., McCaffery J. M., Shaw J. M., **2000** Dnm1p GTPase-mediated mitochondrial fission is a multi-step process requiring the novel integral membrane component Fis1p. J. Cell Biol. **151**: 367–379.

193. Mukherjee S., Forde R., Belton A., Duttaroy A., **2011** SOD2 , the principal scavenger of mitochondrial superoxide , is dispensable for embryogenesis and imaginal tissue development but essential for adult survival. : 39–46.

194. Muliyil S., Krishnakumar P., Narasimha M., **2011** Spatial , temporal and

molecular hierarchies in the link between death , delamination and dorsal closure. **3054**: 3043–3054.

195. Mummery-Widmer J. L., Yamazaki M., Stoeger T., Novatchkova M., Bhalerao S., Chen D., Dietzl G., Dickson B. J., Knoblich J. A., **2009** Genome-wide analysis of Notch signalling in Drosophila by transgenic RNAi. Nature **458**: 987–992.

196. Nagaraj R., Gururaja-rao S., Jones K. T., Slattery M., Negre N., Braas D., Christofk H., White K., Mann R., Banerjee U., **2012** Control of mitochondrial structure and function by the Yorkie / YAP oncogenic pathway.

197. Narbonne K., Besse F., Brissard-zahraoui J., Pret A., Busson D., **2004** polyhomeotic is required for somatic cell proliferation and differentiation during ovarian follicle formation in *Drosophila*. : 1389–1400.

198. Nauseef W. M., **2008** Biological roles for the NOX family NADPH oxidases. J. Biol. Chem. **283**: 16961–16965.

199. Nicholls D. G., Budd S. L., **2000** Mitochondria and Neuronal Survival. **80**: 315–360.

200. Noguchi M., Kasahara A., **2017** *Mitochondrial dynamics coordinate cell differentiation*.

201. Nunnari J., Marshall W. F., Straight a, Murray a, Sedat J. W., Walter P., **1997** Mitochondrial transmission during mating in Saccharomyces cerevisiae is determined by mitochondrial fusion and fission and the intramitochondrial segregation of mitochondrial DNA. Mol. Biol. Cell **8**: 1233–42.

202. Ohsawa S., Sato Y., Enomoto M., Nakamura M., Betsumiya A., Igaki T., **2012** Mitochondrial defect drives non-autonomous tumour progression through Hippo signalling in *Drosophila*. Nature **490**: 547–51.

203. Okada H., Ebhardt H. A., Vonesch S. C., Aebersold R., Hafen E., **2016** phenotype in Drosophila melanogaster. Nat. Commun. **7**: 1–11.

204. Okamoto K., Shaw J. M., **2005** Mitochondrial Morphology and Dynamics in Yeast and Multicellular Eukaryotes. Annu. Rev. Genet. **39**: 503–536.

205. Palmer C. S., Osellame L. D., Laine D., Koutsopoulos O. S., Frazier A. E., Ryan M. T., **2011** MiD49 and MiD51, new components of the mitochondrial

fission machinery. EMBO Rep. **12**: 565–73.

206. Parker D. J., Iyer A., Shah S., Moran A., Hjelmeland A. B., Basu M. K., **2015** RESEARCH ARTICLE A new mitochondrial pool of cyclin E , regulated by Drp1 , is linked to cell-density-dependent cell proliferation. **1**: 4171–4182.

207. Paula W. B. M. De, Lucas C. H., Agip A. A., Vizcay-barrena G., Allen J. F., Allen J. F., **2013** Energy , ageing , fidelity and sex : oocyte mitochondrial DNA as a protected genetic template.

208. Pereira S. L., Grãos M., Rodrigues A. S., Anjo S. I., Carvalho R. A., Paulo J., **2013** Inhibition of Mitochondrial Complex III Blocks Neuronal Differentiation and Maintains Embryonic Stem Cell Pluripotency. **8**: 1–16.

209. Peri F., Bökel C., Roth S., **1999** Local Gurken signaling and dynamic MAPK activation during *Drosophila* oogenesis. Mech. Dev. **81**: 75–88.

210. Perumalsamy L. R., Nagala M., Sarin A., **2010** Notch-activated signaling cascade interacts with mitochondrial remodeling proteins to regulate cell survival. Proc. Natl. Acad. Sci. U. S. A. **107**: 6882–6887.

211. Pich S., Bach D., Briones P., Liesa M., Camps M., Testar X., Palacín M., Zorzano A., **2005** The Charcot-Marie-Tooth type 2A gene product, Mfn2, up-regulates fuel oxidation through expression of OXPHOS system. Hum. Mol. Genet. **14**: 1405–15.

212. Poulton J. S., Deng W.-M., **2007** Cell-cell communication and axis specification in the *Drosophila* oocyte. Dev. Biol. **311**: 1–10.

213. Prober D. a, Edgar B. a, **2000** Ras1 promotes cellular growth in the *Drosophila* wing. Cell **100**: 435–46.

214. Pyakurel A., Savoia C., Hess D., Scorrano L., **2015** Extracellular Regulated Kinase Phosphorylates Mitofusin 1 to Control Mitochondrial Morphology and Apoptosis. Mol. Cell **58**: 244–254.

215. Quinn P. M., Pellissier L. P., Wijnholds J., **2017** The CRB1 Complex : Following the Trail of Crumbs to a Feasible Gene Therapy Strategy. **11**.

216. Quintero M., Colombo S. L., Godfrey A., Moncada S., **2006** Mitochondria as signaling organelles in the vascular endothelium. **103**.

217. Ramamurthy S., Ronnett G. V, **2006** Developing a head for energy

sensing: AMP-activated protein kinase as a multifunctional metabolic sensor in the brain. J. Physiol. **574**: 85–93.

218. Ratnaparkhi A., **2013** Signaling by Folded gastrulation is modulated by mitochondrial fusion and fission. J. Cell Sci. **126**: 5369 LP-5376.

219. Restrepo S., Basler K., **2016** intercellular calcium waves. Nat. Commun. **7**: 1–9.

220. Ribas V., García-Ruiz C., Fernández-Checa J. C., **2016** Mitochondria, cholesterol and cancer cell metabolism. Clin. Transl. Med. **5**: 22.

221. Rikhy R., Kamat S., Ramagiri S., Sriram V., Krishnan K. S., **2007** Mutations in dynamin-related protein result in gross changes in mitochondrial morphology and affect synaptic vesicle recycling at the *Drosophila* neuromuscular junction. Genes, Brain Behav. **6**: 42–53.

222. Rohrbaugh M., Ramos E., Nguyen D., Price M., Wen Y., Lai Z. C., **2002** Notch activation of yan expression is antagonized by RTK/pointed signaling in the *Drosophila* eye. Curr. Biol. **12**: 576–581.

223. Rolls M. M., Albertson R., Shih H. P., Lee C. Y., Doe C. Q., **2003** *Drosophila* aPKC regulates cell polarity and cell proliferation in neuroblasts and epithelia. J. Cell Biol. **163**: 1089–1098.

224. Rossignol R., Gilkerson R., Aggeler R., Yamagata K., Remigton S. J., Capaldi R. A., **2004** Energy substrate modulates mitochondrial structures and oxidative capacityin cancer cells. Cancer Res. **64**: 985–993.

225. Rossignol R., **2004** Energy Substrate Modulates Mitochondrial Structure and Oxidative Capacity in Cancer Cells. Cancer Res. **64**: 985–993.

226. Roth S., Lynch J. a, **2009** Symmetry Breaking During Drosophila Oogenesis. Cold Spring Harb. Prospect. Biol. **1**: 1–21.

227. Röth D., Krammer P. H., Gülow K., **2014** Dynamin related protein 1-dependent mitochondrial fission regulates oxidative signalling in T cells. FEBS Lett. **588**: 1749–1754.

228. Ruiz P. S., Santillán M. L., Rodríguez I. M., Casas A. B., Pérez L., Milán M., **2015** ROS-Induced JNK and p38 Signaling Is Required for Unpaired Cytokine Activation during *Drosophila* Regeneration. : 1–20.

229. Samant S. A., Zhang H. J., Hong Z., Pillai V. B., Sundaresan N. R., Wolfgeher D., Archer S. L., Chan D. C., Gupta M. P., **2014** SIRT3 Deacetylates and Activates OPA1 To Regulate Mitochondrial Dynamics during Stress. Mol. Cell. Biol. **34**: 807–819.

230. Saotome M., Safiulina D., Szabadkai G., Das S., Fransson A., Aspenstrom P., Rizzuto R., Hajnóczky G., **2008** Bidirectional Ca2+-dependent control of mitochondrial dynamics by the Miro GTPase. Proc. Natl. Acad. Sci. U. S. A. **105**: 20728–33.

231. Sasamura T., Matsuno K., Fortini M. E., **2013** Disruption of *Drosophila melanogaster* Lipid Metabolism Genes Causes Tissue Overgrowth Associated with Altered Developmental Signaling (SJ Bray, Ed.). PLoS Genet. **9**: e1003917.

232. Saxton W. M., Hollenbeck P. J., **2012** The axonal transport of mitochondria. J. Cell Sci. **125**: 2095–2104.

233. Scatena R., **2012** Mitochondria and Cancer: A Growing Role in Apoptosis, Cancer Cell Metabolism and Dedifferentiation BT - Advances in Mitochondrial Medicine (R Scatena, P Bottoni, and B Giardina, Eds.). Adv. Exp. Biol. Med. **942**: 287–308.

234. Scha H., Pfeiffer K., **2000** Supercomplexes in the respiratory chains of yeast and mammalian mitochondria. **19**.

235. Schaeffer V., Althauser C., Shcherbata H. R., Wu-Min Deng, Ruohola-Baker and H., **1998** Notch-Dependent Fizzy-Related/Hec1/Cdh1 Expression Is Required for the Mitotic-to-Endocycle Transition in *Drosophila* Follicle Cells. Development **125**: 2457–2467.

236. Schieber M., Chandel N. S., **2014** ROS Function in Redox Signaling and Oxidative Stress. Curr. Biol. **24**: R453–R462.

237. Schieke S. M., Ma M., Cao L., Mccoy J. P., Liu C., Hensel N. F., Barrett A. J., Boehm M., Finkel T., **2008** Mitochondrial Metabolism Modulates Differentiation and Teratoma Formation Capacity in Mouse Embryonic Stem Cells *. **283**: 28506–28512.

238. Schneider H., Lemasters J. J., Hochli M., Hackenbrock C. R., **1980** Liposome-Mitochondrial Inner Membrane Fusion. **255**: 3748–3756.

239. Schnepp B., Donaldson T., Grumbling G., Ostrowski S., Schweitzer R., Shilo B., Simcox A., **1998** EGF domain swap converts a *Drosophila* EGF receptor activator into an inhibitor. : 908–913.

240. Sen J., Goltz J. S., Stevens L., Stein D., **1998** Spatially Restricted Expression of pipe in the Drosophila Egg Chamber Defines Embryonic Dorsal–Ventral Polarity. Cell **95**: 471–481.

241. Sen A., Sun R., Krahn M. P., **2015** Localization and Function of Pals1 Associated Tight Junction Protein in *Drosophila* is Regulated by Two Distinct Apical Complexes. J. Biol. Chem.

242. Senft D., Ronai Z. A., **2016** Regulators of mitochondrial dynamics in cancer. Curr. Opin. Cell Biol. **39**: 43–52.

243. Seo A. Y., Joseph A.-M., Dutta D., Hwang J. C. Y., Aris J. P., Leeuwenburgh C., **2010** New insights into the role of mitochondria in aging: mitochondrial dynamics and more. J. Cell Sci. **123**: 2533 LP-2542.

244. Serasinghe M. N., Weider S. Y., Renault T. T., Asciolla J. J., Yao J. L., Jabado O., Hoehn K., Sesaki H., Chipuk J. E., **2015** Mitochondrial division is requisite to RAS-induced transformation and targeted by oncogenic MAPK pathway inhibitors. Mol. Cell **57**: 521–536.

245. Sereda, S.V. and I. A. K., **2007** Genes affecting wing planarity of *Drosophila* virilis (I): curl. Genetics **92**: 141–142.

246. Sgambato A., Camerini A., Pani G., Cangiano R., Faraglia B., Bianchino G., Bari B. De, Galeotti T., Cittadini A., **2003** Increased expression of cyclin E is associated with an increased resistance to doxorubicin in rat fibroblasts. Br. J. Cancer **88**: 1956–1962.

247. Shaw J. M., Nunnari J., **2002** Mitochondrial dynamics and division in budding yeast. Trends Cell Biol. **12**: 178–84.

248. Shaw R. J., Kosmatka M., Bardeesy N., Hurley R. L., Witters L. A., Depinho R. A., Cantley L. C., **2004** The tumor suppressor LKB1 kinase directly activates AMP-activated kinase and regulates apoptosis in response to energy stress. **101**: 3329–3335.

249. Shcherbata H. R., Althauser C., Findley S. D., Ruohola-Baker H., **2004**

The mitotic-to-endocycle switch in *Drosophila* follicle cells is executed by Notch-dependent regulation of G1/S, G2/M and M/G1 cell-cycle transitions. Development **131**: 3169–81.

250. Sherlekar A., Rikhy R., **2016** Syndapin promotes pseudocleavage furrow formation by actin organization in the syncytial *Drosophila* embryo. Mol. Biol. Cell **27**: 2064–2079.

251. Shilo B., **2003** Signaling by the *Drosophila* epidermal growth factor receptor pathway during development. Exp. Cell Res. **284**: 140–149.

252. Shingleton A. W., Das J., Vinicius L., Stern D. L., **2005** The temporal requirements for insulin signaling during development in *Drosophila*. PLoS Biol. **3**: 1607–1617.

253. Sieber M. H., Thomsen M. B., Spradling A. C., **2016** Electron Transport Chain Remodeling by GSK3 during Oogenesis Connects Nutrient State to Reproduction. Cell **164**: 420–432.

254. Silvestri L., Caputo V., Bellacchio E., Atorino L., Dallapiccola B., Valente E. M., Casari G., **2005** Mitochondrial import and enzymatic activity of PINK1 mutants associated to recessive parkinsonism. Hum. Mol. Genet. **14**: 3477–3492.

255. Sinenko S. a, Shim J., Banerjee U., **2012** Oxidative stress in the haematopoietic niche regulates the cellular immune response in *Drosophila*. EMBO Rep. **13**: 83–9.

256. Sing A., Tsatskis Y., Fabian L., Hester I., Rosenfeld R., Serricchio M., Yau N., Shanbhag R., Jurisicova A., Brill J. A., Mcquibban G. A., **2014** The Atypical Cadherin Fat Directly Regulates Mitochondrial Function and Metabolic State. : 1293–1308.

257. Skulachev V. P., **2001** Mitochondrial filaments and clusters as intracellular power-transmitting cables. Trends Biochem. Sci. **26**: 23–29.

258. Slaninova V., Krafcikova M., Perez-gomez R., Steffal P., Trantirek L., Bray S. J., Krejci A., Krejci A., **2016** Notch stimulates growth by direct regulation of genes involved in the control of glycolysis and the tricarboxylic acid cycle.

259. Small C., Ramroop J., Otazo M., Huang L. H., Saleque S., Govind S.,

2014 An unexpected link between notch signaling and ROS in restricting the differentiation of hematopoietic progenitors in Drosophila. Genetics **197**: 471–483.

260. Smith D. M., **1931** The ontogenetic history of the mitochondria of the hepatic cell of the white rat. J. Morphol. **52**: 485–511.

261. Soares H., Marinho H. S., Real C., Antunes F., **2014** Cellular polarity in aging : role of redox regulation and nutrition.

262. Sotillos S., Campuzano S., **2000** DRacGAP , a novel *Drosophila* gene , inhibits EGFR / Ras signalling in the developing imaginal wing disc. **5438**: 5427–5438.

263. Soubannier V., McBride H. M., **2009** Positioning mitochondrial plasticity within cellular signaling cascades. Biochim. Biophys. Acta **1793**: 154–70.

264. Spradling A. C., **1993** Germline cysts: Communes that work. Cell **72**: 649–651.

265. Steinberg G. R., Kemp B. E., 2009 AMPK in Health and Disease : 1025–1078.

266. Stephen J. McConnell, Leslie C. Stewart, Alec Talin and M. E. Y., **1990** Temperature-sensitive Yeast Mutants Defective in Mitochondrial Inheritance. J. Cell Biol. **111**: 967–976.

267. Struhl G., Greenwald I., **1999** Presenilin is required for activity and nuclear access of Notch in Drosophila. Nature **398**: 522–525.

268. Sturmey R. G., Brison D. R., Leese H. J., **2008** Assessing embryo viability by measurement of amino acid turnover. Reprod. Biomed. Online **17**: 486–496.

269. Sturtevant M. A., Bier E., **1995** Analysis of the genetic hierarchy guiding wing vein development in *Drosophila*. Development **121**: 785 LP-801.

270. Sun J., Deng W.-M., **2005** Notch-dependent downregulation of the homeodomain gene cut is required for the mitotic cycle/endocycle switch and cell differentiation in *Drosophila* follicle cells. Development **132**: 4299–4308.

271. Sun J., Deng W. M., **2007** Hindsight Mediates the Role of Notch in Suppressing Hedgehog Signaling and Cell Proliferation. Dev. Cell **12**: 431–442.

272. Sundaram M. V, **2005** The love − hate relationship between Ras and

Notch The love – hate relationship between Ras and Notch. : 1825–1839.

273. Susin S. a, Lorenzo H. K., Zamzami N., Marzo I., Brenner C., Larochette N., Prévost M. C., Alzari P. M., Kroemer G., **1999** Mitochondrial release of caspase-2 and -9 during the apoptotic process. J. Exp. Med. **189**: 381–394.

274. Suski J. M., Lebiedzinska M., Bonora M., Pinton P., Duszynski J., Wieckowski M. R., **2012** Relation Between Mitochondrial Membrane Potential and ROS Formation BT - Mitochondrial Bioenergetics: Methods and Protocols. In: Palmeira CM, Moreno AJ (Eds.), Humana Press, Totowa, NJ, pp. 183–205.

275. Suzanne M., Irie K., Glise B., Mori E., Matsumoto K., **1999** The Drosophila p38 MAPK pathway is required during oogenesis for egg asymmetric development. : 1464–1474.

276. Sylvain Brun, Vincent Rincheval, Se´ bastien Gaumer B. M. and I. G., **2002** reaper and bax initiate two different apoptotic pathways affecting mitochondria and antagonized by bcl-2 in *Drosophila*. Oncogene **21**: 6458–6470.

277. Szabadkai G., Simoni A. M., Bianchi K., Stefani D. De, Leo S., Wieckowski M. R., Rizzuto R., **2006** Mitochondrial dynamics and Ca2+ signaling. Biochim. Biophys. Acta - Mol. Cell Res. **1763**: 442–449.

278. Taguchi N., Ishihara N., Jofuku A., Oka T., Mihara K., **2007** Mitotic phosphorylation of dynamin-related GTPase Drp1 participates in mitochondrial fission. J. Biol. Chem. **282**: 11521–9.

279. Tanentzapf G., Smith C., Mcglade J., Tepass U., **2000** Apical , Lateral , and Basal Polarization Cues Contribute to the Development of the Follicular Epithelium during *Drosophila* Oogenesis. J. Cell Biol. **151**: 891–904.

280. Tanentzapf G., Tepass U., **2002** giant larvae and bazooka pathways in epithelial polarization. **5**.

281. Tang S., Le P. K., Tse S., Wallace D. C., Huang T., **2009** Heterozygous Mutation of Opa1 in *Drosophila* Shortens Lifespan Mediated through Increased Reactive Oxygen Species Production. PLoS One **4**: e4492.

282. Tatar M., Kopelman A., Epstein D., Tu M.-P., Yin C.-M., Garofalo R. S., **2001** A Mutant *Drosophila* Insulin Receptor Homolog That Extends Life-Span and Impairs Neuroendocrine Function. Science (80-.). **292**: 107–110.

283. Tembe V., Martino-echarri E., Marzec K. A., Mok M. T. S., Brodie K. M., Mills K., Lei Y., Defazio A., Rizos H., Kettle E., Boadle R., Henderson B. R., **2015** The BARD1 BRCT domain contributes to p53 binding , cytoplasmic and mitochondrial localization , and apoptotic function. Cell. Signal. **27**: 1763–1771.

284. Tennessen J. M., Bertagnolli N. M., Evans J., Sieber M. H., Cox J., Thummel C. S., **2014** Coordinated Metabolic Transitions During *Drosophila* Embryogenesis and the Onset of Aerobic Glycolysis. **4**: 839–850.

285. Thaiparambil J. T., Eggers C. M., Marcus A. I., **2012** AMPK Regulates Mitotic Spindle Orientation through Phosphorylation of Myosin Regulatory Light Chain. **32**: 3203–3217.

286. Thayer S. A., Miller R. J., **1990** Regulation of the intracellular free calcium concentration in single rat dorsal root ganglion neurones in vitro. J. Physiol. **425**: 85–115.

287. Thomenius M., Freel C. D., Horn S., Krieser R., Abdelwahid E., Cannon R., Balasundaram S., White K., Kornbluth S., **2011** Mitochondrial fusion is regulated by Reaper to modulate *Drosophila* programmed cell death. Cell Death Differ. **18**: 1640–50.

288. Tian A.-G., Deng W.-M., **2008** Lgl and its phosphorylation by aPKC regulate oocyte polarity formation in *Drosophila*. Development **135**: 463–71.

289. Tomas A., Futter C. E., Eden E. R., **2014** EGF receptor trafficking: consequences for signaling and cancer. Trends Cell Biol. **24**: 26–34.

290. Tomlinson A., Struhl G., **2001** Delta/Notch and Boss/Sevenless signals act combinatorially to specify the *Drosophila* R7 photoreceptor. Mol. Cell **7**: 487–495.

291. Tourmente S., Lecher P., Degroote F., Renaud M., Biotechnologie De, **1990** Mitochondrial development during *Drosophila* oogenesis : distribution , density and in situ RNA hybridizations. : 119–127.

292. Tovar J., Fischer A., Clark C. G., **1999** The mitosome, a novel organelle related to mitochondria in the amitochondrial parasite Entamoeba histolytica. Mol. Microbiol. **32**: 1013–1021.

293. Toyama E. Q., Herzig S., Courchet J., Jr T. L. L., Oliver C., Hellberg K., Young N. P., Chen H., Polleux F., David C., Shaw R. J., **2016** AMP-activated

protein kinase mediates mitochondrial fission in response to energy stress. Science (80-.). **351**: 275–281.

294. Tsou P., Zheng B., Hsu C.-H., Sasaki A. T., Cantley L. C., **2011** A Fluorescent Reporter of AMPK activity and Cellular Energy Stress. Cell Metab. **13**: 476–486.

295. Turley J. M., Ruscetti F. W., Kim S., Fu T., Gou F. V., Birchenall-roberts M. C., **1997** Vitamin E Succinate Inhibits Proliferation of BT-20 Human Breast Cancer Cells : Increased Binding of Cyclin A Negatively Regulates E2F Transactivation Activity.

296. Ushio-Fukai M., Alexander R. W., Akers M., Griendling K. K., **1998** p38 Mitogen-activated protein kinase is a critical component of the redox-sensitive signaling pathways activated by angiotensin II. Role in vascular smooth muscle cell hypertrophy. J. Biol. Chem. **273**: 15022–15029.

297. Valente E. M., Abou-sleiman P. M., Caputo V., Muqit M. M. K., Harvey K., Gispert S., Ali Z., Turco D. Del, Bentivoglio A. R., Healy D. G., Albanese A., Nussbaum R., Gonza R., Deller T., Salvi S., Cortelli P., Gilks W. P., Latchman D. S., Harvey R. J., Dallapiccola B., Auburger G., Wood N. W., **2004** Hereditary Early-Onset Parkinson ' s Disease Caused by Mutations in PINK1. Science (80-.). **304**: 1158–1161.

298. Valsecchi F., Grefte S., Roestenberg P., Joosten-Wagenaars J., Smeitink J. A. M., Willems P. H. G. M., Koopman W. J. H., **2013** Primary fibroblasts of NDUFS4−/− mice display increased ROS levels and aberrant mitochondrial morphology. Mitochondrion **13**: 436–443.

299. Vásquez-Trincado C., García-Carvajal I., Pennanen C., Parra V., Hill J. A., Rothermel B. A., Lavandero S., **2016** Mitochondrial dynamics, mitophagy and cardiovascular disease. J. Physiol. **594**: 509–525.

300. Velde C. Vande, McDonald K. K., Boukhedimi Y., McAlonis-Downes M., Lobsiger C. S., Bel Hadj S., Zandona A., Julien J.-P., Shah S. B., Cleveland D. W., **2011** Misfolded SOD1 associated with motor neuron mitochondria alters mitochondrial shape and distribution prior to clinical onset. PLoS One **6**: e22031.

301. Verburg J., Hollenbeck P. J., **2008** Mitochondrial membrane potential in

axons increases with local nerve growth factor or semaphorin signaling. J. Neurosci. **28**: 8306–15.

302. Verrelli B. C., Eanes W. F., **2001** The functional impact of Pgm amino acid polymorphism on glycogen content in *Drosophila melanogaster*. Genetics **159**: 201–210.

303. Vrailas-Mortimer A., Rivero T. del, Mukherjee S., Nag S., Gaitanidis A., Kadas D., Consoulas C., Duttaroy A., Sanyal S., **2011** A muscle-specific p38 MAPK/Mef2/MnSOD pathway regulates stress, motor function, and life span in Drosophila. Dev. Cell **21**: 783–95.

304. Vyas S., Zaganjor E., Haigis M. C., **2016** Review Mitochondria and Cancer. Cell **166**: 555–566.

305. Wai T., Langer T., **2016** Mitochondrial Dynamics and Metabolic Regulation. Trends Endocrinol. Metab. **27**: 105–117.

306. Wanet A., Arnould T., Najimi M., Renard P., **2015** Connecting Mitochondria, Metabolism, and Stem Cell Fate. Stem Cells Dev. **24**: 1957–1971.

307. Wang S.-H., **2000** Dual role for *Drosophila* epidermal growth factor receptor signaling in early wing disc development. Genes Dev. **14**: 2271–2276.

308. Wang Z. a, Huang J., Kalderon D., **2012** *Drosophila* follicle stem cells are regulated by proliferation and niche adhesion as well as mitochondria and ROS. Nat. Commun. **3**: 769.

309. Wang X., Li H., Zheng A., Yang L., Liu J., Chen C., Tang Y., Zou X., Li Y., Long J., Liu J., Zhang Y., Feng Z., **2014** Mitochondrial dysfunction-associated OPA1 cleavage contributes to muscle degeneration : preventative effect of hydroxytyrosol acetate. : 1–11.

310. Wangler M. F., Reiter L. T., Zimm G., Trimble-morgan J., Wu J., Bier E., **2011** Antioxidant proteins TSA and PAG interact synergistically with Presenilin to modulate Notch signaling in Drosophila. **2**: 554–563.

311. Warburg O., **1956** On the Origin of Cancer Cells On the Origin of Cance. Source Sci. New Ser. **123**: 309–314.

312. Wasserman J. D., Freeman M., **1998** An Autoregulatory Cascade of EGF Receptor Signaling Patterns the Drosophila Egg. **95**: 355–364.

313. Weiss C., Schneider S., Wagner E. F., Zhang X., Seto E., Bohmann D., **2003** JNK phosphorylation relieves HDAC3-dependent suppression of the transcriptional activity of c-Jun. EMBO J. **22**: 3686–3695.

314. Westermann B., **2010** Mitochondrial fusion and fission in cell life and death. Nat. Rev. Mol. Cell Biol. **11**: 872–84.

315. Williams P. a., Morgan J. E., Votruba M., **2010** Opa1 deficiency in a mouse model of dominant optic atrophy leads to retinal ganglion cell dendropathy. Brain **133**: 2942–2951.

316. Wu S.-B., Wei Y.-H., **2012** AMPK-mediated increase of glycolysis as an adaptive response to oxidative stress in human cells: Implication of the cell survival in mitochondrial diseases. Biochim. Biophys. Acta - Mol. Basis Dis. **1822**: 233–247.

317. Xie X., Dubrovsky E. B., **2015** Knockout of *Drosophila* RNase Z(L) impairs mitochondrial transcript processing, respiration and cell cycle progression. Nucleic Acids Res. **43**: 10364–10375.

318. Xu J., Chi F., Guo T., Punj V., Lee W. N. P., French S. W., Tsukamoto H., **2015** NOTCH reprograms mitochondrial metabolism for proinflammatory macrophage activation. **125**: 1579–1590.

319. Yang Y., Ouyang Y., Yang L., Beal M. F., McQuibban A., Vogel H., Lu B., **2008** Pink1 regulates mitochondrial dynamics through interaction with the fission/fusion machinery. Proc. Natl. Acad. Sci. U. S. A. **105**: 7070–5.

320. Youle C. W. and R. J., **2009** The Role of Mitochondria in Apoptosis. Annu. Rev. Genet. **43**: 95–118.

321. Yu T., Robotham J. L., Yoon Y., **2006** Increased production of reactive oxygen species in hyperglycemic conditions requires dynamic change of mitochondrial morphology. **103**: 2653–2658.

322. Yu J., Poulton J., Huang Y.-C., Deng W.-M., **2008** The hippo pathway promotes Notch signaling in regulation of cell differentiation, proliferation, and oocyte polarity. PLoS One **3**: e1761.

323. Zanna C., Ghelli A., Porcelli A. M., Karbowski M., Youle R. J., Schimpf S., Wissinger B., Pinti M., Cossarizza A., Vidoni S., Valentino M. L., Rugolo M.,

Carelli V., **2008** OPA1 mutations associated with dominant optic atrophy impair oxidative phosphorylation and mitochondrial fusion. Brain **131**: 352–67.

324. Zhang W., Thompson B. J., Hietakangas V., Cohen S. M., **2011** MAPK/ERK signaling regulates insulin sensitivity to control glucose metabolism in *Drosophila*. PLoS Genet. **7**: e1002429.

325. Zhao Q., Wang J., Levichkin I. V, Stasinopoulos S., Ryan M. T., Hoogenraad N. J., **2002** A mitochondrial specific stress response in mammalian cells. EMBO J. **21**: 4411–9.

326. Zhao T., Graham O. S., Raposo A., Johnston D. S., **2012** Europe PMC Funders Group Growing microtubules push the oocyte nucleus to polarise the *Drosophila* dorsal-ventral axis. **336**: 999–1003.

327. Zhao J., Zhang J., Yu M., Xie Y., Huang Y., Wolff D. W., Abel P. W., Tu Y., **2013** Mitochondrial dynamics regulates migration and invasion of breast cancer cells. Oncogene **32**: 4814–4824.

328. Zheng B., Cantley L. C., **2006** Regulation of epithelial tight junction assembly and disassembly by AMP-activated protein kinase. **2006**: 2–5.

329. Zick M., Rabl R., Reichert A. S., **2009** Cristae formation—linking ultrastructure and function of mitochondria. Biochim. Biophys. Acta - Mol. Cell Res. **1793**: 5–19.